2009

# Conformationally gated electron transfer studies of iso-1-cytochrome c

Swati Bandi
*The University of Montana*

# CONFORMATIONALLY GATED ELECTRON TRANSFER STUDIES OF ISO-1-CYTOCHROME *C*

By

SWATI BANDI

B. Sc. Microbiology, Devi. Ahilya. Vishwavidyalaya, Indore, M.P, India, 1997

M. Sc. Biochemistry, Devi. Ahilya. Vishwavidyalaya, Indore, M.P, India, 1999

Dissertation

presented in partial fulfillment of the requirements
for the degree of

Doctor of Philosophy
in Chemistry & Biochemistry

The University of Montana
Missoula, MT

May 2009

Approved by:

Perry Brown, Associate Provost for Graduate Education
Graduate School

Dr. J.B. Alexander Ross, Committee Chairperson
Department of Chemistry & Biochemistry

Dr. Bruce E. Bowler, Committee Member
Department of Chemistry & Biochemistry

Dr. Klára Briknarová, Committee Member
Department of Chemistry & Biochemistry

Dr. Michael DeGrandpre, Committee Member
Department of Chemistry & Biochemistry

Dr. Michele A. McGuirl, Committee Member
Division of Biological Sciences

Bandi, Swati, Ph. D., Spring 2009 Chemistry & Biochemistry

Conformationally Gated Electron Transfer Studies of Iso-1-cytochrome *c*

Chairperson: J. B. Alexander Ross

Protein folding is important because all proteins must fold to achieve their active conformer. In many cases, misfolding is the cause of disease and thus, understanding folding may lead to cures for disease. This thesis focuses on the dynamics and thermodynamics of partially unfolded states of proteins that lie near the bottom of a folding funnel. Various studies have provided evidence that partially unfolded proteins can be key intermediates in metabolic processes and in aggregation diseases. Partially unfolded proteins also provide insight into the types of structures that guide/misguide the process of protein folding. Less is known about how stability affects the roughness of an energy landscape at the bottom of the folding funnel. Histidine-heme alkaline conformers of cytochrome *c* are used as a model for a late folding intermediate or partially unfolded state that can be exploited to study roughness near the bottom of a folding funnel.

In my thesis work, I have developed a novel method using electron transfer (ET) reactions to probe these conformational changes and thus provide insight into the dynamics of late folding processes not available through standard stopped-flow methods. This method has helped to probe two factors that affect dynamics near bottom of funnel: overall stability and the position of a residue in a loop that stabilizes a misfold. The main findings from my work include: a decrease in stability decreases the roughness of a folding funnel and changing the position of a residue responsible for misfolding strongly affects stability and dynamics of the misfolded state. The robustness pertaining to the gated ET method highlighted in this work is that it allows extraction of discrete rate constants for conformational changes under conditions where these rate constants cannot usually be measured directly. The method has also been applied to the dynamics of proline isomerization. The data demonstrate that rates of ET in proteins can be tuned efficiently using a combined strategy of modulating the sequence position and nature of the metal ligand involved in conformational gating. Thus, ET gates can be readily tuned for metabolic processes or the development of molecular switches.

## Acknowledgements

*I ask for a moment's indulgence to sit by thy side. The works that I have in hand I will finish afterwards. Away from the sight of thy face my heart knows no rest nor respite, and my work becomes an endless toil in a shoreless sea of toil. Today the summer has come at my window with its sighs and murmurs; and the bees are plying their minstrelsy at the court of the flowering grove. Now it is time to sit quiet, face to face with thee, and to sing dedication of life in this silent and overflowing leisure.* Rabindranath Tagore, *Gitanjali*.

In this moment of indulgence I would like to remember and thank all the people who have helped me in my journey to reach my goals. First of all I want to thank my Advisor Dr. Bruce Bowler for making me a part of his laboratory, for his invaluable guidance, patience, kindness, support and motivation throughout the journey of my PhD education. Working with him is a school by itself, to grow as a student to become a scientist, by learning the skills of not only handling instruments, analyzing data, reasoning and writing, but also hard work, dedication, good management of lab, time and life.

Secondly I want to thank all my committee members Drs. J. B Alexander Ross, Michele McGuirl, Klára Briknarová, and Michael DeGrandpre for their time, encouragement and guidance. I also want to thank Drs. E. Rosenberg and E. Adams for their guidance with N.M.R and all my professors from India and the University of Denver for their mentoring, and guidance.

I would like to thank all the past and present Bowler group members especially, Eydiejo, Franco, Jasmina, Melisa, Michael, Michaela, Mike, Saritha, Sudhindra, Tanveer and Bryan for their mentoring, valuable discussions, friendship, help and being my academic family. I want to thank Ayesha for helping me with ATR and NMR. I also want to thank all my friends from India, Denver (especially Jeff, Tom, Edmir, and Sara), Missoula and all my room mates for being an integral part of this journey. I especially want to thank Vaishali, Gianna, and Varadharajan for being with me in my difficult times at Missoula and for their unconditional support.

I especially would like to thank my Parents, Grandparents (paternal & maternal), brother, sister-in-law, all my aunts, uncles, and cousins for their endless support, encouragement and trust in me. Finally want to thank my Gurus and GOD for there blessings and being with me always.

## Table of Contents


Abstract ii

Acknowledgements iii

Table of Contents iv

List of Figures vii

List of Tables xi

Chapter 1 *Introduction*

1.1 Protein Folding and Partially Unfolded Proteins 1

1.2 Cytochrome *c* 8

1.3 Alkaline Conformational Transition 15

1.4 Electron Transfer 20

1.5 Goals of Dissertation 26

Chapter 2 *The Alkaline Conformational Transition and Gated Electron Transfer with a Lys 79 → His Variant of Iso-1-cytochrome c*

2.1 Introduction 29

2.2 Materials and Methods 32

2.3 Results 44

2.4 Discussion 63

2.5 Conclusions 69

Chapter 3 *Probing the Bottom of the Folding Funnel using Conformationally Gated Electron Transfer with the AcH73 Variant of Iso-1-cytochrome c*

3.1 Introduction 70

3.2 Materials and Methods 73

3.3 Results 79

3.4 Discussion 105

3.5 Conclusions 111

Chapter 4 *Kinetics of Proline Isomerization Monitored through Conformationally Gated Electron Transfer in the A79H73 Variant of Iso-1-cytochrome c*

4.1 Introduction 112

4.2 Materials and Methods 118

4.3 Results 119

4.4 Discussion 128

4.5 Conclusions 137

Chapter 5 *Modification in the Dynamics of the Alkaline Transformation by Mutations in the Ω-loop of Iso-1-cytochrome c*

5.1 Introduction 138

5.2 Materials and Methods 142

5.3 Results 149

5.4 Discussion 178

5.5 Conclusions 187

Chapter 6 *Conformationally Gated Electron Transfer Studies by Flash Photolysis*

6.1 Introduction 188

6.2 Materials and Methods 192

6.3 Results and Discussion 195

6.4 Conclusions 198

References 200

Appendices 216

Appendix A 216

Appendix B 222

Appendix C 241

Appendix D 249

Appendix E 258

Appendix F 267

Appendix G 274

Appendix H 275

Appendix I 276

Appendix J 277

# List of Figures


| FIGURE | | PAGE |
|---|---|---|
| 1.1 | Basic protein structure | 2 |
| 1.2 | Folding funnel energy landscape models | 4 |
| 1.3 | Phase diagrams for protein folding | 5 |
| 1.4 | Folding funnel energy landscape | 6 |
| 1.5 | Schematic of the electron transfer chain | 9 |
| 1.6 | Schematic representation of apoptosis and role of cytochrome *c* | 11 |
| 1.7 | The cooperative units in horse heart cytochrome *c* | 13 |
| 1.8 | Structure of heme | 14 |
| 1.9 | Sequential unfolding and refolding pathway of cytochrome *c* | 15 |
| 1.10 | Summarized spectral states of alkaline transition | 16 |
| 1.11 | Positions of possible lysine ligands of iso-1-cytochrome *c* | 17 |
| 1.12 | Heme ligation scheme in alkaline transition of iso-1-cyt *c* | 18 |
| 1.13 | Schematic representation of the ligands replacing Met80 in the alkaline conformational transition of the K73H variant of iso-1-cytochrome *c* | 19 |
| 1.14 | Schematic representation of electron transfer reaction | 20 |
| 1.15 | Electron transfer square scheme for iso-1-cytochrome *c* | 25 |
| 1.16 | Electronic absorption spectra of oxidized and reduced horse cytochrome *c* | 26 |
| 2.1 | Ribbon diagram of iso-1-cyt *c* showing the engineered histidine at position 79 | 31 |
| 2.2 | Schematic representation of the ligands replacing Met80 in the alkaline conformational transition of K79H iso-1-cytochrome *c*. | 32 |
| 2.3 | Schematic representation of pRS/C7.8 phagemid vector | 33 |
| 2.4 | CD denaturation curve for H79 variant | 45 |
| 2.5 | Partial denaturation curve for wild type and H79 variant | 47 |
| 2.6 | pH titration comparative curve for wild type and H79 variant | 48 |
| 2.7 | Plots for determination of isosbestic points of K79H iso-1-cytochrome *c* | 50 |
| 2.8 | NMR spectra of K79H iso-1-cytochrome *c* | 54 |
| 2.9 | Representative kinetic traces from pH jump kinetics of K79H iso-1-cytochrome *c* | 56 |
| 2.10 | Plots of fast phase rate constant and its amplitude for K79H iso-1-cytochrome *c* | 57 |

| | | |
|---|---|---|
| 2.11 | Plots of slow phase rate constant and its amplitude for K79H iso-1-cytochrome *c* | 58 |
| 2.12 | Representative kinetic traces from electron transfer kinetics of K79H iso-1-cytochrome *c* | 62 |
| 3.1 | Ribbon diagram of iso-1-cyt *c* showing the engineered histidine at position 73 | 72 |
| 3.2 | CD denaturation and partial unfolding curves of AcH73 variant | 81 |
| 3.3 | pH titration curves for AcH73 at different [gdnHCl] | 82 |
| 3.4 | Representative for forward and backward pH titration curves of AcH73 variant | 83 |
| 3.5 | Plots of free energy as a function of gdnHCl concentration for the AcH73 variant | 85 |
| 3.6 | Plots for determination of isosbestic points of AcH73 variant of iso-1-cytochrome *c* | 87 |
| 3.7 | Acid and alkaline transition curves monitored at 380 and 398 nm | 88 |
| 3.8 | Representative kinetic traces from pH jump kinetics of AcH73 | 90 |
| 3.9 | Plots of fast phase rate constant and its amplitude for AcH73 | 92 |
| 3.10 | Plots of slow phase rate constant and its amplitude for K79H iso-1-cytochrome *c* | 93 |
| 3.11 | Representative kinetic traces from electron transfer kinetics of AcH73 variant as a function of pH and $[a_6Ru^{2+}]$ | 95 |
| 3.12 | Plots of fast phase rate constant as a function of pH and $[a_6Ru^{2+}]$ | 97 |
| 3.13 | Plot of electron transfer rate constant as a function of pH. | 98 |
| 3.14 | Schematic representation of gated electron transfer kinetic mechanism | 98 |
| 3.15 | Plots of faster intermediate rate constant as a function of $[a_6Ru^{2+}]$ at different pH's | 99 |
| 3.16 | Plots of slower intermediate and slow rate constant at 5 mM $[a_6Ru^{2+}]$ as a function of pH | 100 |
| 3.17 | Plots of fractional amplitude for the four phases obtained from ET kinetics as a function of pH | 102 |
| 3.18 | Downfield NMR spectra of AcH73 | 104 |
| 3.19 | Summarized thermodynamic results and the dual-well landscape for AcH73 and K73H proteins at pH 7.5 | 106 |
| 3.20 | Summarized conformational kinetic results for the AcH73 and K73H | 109 |
| 3.21 | Summarized thermodynamics and conformational kinetics for | 111 |

| | | |
|---|---|---|
| | AcH73 and K73H proteins at pH 7.5 | |
| 4.1 | Schematic representation of the proline *cis trans* isomerization | 112 |
| 4.2 | Ribbon diagram of iso-1-cyt *c* showing the positions of proline | 115 |
| 4.3 | Schematic representation of the conformationally gated electron transfer and proline isomerization kinetic mechanism | 118 |
| 4.4 | Representative kinetic traces from electron transfer kinetics of A79H73 variant as a function of pH and $[a_6Ru^{2+}]$ | 121 |
| 4.5 | Plots of fast phase rate constant as a function of pH and $[a_6Ru^{2+}]$ | 123 |
| 4.6 | Plot of electron transfer rate constant as a function of pH | 124 |
| 4.7 | Plots of faster intermediate rate constant as a function of $[a_6Ru^{2+}]$ at different pH's | 124 |
| 4.8 | Plots of slower intermediate rate constant at as a function of pH. | 125 |
| 4.9 | Plots of slowest rate constant at as a function of pH. | 126 |
| 4.10 | Plots of fractional amplitude for the four phases obtained from ET kinetics as a function of pH | 128 |
| 4.11 | Summarized conformationally gated kinetic results for A79H73 variant | 132 |
| 4.12 | Summarized proline isomerization kinetic results for A79H73 variant | 133 |
| 4.13 | Plots of amplitude for the faster intermediate and the slowest phase as a function of pH from ET data. | 135 |
| 5.1 | Ribbon diagram of iso-1-cyt *c* showing the positions of engineered mutations in the Ω-Loop D | 141 |
| 5.2 | CD denaturation curves of the variants of iso-1-cyt *c* | 151 |
| 5.3 | Partial denaturation curve for the H81 variant | 152 |
| 5.4 | pH titration curves for His81 variant at different [gdnHCl] | 153 |
| 5.5 | Plots of free energy as a function of gdnHCl concentration for the H81 variant | 155 |
| 5.6 | Plots for determination of isosbestic points of His81 variant of iso-1-cytochrome *c* | 156 |
| 5.7 | Fractional population of H81 as a function of pH | 157 |
| 5.8 | pH titration curves for A72H76 variant at 0 M [gdnHCl] | 158 |
| 5.9 | Plots for determination of isosbestic points of A72H76 variant of iso-1-cytochrome *c* | 159 |
| 5.10 | Plots of fast phase rate constant and its amplitude for H81 variant | 162 |
| 5.11 | Plots of intermediate phase rate constant and its amplitude of H81 | 163 |

variant
5.12 Plots of slow phase rate constant and its amplitude of H81 164
5.13 Plots of fast phase rate constant and its amplitude for A72H76 variant 166
5.14 Plots of slow phase rate constant and its amplitude for A72H76 variant 168
5.15 Plots of fast phase rate constant as a of $[a_6Ru^{2+}]$ at pH 7.5 for H81 variant 170
5.16 Plots of intermediate phase rate constant as a function of $[a_6Ru^{2+}]$ at pH 7.5 for H81 variant 171
5.17 Plots of slow phase rate constant as a function of $[a_6Ru^{2+}]$ at pH 7.5 for H81 variant 171
5.18 Plots of fast phase rate constant as a function of $[Co(terpy)_2]^2$ at pH 7.5 for H81 variant 173
5.19 Plots of intermediate phase rate constant as a function of $[Co(terpy)_2]^2$ at pH 7.5 for H81 variant 173
5.20 Plots of slowest phase rate constant as a function of $[Co(terpy)_2]^2$ at pH 7.5 for H81 variant 174
5.21 Plots of fast phase rate constant as a function of $[a_6Ru^{2+}]$ at pH 7.5 for A72H76 variant 175
5.22 Plots of intermediate phase rate constant as a function of $[a_6Ru^{2+}]$ at pH 7.5 for A72H76 variant 175
5.23 Plots of slow phase rate constant as a function of $[a_6Ru^{2+}]$ at pH 7.5 for A72H76 variant 176
5.24 Plots of fast phase rate constant as a function of $[Co(terpy)_2]^2$ at pH 7.5 for H81 variant 177
5.25 Plots of slow phase rate constant as a function of $[Co(terpy)_2]^2$ at pH 7.5 for H81 variant 177
5.26 Summary of the ET gate lifetimes for the variants of iso-1-cyt *c* 186
5.27 Summary of the energy states for the variants of iso-1-cyt *c* 186
6.1 Figure of cytochrome *c* showing the extent of the electronic coupling with the heme center 189
6.2 Schematic representation of intramolecular ET reaction 190
6.3 Schematic representation of intramolecular ET reaction during the alkaline conformational transition 192
6.4 CD denaturation curves of the S47H related variants of iso-1-cyt *c* 196
6.5 CD denaturation curves of the D50H related variants of iso-1-cyt *c* 197

# List of Tables


| TABLE | | PAGE |
|---|---|---|
| 2.1 | Thermodynamic parameters from pH titration for H79 variant | 52 |
| 2.2 | Kinetic parameters from pH jump for H79 variant | 59 |
| 2.3 | Kinetic parameters from ET experiments for H79 variant | 63 |
| 3.1 | Thermodynamic parameters for forward and backward pH trations for the AcH73 variant | 83 |
| 3.2 | Thermodynamic parameters from pH titration of AcH73 variant | 84 |
| 3.3 | Thermodynamic parameters from pH titration in the acidic region at 380 and 398 nm for the AcH73 variant | 89 |
| 3.4 | Thermodynamic parameters from pH titration in the alkaline region at 380 and 398 nm for the AcH73 variant | 89 |
| 3.5 | Kinetic parameters from pH jump for AcH73 variant | 94 |
| 5.1 | Oligonucleotide primers used for site directed mutagenesis | 145 |
| 5.2 | Expected and determined m/z for the main peak from HPLC. | 146 |
| 5.3 | Thermodynamic parameters from global unfolding of variants of iso-1-cyt *c* | 151 |
| 5.4 | Thermodynamic parameters from pH titration for H81 variant | 154 |
| 5.5 | Thermodynamic parameters from pH titration for A72H76 variant | 158 |
| 5.6 | Kinetic parameters from pH jump for H81 variant | 164 |
| 5.7 | Kinetic parameters from pH jump for A72H76 variant | 168 |
| 5.8 | Kinetic parameters from ET experiments for H81 and A72H76 variants | 178 |
| 5.9 | Comparative conformationally gated rate constant for variants of iso-1-cyt *c* | 185 |
| 6.1 | Oligonucleotide primer used as mutagenic primer for site directed mutagenesis | 194 |
| 6.2 | Expected and determined m/z for the main peak from HPLC | 195 |
| 6.3 | Thermodynamic parameters for global unfolding of variants of iso-1-cyt *c* | 198 |

# CHAPTER 1

# *INTRODUCTION*

## 1.1 Protein Folding and Partially Unfolded Proteins

Proteins are the workhorses of biological systems that carry out most of the biochemical processes and constitute the majority of cellular structures [1]. They are made up of 20 different amino acids arranged in a linear chain and joined together by peptide bonds between the carboxyl group of one amino acid and the amino group of the following amino acid residue. Regular repeating local structure stabilized by hydrogen bonds leads to formation of secondary structures like alpha helix or beta sheet as shown in figure 1.1.

To carry out their function proteins must fold into complex three dimensional (3D) structures. In 1958, more than fifty years ago, John Kendrew and coworkers published the first paper showing the 3D structure of the protein myoglobin [2]. Since then various landmarks have been achieved in the protein science field. These include the famous experiment by Christian Anfinsen on ribonuclease which suggested the relation between the amino acid sequence of a protein and its conformation, and the predictability of folding and unfolding pathways [3]. In 1969, Cyrus Levinthal pointed out that it is impossible for an unfolded protein to fold on the biological timescale if a complete conformational search is necessary [4]. Oleg Ptitsyn suggested a hierarchical process with the rapid initial formation of secondary structures, such as alpha helices or beta sheets. At each step stabilization is achieved by interaction with previously formed structure. The initial structure formed is partially folded; it is referred as a molten globule [5]. It can be

further defined as a stable, partially folded protein state found in mildly denaturing conditions, occurring between denatured and fully native states of a protein.

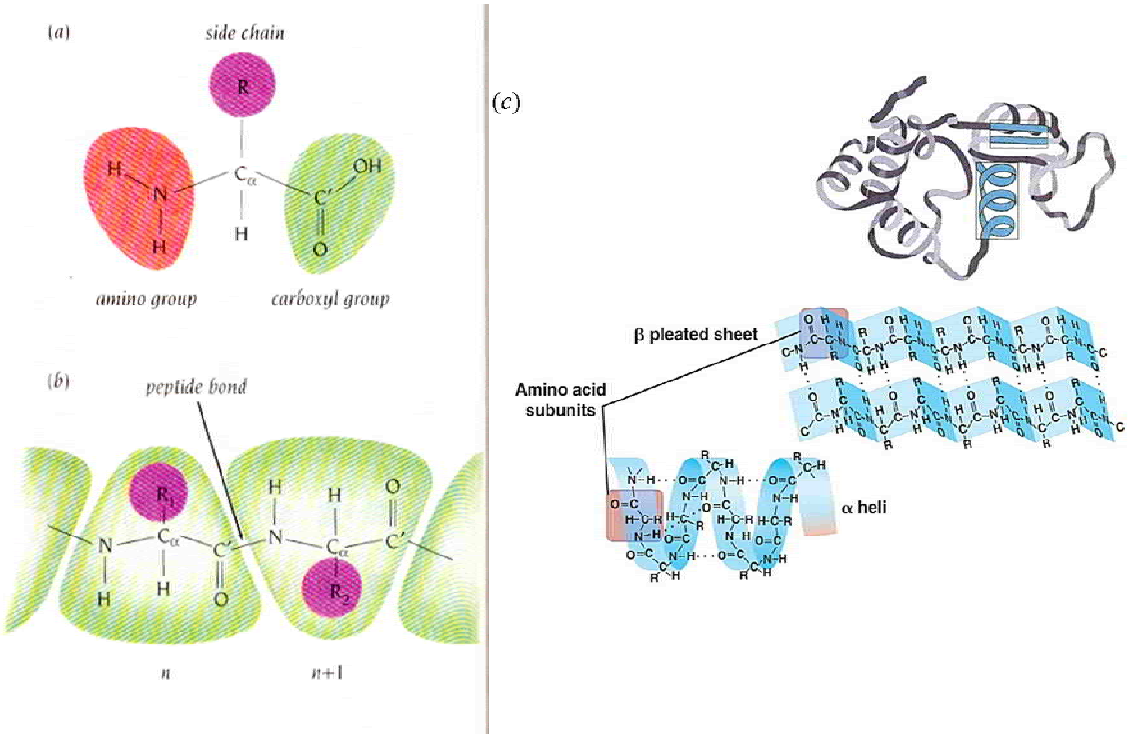


**Figure 1.1** (a) Basic protein structure showing carboxyl group and amino group with side chain R connected to the α-carbon atom. (b) Two amino acids connected through a peptide bond between the carboxyl group of one amino acid (n) and the amino group of the adjacent amino acid (n+1) to form the primary protein structure. Panel (c), shows primary structure connected through hydrogen bonds to form the secondary structures, α-helix and β-sheet, which are part of the tertiary structure of a globular protein. Figures (a) and (b) are taken from: tigger.uic.edu/.../phys/phys461/phys450/ANJUM05/ and figure (c) is taken from http://kvhs.nbed.nb.ca/gallant/biology/secondary_structure.jpg

Hydrophobic collapse is a hypothesized event that occurs during the folding process of globular proteins (soluble in aqueous solution). In this hydrophobic collapse, amino acids with non-polar side chains are buried in the protein interior to form the hydrophobic core and most of the amino acids with polar side chains are exposed to the solvent forming the protein surface. This is considered to be a relatively early step in the

folding pathway, occurring before the formation of the secondary structure and native contacts. Pitsyn proposed rapid hydrophobic collapse of a protein to form a molten globule in which the native secondary structure leads to formation of native tertiary structure [6].

Tremendous amounts of experimentation have been done since Ptitsyn's proposal dealing with understanding the thermodynamics and kinetics of protein folding. Prior to the mid-1980s, protein folding was considered to be the sum of many different small interactions such as hydrogen bonds, ion pairs, van der Waals attractions and water mediated hydrophobic interactions. However, hydrophobic interactions have emerged as the dominant component in protein folding. Various models arose in 1980's and 1990's to probe the shape of the energy landscape and the nature of the conformational space of a protein. These studies led to the conclusion that proteins have funnel shaped energy landscapes, i.e., many high energy states and few low energy states. Figure 1.2 represents four types of possible protein folding energy landscapes, leading to different folding mechanisms. Figure 1.2a represents a simple funnel for fast folding, figure 1.2b represents a rugged energy landscape with kinetic traps, figure 1.2c represents a golf course energy landscape in which folding is dominated by a diffusional conformational search and figure 1.2d represents a moat landscape, where folding must pass through an obligatory intermediate [7]. A funnel describes the heterogeneous nature of the process by which a protein attains the native state, which is confirmed by various experiments including studies on the folding of the seven repeats of the Notch receptor ankyrin domain [8]. These experiments suggest that chain entropy increases as protein structure becomes less stable, that there are multiple folding routes and that different routes

dominate under different folding conditions [7]. It is also believed that proteins with similar functions rather than similar structure have similar energy landscapes [9].

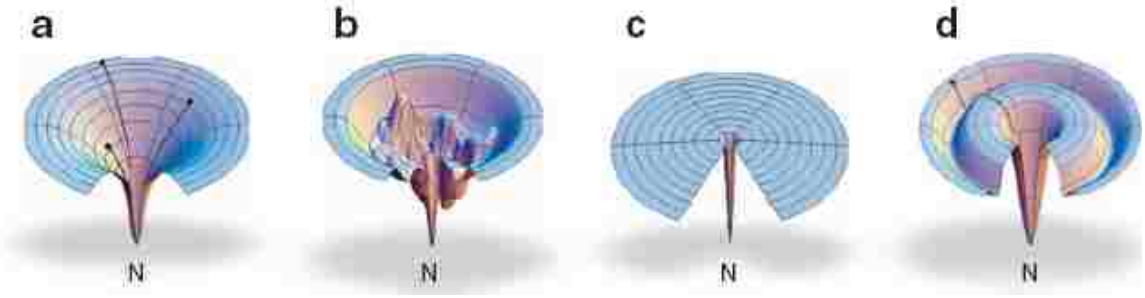


**Figure 1.2** Folding funnel energy landscape cartoon taken from reference 7 showing the possible paths a protein can follow to attain the low energy native (N) state from the high energy denatured state. (a) A smooth energy landscape for a fast folder, (*b*) a rugged energy landscape with kinetic traps, (*c*) a golf course energy landscape in which folding is dominated by a diffusional conformational search, and (*d*) a moat landscape, where folding must pass through an obligatory intermediate [7].

The rugged funnel model (figure 1.2b) is accepted as the most realistic model of the four shown in figure 1.2, which can be applicable to many types of proteins. This statistical energy landscape is built with three tools: the statistical mechanics of disordered systems like glasses, where material is arranged randomly in space, the properties of polymers, and the properties of phase transitions in finite systems. The phase transition of a protein is shown in figure 1.3. This phase diagram is based on three axes, hydrophobicity, ratio of temperature and solvent energy changes, and the free energy change. This shows the conversion of a random coil to a molten globule followed by a collapsed glassy state and finally attaining the native state, on the right hand side for slow folding proteins. The left

hand side, where a random coil directly goes to the formation of native state represents the fast folding protein phase transition.

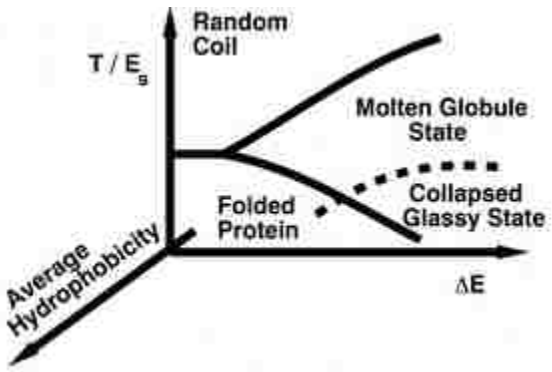


**Figure 1.3** The phase diagram is taken from reference 10. The phase diagram along a line of some average sequence hydrophobicity shows the possible thermodynamic states of a protein modeled as a minimally frustrated heteropolymer. Varying the hydrophobicity by changes in solvent ($E_s$, solvent energy) and temperature (T) can modify the number of phases observed in the folding process [10].

According to this model a protein is considered to be a minimally frustrated heteropolymer. The main point from this statistical energy landscape theory is that globally the folding landscape resembles a funnel which is to some extent rugged i.e., riddled with traps in which a protein can temporarily reside. The early folding steps lead to a collapsed structure with the overall topology of the native protein. There is not a single pathway but multiple pathways or routes of folding. Figure 1.4 represents the folding landscape of a small helical protein which is funnel-like, with a preferred direction of flow to attain the unique native state. The upper broad part of this figure represents the denatured state with higher entropy, higher free energy and little ordered structure. The lower tapered part represents less entropy and lower free energy as the

protein approaches structural similarity with the native state. In between these states lies the molten globule state, which is a partially folded structure of the protein. The molten globule state is above the glass transition temperature ($T_g$) [11] and behaves like a viscous liquid.

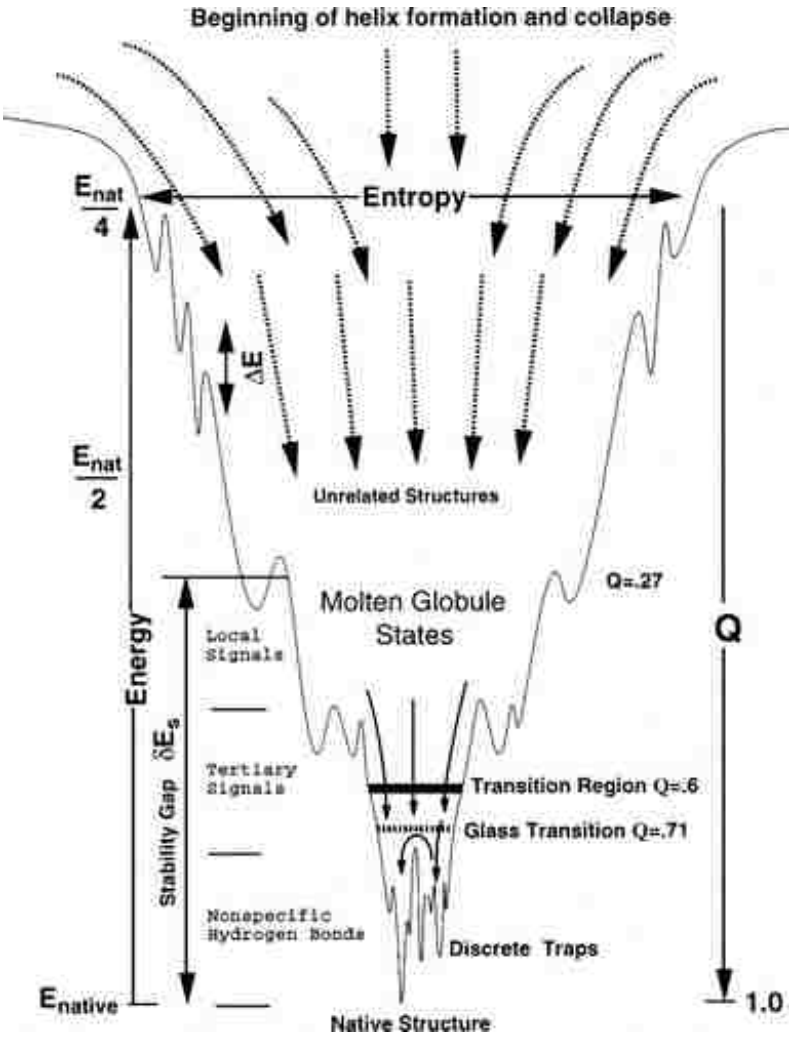


**Figure 1.4** A rugged folding landscape of a small helical protein taken from reference 10. The upper part of funnel represents the denatured state with high free energy and high entropy while lower part refers to the native state of protein with low free energy and low entropy. E, represents the solvent-averaged energy, Q represents the fraction of native like contacts, describing the position of an ensemble of states within the funnel. $\Delta E$ is the average ruggedness and $\delta E_S$ is the stability gap between the compact misfolded or molten globule state and the native state [10].

Below $T_g$, transition rates between different low energy states slow down and protein now has more glass-like transitions between partially unfolded forms of the protein. A glass transition occurs at a temperature where there are too few states available, so the system remains frozen in one of a few distinct states. At the folding temperature ($T_f$), the probability of being in the folded state is equal to the probability of being in a misfolded state. As shown in figure 1.4 some routes can lead to a low energy misfolded conformation from which the protein has to partially unfold to reach the native state. Efficient folding requires that this commitment to folding occurs before the glass transition ($T_f > T_g$). If not, a frustrated landscape results with deep, slowly interconverting traps below the glass transition. For small proteins like cytochrome *c*, which is used in this study, discrete pathways emerge only in the late folding process when the protein has already achieved a correct global configuration. Such late folding intermediates are observable because they occur below the glass transition where the kinetics are slow [10].

One of the approaches to understand late folding processes below the glass transition is to study partially unfolded states of proteins. Partially unfolded states exist in a wide range of structures [12-16] and can be close to the secondary structure of the native state. Partially unfolded states provide clues for understanding folding and misfolding. NMR studies of the SH3 module of P13 kinase have shown that at low pH, where the protein is at least partially unfolded, the solution turns into a viscous gel after several hours [17]. Electron microscopy showed this gel to contain well-defined fibrils as seen in amyloid diseases like Alzheimer's disease, Parkinson's disease, Mad Cow Disease (thus there is a role for partially unfolded proteins in prion disease), Huntington's disease, Rheumatoid arthritis, Aortic medial amyloid, Atherosclerosis, Cardiac arrhythmias and

many more [18]. Partially unfolded states have been closely associated with performing various vital metabolic processes, which include binding of enzymes to substrate, transfer of ions and metals, electron transfer reactions, and various catabolic and anabolic processes in biological systems. It is also known that partially unfolded and/or molten-globule like states play an important role *in vitro*, in particular for photoreceptor-mediated signaling [19]. Studies have shown that partially unfolded proteins efficiently penetrate cell membranes which can be used for oral drug delivery [20].

## 1.2 Cytochrome *c*

Cytochrome *c* (cyt *c*) provides a unique opportunity to study protein folding mechanisms. One can study the early mechanism of folding from the denatured state or the partially folded state [21] and also the late stages of formation of the native state, i.e., the partially unfolded state [22-24].

Cyt *c* is a 12-13 kDa protein encoded by a nuclear gene. It normally resides in the space within the lumen of the cristae of the inner mitochondrial membrane (IMM). On the surface of the inner mitochondrial membrane, cyt *c* participates in the mitochondrial electron transport chain, using its heme group as a redox intermediate to shuttle electrons between cytochrome *c* oxido-reductase (Complex III) and Cytochrome *c* oxidase (Complex IV) (figure 1.5). Ubiquinone (Q) acts as a carrier in transfer of electrons from NADH dehydrogenase complex (complex II) to complex III. The transfer of electrons yields a highly exergonic reaction which is used to pump protons out of the mitochondrial matrix. This generates the membrane potential across the IMM and electrochemical energy, in the form of a proton motive force. The proton motive force then drives the

synthesis of ATP (energy currency of intracellular processes) as protons flow passively back into the mitochondrial matrix through a proton pore that is associated with ATP synthase.

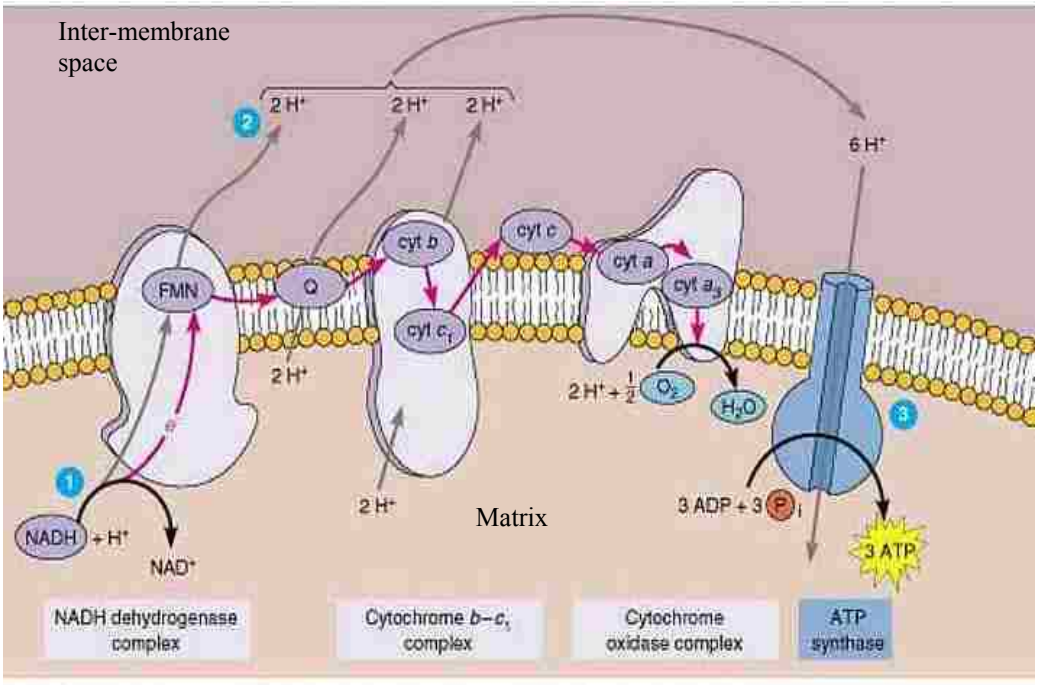


**Figure 1.5** A schematic of the electron transport chain occurring in the inner mitochondrial membrane. Figure extracted from the website, http://www.columbia.edu/cu/biology/courses/c2005/handouts/etccomplexes.jpg

The role of cytochrome *c* in the electron transfer mechanism both in aerobic and anaerobic respiration is long known, but its function goes beyond this process which is often referred to as cellular respiration and is considered its life supporting function. One of the minor but interesting roles of cytochrome *c* in eukaryotes is in the pathway of hydrogen peroxide scavenging. Cytochrome *c* is also widespread in the bacterial world, where it takes part in biochemical processes such as respiration and $H_2O_2$ scavenging, as

well as in a number of other pathways. Cytochome *c* in the presence of $H_2O_2$ is also known to cause tyrosine dependent *in vitro* peroxidative aggregation of proteins [25]. In particular, it is sometimes fused to redox enzymes and constitutes an entry and exit point for electrons in the catalytic cycle of the enzyme [26].

Research studies from the last 10 to 15 years have shown the important role of cytochrome *c* in apoptosis [27]. Apoptosis, also referred to as programmed cell death, is crucial for life in that it eliminates unwanted cells and is vital for embryonic development, homeostasis and immune defense. Deregulation of this process can lead to disease or death. There are extrinsic and intrinsic pathways for this process. The extrinsic pathway is initiated by the engagement of a trans-membrane death receptor by an extracellular ligand. This interaction leads to assembly of the death indicating signaling complex (DISC) as shown in figure 1.6b.

The intrinsic pathway is also known as the mitochondrial pathway. This is activated by apoptotic stimuli, which lead to the permeabilization of the outer mitochondrial membrane and release of cytochrome *c* from the intermembrane space of mitochondria as shown in figure 1.6b. Cytochrome *c* regulates caspase activity and thus induction of apoptosis [27].

Cytochromes were first discovered by Charles A. MacMunn (1886) [28] and re-discovered by David Keilin (1926) [29-31] who also identified their function in cell respiration. Since then this has been an extremely popular protein. More than 84,300 articles can be found on Scifinder Scholar with the word cytochrome *c* either in the title or abstract. Out of these, 36,727 articles were published between the years 1999 and March 2009.

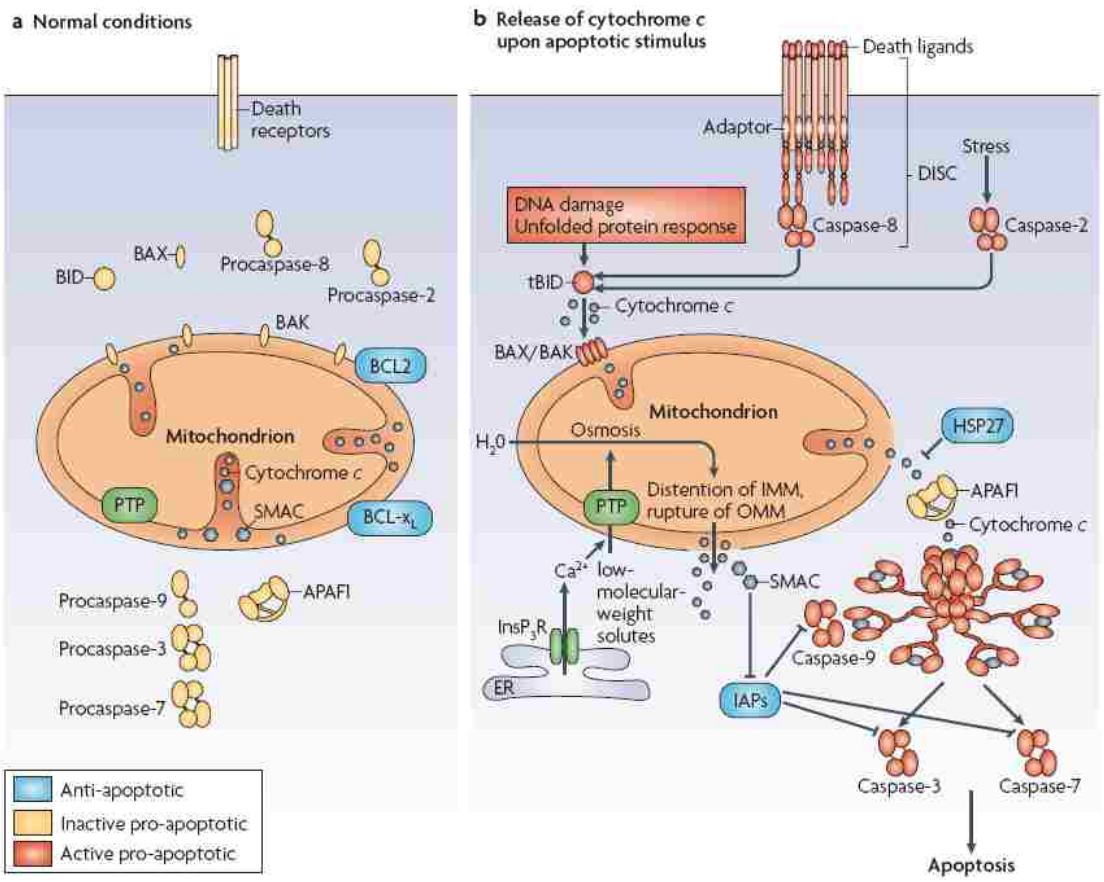


**Figure 1.6** Release of cytochrome *c* and its downstream effects during apoptosis. This figure is taken from reference [27].

Some of the reasons for the widespread popularity of cytochrome *c* are as follows: (i) it is small, stable, monomeric, possesses a single tryptophan residue, a heme moiety and it can reversibly withstand extreme conditions; (ii) it is easy to express in bacteria and yeast and its purification procedure is straightforward via cation exchange chromatography; (iii) it can be obtained in large amounts in pure form and dissolves at high concentrations, which has made it popular for various spectroscopic techniques like EPR, NMR, fluorescence, EXAFS, Mössbauer, and resonance Raman; (iv) it is widely distributed from prokaryotes to eukaryotes providing a large resource to study the differences due to structural variations; (v) early determination of its amino acid sequence

made it a prime object for studies of protein evolution and the relation between phylogeny and protein primary structure [32]; (vi) and it can be easily modified and since it is a very well-studied protein it is ideal for use with new techniques like single molecule studies [33].

It is of historical interest that cytochrome *c* was prepared from bakers yeast and fundamental properties were established related to this protein between 1930 and 1935 [31, 34]. Iso-1-cytochrome *c* was the major fraction obtained from chromatographic separation containing approximately 95% of the total complement of cytochrome *c* in yeast [35]. Iso-1-cytochrome *c* is a small protein (MW = 12,710 D for the naturally occurring sequence). It contains 108 amino acid residues in a single polypeptide chain and the fold of the protein consists of α-helical and loop structures. According to R.P. Ambler's classification of *c*-type cytochromes in 1991 [36, 37], iso-1-cytochrome *c* (iso-1-cyt *c*) belongs to Class I of type *c* cytochrome.

Class I cytochromes *c* include the low spin soluble cytochrome *c* found in mitochondria and in bacteria. The heme attachment site is towards the N-terminus, and the sixth ligand is provided by a methionine residue which is situated about 40 residues further on towards the C-terminus. The protein contains three conserved core helices (blue color N and C helix, and, green color 60's-helix in figure 1.7) which form a basket around the heme group with one heme edge exposed to the solvent [38].

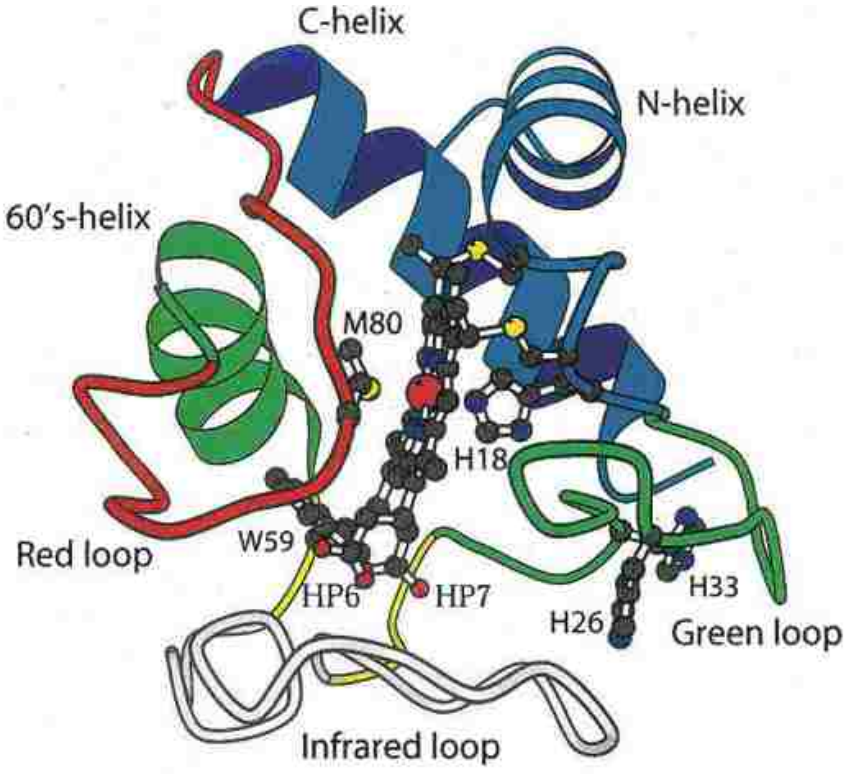


**Figure 1.7** The cooperative units in horse heart cytochrome *c*. The five foldons in decreasing order of stability are, the Blue unit (N and C-terminal helices), the Green unit (60's helix and 20's-30's Ω loop), the outer yellow neck (a short anti-parallel β-sheet; residues 37-39, 58-61), the Red unit (71-85 Ω loop) and the Infrared or N-yellow Ω loop (shown in gray, residues 40-57). The outer Yellow neck and the N-yellow Ω loop constitute the Yellow unit (residues 37-61). Figure is taken from *ref* [39].

The two original vinyl groups of the heme are converted into thioether bonds (figure 1.8) following the addition of thiol sulfurs from two cysteines of a CXXCH motif within the protein to the α-carbons of the heme vinyls [40]. The presence of heme gives a strong characteristic α/β band near 550 nm. An absorbance band in the spectroscopic region from 390-430 nm, which is also known as the heme Soret band, provides information about the heme environment. Both these bands are due to $\pi \rightarrow \pi^*$ transitions [41].

**Figure 1.8** Structure of heme. A schematic representation of the atomic skeleton of the heme group of cytochrome *c*. Iron is coordinated with the four pyrrole rings that form the porphyrin ring. Cys 14 and Cys 17 form thioether bonds to the heme. Positions are labeled using the Fischer system of nomenclature.

In iso-1-cyt *c* used in this study, two cysteines are present at positions 14 and 17 and the fifth ligand for the iron in the porphyrin ring is provided by His18, (see figure 1.7 for analogous heme ligation in horse cyt *c*). Heme synthesis is completed through the action of ferrochelatase in the mitochondrial matrix. Cytochrome *c* is first formed as apocytochrome *c*, which is produced by translation and co-translational modification in the cytosol. Apocytochrome *c* is then translocated to the mitochondrial intermembrane space where the heme moiety is covalently attached by cytochrome *c* heme lyase. Heme lyase, encoded by the *CYC3* gene, is considered to act like a chaperone or as a catalyst, although its role is still not clear for the formation of bond between the thiols of the cysteines and the vinyl groups of heme. Heme attachment causes the partially extended conformation of apocytochrome *c* to become the fully folded holocytochrome *c*.

The structure of horse cyt *c* is shown in figure 1.7. Horse cyt *c* is composed of five cooperative folding units. The folding units from order of stability from most to least stable are, blue, N and C helices; green, 60's helix and loop; yellow; red, Ω-loop; and infrared, Ω-loop [39]. Recent studies from Englander's lab with horse heart cytochrome *c* have shown branching in this sequential folding pathway as shown in figure 1.9. According to this study, either the infrared or red loop can unfold first followed by the yellow loop, then branching can take place again with either the green loop or green helix unfolding and finally unfolding of the most stable blue helices takes place [42].

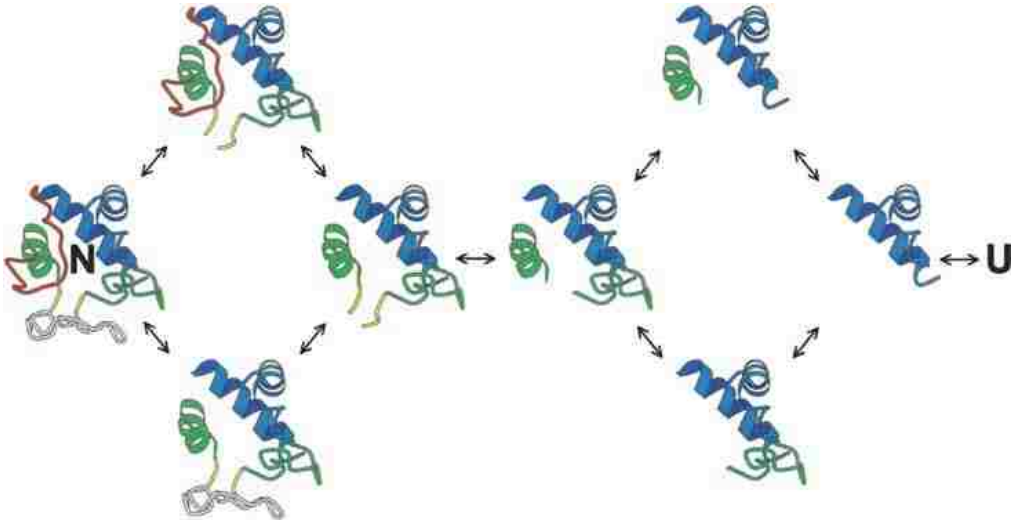


**Figure 1.9** Sequential unfolding and refolding pathway of Cyt *c*. Pathway steps are determined by the intrinsically cooperative protein foldons. The pathway order is determined by the sequential stabilization mechanism in which previously formed structure templates the formation of and stabilizes subsequent foldons, all in the native context, to progressively build the target native structure. This figure is taken from reference [42].

## 1.3 Alkaline Conformational Transition

Theorell and Åkesson in 1941 [43] observed five distinct electronic spectra for ferricytochrome *c* over the pH range 0 to 14. These five spectral states displayed by oxidized protein were linked by protonation events corresponding to four distinct p*K*

values. The reduced protein has three states linked by two deprotonation steps. These results are summarized in figure 1.10 [44]. In the case of ferrocytochrome *c*, state III (figure 1.10), which appears at alkaline pH is unfolded. No stable intermediate is known to appear in between the folded and unfolded state.

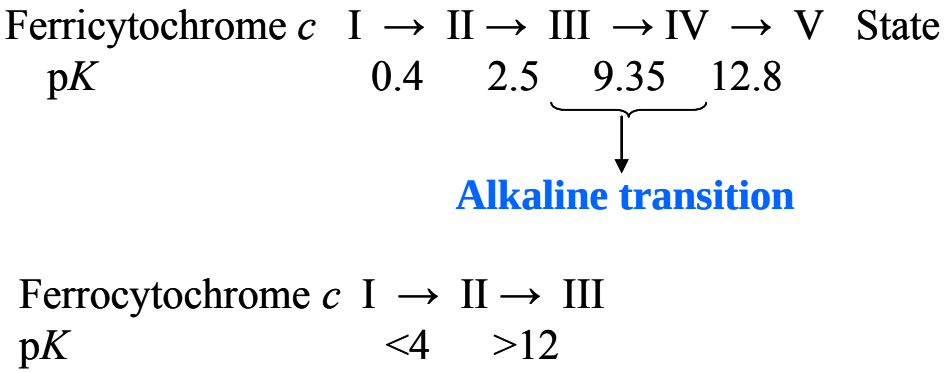


**Figure 1.10** Summarized spectral states for reduced and oxidized cytochrome *c* observed by Theorell and Åkesson [43].

Ferrocytochrome *c* is likely to be present in the reductive intracellular milieu after post-translational modification but most of the studies have been done on the oxidized form of cytochrome *c*, i.e., ferricytochrome *c*. The redox potential of ferrocytochrome *c* is -164 mV in the unfolded state and that for the folded form is 254 mV. As a result, reduced heme is extremely susceptible to oxidation by molecular oxygen dissolved in solution. Thus, studies on ferrocytochrome *c* must be done in degassed solutions containing an excess of sodium dithionite. This requirement of a highly basic environment to unfold ferrocytochrome *c*, (p*K* >12), and the need to work under anaerobic conditions makes experimental studies very difficult with ferrocytochrome *c* [45].

State III in ferricytochrome *c* dominates near neutral pH and is regarded as the native conformation of the protein. This state gives a characteristic spectroscopic band at 695 nm in the visible region which is due to methionine 80 bound to heme. This band is due to a ligand-to-metal (Fe) charge transfer band with very low extinction coefficient ~0.7 $mM^{-1}$ $cm^{-1}$ [46]. The biological role of State V, the unfolded state of the protein, is still not clear. State IV is referred to as the alkaline state. In state IV, Met 80 is replaced by one of the many lysine residues present on the surface of the protein. There are 16 lysine residues in iso-1-cyt *c* from yeast. Out of these, lysine at positions 73, 79, 86, 87 and 88 were proposed as possible ligands, as shown in figure 1.11 [47].

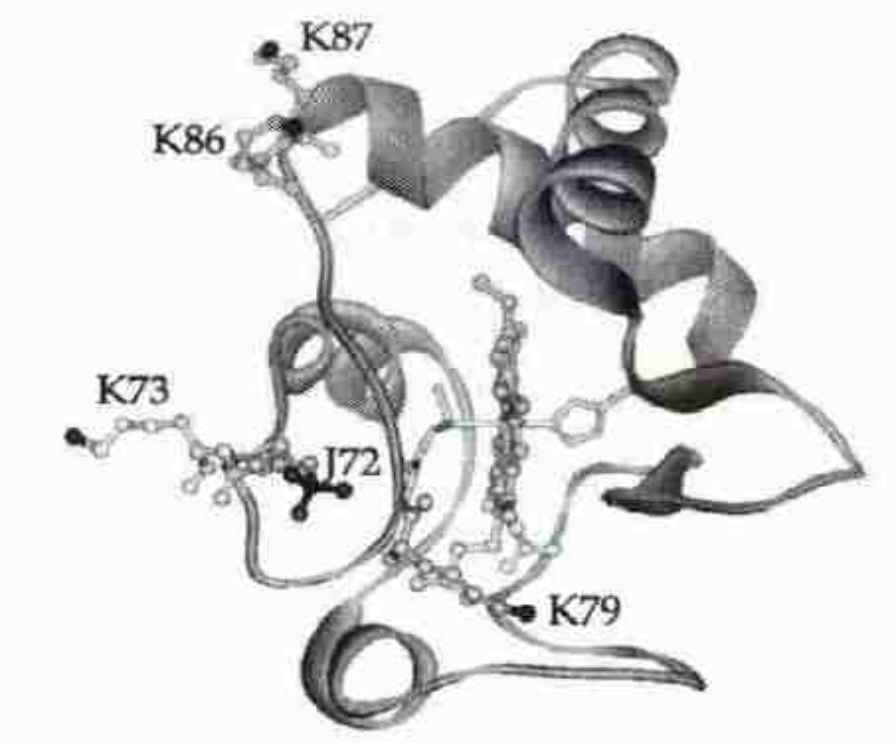


**Figure 1.11** This figure is taken from reference 47, showing the crystal structure of oxidized iso-1-cytochrome *c*, with lysine residues as the possible ligands to participate in the alkaline transition [47].

But $^{1}$H NMR and EPR studies established the lysines at position 73 and 79 as the ligands replacing Met 80 as shown in figure 1.12. Lysine 72 is trimethylated in yeast cytochrome *c* but not in bacteria or mammalian cytochrome *c* [48].

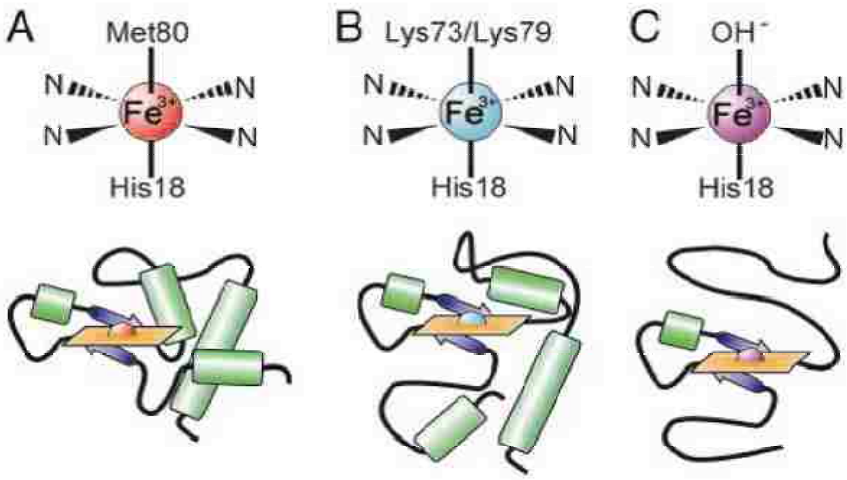


**Figure 1.12** Heme ligation schemes (upper) and structural models (lower) for ferricytochrome *c* state III (A) as shown in figure 1.9 with Methionine 80 bound heme, state IV, the alkaline state (B) Lys73/Lys79 bound form, and state V, unfolded form (C). Two possible conformers exist as either of Lys 73 or 79 can act as the sixth axial heme ligand in the alkaline state. Heme is shown as a yellow square with iron in the center, helices are shown as green bundles, beta sheets are shown as blue arrows and loops are shown in black. This figure is taken from *ref* [33].

These lysines are present in the red loop of iso-1-cyt *c* (the 70-85 or Ω-loop D as shown in figures 1.7 and 1.11). This Ω-loop D participates in the first step of unfolding of iso-1-cyt *c* (as shown in figure 1.9). As a result, this base induced conformational transition represents a partially unfolded state of iso-1-cyt *c* that can serve as a model for a late folding intermediate [23]. This transition is coupled to a large redox potential change [49]. Thus, for mitochondrial cytochrome *c*, state IV is proposed to have a functional role in the control of the electron transfer pathway and hence in energy transduction [47, 50-54]. Other than high pH, high temperature, exposure of the protein at neutral pH to the action of protein denaturants (urea, guanidine hydrochloride) and other

choatropic agents (lithium perchlorate) can also induce this conformational change [44]. These alkaline forms are also considered to play a role in apoptosis [55].

Studies have been done to understand the alkaline conformational transition in other labs by mutating lysines in the Ω-loop to alanine [48, 56-60] and in our lab by mutating these lysines to histidine [23, 61-63]. Previous studies with a Lys 73→ His (K73H) variant of iso-1-cyt *c* suggest that histidine is the ligand bound to heme near neutral and mildly acidic pH (pH 6-8) and lysine the ligand bound to heme at more alkaline pH (pH 8-11) [23, 61]. This can be represented as shown in figure 1.13:

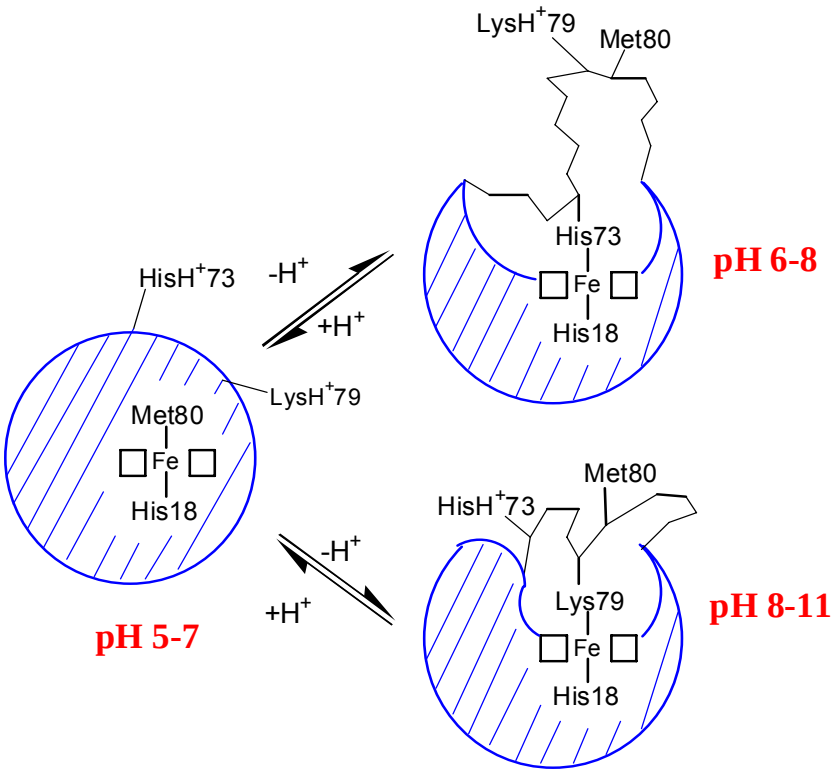


**Figure 1.13** schematic representations of the ligands replacing Met 80 in the alkaline conformational transition of the K73H variant of iso-1-cyt *c*. The Met 80-heme bound form is the native state, the His73-heme bound form and the Lys79-heme bound form are alkaline conformers at lower and higher alkaline pH, respectively. Figure is adapted from [64].

## 1.4 Electron Transfer

Electron transfer (ET) is the process by which an electron moves from one atom or molecule to another atom or molecule; one being oxidized and the other reduced, as shown in figure 1.13. A* represents the reduced form and B represents the oxidized form. Transfer of an electron leads to the generation of $A^+$ (electron deficient species) and $B^-$ (electron rich species).

$$A_{red} + B_{ox} \longrightarrow A_{ox} + B_{red}$$

**Figure 1.14** Representation of the change of state before and after an electron transfer reaction.

Initial studies on ET started after World War II because of the availability of radioactive isotopes, which permitted studies on isotopic exchange reactions in aqueous solution. Numerous ET experiments have been carried out since then in other areas like solar energy conversion semiconductors, electrochemistry, chemiluminescence, etc.

ET reactions are integral to biological processes like oxygen binding and/or transport, photosynthesis or respiration, metabolic syntheses, and detoxification of reactive species. ET reactions commonly involve transition metal complexes, but there are now many examples of ET in organic molecules. This involvement of ET reactions in various fields led to the development of theory and experiment to better understand the chemical and biological systems around us. Rudolph Marcus received the Nobel Prize in Chemistry in 1992 for his semi-classical electron transfer theory. This theory is used in various aspects of chemistry and biology, including photosynthesis, corrosion, etc., and is

considered as the dominant theory for understanding ET chemistry. The basic equation for Marcus theory [65] is:

Equation 1.1
$$k_{ET} = \frac{2\pi}{\hbar} H_{AB}^2 \frac{1}{\sqrt{4\pi k_b T}} \exp\left( \frac{-\left(\lambda + \Delta G^{\circ}\right)^2}{4\lambda k_b T} \right)$$

where $k_{ET}$ is the rate of electron transfer, $H_{AB}$ is the electronic coupling between the initial and final states, $\lambda$ is the reorganization energy between the product and the reactant states at the equilibrium nuclear configuration of the reactant (i.e., the minimum free energy), $\Delta G^{\circ}$ is the total Gibbs free energy change for the electron transfer reaction, $k_b$ is the Boltzmann constant, $\hbar$ is Plank's constant divided by $2\pi$ and $T$ is the temperature of the reaction.

$H_{AB}$, also referred to as the tunneling matrix element, is a measure of the electronic coupling between the donor and the acceptor at the transition state. Its magnitude depends upon donor-acceptor separation, orientation, and the nature of the medium where this reaction is to take place. In simple models, the electronic-coupling strength is predicted to decay exponentially with increasing donor-acceptor separation [65, 66].

The reorganization energy, $\lambda$, contains both inner and outer sphere components. As can be seen in eq 1.1, variation in $\lambda$ can have a large impact on electron transfer rates. The inner sphere reorganization energy ($\lambda_i$) is the free energy change associated with changes in the bond lengths and angles of the reactants. The outer sphere reorganization energy ($\lambda_o$) includes contributions from the size of the reactants, the separation distance between the reactants and changes in the polarization of solvent molecules during electron transfer (taking into consideration the dielectric constant and the refractive index

of the medium). The response of $\lambda_o$ to solvent polarity suggests that metalloenzymes that contain buried redox cofactors need not experience large outer sphere reorganization energies [67].

The $\Delta G^{\circ}$ for ET reactions depends on the electrochemical potential of the system ($E^{o}$). The change in the free energy of electron transfer, $\Delta G^{\circ}$ (in eq 1.1), can be related with the electro potential of the system through the Nernst equation (equation 1.2).

Equation 1.2 $$\Delta G = -nFE$$

where n is the number of moles of electrons associated with the oxidation/reduction process, $F$ is the Faraday constant and $E$ is the electrode potential of the system which in turn is related to the standard electrode potential as given in Equation 1.3,

Equation 1.3 $$E = E^{\circ} + \frac{RT}{nF} \ln K$$

where $K$ is the equilibrium constant of the oxidation-reduction reaction, $R$ is the gas constant, $E^{o}$ is the standard cell potential which is referenced to the standard hydrogen electrode potential (NHE).

Factors that influence $E^{o}$ include ligands for metal cofactors, protein imposed constraints on organic cofactor conformation or metal ligation geometry, hydrogen bonding around the cofactor, the presence of water, hydrophobicity and electrostatic effects [68].

As all these above parameters can be determined experimentally, studies on ET can provide the insight to understand and solve some of the mechanistic problems related to drug delivery, collagen synthesis, steroid metabolism, immune response, drug activation, neurotransmitter metabolism, nitrogen fixation, respiration, and photosynthesis.

In biological systems the role of conformational changes has been recognized as an important factor in controlling ET reactions. Studies with these systems have led to development of kinetic models by Victor L. Davidson [50, 51] for inter-protein and intra-protein ET reactions. These reaction models can be summarized as follows:

**Inter-protein ET:**

$$A_{ox} + B_{red} \underset{}{\overset{K_a}{\rightleftharpoons}} A_{ox}/B_{red} \underset{k_{-x}}{\overset{k_x}{\rightleftharpoons}} [A_{ox}/B_{red}]^* \underset{k_{-ET}}{\overset{k_{ET}}{\rightleftharpoons}} A_{red}/B_{ox}$$

**Intra-protein ET:**

$$A_{ox}\text{-}B_{red} \underset{k_{-x}}{\overset{k_x}{\rightleftharpoons}} [A_{ox}\text{-}B_{red}]^* \underset{k_{-ET}}{\overset{k_{ET}}{\rightleftharpoons}} A_{red}\text{-}B_{ox}$$

True ET: $k_{ET} << k_x$ and $k_x / k_{-x} >> 1$; $k_{obs} = k_{ET}$

Gated ET: $k_x << k_{ET}$; $k_{obs} = k_x$

Coupled ET: $k_{ET} << k_x$ and $k_x / k_{-x} << 1$; $k_{obs} = K_x^* k_{ET}$

where $K_a$ is the association constant, $k_x$ and $k_{-x}$ are the rate constants for the gating step or the conformational change preceding the electron transfer and $k_{ET}$ and $k_{-ET}$ are the forward and backward rate constants for electron transfer.

In Davidson's models for both inter and intra-protein ET reactions, the donor and acceptor species have to be conformationally reorganized to attain optimal geometry for the efficient transfer of the electron, which is represented by the middle part of the equations. Three conditions highlighted from these equations are based on the limiting rate constants. A reaction is considered to be a True ET reaction when $k_{ET}$ is rate limiting, $k_{-ET}$, backward flow of the electron is negligible and the forward rate constant for the conformational change is dominant over that for the backward reaction.

When the forward rate constant of the conformational change is rate limiting and the backward conformational rate constant is small compared to ET, the conformational change has to take place before ET. This condition is referred as Gated ET. But when forward and backward conformational rate constants are rapid compared to ET, then ET is dependent on both $k_x$ and $k_{-x}$. This situation is referred to as Coupled ET [50, 51].

Understanding the conformational dependence of ET in ferricytochrome *c* is of interest for several reasons. Firstly, various proteins like plastocyanin [69], growth hormones [70] and influenza virus hemagglutinin [71] have been recognized to exhibit pH linked conformational diversity. Ferricytochrome *c* is an excellent model for such systems and a variety of spectroscopic techniques can be applied for characterization of the mechanism of its conformational change. Secondly, the structure of cytochrome *c* changes with pH and also leads to a change in the functional properties of the protein as mentioned earlier. Native cytochrome *c* has a redox potential of 262 mV vs NHE and that of a His-heme conformer of iso-1-cyt *c* has been found to be 41 mV when methionine at position 80 is mutated to histidine [49]. For these reasons, the inter-conversion of native and His-heme alkaline cytochrome *c* can act as an efficient switch that has a dramatic effect on the activity of the protein electron transfer reaction. Thirdly pH-linked conformational changes of cytochrome *c* have shown local structural changes in the heme pocket as well as global changes to the protein matrix. Lastly magnetic circular dichroic (MCD) and circular dichroic (CD) studies have provided evidence that the structural changes occurring at high pH may be related to those associated with the electron transfer process of cytochrome *c* in complex with its natural partners [72].

Based on these studies, a scheme for conformationally gated electron transfer was proposed for iso-1-cyt *c* by the Bowler lab as shown in figure 1.14 [73]. According to this scheme, either electron transfer can take place before the conformational change (Path A) or the conformational change can precede the ET reaction (Path B).

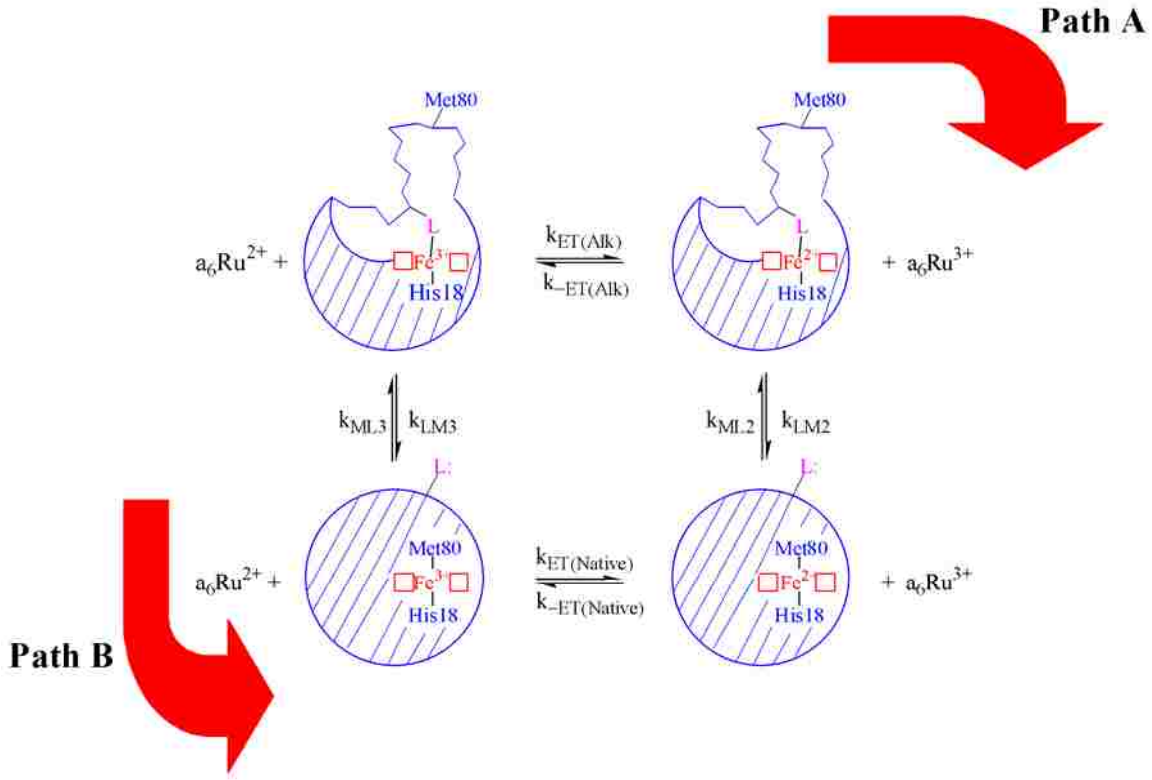


**Figure 1.15** ET square scheme for the reaction of oxidized iso-1-cyt *c* with hexaammineruthenium(II) ($a_6Ru^{2+}$). Horizontal equilibria represent ET, and vertical equilibria are conformational changes. The oxidized and reduced alkaline conformers of iso-1-cyt *c* are shown in the upper row of the ET square scheme. The alkaline state iron ligand is shown as L, The oxidized and reduced native conformers of iso-1-cyt *c* are shown in the lower row of the ET square scheme. The rate constants controlling the conformational change in the oxidized ($Fe^{3+}$) state of iso-1-cyt *c* are $k_{LM3}$ and $k_{ML3}$ and in the reduced ($Fe^{2+}$) state of iso-1-cyt *c* are $k_{LM2}$ and $k_{ML2}$. The rate constants controlling ET in the alkaline state are $k_{ET(Alk)}$ and $k_{-ET(Alk)}$ and in the native state are $k_{ET(Native)}$ and $k_{-ET(Native)}$. Path B is expected to be dominant for the reaction of the oxidized alkaline state of iso-1-cyt *c* with $a_6Ru^{2+}$. Therefore, gated ET will be controlled by the rate constant $k_{LM3}$ and direct ET by the rate constant $k_{ET(Native)}$. This figure is taken from *ref* [73].

Since the alkaline conformer requires strong reductants to be reduced, Path B involving conformationally gated ET reaction is favored for iso-1-cyt *c*. In this scheme, reduced hexaaminеruthenium is used as an electron donor. For this reaction, a stopped flow apparatus can be used to follow the kinetics. The difference in molar extinction coefficient of oxidized and reduced cytochrome *c* is ~18.5 x $10^3$ at 550 nm [74]. As a result, an increase in absorbance is observed (figure 1.15) in these ET kinetic experiments at 550 nm. Using known concentrations of reduced ruthenium and the alkaline conformer of cytochrome *c* one can determine the rate of electron transfer, and the forward and backward rates of the conformational change.

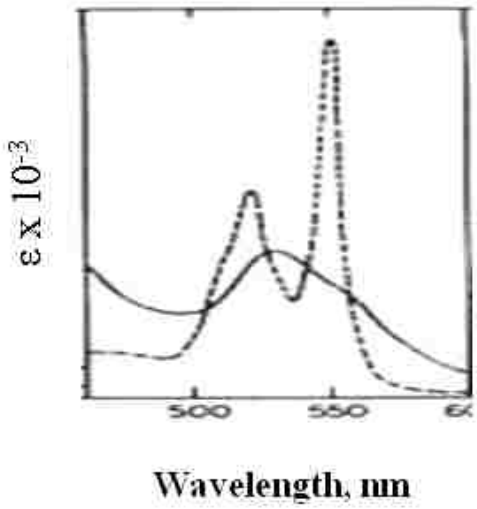


**Figure 1.16** Electronic absorption spectra of Horse cytochrome *c* at pH 7.0. Solid line is for oxidized cytochrome *c* and dashed line is for reduced cytochrome *c*. This figure is taken from *ref* [41].

## 1.5 Goals of Thesis

1. Lys73 and Lys79 have been identified as the ligands replacing Met80 in the alkaline state of yeast iso-1-cytochrome *c*. The alkaline transition kinetics of a

Lys73→His (K73H) variant of iso-1-cytochrome *c* have been found to be triggered by three ionizable groups [61]. The goal for the project described in Chapter 2 is to probe the mechanism of the alkaline conformational transition and its effect on the dynamics of gated electron transfer reactions with a Lys 79→ His variant of iso-1-cyt *c*. In particular, it is of interest to understand how the position and nature of the alkaline state ligand affects the dynamics of the conformational change. The main focus is on the effect of this mutation on stability, the number of ionizable groups triggering the alkaline transition, the rate of formation of this conformer and the rate of electron transfer.

2. The goal for the project described in Chapter 3 is to probe the bottom of a folding funnel using conformationally gated ET reactions with the AcH73 variant of iso-1-cyt *c*. The AcH73 variant lacks a naturally-occurring hydrogen bond between the green and the infrared loops, which stabilizes the protein [75]. This less stable AcH73 variant is compared with the more stable K73H variant in this study. The main point of emphasis in this study is to see how stability can affect the dynamics of a late folding intermediate as modeled by the alkaline conformer. In this study, thermodynamic and kinetic studies are undertaken to understand the mechanism of partial unfolding. For this study, ET reactions are used as a tool to gain insight into the complexities of a folding mechanism using hexaaminеruthenium(II) chloride and the oxidized Ac73H variant of iso-1-cyt *c*.

3. Studies done on an A79H73 variant (K73H, K79A, C102S) of iso-1-cyt *c* [62] in the Bowler lab have shown the presence of a slow phase on the time scale relevant to proline isomerization during the alkaline transition. The goal for the project described in Chapter 4 is to gain insight into the effect of pH on proline isomerization. This study mainly focuses on the determination of the change in the kinetics of this slowest phase using ET reactions with hexaammineruthenium(II) chloride over a pH range of 5 to 9.5.

4. The goal of the project described in Chapter 5 is to vary the position of a histidine alkaline state ligand in the red loop of iso-1-cyt *c*, beyond the naturally-occurring positions (73 and 79) used for the alkaline state. We thus probe more broadly the effect of ligand position in the loop on the dynamics of the alkaline transition. These studies also probe the role of proline at position 76 in the alkaline transition. Besides hexaammineruthenium(II) chloride, we also test the ability of tris(terpyridyl)Cobalt(II) to probe slower conformational dynamics.

5. The goal for the project described in Chapter 6 deals with intraprotein ET by flash photolysis using ruthenium bipyridine complexes to initiate ET. For this project mutations were designed based on the efficiency expected for ET reactions from the protein surface to the heme. The results in this chapter are preliminary and focus on expression of variants in both yeast and bacteria and measurement of their stabilities by guanidine hydrochloride denaturation.

# CHAPTER 2

## *THE ALKALINE CONFORMATIONAL TRANSITION AND GATED ELECTRON TRANSFER WITH A LYS 79 → HIS VARIANT OF ISO-1-CYTOCHROME C*

### 2.1 Introduction

Iso-1-cytochrome *c* from yeast is an electron transfer protein with a covalently-bound heme. It is a class I cytochrome *c* which includes low spin soluble cytochrome *c* of mitochondria and bacteria with the CXXCH heme attachment site towards the N-terminus and the 6$^{th}$ ligand provided by a methionine located near the C-terminus [76]. Cytochrome *c* undergoes a base induced conformational transition, commonly called the alkaline transition. This transition is characterized by the loss of the heme-Met 80 ligation of the native state of the protein [44]. Due to the small difference in the enthalpy of the fully folded and this partially unfolded state (alkaline conformational transition), cyt *c* has been used as a model to understand late folding intermediates [23, 39, 77].

Lys73 and Lys79 have been identified as the ligands replacing Met80 in the alkaline state of yeast iso-1-cyt *c* [48, 60], although for iso-1-cyt *c* expressed in *Escherichia coli*, Lys72 is not trimethylated, and it becomes an important ligand in the alkaline state [56, 57]. For the Lys73-heme alkaline conformer, NMR structural data is available [58]. The alkaline state ligands have been replaced by alanine [48, 56-60] and by histidine [23, 61-63] to obtain more insight into the alkaline transition. Studies done in our lab [61, 62] have shown the alkaline transition kinetics of Lys73→His variants of iso-1-cyt *c* to be modulated by three ionizable groups. Kinetic data have provided the acid constants, p$K_H$, for the triggering groups, one of which is consistent with ionization of the histidine ligand. The identity of the two other ionizable groups affecting the

kinetics of this conformational change is more speculative [59, 61, 62]. Recent data suggest that the lysine ligand may be the triggering ionizable group for formation of lysine-heme alkaline conformers [57].

In this work, we have mutated Lys79 to His generating a K79H variant of iso-1-cyt *c* to probe how ligands at position 79 affect the alkaline transition. The histidine introduced at position 79 in this variant is located in the next to least stable surface loop (red loop, Figure 2.1) of the protein (residues 70-85 or Ω-loop D, [78, 79]), which appears to be substantially disrupted in the Lys73-heme alkaline conformer [58]. Lys79 is closer to the native state heme ligand, Met80, and thermodynamic data indicate that the structural disruption is smaller [23, 56, 63]. Figure 2.2 represents the expected behavior for this variant based on studies done previously [23, 61-63]. The specific goals for this study are firstly to find whether the Lys79→His mutation makes the alkaline conformer more or less stable than for the Lys73→His mutation [23] and secondly to determine if the kinetic mechanism involves the same number of ionizable groups [61, 62].

Conformationally-gated electron transfer (ET) reactions can regulate metabolic processes [50] and several studies have suggested a role for the alkaline state in modulating the ET dynamics of cyt *c* in the electron transport chain [47, 48, 58, 80]. Recent studies in our lab have shown the usefulness of different alkaline state ligands in modulating the dynamics of conformational gates that control cyt *c* ET reactions [73, 81]. Conformational gates operating at near neutral pH can be of biophysical importance, potentially serving as molecular switches. This serves as the third goal of this study, to correlate the thermodynamic and kinetic properties of the His79-heme alkaline state with the conformationally-gated ET reactions of K79H iso-1-cyt *c* and to determine whether

moving the position of the alkaline state ligand in Ω-loop D can modulate the dynamics of gated ET.

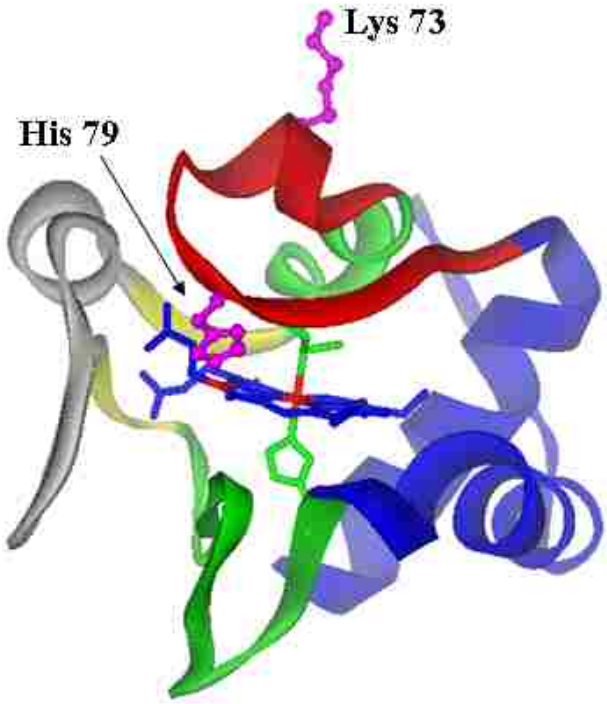


**Figure 2.1** Ribbon diagram of iso-1-cyt *c* showing the engineered histidine at position 79 in magenta. Lysine73 the other alkaline state ligand is also shown in magenta. The colors on the ribbon diagram outline the substructures of cytochrome *c* from least to most stable in the order gray, red, yellow, green and blue as defined by the native state hydrogen exchange experiments of Englander and coworkers [78, 79]. The gray and red substructures are disrupted in the alkaline form of cyt *c*.

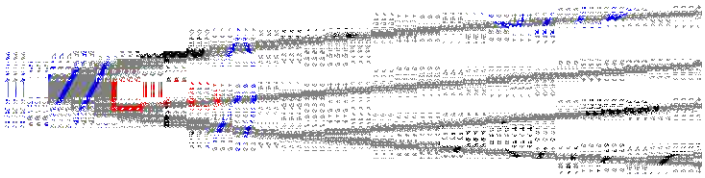

**Figure 2.2** Schematic representation of the ligands replacing Met80 in the alkaline conformational transition of K79H iso-1-cyt *c*.

## 2.2 Materials and Methods

### *2.2.1 Preparation of the K79H Variant.*

The Lys79→His mutation was introduced with the unique restriction site elimination site-directed mutagenesis method [82] using the pRS/C7.8 phagemid vector, which carries the pseudo wild type iso-1-cyt *c* gene, (pWT, C102S, prevents dimerization of iso-1-cyt *c*) as previously described [83, 84]. The pRS/C7.8 phagemid vector (figure 2.3) has two unique restriction sites *Sac* I and *Sac II* that are adjacent to each other and upstream of the iso-1-cyt *c* gene (*CYC1*, [85]).

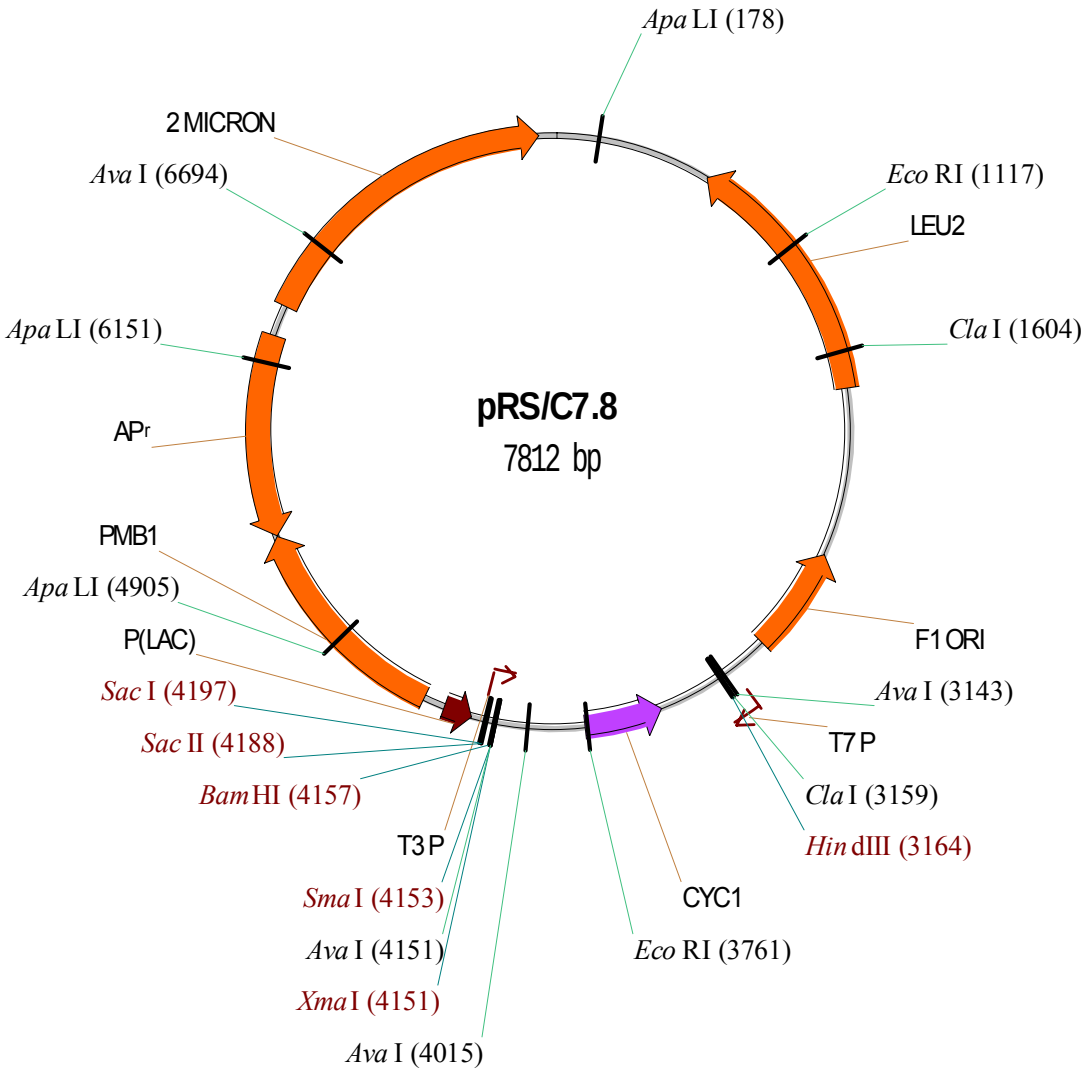


**Figure 2.3** Schematic representation of pRS/C7.8 phagemid vector used for preparation of the H79 variant of iso-1-cyt *c*. 2 Micron allows for replication as a multicopy phagemid in yeast. F1 ORI allows production of ssDNA, $Ap^r$ confers ampicillin resistance and Leu2 complements the leucine deficiency in GM-3C-2 *S. cerevisiae*.

The selection oligonucleotide $SacI^{-}II^{+}$ (5'-d(GCC ACC GCG GTG CAG CTC CAG C)-3') [84] was used to eliminate the unique *Sac* I (GAG sequence was changed to the underlined sequence in the parenthesis) restriction enzyme site upstream from the iso-1-cyt *c* gene (*CYC1, ref* [85]) and restore the *Sac* II restriction enzyme site (which is

CCG CGG). The mutagenic oligonucleotide K79H {5′-d(CAAAGGCCATGTGGGTACCAGG)-3′); site of mutation is underlined} was purchased from Operon Biotechnologies, Inc. (Huntsville, Alabama). The sequence analysis to confirm the mutation was done using a Beckman CEQ 8000 capillary electrophoresis autosequencer.

After confirming the K79H mutation, large-scale preparation of pRS/C7.8 dsDNA was carried out using a Qiagen MidiPrep kit followed by spectrophotometric quantitation ($\varepsilon_{260}$ = 6600 $M^{-1}cm^{-1}$) and restriction analysis using the *Hind*III and *Sac*II restriction enzymes to confirm the presence of the *CYC1* fragment [86]. Phagemid DNA was transformed into the GM-3C-2 strain ([87] deficient in *CYC1* gene) of *Saccharomyces cerevisiae* by the LiCl method [88].

As previously described [83], the transformants were evaluated for the functionality of the variant cyt *c*, by curing to confirm the phagemid-based expression and by phagemid recapture and re-sequencing to eliminate the possibility of further mutation under the selective conditions used to express iso-1-cyt *c*. The K79H and pWT iso-1-cytochromes *c* were isolated and purified as described previously [89-91]. Both the K79H and pWT proteins contain the C102S mutation to prevent formation of intermolecular disulfide dimers during physical studies.

### *2.2.2 Molecular Weight Determination by MALDI-TOF Mass Spectroscopy.*

The purification of the K79H protein by cation-exchange HPLC gave two small pre-peaks, one main peak (highest intensity) and 1 small post-peak. Mass spectrometry was carried out as described previously using synapic acid as matrix [59]. The main peak

gave m/z = 12,697.2 ± 2.3 (average and standard deviation of two independent spectra), consistent with the expected molecular mass of 12,687.26 g/mol for the K79H variant. All experiments were carried out with this material.

### *2.2.3 Oxidation of Protein.*

To ensure that the purified protein was fully oxidized, 5 mg of $K_3Fe(CN)_6$ per mg of protein was added and the solution was incubated at 4 °C for 1 hr. To remove oxidizing agent, it was then run through a G-25 size exclusion column pre-equilibrated with the buffer appropriate to the experiment. The concentration and degree of oxidation of the protein were determined, as described previously [83].

### *2.2.4 GdnHCl Denaturation Monitored by Circular Dichroism Spectroscopy.*

Global stability of the protein was determined by gdnHCl denaturation monitored by circular dichroism (CD) spectroscopy using an Applied Photophysics π*-180 spectrophotometer coupled to a Hamilton Microlab 500 titrator, as previously described [63]. The experiments were carried out in CD buffer (20 mM Tris, 40 mM NaCl, pH 7.5) at 25 °C. A 6 M gdnHCl stock solution was prepared in the same buffer and its concentration was determined using refractive index measurements [92]. Ellipticity was measured at 222 nm and the ellipticity at 250 nm was used as a baseline. The ellipticity measured at 222 nm as a function of gdnHCl concentration was fitted to equation 2.1 [83] which assumes a linear free energy relationship and two-state unfolding [92, 93].

**Equation 2.1**

$$\theta = \frac{\theta_N^{\circ} + \left[\left(\theta_D^{\circ} + m_D[gdnHCl]\right)\exp\left\{\frac{m[gdnHCl] - \Delta G_u^{\circ}(H_2O)}{RT}\right\}\right]}{1 + \exp\left\{\frac{m[gdnHCl] - \Delta G_u^{\circ}(H_2O)}{RT}\right\}}$$

where $\theta$ is the ellipticity of the sample, $\theta^{\circ}_N$ is the ellipticity of native protein at 0 M gdnHCl, $\theta^{\circ}_D$ is the ellipticity of denatured protein at 0 M gdnHCl, $m_D$ is the denaturant dependence of the ellipticity of the denatured state, $m$ is the gdnHCl concentration dependence of the free energy of unfolding, $\Delta G_u$, and $\Delta G^o_u$ ($H_2O$) is the free energy of unfolding extrapolated to 0 M gdnHCl. A set of four titrations were done, and the parameters were averaged.

### *2.2.5 Partial Unfolding by GdnHCl Monitored at 695 nm.*

Partial unfolding of protein was monitored at 695 nm, $A_{695}$, as a function of gdnHCl concentration using Beckman DU 640 or DU 800 spectrophotometers. This band is sensitive to the presence of Met 80-heme ligation [94]. Studies were done at pH 5 in acetate buffer (20 mM sodium acetate, 40 mM NaCl, pH 5) and pH 7.5 in CD Buffer with ~100 μM or ~200 μM protein at 25 $^{o}$C. Equal volumes of the appropriate buffer and 2x protein stocks (~200 μM or ~400 μM) protein in the appropriate buffer) were mixed to produce a 500 μL protein sample and the gdnHCl concentration was gradually increased from 0 to 2 M using previously described titration procedures [63]. Absorbance at 750 nm was used as the background wavelength to control for small variations in the baseline yielding $A_{695corr} = A_{695} - A_{750}$. The concentration of the titration solution at 0 M gdnHCl was evaluated at 570 and 580 nm using oxidized state extinction coefficients [95] and

used to convert $A_{695corr}$ to $\varepsilon_{695corr}$. Then $\varepsilon_{695corr}$ as a function of pH was fit to equation 2.2, which assumes that the dependence of $\Delta G_u$ on gdnHCl concentration is linear and that protein folding can be approximated as a two state process [92, 93].

**Equation 2.2**

$$\varepsilon_{695corr} = \frac{\varepsilon_N + \left[ \varepsilon_D * \exp\left\{ \frac{m[gdnHCl] - \Delta G_u^{\circ}(H_2O)}{RT} \right\} \right]}{1 + \exp\left\{ \frac{m[gdnHCl] - \Delta G_u^{\circ}(H_2O)}{RT} \right\}}$$

In eq 2.2, $\varepsilon_N$ and $\varepsilon_D$ are the corrected extinction coefficients at 695 nm of the Met80 bound native state and the denatured state, respectively, and other parameters are as in eq 2.1. Since the K79H variant does not appear to fully attain the native state, the change in the $\varepsilon_{695corr}$ for native versus denatured pWT iso-1-cyt *c*, $\Delta\varepsilon_{695corr} = \varepsilon_N - \varepsilon_D$, was determined using data obtained at pH 5 [96], yielding $\Delta\varepsilon_{695corr} = 0.57 \pm 0.02$ $mM^{-1}cm^{-1}$. $\Delta\varepsilon_{695corr}$ was used to constrain $\varepsilon_N$ relative to $\varepsilon_D$ when fitting data for the K79H variant.

### *2.2.6 pH Titration Experiments.*

The alkaline conformational transition for the K79H variant was monitored, as previously described [62], at 22 ± 1 °C as a function of pH in 100 mM NaCl using the 695 nm absorbance band. Briefly, the initial sample was made by mixing 500 µL of ~400 µM oxidized protein in 200 mM NaCl (2x protein in 2x buffer) with 500 µL of doubly deionized water ($ddH_2O$). The solution was mixed with a 1000 µL pipet and pH was adjusted to about 2 by adding equal amounts of 2x protein and 3 M HCl solution. The pH was measured with an Accumet AB15 pH meter (Fisher Scientific) using an Accumet semimicro calomel pH probe (Fisher Scientific Cat. No. 13-620-293). 100 mM NaCl was

used as blank. Equation 2.3 (analogous to eq 8 in *ref* [59]) based on Scheme 2.1, was used to fit the curve obtained from a plot of $\varepsilon_{695corr}$, evaluated as described above, as function of pH.

**Scheme 2.1**

$$\text{A1} \underset{}{\overset{K_{\text{obs},1}}{\rightleftharpoons}} \text{A2} \overset{K_{\text{obs},2}}{\rightleftharpoons} \text{N} \overset{K_{\text{obs},3}}{\rightleftharpoons} \text{Alk}$$

**Equation 2.3**

$$\varepsilon_{695corr} = \varepsilon_{Alk} + \frac{\left(\varepsilon_{A1} - \varepsilon_{Alk}\right) + K_{obs,1}\left\{\left(\varepsilon_{A2} - \varepsilon_{Alk}\right) + K_{obs,2}\left(\varepsilon_{N} - \varepsilon_{ALk}\right)\right\}}{1 + K_{obs,1}\left\{1 + K_{obs,2}\left(1 + K_{obs,3}\right)\right\}}$$

In eq 2.3, $\varepsilon_N$ is the corrected extinction coefficient at 695 nm of the Met80–heme bound native state, $\varepsilon_{Alk}$ is the corrected extinction coefficient at 695 nm of the alkaline state, $\varepsilon_{A1}$ and $\varepsilon_{A2}$ are the corrected extinction coefficients at 695 nm of the low pH acid state, A1, and higher pH acid state, A2. $K_{obs}$ has the form shown in eq 2.4 (see *ref* [59], equation 6) for $K_{\text{obs},1}$ and $K_{\text{obs},2}$

**Equation 2.4**

$$K_{obs} = \frac{K_C}{1 + \left(\frac{H^+}{K_H}\right)^n} = \frac{10^{-pK_C}}{\left(1 + 10^{n(pK_H - pH)}\right)}$$

where $K_C$ ($pK_C$) is the conformational equilibrium constant associated with the A1 to A2 or A2 to N conformational transitions, $n$ is the number of protons associated with each conformational transition and $K_H$ ($pK_H$) is the acid dissociation constant for the ionizable groups triggering each conformational transition. $pK_{H1}$ was arbitrarily set to 4, which assumes that an Asp or a Glu side chain triggers the A1 to A2 transition. $pK_{H2}$ was arbitrarily set to 6, which assumes a heme propionate or a histidine triggers the A2 to N transition. The value for $\varepsilon_{A2}$ - $\varepsilon_{Alk}$ was constrained empirically based on the magnitude of

$\varepsilon_{695corr}$ near pH 3.3, where there is a shift in the position of the isosbestic points during the acid transition (see figure 2.7). Since the K79H variant does not appear to fully attain the native state near neutral pH, the value for ($\varepsilon_N$ - $\varepsilon_{Alk}$) was set to 0.66 ± 0.02 $mM^{-1}cm^{-1}$ based on the pH titration data for pWT iso-1-cyt *c*. For the K79H variant, $K_{obs,3}$ in eqn. 2.5 is analogous to $K_{1,2}$(obs) from eq 16 in *ref* [23] representing the transition from the native to the alkaline state, shown in Scheme 2.2. The alkaline transition of the K79H variant yields a biphasic transition as for the K73H variant of iso-1-cyt *c* [23].

In Scheme 2.2, $T_2$ and $T_3$ are the triggering ionizable groups, which may be the same as the His79 and Lys73 ligands replacing Met80 in the alkaline conformer [57, 61, 62].

**Scheme 2.2**

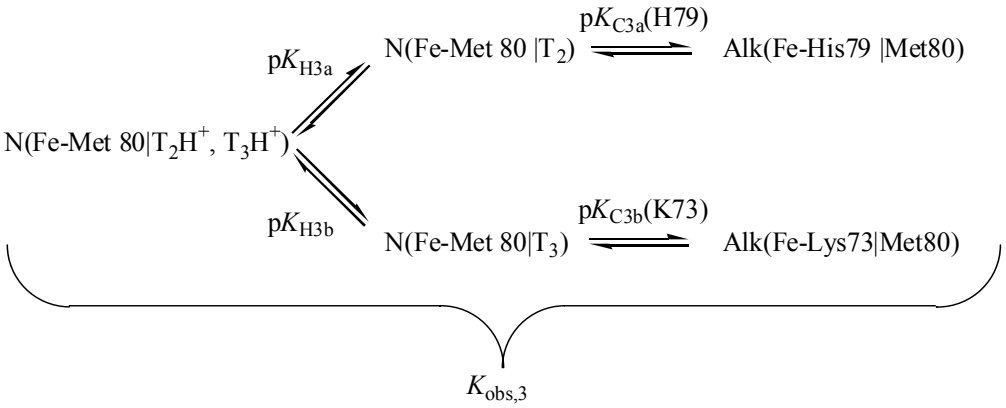


**Equation 2.5**

$$K_{obs,3} = \frac{K_{C3a}(H79)}{1+\left(\frac{[H^+]}{K_{H3a}}\right)} + \frac{K_{C3b}(K73)}{1+\left(\frac{[H^+]}{K_{H3b}}\right)} = \frac{10^{pK_{C3a}(H79)}}{1+10^{(pK_{H3a}-pH)}} + \frac{10^{-pK_{C3b}(K73)}}{1+10^{(pK_{H3b}-pH)}}$$

Equation 2.5 describes the pH dependence of $K_{obs,3}$, where $K_{C3a}$(H79) (p$K_{C3a}$(H79)) and $K_{C3b}$(K73) (p$K_{C3b}$(K73)) are the conformational equilibrium constants associated with the replacement of Met 80 with His79 or Lys73, respectively, during the alkaline transition. $K_{H3a}$ (p$K_{H3a}$) and $K_{H3b}$ (p$K_{H3b}$) are acid dissociation constants for the triggering deprotonation equilibrium constants. For curve fitting, the magnitude of p$K_{H3b}$ was set to 10.8 to be consistent with analysis reported for the K73H variant [23]. All other parameters in eq 2.5 were obtained from the fit of eq 2.3 to the data; using non-linear least squares methods (SigmaPlot, 2001).

### *2.2.7 NMR Studies.*

NMR studies on the oxidized K79H variant were done at 25 $^{o}$C, 2.5 mM protein concentration in 0.1 M NaCl $D_2O$ solution. The pH was adjusted by using 1 M NaOD or 1 M DCl. pH$^{*}$ was measured before and after each spectrum as previously described [23] and is not corrected for the solvent isotope effect. Spectra were obtained with a 500 MHz Varian Innova NMR spectrometer at the University of Colorado Health Sciences Center with 512 scans and a sweep width of 40,000 Hz. The residual HOD signal was suppressed using the pre-saturation pulse sequence.

### *2.2.8 pH Jump Stopped-Flow Experiments.*

After oxidation with ferricyanide as described above, the protein concentration was determined spectrophotometrically. The protein was then adjusted to a concentration of 20 μM and an initial pH of 5 in 0.1 M NaCl for upward pH jump experiments and an initial pH of 7.8 in 0.1 M NaCl for downward pH jump experiments. Buffers used for

controlling the final pH were 20 mM prepared in 0.1 M NaCl. Buffers used in these experiments were acetic acid (pH 5 – 5.4), MES (pH 5.6 – 6.6), $NaH_2PO_4$ (pH 6.8 – 7.6), Tris (pH 7.8 – 8.8), $H_3BO_3$ (pH 9 – 10) and CAPS (pH 10 – 11.2). Buffer pH was adjusted with HCl or NaOH. Stopped flow mixing was done using an Applied Photophysics π*-180 spectrophotometer operating in kinetics mode, as described previously [59, 61, 62]. Protein at pH 5 or 7.8 and final buffer at each specific pH were mixed in equal volumes to achieve the desired pH. The final conditions after mixing were 10 μM protein in 10 mM buffer and 0.1 M NaCl.

All pH jump experiments were carried out at 25 $^{o}$C and the conformational change from the native to alkaline state was monitored by absorption spectroscopy at 405 nm, which is the wavelength of maximum change in absorbance for the conversion of native (Met80-heme ligation) to the histidine – heme alkaline state [23, 61]. At every pH, at least 3 to 5 kinetic trials were acquired. A total of 1000 points on a logarithmic time scale were collected for each trial. Data were collected on 5 s and 50 s time scales. Each trial of upward pH-jump data was fit using single or double exponential rise to maximum equations, as appropriate, for both time ranges. Each trial of downward pH jump data was fit to a single or double exponential decay equation, as appropriate.

The $k_{obs}$ and amplitude data as a function of pH for the slow phase were fit to the usual mechanism for the alkaline conformational transition [97], a rapid protonation equilibrium followed by a conformational change, which yields equation 2.6 for $k_{obs}$ versus pH:

**Equation 2.6**

$$k_{obs} = k_b + k_f \left\{ \frac{1}{1+10^{(pK_H - pH)}} \right\}$$

where $k_{obs}$ is the observed rate constant, $k_f$ and $k_b$ are the forward and backward rate constants for the alkaline transition, respectively, and $K_H$ ($pK_H$) is the equilibrium constant for the deprotonation reaction. The pH dependence of the amplitude data was fit to eq 2.7:

**Equation 2.7**

$$\Delta A_{405} = \Delta A_{405t}\left(\frac{1}{1+\left(\frac{k_b}{k_f}\right)\left(1+10^{(pK_H-pH)}\right)}\right)$$

where $\Delta A_{405}$ is the change in amplitude at 405 nm, $\Delta A_{405t}$ is the limiting change in amplitude at high pH and other parameters are the same as described for eq 2.6. In fitting eq 2.7, $k_f$ and $k_b$ were set to the values obtained from fits of slow phase $k_{obs}$ versus pH data to eq 2.6.

The $k_{obs}$ data as a function of pH for the fast phase were fit to a mechanism for the alkaline conformational transition involving two ionizable groups (Scheme 2.3), as previously described (Supporting Information in *ref* [61]) The mechanism assumes that the ligand, L, replacing Met 80 must be deprotonated ($K_{HL}$) for the alkaline transition to occur and it yields eq 2.8 for the pH dependence of $k_{obs}$. In eq 2.8, $k_{f1}$ and $k_{b1}$ are the rate constants for the forward and backward reactions respectively, when the ionizable group, X, corresponding to $K_{H2}$ is protonated and $k_{f2}$ and $k_{b2}$ are those rate constants when that ionizable group is deprotonated. The pH dependence for the amplitude up to pH 10 was fit with eq 2.9. Eqs 2.8 and 2.9 were fitted using an iterative procedure described in the footnotes to Table 2.2

**Scheme 2.3**

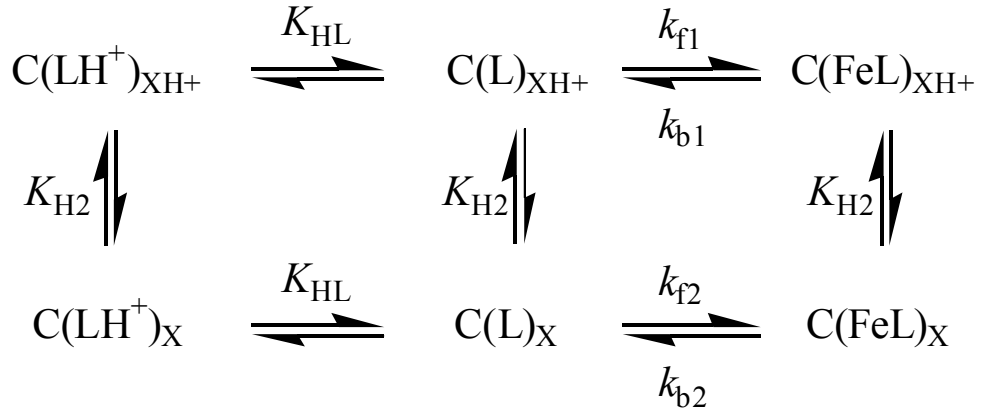


**Equation 2.8**

$$k_{obs} = \left(\frac{K_{HL}}{K_{HL} + [H^+]}\right)\left(\frac{k_{f1}[H^+] + k_{f2}K_{H2}}{K_{H2} + [H^+]}\right) + \left(\frac{k_{b1}[H^+] + k_{b2}K_{H2}}{K_{H2} + [H^+]}\right)$$

**Equation 2.9**

$$\Delta A_{405} = \Delta A_{405t}\left(\frac{1}{1 + \left(\frac{k_{b1}[H^+] + k_{b2}K_{H2}}{k_{f1}[H^+] + k_{f2}K_{H2}}\right)\left(1 + \frac{[H^+]}{K_{HL}}\right)}\right)$$

### *2.2.9 Electron Transfer Experiments by the Stopped Flow Method.*

Hexaammineruthenium(II) chloride ($a_6Ru^{2+}$) was prepared by reducing commercially available $[Ru(NH_3)_6]Cl_3$ (Strem Chemicals) with zinc by the method of Fergusson and Love [98]. Briefly, 0.5 grams of $[Ru(NH_3)_6]Cl_3$ was dissolved in 2.5 mL of ammonia solution (concentration ~15 M and density ~0.88) by stirring for a brief time. To this homogeneous solution, 0.1 grams of zinc granules were added and the solution was boiled for 3 - 4 mins. This hot solution was filtered immediately to remove excess Zn and then kept on ice for 10 to15 mins producing yellow crystals of $a_6Ru^{2+}$. The yellow

crystals were then filtered and washed with a minimum amount of cold ammonia solution. The $[Ru(NH_3)_6]Cl_2$ was dried in a vacuum dessicator which was refilled with Argon. The approximate yield obtained was 20-30%. Ruthenium metal is produced if the reduction is allowed to proceed for a longer time. The solution turns deep purple or magenta and no formation of crystals is seen if dilute ammonia is used. The product was stored at -20 °C. Formation of $a_6Ru^{2+}$ was confirmed by IR spectroscopy using the 1217 $cm^{-1}$ band which is characteristic of the Ru(II) complex [99].

The day before ET experiments syringes and the flow cell were soaked in solution of 50 μM riboflavin and 1 mM EDTA to scavenge oxygen. Experiments were done with 10 mM $NaH_2PO_4$ in 0.1 M NaCl, pH 7.5 buffer. Argon gas that was further purified with an oxy-trap column (Alltech, Inc) was used to degas all solutions for anaerobic work. Stopped-flow mixing of oxidized K79H iso-1-cyt *c* with $a_6Ru^{2+}$ was done, as described previously [81, 82].

Reduction of the heme was monitored at 550 nm. At each concentration of $a_6Ru^{2+}$, five kinetic traces were collected. For all traces, 1000 points were collected logarithmically on either a 5 sec or 50 sec time scale. Analysis of the data was done using the curve fitting program, SigmaPlot (v. 7.0). The data were fit to a double exponential rise to maximum equation for both 5 sec and 50 sec time scale data.

## 2.3 Results

### *2.3.1 Global Unfolding by GdnHCl Denaturation.*

GdnHCl denaturation monitored by CD spectroscopy was used to determine the overall stability of the K79H variant of iso-1-cyt *c* (figure 2.4). The experiments were

done at pH 7.5, so that His79 would be predominantly deprotonated. The fit to the data (eq 2.1, Materials and Methods) gives $\Delta G^{o}_{u}(H_2O)$ = 4.45 ± 0.30 kcal/mol, $m$ = 3.53 ± 0.25 kcal/(mol×M) and a titration midpoint, $C_m$ = 1.26 ± 0.01 M. These values compare well to those observed for the previously reported K73H variant of iso-1-cyt *c* ($\Delta G^{o}_{u}(H_2O)$ = 4.32 ± 0.11 kcal/mol, $m$ = 3.59 ± 0.01 kcal/(mol×M) and a titration midpoint, $C_m$ = 1.15 ± 0.01 M, see *ref* [100].

The similarity of $\Delta G^{o}_{u}(H_2O)$ and the *m*-value for these two variants indicates that the global unfolding transitions are similar in character and different from that for pWT iso-1-cyt *c* which has a much larger denaturant *m*-value ($\Delta G^{o}_{u}(H_2O)$ = 5.77 ± 0.40 kcal/mol, $m$ = 5.11 ± 0.36 kcal/(mol×M), see *ref* [101]).

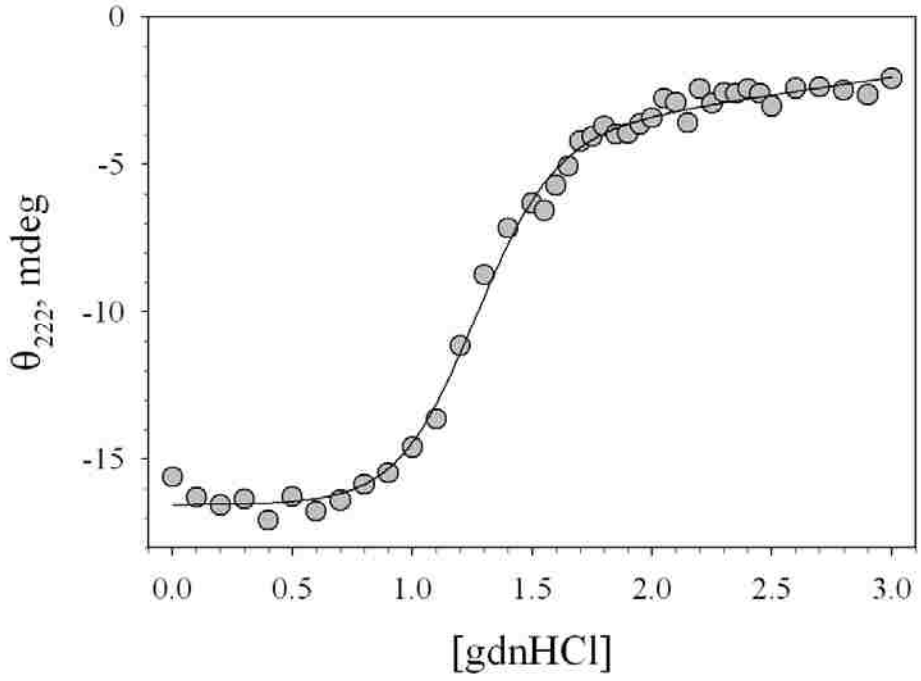


**Figure 2.4** Plot of ellipticity observed at 222 nm as a function of gdnHCl concentration for the K79H variant of iso-1-cytochrome *c*. Data were acquired at 25 ºC in 20 mM Tris, pH 7.5, 40 mM NaCl and at 4 μM protein concentration. The solid curve is a fit of the data to eq 1 in Materials and Methods.

### *2.3.2 Partial Unfolding by GdnHCl.*

The low *m*-value observed for global unfolding of the K79H variant suggests that its global unfolding transition at pH 7.5 occurs from a partially unfolded form of the protein involving His79-heme ligation, paralleling the role of His73-heme ligation in the unfolding of the K73H variant [23, 96, 100]. To test this hypothesis, partial unfolding of the K79H variant was studied at both pH 5.0 and 7.5 as a function of gdnHCl concentration by monitoring the loss of Met80-heme ligation at 695 nm. At pH 7.5, absorbance at 695 nm was very low and the titration data were too noisy to be fit to eq 2.2 (Materials and Methods).

Previous studies [23, 96, 100] have shown that the absorbance at 695 nm is maximal near pH 5 for iso-1-cyt *c* variants with a histidine at position 73, as the protein is in its fully native state. At pH 5 we find that $A_{695corr}$ decreases with increasing gdnHCl concentration, however the signal is much weaker than observed for the WT protein under the same conditions (figure 2.5) suggesting that the K79H variant is not fully native in the absence of denaturant even at pH 5. Fitting the data for this variant to eq 2.2 as described in Materials and Methods yields $\Delta G^{o}_{u}(H_2O)$ = -0.34 ± 0.06 kcal/mol and *m* = 1.0 ± 0.1 kcal/(mol×M). Thus, the maximal population of the native state by this analysis is ~35% at pH 5. The difficulty in following loss of the heme-Met80 ligation at pH 7.5 indicates that the native form of the K79H variant has much lower population at pH 7.5, even at 0 M gdnHCl. Thus, the gdnHCl unfolding data at 695 nm are consistent with global unfolding at pH 7.5 monitored by CD occurring from a partially unfolded state.

The *m*–value of ~1 kcal/(mol×M) obtained for partial unfolding at pH 5 is similar to values of 0.8-1.1 kcal/(mol×M) obtained for formation of the Lys79-heme alkaline

conformer [23, 63] and less than the *m*-value of 1.4 to 1.8 kcal/(mol×M) observed for partial unfolding mediated by His73-heme ligation [23, 63, 100]. Thus, *m*-value data are consistent with the smaller structural disruption expected when His79 (versus His 73) replaces Met80 (see figure 2.1 and *ref* [48]).

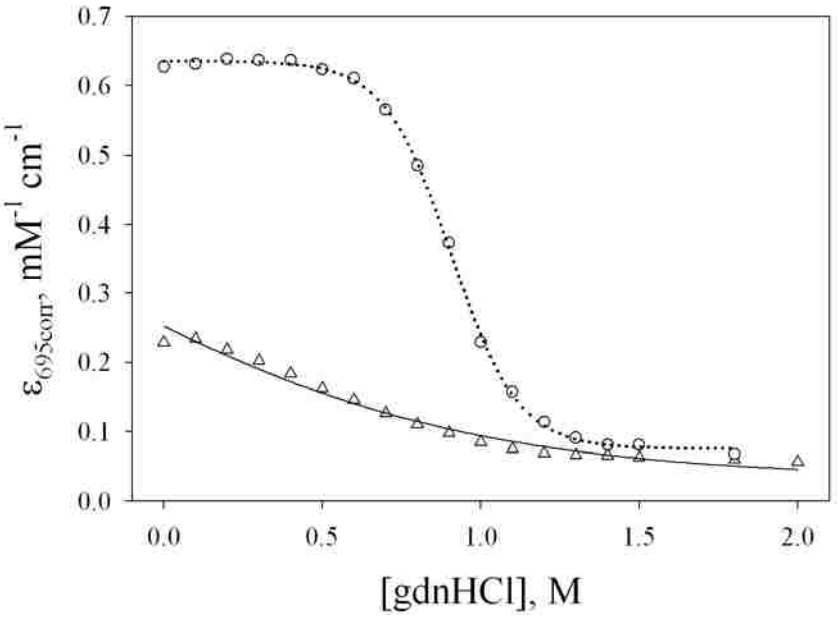


**Figure 2.5** Plot of $\varepsilon_{695corr}$ versus gdnHCl concentration for K79H (Δ) and WT (○) iso-1-cytochromes *c*. Data were acquired at 25 ± 1 ºC in the presence of 20 mM sodium acetate, pH 5.0, 40 mM NaCl. The WT data is from ref. [96]. The solid and dotted curves are fits of the data to eq 2.2 as described in Materials and Methods.

### *2.3.3 pH Dependence of the Stability of the Native Heme-Met 80 Conformer.*

To more fully characterize the heme ligation state of the K79H variant, the absorbance at 695 nm was monitored from pH 2 to 11 in the absence of gdnHCl. This method provides another means of assessing the stability of the native state relative to His-heme and Lys-heme alkaline conformers, as shown in previous work from our lab

[23, 59, 62, 63]. The data for the K79H variant are compared to data for the WT protein in figure 2.6.

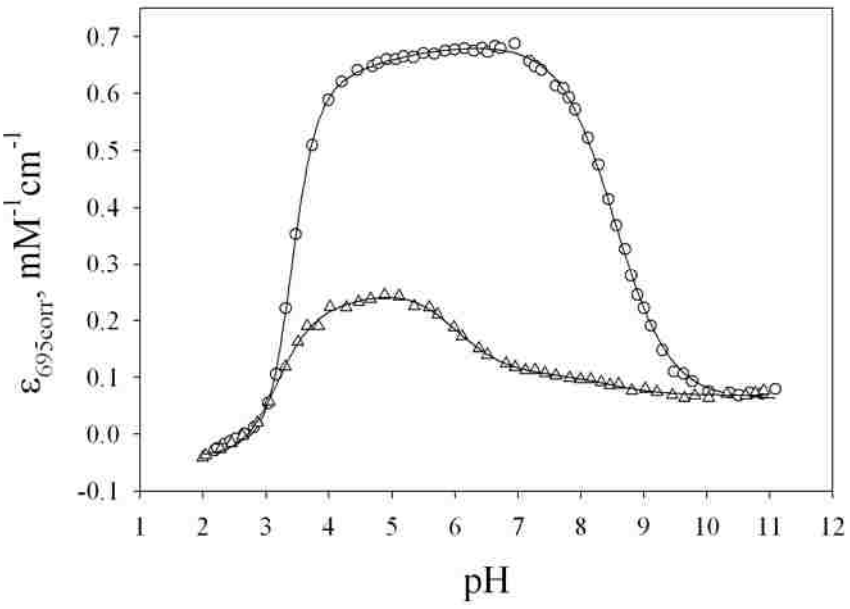


**Figure 2.6** Plot of $\varepsilon_{695corr}$ versus pH for K79H (Δ) and WT (○) iso-1-cytochromes *c* at room temperature (22 ± 1 ºC) in 0.1 M NaCl. The solid curves are fits to eq 2.3 as described in Materials and Methods.

It is immediately apparent that $\varepsilon_{695corr}$ for the K79H variant never reaches the magnitude observed for the fully native state of the WT protein. It is also evident that the alkaline transition observed above pH 5 is biphasic; $\varepsilon_{695corr}$ decreases rapidly from pH 5 to 7 and then more slowly from pH 7 to 10. Similar behavior is observed for the alkaline transition of the K73H variant [23], where the alkaline transition involves both histidine and lysine ligation (See figure 2.2). Initial attempts to fit the pH dependent data for the K79H variant to a four-state equilibrium involving an Acid state, a Native state and two alkaline conformers produced unsatisfactory fits. Closer inspection of the pH dependent spectral data (figure 2.7) reveals significant complexities in the acid to native state

transition, indicating that this transition deviates from two-state behavior. Similar results are observed for the WT protein (figure S3 in *ref* [64]) and for other mitochondrial cytochromes *c* [94, 102-106]). In fact, two variants of iso-1-cyt *c* with K79A mutations undergo acid unfolding through a well-defined intermediate [59, 62].

Thus, data for both K79H and pWT iso-1-cytochromes *c* were fit to a more complex equilibrium model (Schemes 2.1 and 2.2, Materials and Methods) involving two acid states which yielded improved fits. Previous data indicate that the magnitude of $\varepsilon_{695}$ in the native state of cyt *c* may depend on the conformational constraints on the Met80 ligand [107, 108]. NMR data demonstrating Met80-heme ligation when this band is decreased in magnitude or absent have been observed for both wild type and variant cyt *c* [108, 109]. Thus, we have fit the pH dependent $\varepsilon_{695corr}$ data for the K79H variant in two ways. In the first, we use the value of $\varepsilon_N$-$\varepsilon_{Alk}$ from fits of the pH titration data for pWT iso-1-cyt *c*. In the second, we assume that the observed $\varepsilon_N$-$\varepsilon_{Alk}$ value for the K79H variant near pH 5 approaches a fully native state (parameters in brackets in Table 2.1). These two extremes for $\varepsilon_N$-$\varepsilon_{Alk}$ provide limits for the range of the thermodynamic parameters in Schemes 2.1 and 2.2.

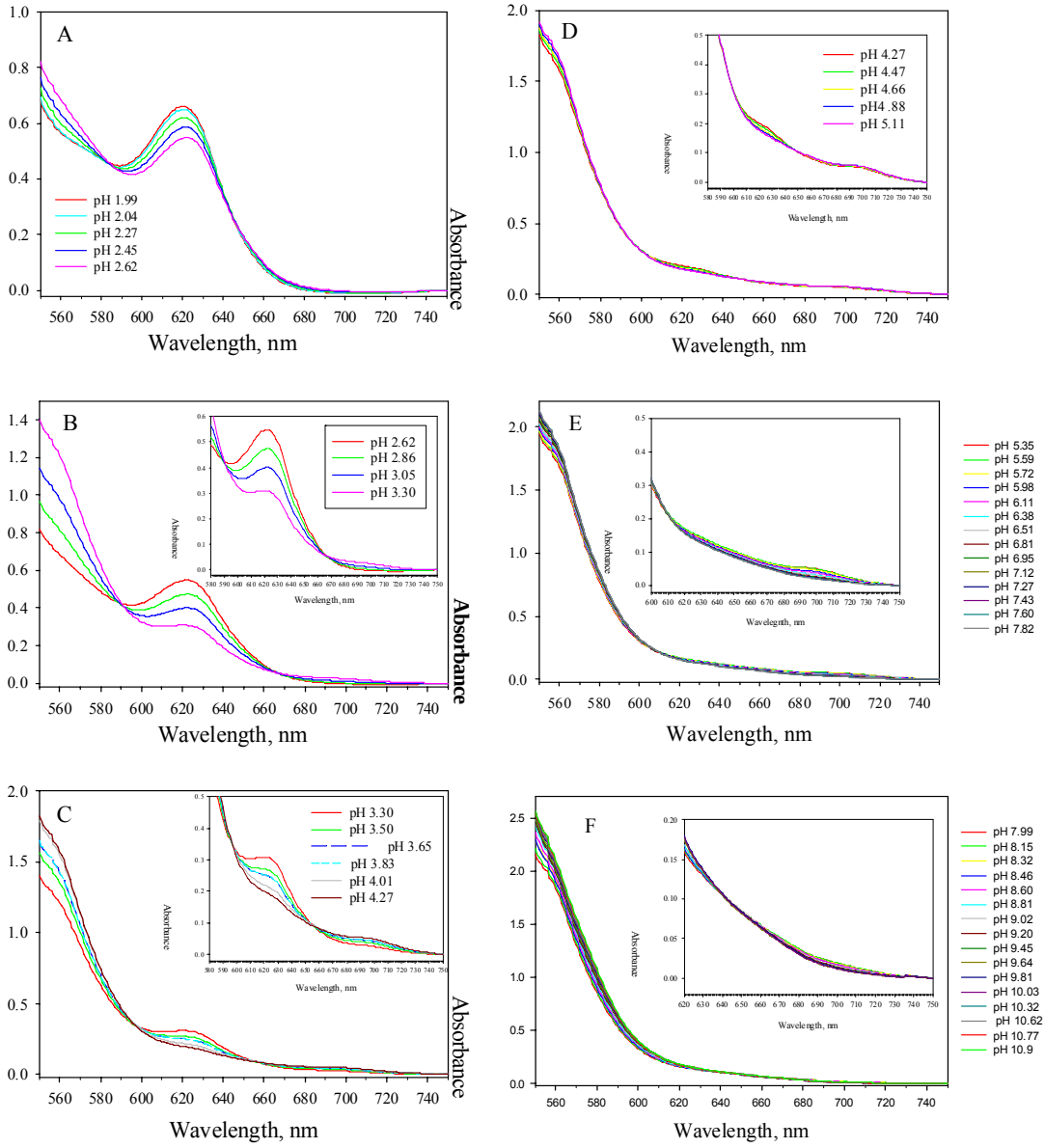


**Figure 2.7** Plot of absorbance spectra as a function of pH for the K79H variant of iso-1-cyt *c* at 22 ± 1 ºC in the presence of 0.1 M NaCl. The absorbance at 750 nm was subtracted from all wavelengths at each pH to correct for variation in background absorbance. (A) pH 2.0 – 2.6 (B) pH 2.6 – 3.3 (C) pH 3.3 – 4.3 (D) pH 4.3 – 5.1 (E) pH 5.4 – 7.8 and (F) pH 8.0 – 10.9 (inset is pH 8 – 10).

An inspection of Table 2.1 shows that the A1 to A2 transition involves uptake of ~2 protons and the A2 to N process ≤0.5 protons, consistent with previous observations that acid unfolding of cyt *c* is a 2 to 3 proton process [94, 96]. The alkaline transition is well-fit as a one proton process and the p$K_{H3a}$ of ~6.6 obtained for the low pH phase of this transition is consistent with the requirement that His 79 ionize for the His79-heme alkaline conformer to form. The native state is clearly disfavored by the K79H mutation compared to the K73H and pWT proteins irrespective of which assumption is made regarding $\varepsilon_N$-$\varepsilon_{Alk}$. In particular, the magnitude of p$K_{C3a}$ for the histidine-heme alkaline conformer is more negative than for the K73H protein and p$K_{C3b}$ for the lysine-heme alkaline conformer is more negative than for both the pWT and K73H proteins.

The maximum population of the His79-heme alkaline conformer occurs at approximately pH 7.3 and is ~75%, whereas the maximal population of the His73-heme alkaline conformer is ~ 30% in 0.1 M NaCl [23]. Thus, the His79-heme alkaline conformer is significantly more stable than the His73-heme alkaline conformer.

**Table 2.1.** Thermodynamic parameters from pH titration in 0.1 M NaCl at 25 ºC for the K79H variant of iso-1-cytochrome *c*.[a]

| Thermodynamic Parameter | Variant | | |
|---|---|---|---|
| | K79H | pWT | K73H[b] |
| $pK_{C1}$ | -1.6 ± 0.3 | -0.9 ± 0.6 | n.d. |
| | (-1.3 ± 0.3)[c] | | |
| $n_1$ | 1.9 ± 0.3 | 2.1 ± 0.1 | n.d. |
| | (1.7 ± 0.3)[c] | | |
| $pK_{C2}$ | 0.12 ± 0.06 | -1.72 ± 0.04 | n.d. |
| | (-1.5± 0.2)[c] | | |
| $n_2$ | 0.20 ± 0.02 | 0.5 ± 0.1 | n.d. |
| | (0.55 ± 0.05)[c] | | |
| $pK_{C3a}$(H79) | -1.20 ± 0.03 | | 0.28 ± 0.01 |
| | (-0.63 ± 0.08)[c] | | |
| $pK_{H3a}$ | 6.61 ± 0.08 | | 6.60 ± 0.06 |
| | (6.71 ± 0.07)[c] | | |
| $pK_{C3b}$(K73) | -3.5 ± 0.2[d] | -2.2 ± 0.1[d] | -2.2 ± 0.1[d] |
| | (-2.9 ± 0.2)[c] | | |

[a] Parameters are from fits of the data to eq 2.3 in Materials and Methods.

[b] Data are from Table 2, *ref* [23], where $pK_{C3a}$ and $pK_{H3a}$ involve His73-heme binding.

[c] Alternate data fit assuming the maximal value of $\varepsilon_{695corr}$ approaches that of the fully native state of the K79H variant.

[d] $pK_{H3}$ for the Lys79-heme alkaline transition was taken as 10.8 based on kinetic data in *ref* [48]. The same value was used for the $pK_{H3b}$ of the K79H variant to allow direct comparison to the $pK_{C3b}$ values for the pWT (Lys73/79-heme binding) and K73H (Lys79-heme binding) proteins.

### *2.3.4 $^1$H NMR Spectroscopy.*

NMR studies were done to further characterize the conformational properties of the K79H variant as a function of pH. The paramagnetically shifted heme-methyl substituents were used to monitor the alkaline conformational transition as a function of pH* as shown in figure 2.8. At pH* 5.04, it is evident that NMR resonances due to the Met80 and heme methyl groups of the native state near -21, and at 32 and 34 ppm, respectively, are low in intensity. By comparison, the heme methyl NMR resonances near 12, 16, 22 and 25 ppm (assignments based on *ref* [23, 48]) due to the Lys73-heme alkaline conformer at pH* 10.15 are much more intense, indicating that the native state is either not fully populated at pH 5 or is very dynamic. The resonances due to the native state decrease both above and below pH* 5. From pH* 6.3 to 8.3, the heme methyl peaks for His79-heme ligation are clearly present as broad peaks near ~17 and ~19 ppm (assignments based on *ref* [23]). $^1$H NMR resonances characteristic of the His79-heme alkaline conformer can also be seen at -10 and -14 ppm over the same pH range. Broad peaks persist in the regions attributable to His-heme ligation at pH* 4.5 to 5.3. This observation suggests that His-heme ligation persists in the A2 state of the K79H variant. Unfortunately, the $^1$H NMR resonances attributable to His-heme ligation are too broad to be integrated reliably, thus the NMR data provide only qualitative information.

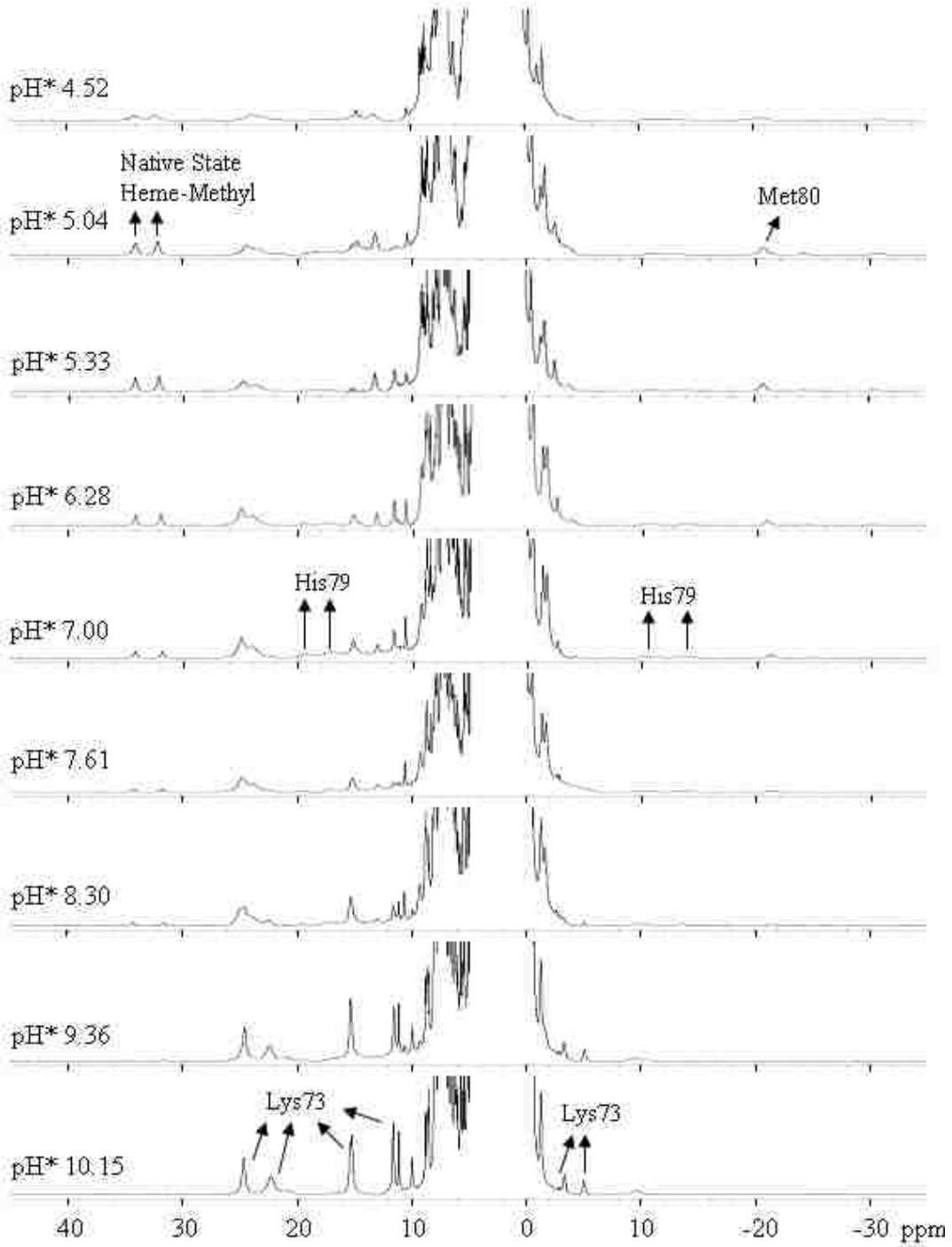


**Figure 2.8** NMR spectra in 0.1 M NaCl, $D_2O$ solution at 25 ºC as a function of pH* for the K79H variant of iso-1-cyt *c*.

### *2.3.5 Stopped–Flow Kinetic Studies of the Alkaline Transition for the K79H Variant of Iso-1-cyt c.*

Kinetic studies were carried out to gain further insight into the alkaline transition caused by His79–heme ligation using pH jump stopped-flow methods. Upward pH jumps were initiated at pH 5 where the K79H variant is maximally in its native state. Data were collected at final pH values from 5.6 to 11.2, to provide data that progress from the region dominated by the His79-heme alkaline conformer to that dominated by the Lys73-heme alkaline conformer. Downward pH jump experiments were initiated at pH 8, where the His79-heme alkaline conformer is expected to dominate to provide rate constant data from pH 5 to 6.6. Representative kinetic data for upward and downward pH jump experiments are shown in the figure 2.9. Two kinetic phases are observed, a fast (100 ms to 1 s time scale) and a slow (2 to 30 s time scale) phase (figures 2.10 and 2.11). The amplitude of the fast phase increases from pH 5.6 to 8 (figure 2.10, inset) as expected for the His79-heme alkaline conformer from equilibrium pH titrations. Thus, we assign the fast phase to formation of the His79-heme alkaline conformer. Similarly, the amplitude for the slow phase grows from pH 8 to 10 (figure 2.11, inset), as expected for formation of a lysine-heme alkaline conformer. A fit of the growth in the slow phase amplitude to the Henderson-Hasselbalch equation yields an apparent p$K_a$ of 8.59 ± 0.02, similar in value to the apparent p$K_a$ of 8.44 ± 0.01 reported for equilibrium formation of a Lys73-heme alkaline conformer with a K79A variant of iso-1-cyt *c* [48]. Thus, we assign the slow kinetic phase to formation of the Lys 73-heme alkaline conformer.

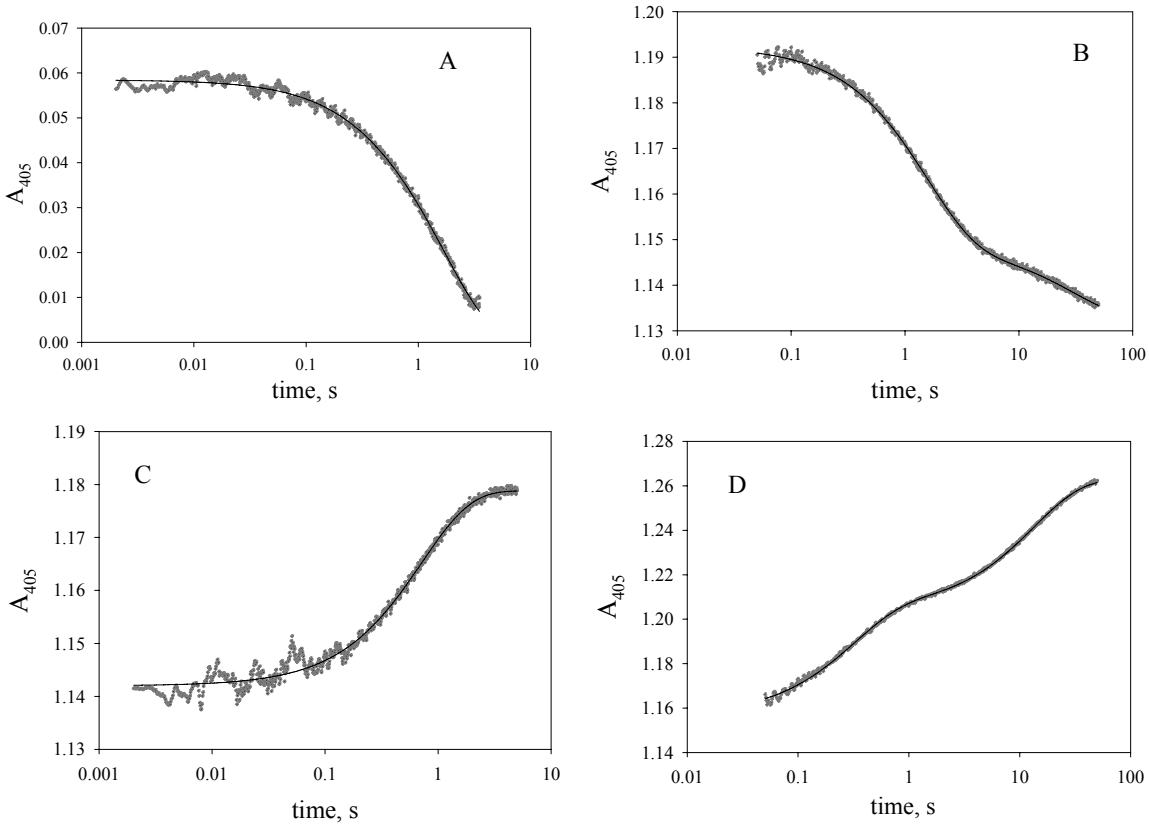


**Figure 2.9** Plot of Absorbance at 405 nm as a function of time from (A) 5 s and (B) 50 s downward pH jumps for pH 5. Buffer used was 10 mM Acetate, pH 5 in the presence of 0.1 M NaCl. (C) 5 s upward pH jump data for pH 6.2. Buffer used was 10 mM MES, pH 6.2 in the presence of 0.1 M NaCl. (D) 50s upward pH jump to pH 9. Buffer used was 10 mM $H_3BO_3$, pH 9 in the presence of 0.1 M NaCl. Solid lines are fits to single or double exponential equations. All pH jump data were collected at 25º C. Time scale is logarithmic.

The rate constant for the fast phase slowly increases with pH (figure 2.10), reaching its maximum near pH 8, after which it slowly declines finally leveling off near pH 10. Above pH 10, the magnitude of the rate constant increases rapidly likely due to the onset of alkaline denaturation of the protein. The pH dependence of the fast phase amplitude follows a similar profile. Over the range pH 5 to 10, the data are consistent with formation of the His79-heme alkaline conformer being modulated by two ionizable

groups. The kinetic model in Scheme 2.3 was used to fit both the fast phase rate constant and amplitude data as a function of pH (figure 2.10).

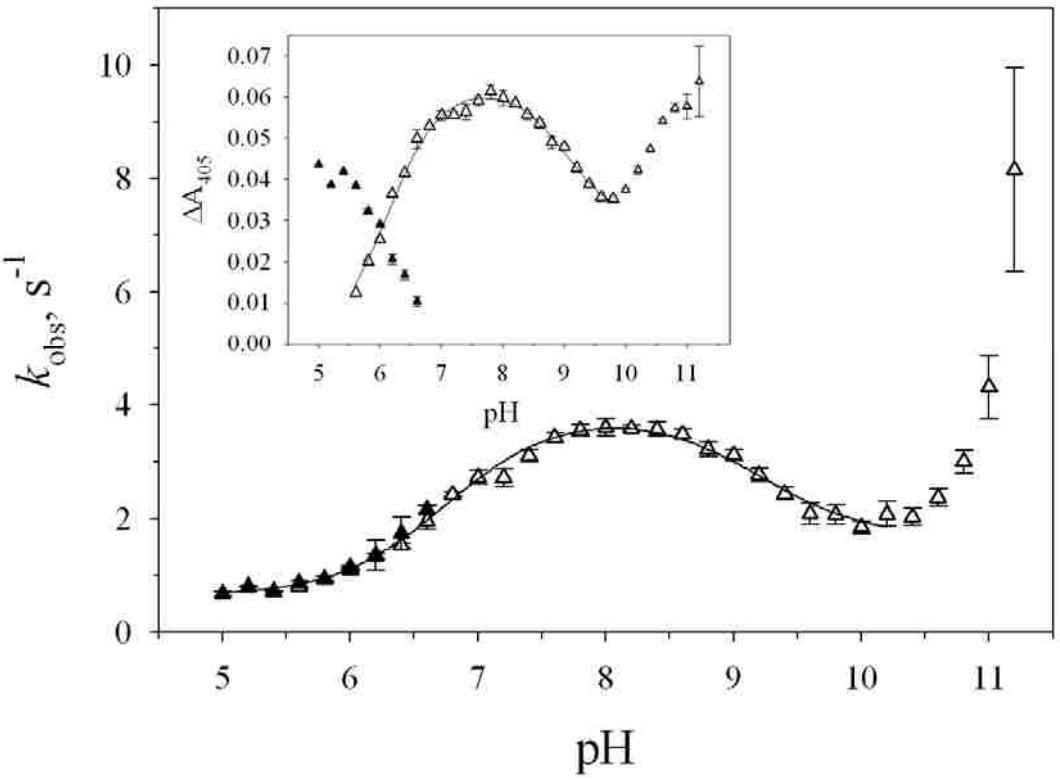


**Figure 2.10** Plots of rate constant and amplitude (inset) data for the fast phase from 50 s data collected at 25 ºC as a function of pH in 10 mM buffer and 0.1 M NaCl. Open triangles are data from upward pH jump experiments and solid triangles are data from downward pH jump experiments. The solid curve is a fit of upward and downward pH jump rate constants from pH 5 to 10 to eq 2.8 in Materials and Methods. The solid curve in the inset is a fit of upward pH jump amplitudes from pH 5.6 to 10 to eq 2.9 in Materials and Methods. Rate constants and amplitudes in this figure are collected in Tables A1, A3 and A5 in Appendix A.

The parameters from these fits are collected in Table 2.2. Both the rate constant and amplitude data for the fast phase yield p$K_{HL}$ ~ 6.8, consistent with p$K_{H3a}$ ~ 6.6 obtained from equilibrium measurements (Table 2.1). For the second ionization, the agreement between the amplitude and rate constant data is less good, but indicates that

p$K_{H2}$ is near 9. For iso-1-cyt *c* variants which form His 73-heme alkaline conformers, values for p$K_{H2}$ range from 8.6 to 9.3 [61, 62]. Thus, there appears to be general agreement that an ionizable group with a p$K_a$ near 9 modulates the kinetics of the alkaline transition. Unlike variants which form a His73-heme alkaline conformer, the kinetics of the formation of the His79-heme alkaline conformer are not affected by an ionizable group with a p$K_a$ between 5 and 6.

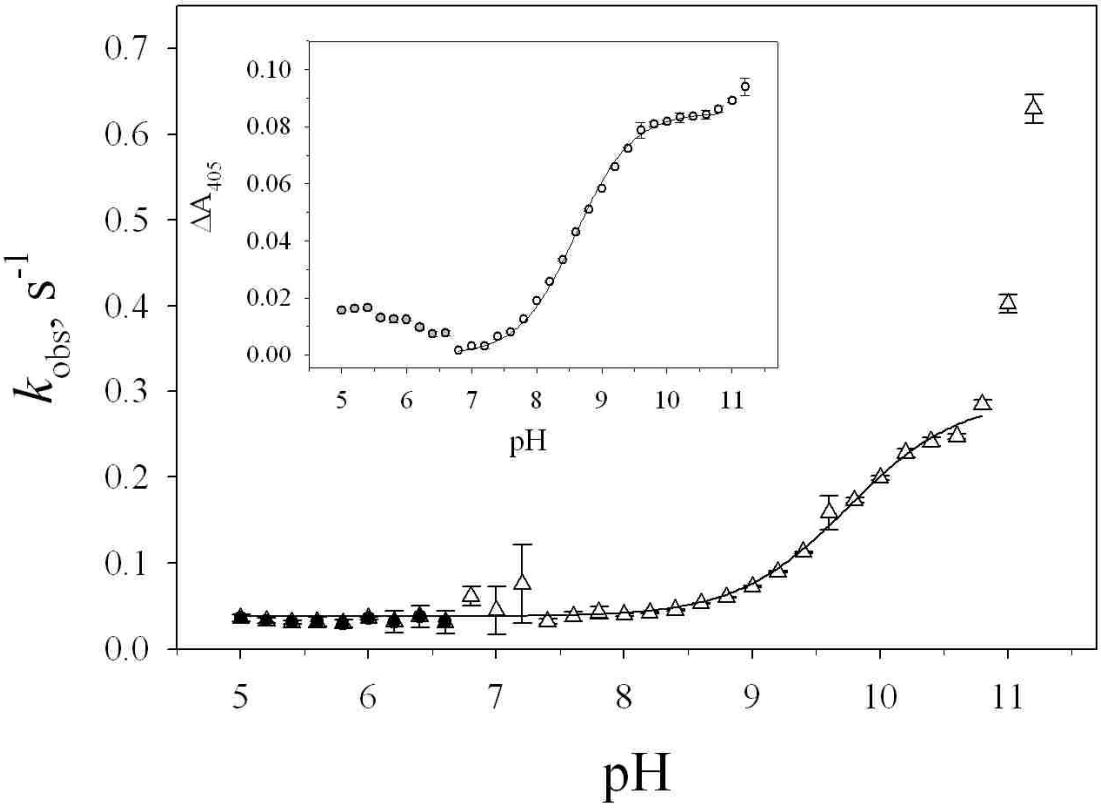


**Figure 2.11** Plots of rate constant and amplitude (inset) data for the slow phase from 50 s data collected at 25 ºC as a function of pH in 10 mM buffer and 0.1 M NaCl. Open triangles are data from upward pH jump experiments and solid triangles are data from downward pH jump experiments. The solid curve is a fit of upward and downward pH jump rate constants from pH 5 to 10.8 to eq 2.6 in Materials and Methods. The solid curve in the inset is a fit of upward pH jump amplitudes from pH 6.8 to 10.8 to eq 2.7 in Materials and Methods. Rate constants and amplitudes in this figure are collected in Tables A2, A4 and A6 in Appendix A.

**Table 2.2** Rate and ionization constants associated with the fast and slow phase of the alkaline transition of K79H iso-1-cyt *c*.

| Parameter | Fast phase[a,b] | Slow phase[c] |
|---|---|---|
| $k_{f1}$, $s^{-1}$ | 3.3 ± 0.2 | 0.23 ± 0.03 |
| $k_{b1}$, $s^{-1}$ | 0.7 ± 0.2 | 0.037 ± 0.001 |
| $k_{f2}$, $s^{-1}$ | 0.7 ± 0.1 | |
| $k_{b2}$, $s^{-1}$[a] | 1.1 ± 0.1 | |
| p$K_{HL}$ ($k_{obs}$ data) | 6.75 ± 0.04 | |
| p$K_{HL}$ (Amp. data) | 6.8± 0.2 | |
| p$K_{H2}$ ($k_{obs}$ data) | 9.21 ± 0.02 | 9.6 ± 0.2 |
| p$K_{H2}$ (Amp. data) | 8.64 ± 0.02 | 9.44 ± 0.06 |

[a]The value for $k_{b2}$ was calculated from $k_{f2}$ iteratively. To fit $k_{obs}$ versus pH data to eq 2.8, an initial guess at the $k_{f2}/k_{b2}$ ratio was made based on the decrease in amplitude for the fast phase between pH 8 and 10. The values for $k_{f1}$, $k_{b1}$ and $k_{f2}$ were then used in fitting amplitude data for the fast phase to eq 2.9, $k_{b2}$ was allowed to vary to obtain the best fit. The $k_{f2}/k_{b2}$ ratio obtained by this procedure was then used in the final fit of the fast phase $k_{obs}$ versus pH data to eq 2.8. A final fit of the fast phase amplitude data to eq 2.9 was made using the rate constants obtained in the second fit of the fast phase $k_{obs}$ versus pH data.

[b]Parameters are averages and standard deviations obtained from fits of $k_{obs}$ and amplitude versus pH data from two data sets to eqs 2.8 and 2.9, respectively. One data set was collected on a 5 s time scale and the other on a 50 s time scale. Parameters from fits of $k_{obs}$ and amplitude versus pH data from pH 5 to 8 from a third 5 sec data set fit to eqs 2.6 and 2.7 were used in the averages for $k_{f1}$, $k_{b1}$ and p$K_{HL}$.

[c]Parameters are the averages from the fits of $k_{obs}$ and amplitude versus pH data from two independent data sets collected on a 50 s time scale to equations 2.6 and 2.7, respectively.

The ratio of $k_{f1}/k_{b1}$ is ~4.7, consistent with the maximal population of ~75% for the His79-heme alkaline conformer observed near pH 7.3 in equilibrium pH titrations. This observation suggests that the A2 and native states behave similarly in kinetics with regard

to formation of the His79-heme alkaline conformer and thus the exact proportioning between these states is unimportant for formation of the His79-heme alkaline conformer.

As is typical for lysine-heme alkaline conformers, the slow Lys73-heme phase of the alkaline transition can be fit to a simpler kinetic model involving a single ionizable group. Fits of the slow phase $k_{obs}$ and amplitude data versus pH to this model (figure 2.11), yield a p$K_a$ for this ionization near 9.5. Kinetic data from our laboratory on a K79A/N52G variant which forms a Lys73-heme alkaline conformer also yielded a p$K_a$ of ~9.5 for the ionizable group triggering the Lys73-heme alkaline conformer. At pH 10, $k_{obs}$ for formation of the Lys73-heme alkaline conformer of the K79H variant is 5 to 10-fold lower than for formation of the Lys73-heme alkaline conformers of the K79A [48] and K79A/N52G variants [59].

### *2.3.6 Anaerobic Stopped-Flow Kinetic Measurements.*

The alkaline state of iso-1-cyt *c* can lead to conformationally gated ET processes, as has been shown previously [52-54, 73, 81]. Our interest in gated ET with the K79H variant is two-fold. By changing the ligand involved in the alkaline conformer and its sequence position, we aim to adjust the rate of the gated ET. Secondarily, gated ET can be used to measure microscopic rate constants for conformational changes under solution conditions where normally a pure rate constant can not be obtained. In particular, as pH increases the rate constant for the alkaline conformational transition becomes the sum of forward and backward rate constants (eqs 2.6 and 2.8). In principle, gated ET will allow the backward rate constant, $k_b$, for the alkaline conformational transition to be measured directly at any pH, not just low pH.

Near pH 7.5 the His79-heme alkaline conformer is predominant for the K79H variant and is expected to have a low reduction potential (~50 mV vs NHE, see *refs* [49, 110]). A small amount of the native form (Met80-heme ligation) is present with a high reduction potential (~290 mV vs NHE, see *ref* [48]). Thus, immediately after mixing $a_6Ru^{2+}$with the K79H variant at pH 7.5 a fast intermolecular reaction with the native state is expected. This fast phase should depend on the concentration of $a_6Ru^{2+}$. The rate of ET to the His79-heme alkaline conformer should depend on the rate of the slower conformational change back to the native state. This conformationally gated ET should not depend on [$a_6Ru^{2+}$]. At pH 7.5, the rate constant for gated ET should correlate with $k_{b1}$ measured by pH jump methods. Over a 5 s time scale, two ET phases, on ~10 ms and ~1 s time scales, are observed (figure 2.12). The faster phase is dependent on [$a_6Ru^{2+}$] and its amplitude is consistent with direct bimolecular reduction of the native state of K79H iso-1-cyt *c* (Table 2.3). Within error, the ~1 s time scale phase is independent of [$a_6Ru^{2+}$] consistent with gated ET. The rate constant for this phase, averaged over all [$a_6Ru^{2+}$] is 0.63 ± 0.02 $s^{-1}$ agreeing well with the magnitude of $k_{b1}$ for the His79-heme alkaline conformational transition (Table 2.2).

A much slower kinetic phase is observed when the ET reaction of K79H iso-1-cyt *c* with $a_6Ru^{2+}$ is observed over the course of 50 s (figure 2.12). The amplitude of this rate constant is consistent with an ET reaction involving the Lys73-heme alkaline conformer. This rate constant appears to be dependent on [$a_6Ru^{2+}$]. A linear fit of $k_3$ versus [$a_6Ru^{2+}$] extrapolates to a rate constant of 0.045 ± 0.003 $s^{-1}$ at 0 M $a_6Ru^{2+}$ reasonably consistent with $k_b$ = 0.037 ± 0.001 for the Lys73-heme alkaline conformer in Table 2.2. The concentration dependence observed for this phase may be due to a slow direct

bimolecular reaction of $a_6Ru^{2+}$ with the Lys73-heme alkaline conformer (also see *ref* [54]).

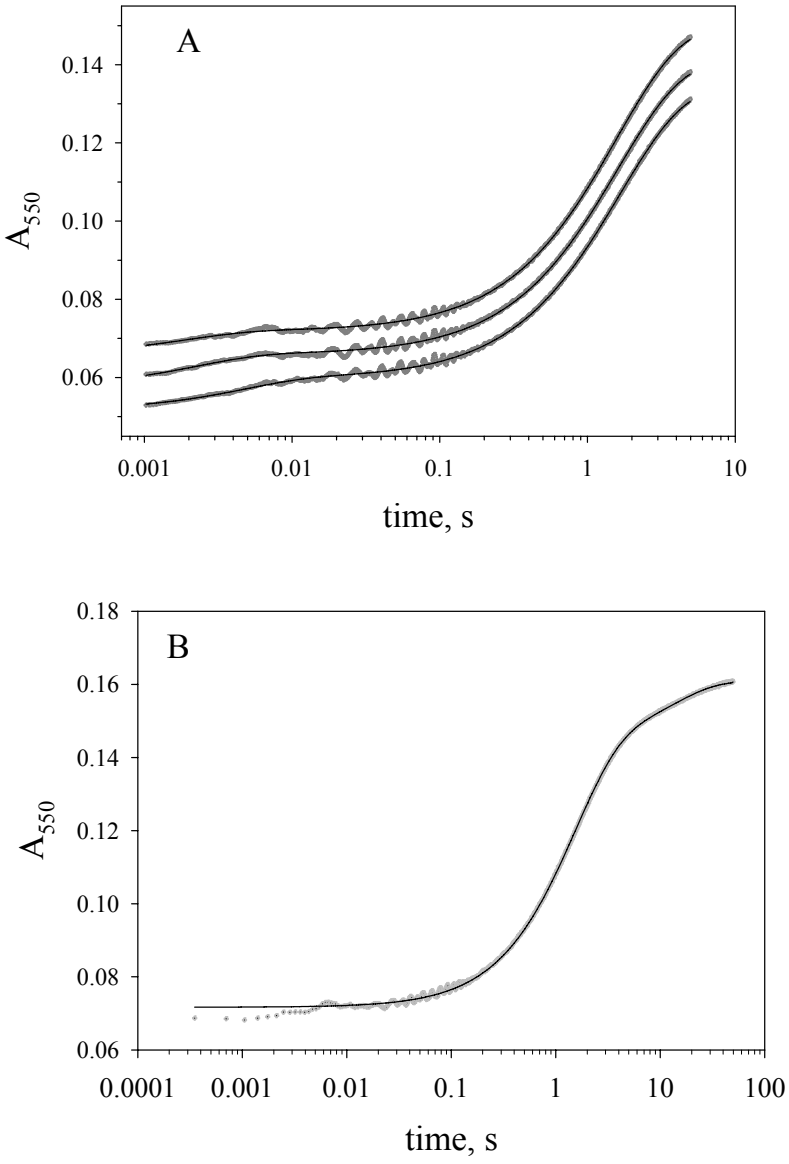


**Figure 2.12** Plot of absorbance at 550 nm versus time (on logarithmic scale) for reduction of the K79H variant of iso-1-cyt *c* with hexammineruthenium(II) chloride at pH 7.5 and 25 ºC for data collected on a (A) 5 s and (B) 50 s time scale. In part A, the $a_6Ru^{2+}$ concentration is 5.0, 2.5 and 1.25 mM from top to bottom. In part B, the $a_6Ru^{2+}$ concentration is 5.0 mM. The buffer used was 10 mM $NaH_2PO_4$ in 0.1 M NaCl, pH 7.5. The solid curves are fits of the data to a double exponential rise to maximum equation.

**Table 2.3.** Rate constants and amplitudes for the reduction of K79H iso-1-cyt *c* by $a_6Ru^{2+}$ at 25 ºC and pH 7.5.

| ($a_6Ru^{2+}$), mM | $k_1$, $s^{-1a}$ | $A_1$, a.u.[a] | $k_2$, $s^{-1b}$ | $A_2$, a.u.[b] | $k_3$, $s^{-1c}$ | $A_3$, a.u.[c] |
|---|---|---|---|---|---|---|
| 1.25 | 124 ± 22 | 0.008 ± 0.001 | 0.62 ± 0.02 | 0.074 ± 0.001 | 0.051 ± 0.004 | 0.0176 ± 0.0002 |
| 2.5 | 290 ± 90 | 0.008 ± 0.002 | 0.63 ± 0.02 | 0.074 ± 0.002 | 0.062 ± 0.003 | 0.0179 ± 0.0001 |
| 5 | 450 ± 160 | 0.005 ± 0.001 | 0.65 ± 0.02 | 0.075 ± 0.003 | 0.074 ± 0.002 | 0.0176 ± 0.0002 |

[a]Parameters are average and standard deviation obtained from the 5 s data set.

[b]Parameters are average and standard deviation obtained from both 5 and 50 s data sets

[c]Parameters are average and standard deviation obtained from the 50 s data set.

## 2.4 Discussion

### *2.4.1 Stability of His 73-heme versus His 79-heme Alkaline Conformers.*

A primary motivation of this work was to determine how the position of a histidine in Ω-loop D impacts the stability of His-heme alkaline conformers. The results in Table 2.1 clearly show that the His79-heme alkaline conformer is more stable than the His73-heme alkaline conformer. Kinetics data provide additional insight into the reason for the increased stability of the His79-heme alkaline conformer relative to the native state. The forward rate constant, $k_f$, for both the His73-heme and His79-heme alkaline transitions is near 3.5 $sec^{-1}$ over the pH range 6.0 to 8.0. For the His79-heme alkaline state $k_{b1}$ is 0.7 $s^{-1}$ which is ten times slower than for the His73-heme alkaline conformer ($k_b \sim 7$ $s^{-1}$ for the K73H variant in this pH regime, see *ref* [61]. This result indicates that the primary cause of the increased favorability of formation of the His79-heme alkaline conformer is stabilization of the alkaline conformer and not destabilization of the native

state by the K79H mutation. The greater stability of the His79-heme alkaline conformer may be due to the smaller structural disruption that occurs when this state forms (*m*-value of ~1 kcal/(mol×M) for partial unfolding at 695 nm versus ~1.7 kcal/(mol×M) for the K73H variant, see *refs* [23, 100]. Further support for a smaller structural disruption for the His79-heme alkaline conformer comes from the lack of a slow proline isomerization phase in the kinetics of its formation. By contrast proline isomerization attributable to Pro76 [111] does occur during formation of the His73-heme alkaline conformer [61, 62]. For lysine-heme alkaline conformers, only lysines in Ω-loop D are capable of forming alkaline conformers [48]. The pWT protein which has histidines at positions 26, 33 and 39, does not give a biphasic alkaline transition (figure 2.5). The low stability of the Ω-loop D substructure [78, 79] presumably accounts for this observation.

### *2.4.2 Insights into the Triggering Mechanism of the Alkaline Transition.*

The debate over the nature of the ionizable group(s) involved in triggering the alkaline transition is ongoing [44, 48, 94]. In the case of the His-heme alkaline conformers studied in this laboratory, the evidence is strong in support of ionization of the histidine ligand being the primary trigger for the conformational transition [61, 62]. In all cases, the magnitude of p$K_{HL}$ is near 6.6 (see Scheme 2.3 and Table 2.2). Recent studies on a set of yeast iso-1-cyt *c* variants show a strong correlation between the apparent p$K_a$ for the alkaline transition and the p$K_a$ for the lysine in Ω-loop D with the lowest calculated p$K_a$ [57]. This observation is consistent with an important role for ionization of the incoming lysine in triggering the alkaline transition. Thus, the ionization

of the ligand replacing Met80 seems to play a primary role in triggering the alkaline transition.

Our studies on His73-heme alkaline conformers indicate that two other ionizable groups modulate the kinetics of the alkaline transition [61, 62], a low pH ionization near 5.5 and a high pH ionization near 9. Groups with perturbed ionizations are often important in promoting conformational transitions. In this pH regime, His26 has a p$K_a$ < 3.6, and one heme propionate is believed to have a p$K_a$ < 4.5 and the other > 9 [94].

For the His73-heme alkaline conformer of the K73H variant, protonation of the group with a p$K_a$ near 5.5 increases the rate of return to the native state [61]. The addition of the mutation, K79A, in a K73H/K79A variant shifts the p$K_a$ of this ionization [62]. In the current work, this ionization is not observed for formation of a His79-heme alkaline conformer. Lys79 is involved in the buried hydrogen bond network of iso-1-cyt *c* [112], which is believed to modulate the strength of the His26/Glu44 hydrogen bond [75, 91]. This hydrogen bond is an important cooperative stabilizer of iso-1-cyt *c* [75, 91] and likely stabilizes the least stable substructure (gray in figure 2.1) of cyt *c* [39, 79] and thus the native state relative to the alkaline state. However, the ionization near 5.5 is unlikely due to protonation of His26 since His26 acts as an H-bond acceptor in the Glu44/His26 hydrogen bond. Thus, an indirect effect on this hydrogen bond via the buried hydrogen bond network through protonation of a group, such as the heme propionate adjacent to Lys79 (heme propionate D), is more likely. The smaller structural disruption involved in the His79-heme alkaline conformer may preserve the Glu44/His26 hydrogen bond (which is broken when a position 73 ligand binds to the heme, *ref* [58]), diminishing the impact of the low pH ionization.

The kinetics of formation of all His-heme alkaline conformers is modulated by ionization near pH 9. For His73-heme conformers [61, 62] this ionization causes $k_{obs}$ to increase, whereas it decreases $k_{obs}$ for the His79-heme alkaline conformer described here (figure 2.10). An ionization between 9 and 9.5 is also observed for formation of lysine-heme alkaline conformers of the K79H (Table 2.3) and K79A/N52G [59] variants, as well as for several position 82 variants of iso-1-cyt *c* [113]. Thus, a protein group with a p$K_a$ in this region appears to be a general modulator of this transition. In previous work, we have suggested that this ionization may involve Tyr67 [59] based on evidence of a high spin intermediate in the kinetics of formation of the alkaline conformer of a Trp82 variant of iso-1-cyt *c* [114]. However, this assignment is difficult to reconcile with kinetic data for the His73-heme alkaline transition of the K73H variant [61]. No change in amplitude is observed for formation of the His73-heme alkaline conformer as $k_{obs}$ increases between pH 8 and 10, implying stabilization of the transition state with respect to the native and alkaline conformers with little change in the relative stability of the native and His73-heme alkaline states. Since the hydroxyl group of Tyr67 is solvent exposed in the NMR structure of the Lys73-heme alkaline conformer [58] whereas it is buried in the native state [112], the relative stabilities of the native and His73-alkaline conformers would be expected to change upon ionization of Tyr67.

The ionizable group with a p$K_a$ near 9 must be able to stabilize the transition state for formation of the His73-heme alkaline conformer and slow down the rate of formation of the His79-heme alkaline conformer while having a lesser impact on the backward rate constant. Our data are consistent with significant differences in the structure of the His79-heme and His73-heme alkaline conformers, so such effects are possible. The

transition state for the His73-heme alkaline conformer may better solvate a charged group produced by this ionization than either the native or His73-heme alkaline conformers. It is possible that the transition state for the His79-heme alkaline conformer is sufficiently different that it solvates this group less well. One of the heme propionates has a p$K_a$ near 9 [94, 115] and this group has been put forward as a possible trigger group for the alkaline transition [44, 94, 116]. The heme propionates make close contacts with a number of polar groups in the native state [112], whereas these contacts are largely disrupted in the NMR structure of the Lys73-heme alkaline conformer [58]. Heme propionate D (outer) is reasonably solvent-exposed whereas heme propionate A (inner) is poorly solvent-exposed in the NMR structure of the Lys73-heme alkaline conformer and both propionates might be poorly exposed in a His79-heme alkaline conformer and also have the polar contacts of the native state disrupted. Thus, it is plausible that ionization of a heme propionate near pH 9 could destabilize the His79-heme alkaline conformer and the transition state relative to the native state.

### *2.4.3 Gated ET*

Electron transfer reactions have been used to initiate fast protein folding [117]. Gated ET on the other hand can allow a conformational change – here the formation of the native state of iso-1-cyt *c* from a partially unfolded form – to be detected by its control of the rate of an ET reaction. The advantage of gated ET is it can permit a direct evaluation of a rate constant for a conformational change under conditions not accessible by standard mixing methods. In the present work, pH jump mixing can only provide $k_{obs} = k_f + k_b$ at pH 7.5, not the individual rate constants. The individual rate constants can only be

obtained from fitting the data to a kinetic model. The gated ET reaction, however, requires the native oxidized state of the K79H variant to form before $a_6Ru^{2+}$ can rapidly reduce the protein. Thus, $k_b$ is obtained directly at pH 7.5. The match obtained between $k_b$ obtained by gated ET and from our pH jump kinetics model provides strong confirmation of the validity of the model.

Gated ET appears to be important in modulating ET reactions of a number of enzymes and may be important in controlling the rates of metabolic pathways [50]. Thus, understanding how the rates of conformational ET gates are controlled will be useful in manipulating metabolic control and could be useful in developing switches for protein-based molecular electronics. To this end we have pursued a strategy of manipulating both the nature of the alkaline state ligand and its sequence position to modulate the rate of gated ET. In previous work, we have shown that the His73-heme ET gate operates on a 75–200 ms, time scale [73, 81]. Lysine-heme alkaline conformers gate ET on a 15-30 s time scale [52-54, 81] and through rational mutagenesis can provide gated ET at physiological pH [81]. The current work shows that we can significantly slow the rate of a His-heme ET gate by changing the position of the histidine ligand used in the alkaline state. Gated ET due to the His79-heme alkaline conformer occurs with a time constant, $\tau$, of $1.58 \pm 0.05$ s filling in the gap between the ~100 ms gating of the His73-heme ET gate and the ~10 s gating of the lysine-heme alkaline conformers. Thus, modulating the nature and the position of an alternate ligand to a redox active metal in a protein appears to be a flexible strategy for manipulating the rate of an ET gate. An ET gate involving the copper in plastocyanin [118] has been shown to operate on a microsecond time scale indicating

that the nature of the metal is important, too. Thus, nature appears to have a versatile toolbox for tuning rates of gated ET to suit a particular metabolic need.

## 2.5 Conclusions

These studies show that K79H variant produces an alkaline conformational transition with distinctly different properties compared to the alkaline conformer produced by the K73H variant. In particular, a more stable His-heme alkaline conformer is produced. The *m*-value for the conformational transition is smaller indicating lesser structural disruption than for the His73-heme alkaline conformer. This structural difference appears to eliminate the low pH triggering ionization and proline isomerization seen with the His73-heme alkaline conformer and to slow rather than enhance the kinetics of the alkaline transition at higher pH. Kinetic data provide additional evidence for a primary role of ionization of the alkaline state ligand in triggering this conformational change. We speculate that the heme propionates may provide auxiliary ionizations that modulate this transition.

We also demonstrate that gated ET provides a useful means to extract discrete rate constants for conformational changes under conditions where these rate constants cannot usually be measured directly. The gated ET data provide further evidence for the efficacy of tuning the rate of an ET gate using a combined strategy of modulating the sequence position and nature of the metal ligand.

# CHAPTER 3

## *PROBING THE BOTTOM OF THE FOLDING FUNNEL USING CONFORMATIONALLY GATED ELECTRON TRANSFER WITH THE ACH73 VARIANT OF ISO-1-CYTOCHROME C*

### 3.1 Introduction

The folding funnel concept [119, 120] has provided a useful and effective means of interpreting and understanding the process of protein folding. A key aspect of this model is that foldable proteins favor contacts that lock in the correct topology and thus commit a protein to fold before the protein becomes so compact that the rate of conformational rearrangement becomes slow or glassy. Such minimally frustrated energy landscapes leads to efficient folding, the rate of which increases as the stability of a protein increases [121, 122]. Due to the funneling of the energy landscapes of foldable proteins, less is known about the rate of conformational rearrangements at the bottom of a folding funnel [122]. While it is clear that decreased protein stability slows the overall rate of protein folding, experimental measurements of the effect of decreased stability on the glassy kinetics at the bottom of a funneled protein folding landscape are lacking. Here, we use engineered proteins in conjunction with novel conformationally-gated electron transfer (ET) methods to assess the response of the kinetics at the bottom of a folding funnel to global stability. We also use gated ET methods with the same destabilized variant of iso-1-cytochrome *c* (iso-1-cyt *c*) to probe in detail the dynamics of the alkaline conformation transition.

The alkaline conformation of cytochrome *c* represents a model for a late folding intermediate or partially unfolded state of cytochrome *c* [39, 77]. Studies with iso-1-cyt *c* show that Lys73 and Lys79 are the ligands that replace Met 80 in the alkaline

conformational transition [48]. Lys73 and 79 have been replaced by Ala [48] and His [61, 64] to gain insight into the mechanism of this transition. These results have shown some interesting differences in the triggering mechanism of His at position 73 [23, 61] as compared to position 79 [64]. With regard to folding landscapes, an interesting aspect of the His-heme alkaline conformers is that they are very close in stability to the native structure near physiological pH. Thus, the variants with His at positions 73 or 79 have double-welled folding funnels with a "native" state and a late folding intermediate (the alkaline conformational state) with similar energies. Since the alkaline transition is proton-coupled, the transition between this late folding intermediate and the native state is readily measured.

A prediction of folding landscape theory is that more stable protein folds faster. This prediction has been verified experimentally [122, 123]. In the current study, we have investigated a highly destabilized variant with a histidine at position 73, AcH73, and compare its properties to the K73H variant of iso-1-cyt *c*. The latter has approximately twice the global stability of the former. An important question is how a transition between a model for a late folding intermediate and the native state, presumably occuring below the glass transition, will behave when the global stability of the protein is compromised.

The AcH73 variant of iso-1-cyt *c* [83] has five mutations beyond that producing His73 in the K73H variant. Two of these lead to N-terminal acetylation (T(-5)S and K(-2)L, note that horse numbering is used, so the N-terminal amino acid is -5) and three of these mutated histidines that are removed at or near the surface of the protein (H26N, H33N and H39Q). The loss in global stability is attributed to the mutation at position 26,

which leads to the disruption of hydrogen bond between Asn31 and Glu44 (green and gray surface loops in figure 3.1) [75].

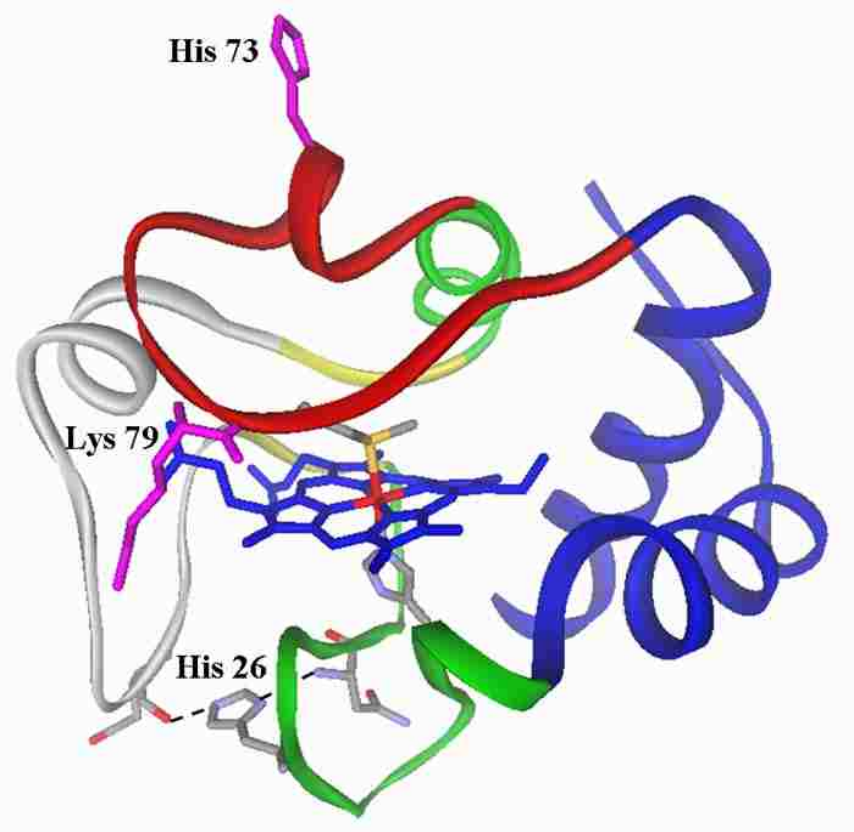


**Figure 3.1** Iso-1-cyt *c* showing the side chains of His73 (K73H mutation) and Lys79 as stick models. The heme cofactor is shown in blue with the heme ligands Met80 and His18 colored by atom type. The side chain of His26 is shown hydrogen-bonded to the carbonyl of Glu44 and the amide NH of Asn31. The substructures of cytochrome *c* as defined by Englander and co-workers [77, 78] are shown from least to most stable in the colors gray, red, yellow, green, and blue. Figure is taken from *reference* [24].

Histidine at position 26 has been shown to have stabilizing effects with the formation of two hydrogen bonds that bridge between the two substructures of the wild type protein [39, 75, 79, 91]. All other mutations (T(-5)S, K(-2)L, H33N and H39Q) have small effects on the stability of the protein [75, 83, 101]. We have speculated that His 26 may have a role in one of the two auxiliary ionizations observed for the His-heme

alkaline transition of cytochrome *c* [61, 62], although other data suggest the role is at most indirect (see chapter 2 and *ref* [64]). Weakening of this H26/Glu44 hydrogen bond is considered to facilitate partial unfolding of the protein [62]. Thus, a secondary aim of this work was to directly investigate the effect of the absence of His26 on the kinetics of the alkaline transition.

To provide appropriate context for this work, we initially provide a careful characterization of the thermodynamics of the His73-heme alkaline transition of the AcH73 variant. We then study the kinetics of the interconversion between the native and partially-unfolded His73-heme alkaline conformer using standard pH jump methods and a novel electron transfer (ET) method that takes advantage of a conformationally-gated ET reaction.

Gated ET methods allow resolution of rate constants for the interconversion between the native and partially unfolded protein that cannot be obtained from modeling the pH jump data in a pH regime that is critical for understanding how the removal of His 26 affects the alkaline conformational transition. We also find that the kinetics of interconversion between the native and partially unfolded alkaline state are faster for the less stable AcH73 variant, showing that compressing the energy dimension of a folding funnel acts to decrease the barriers between low energy "trapped" states.

## 3.2 Materials and Methods

### *3.2.1 Isolation and Purification of Proteins*

The AcH73 variant was isolated and purified from *Saccharomyces cerevisiae* as described previously [89].

### *3.2.2 Molecular Weight Determination by MALDI-TOF Mass Spectroscopy.*

The purification of the AcH73 protein by cation-exchange HPLC gave one main peak (highest intensity) and one small post-peak. The peaks were collected separately and concentrated using centricon concentrators (10,000 MWCO, Millipore), exchanged into 50 mM sodium phosphate buffer, pH 7, and concentrated to a final volume of ~500 µL. Mass spectrometry was carried out using an Applied BioSystems, Voyager–DE Pro Biospectrometry Workstation as described previously [59]. The main peak gave m/z = 12,672.46 ± 2.5 (average and standard deviation of four independent spectra), and the small peak gave m/z = 12,674.22 ± 2.5 (average and standard deviation of four independent spectra). Spectroscopically the main peak was found to be the reduced ($Fe^{II}$) and the second peak the oxidized ($Fe^{III}$) form of the protein, consistent with the expected molecular mass of 12,675.21 g/mol for the AcH73 variant. All experiments were carried out with this material.

### *3.2.3 Oxidation of Protein*

Protein was oxidized and separated from oxidizing agent as described previously in Materials and Methods section 2.2.3 of Chapter 2. The concentration and degree of oxidation of the protein were determined, as described previously [83].

### *3.2.4 Guanidine Hydrochloride Denaturation Monitored by Circular Dichroism Spectroscopy*

Global stability of the protein was determined in the same manner as described previously in the Materials and Methods section 2.2.4 of Chapter 2.

### *3.2.5 Partial Unfolding by GdnHCl Monitored at 695 nm*

Partial unfolding of protein was monitored at 695 nm, $A_{695}$, as a function of gdnHCl concentration using a Beckman DU 640 spectrophotometer as described previously in Materials and Methods section 2.2.5 of Chapter 2.

### *3.2.6 pH Titration Experiments Monitored at 695 nm*

The alkaline conformational transition caused by His73 was monitored as a function of pH at 0, 0.1, 0.2 and 0.3 M gdnHCl concentrations using the 695 nm absorbance band. The experiment was done at 25 ± 1°C. The initial sample was made by mixing 500 µl of ~400 µM protein in 200 mM NaCl or 20 mM MES in 200 mM NaCl (2x protein in 2x buffer) with 500 µl of doubly deionized water ($ddH_2O$). For 0.1, 0.2 and 0.3 M, back titrations were also done. The solution was mixed by a 1000 µl pipet and pH was adjusted to either 4.5 or 5.7 by adding 3 M HCl and an equal volume of 2x protein. The pH was measured with an Accumet AB15 pH meter (Fisher Scientific) using an Accumet semimicro calomel pH probe (Fischer Scientific Cat. No.13-620-293). The experiment was carried out as described previously in Materials and Methods section 2.2.6, of Chapter 2. Absorbance at 750 nm was used as the background wavelength to control for small variations in the baseline yielding $A_{695corr} = A_{695} - A_{750}$. The molar extinction coefficient at each pH was calculated for all pH titrations as described previously in Materials and Methods section 2.2.6, of Chapter 2 and in *ref* [64]. The concentration was determined from absorbance ~ pH 5 (cyt *c* being maximally in the native form at this pH) using absorbance at 570 and 580 nm as described in Materials and

Methods section 2.2.6 of Chapter 2 [95]. The molar extinction coefficient at 695 nm versus pH data was fitted to equation 3.1 [23].

**Equation 3.1**

$$\varepsilon_{695corr} = \frac{\varepsilon_N + \varepsilon_{alk}\left[\left(\frac{10^{-pK_{C1}}}{1+10^{(pK_{H1}-pH)}}\right)+\left(\frac{10^{-pK_{C2}}}{1+10^{(pK_{H2}-pH)}}\right)\right]}{1+\left[\left(\frac{10^{-pK_{C1}}}{1+10^{(pK_{H1}-pH)}}\right)+\left(\frac{10^{-pK_{C2}}}{1+10^{(pK_{H2}-pH)}}\right)\right]}$$

In eq 3.1, $\varepsilon_{695corr}$ is the observed molar extinction coefficient at 695 nm during the alkaline transition, $\varepsilon_N$ is the molar extinction coefficient at 695 nm of the Met80–bound native state, $\varepsilon_{alk}$ is the corrected molar extinction coefficient at 695 nm of the alkaline state. In fitting the data for the AcH73 variant, we have constrained $\varepsilon_{Alk}$ to be ($\varepsilon_N$ - 0.53) as observed in pH titration studies with the K73H variant [23]. $K_C$ is the equilibrium constant associated with the replacement of Met80 with an alternative ligand and $K_H$ is the triggering deprotonation equilibrium. For p$K_{C1}$, the alternate ligand is His73 and for p$K_{C2}$ the alternate ligand is Lys79. p$K_{H2}$ was set to 10.8 [48].

### *3.2.7 pH Titration Experiments Monitored at 380 and 398 nm*

Studies were carried out with oxidized iso-1-cyt *c* at a concentration of approximately 10 μM in 100 mM NaCl. The spectrum was scanned from 350 to 450 nm at each pH step. The titration method is the same as described in the Materials and Methods section 2.2.6 of Chapter 2.

### *3.2.8 pH Jump Experiments*

All pH jump experiments were carried out at 25 $^{o}$C and data were collected on 5 and 50 s time scales, as described previously in the Materials and Methods section 2.2.8 of Chapter 2 and in *ref* [61]. Each trial of upward pH jump data was fit to single or double exponential rise to maximum equations. Data for downward pH jumps were fit to single or double exponential decay equations, as appropriate. The $k_{obs}$ and amplitude data as a function of pH for the fast and slow phase were fit to the usual mechanism for the alkaline conformational transition involving a single ionizable group using eq 2.6 and 2.7, respectively, from Chapter 2, Materials and Methods section 2.2.8. In fitting amplitude data versus pH to eq 2.7, $k_f$ and $k_b$ were set to the values obtained from fits of $k_{obs}$ versus pH data to eq 2.6.

### *3.2.9 Electron Transfer Experiments by the Stopped Flow Method*

Experiments were done using hexaammineruthenium(II) chloride ($a_6Ru^{2+}$) with an Applied Photophysics SX20 stopped flow spectrophotometer, as described previously in Materials and Methods section 2.2.9 of Chapter 2. The dead time of this instrument was determined to be 0.8 ms using the method described in Applied Photophysics SX.18MV Application Note 1 and in *ref* [124]. The stopped flow assembly was made anaerobic by soaking the syringe assembly in 0.1 M sodium dithionite prepared in 0.1 M dibasic sodium phosphate overnight followed by 2 – 3 hrs of soaking in fresh solution on the day of the experiment. The syringe assembly was then thoroughly washed with 10 mM buffer prepared in 0.1 M NaCl [125]. The 10 mM buffers used for these experiments were acetic acid (pH 5 & 5.5), MES (pH 6 & 6.5), $NaH_2PO_4$ (pH 7 & 7.5), Tris (pH 8 & 8.5) and

$H_3BO_3$ (pH 9). The protein concentration after mixing with $a_6Ru^{2+}$ was ~5 μM. Experiments were done at six different concentrations of $a_6Ru^{2+}$; 0.625, 1.25, 2.5, 5, 10 and 20 mM.

Initial sets of experiments gave irregular results. The cause of this problem was unclear. The stability of the $a_6Ru^{2+}$ was characterized by monitoring the UV-Vis spectrum as a function of time at 1, 5, 10 and 20 mM concentrations in different buffers. The buffers used for these studies were MES, pH 6 and sodium phosphate, ammonium sulphate, ammonium acetate, MOPS and ammonium phosphate at pH 7.5, all at a concentration of 10 mM. These studies suggested either gradual oxidation of $a_6Ru^{2+}$ with time or substitution of ammonia ligands. At long times (30-90 mins), a color change from yellow to magenta was sometimes observed. Studies have suggested this color change could be due to the formation of Ru (IV) species or acid catalyzed substitution reactions [126]. In order to minimize substitution reactions or oxidation, experiments were done with minimal delay, i.e., from the time of weighing $a_6Ru^{2+}$ and preparation of solution under anaerobic conditions to actual experiments.

Also the electronic absorption spectrum (250 - 500 nm) was taken for $a_6Ru^{2+}$ prepared in the argon-purged buffer, before and after the experiment to measure the actual $a_6Ru^{2+}$ concentration. Direct concentration measurements turned out to be the critical factor in obtaining reproducible plots of $k_{obs}$ versus $a_6Ru^{2+}$ concentration. Concentration calculated from absorbance at 390 nm ($\varepsilon_{390}$ = 35 $M^{-1}$ $cm^{-1}$) and 400 nm ($\varepsilon_{390}$ = 30 $M^{-1}$ $cm^{-1}$) [127, 128] were averaged to obtain the concentration of $a_6Ru^{2+}$.

Reduction of the heme after mixing the AcH73 variant with $a_6Ru^{2+}$ was monitored at 550 nm. At each concentration of $a_6Ru^{2+}$, five kinetic traces were collected. For all

traces, 5000 points were collected logarithmically on a 50 sec time scale. Analysis of the data was done using the curve fitting program, Sigma Plot (v.7.0). The data were fit to a quadruple exponential rise to maximum equation for the 50 sec time scale data.

### *3.2.10 NMR Studies.*

NMR studies on the oxidized AcH73 variant were done at 25 $^{o}$C, with ~1 mM protein concentration in 0.1 M NaCl $D_2O$ solution as described previously in the Materials and Methods section 2.2.7 of Chapter 2. Spectra were obtained with 500 MHz and 600 MHz Varian Direct Drive NMR spectrometers at the University of Montana with 512 and 1024 scans, respectively, and sweep widths of 35714.3 and 46296.3 Hz, respectively. The residual HOD signal was suppressed using the pre-saturation or Watergate pulse sequences.

## 3.3 Results

### *3.3.1 Global Unfolding by GdnHCl Denaturation.*

The overall stability of the AcH73 variant of iso-1-cytochrome *c* was determined by gdnHCl denaturation monitored by circular dichroism (CD) (figure 3.2, open circles). The experiments were done at pH 7.5, so that His73 would be predominantly deprotonated. The fit to the data (eq 2.1, Materials and Methods section 2.2.4 of Chapter 2) gives $\Delta G^{o}_{u}(H_2O)$ = 2.02 ± 0.15 kcal/mol, $m$ = 2.68 ± 0.21 kcal/(mol×M) and a titration midpoint, $C_m$ = 0.75 ± 0.05 M. These values compare well to those observed previously for this variant ($\Delta G^{o}_{u}(H_2O)$ = 2.25 ± 0.04 kcal/mol, $m$ = 2.79 ± 0.09, $C_m$ = 0.81 ± 0.01 M see *ref* [83].

### *3.3.2 Partial Unfolding by GdnHCl.*

Partial unfolding of the AcH73 variant was studied at pH 7.5 using increasing concentrations of gdnHCl; the loss of Met80-heme ligation was monitored at 695 nm. At pH 7.5, absorbance at 695 nm was very low as shown in figure 3.2 (open squares) in the form of millimolar extinction coefficient. The fit to the data (eq 2.2, Materials and Methods section 2.2.5 of Chapter 2) gives $\Delta G^{o}_{u}(H_2O)$ = -0.78 ± 0.05 kcal/mol, and $m$ = 1.56 ± 0.27 kcal/(mol×M). Partial denaturation studies were further carried out at pH 5 (figure 3.2, open triangles). The fit to the data (eq 2.2, Materials and Methods section 2.2.5 of Chapter 2) gives $\Delta G^{o}_{u}(H_2O)$ = 2.01 ± 0.15 kcal/mol, and $m$ = 3.66 ± 0.29 kcal/(mol×M). The $\Delta G^{o}_{u}$ value is more negative at pH 7.5 suggesting that His73 binding to heme is more favorable at this pH than at pH 5. The $m$-value is less at pH 7.5 as compared with the value at pH 5, suggesting that at pH 5 unfolding monitored at 695 nm more closely corresponds to global unfolding.

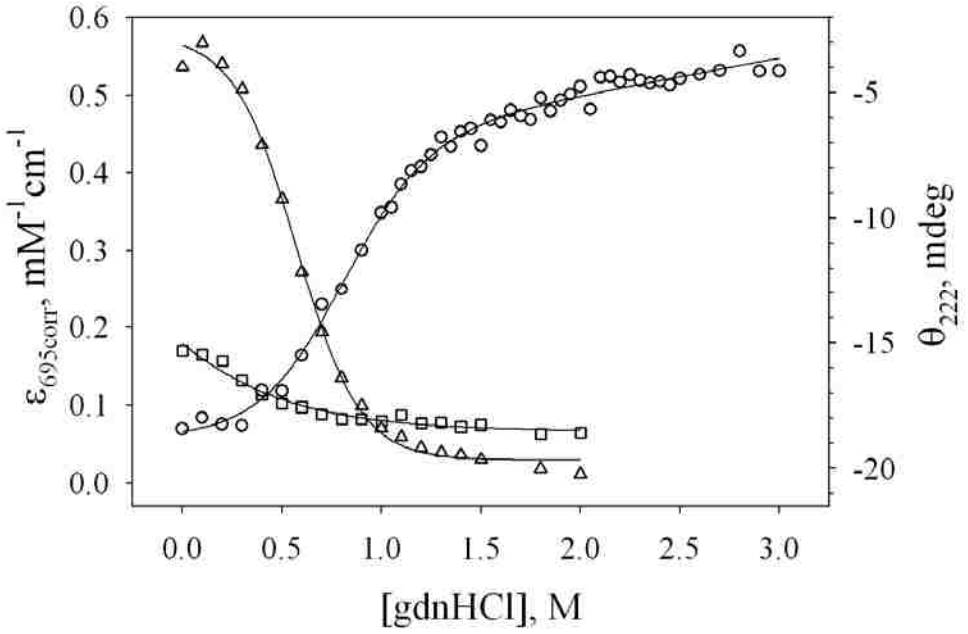


**Figure 3.2** Plot of ellipticity observed at 222 nm as a function of gdnHCl concentration (○) for the AcH73 variant of iso-1-cyt *c*. Data were acquired at 25 ºC in 20 mM Tris, pH 7.5, 40 mM NaCl and 4 μM protein concentration. The solid curve is a fit of the data to eq 2.1 in the Materials and Methods section 2.2.4 of Chapter 2. Plot of $\varepsilon_{695corr}$ versus gdnHCl concentration for AcH73 iso-1-cyt *c*. Data were acquired at room temperature (22 ± 1 ºC) in the presence of 20 mM sodium acetate, pH 5.0, 40 mM NaCl (Δ) and 20 mM Tris, pH 7.5, 40 mM NaCl (□).The solid curves are fits of the data to eq 2.2 as described in Materials and Methods section 2.2.5 of Chapter 2.

### *3.3.3 pH Dependence of the Stability of the Native Heme-Met80 Conformer.*

The conformational transition caused by His73 was monitored as a function of pH and gdnHCl concentration using the 695 nm absorbance band, which is sensitive to the presence of heme-Met80 ligation. A loss in this band is observed which is associated with the alkaline transition. pH titration at 0 and 0.1 M gdnHCl were initiated at pH 5.7 and not lower as the AcH73 variant tended to aggregate at lower pH. The AcH73 variant shows a biphasic pH titration curve at all gdnHCl concentrations (figure 3.3), which was readily fitted to eq 3.1 (Materials and Methods). The low pH phase of the transition does

not completely eliminate the 695 nm band and in the higher pH phase of the transition, the 695 nm band is completely lost. Background subtraction was used to correct for light scattering due to a small amount of aggregation owing to the low stability of the protein. Forward and backward pH titrations were performed with the same sample at 0.1, 0.2 and 0.3 M gdnHCl (figure 3.4) to check the robustness of this method of analysis. Good agreement between thermodynamic parameters from forward and backward pH titration was observed (Table 3.1) indicating that the effect of light scattering due to a small amount of aggregation is adequately removed by background subtraction. Thermodynamic parameters are summarized in Table 3.2.

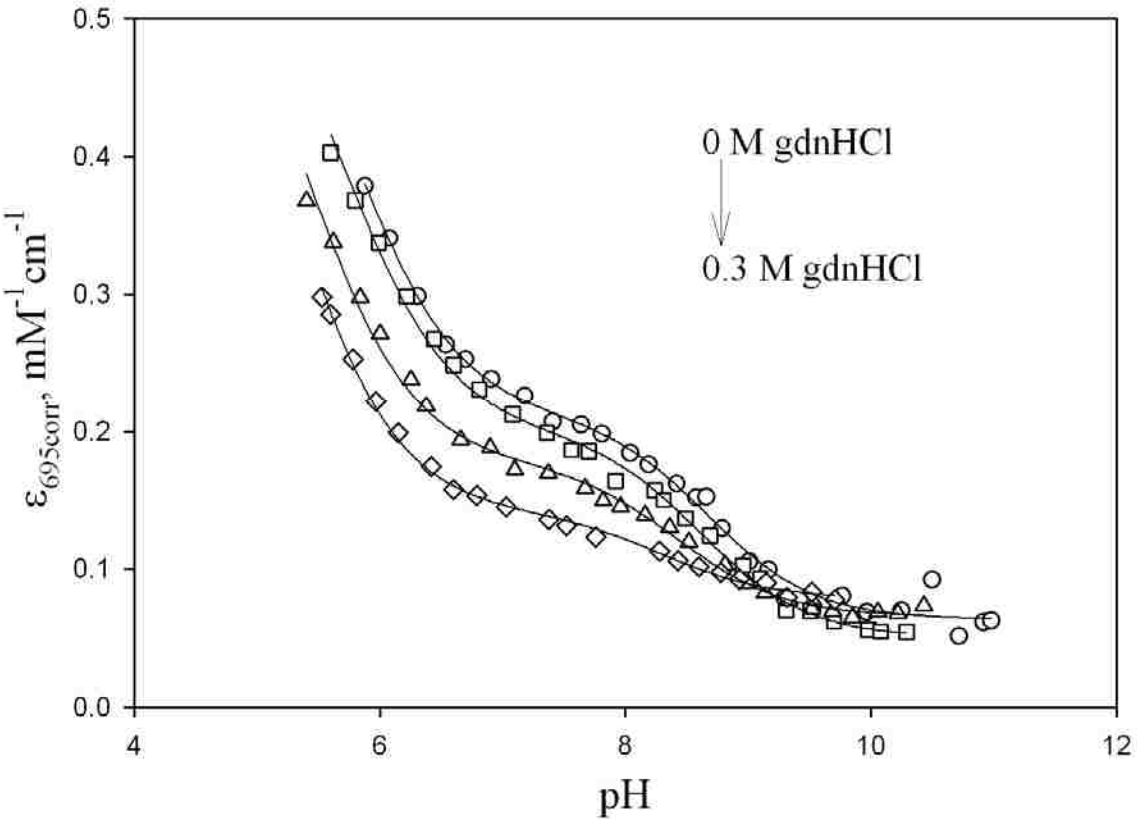


**Figure 3.3** Plot of $\varepsilon_{695corr}$ versus pH for AcH73 iso-1-cytochrome *c* at different concentrations of gdnHCl. Data were collected at room temperature (22 ± 1 ºC) in 0.1 M NaCl with 0 (○), 0.1 (□), 0.2 (Δ) and 0.3 (◊) M gdnHCl. The solid curves are fits to eq 3.1 as described in Materials and Methods.

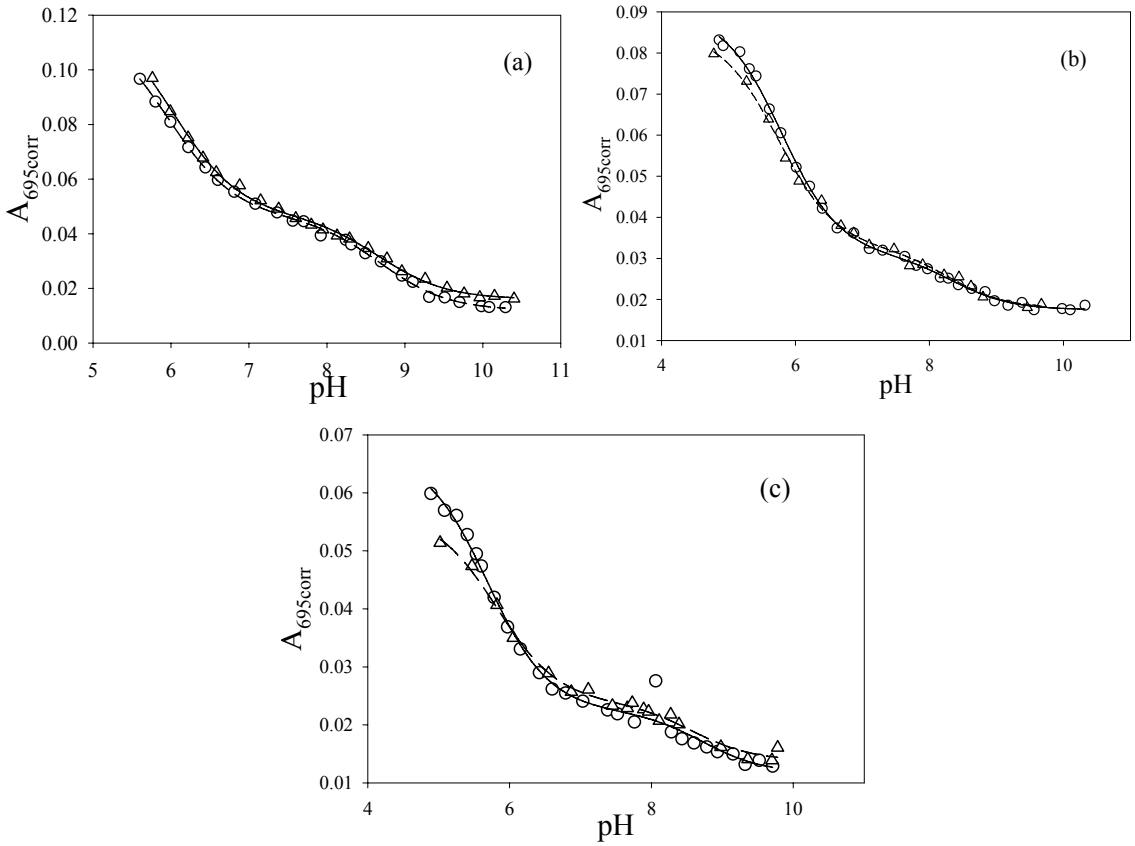


**Figure 3.4** Plot of $A_{695\ corr}$ versus pH for AcH73 iso-1-cytochrome *c* at room temperature (22 ± 1 ºC) in 0.1 M NaCl in the presence of (a) 0.1 M, (b) 0.2 M and (c) 0.3 M gdnHCl showing forward (○) and backward (Δ) titration curves for the sample. The solid curves are fits to eq 3.1 as described in Materials and Methods.

**Table 3.1.** Thermodynamic parameters from pH titration in 0.1 M NaCl at 25 ºC for the AcH73 variant of iso-1-cytochrome *c*.[a]

| [gdnHCl] (M) | p$K_{C1}$ | p$K_{H1}$ | p$K_{C2}$ |
|---|---|---|---|
| 0.1 (Forward) | -0.44 ± 0.08 | 6.29 ± 0.17 | -2.92 ± 0.50 |
| 0.1 (Backward) | -0.66 ± 0.18 | 6.21 ± 0.31 | -3.04 ± 0.43 |
| 0.2 (Forward) | -0.74 ± 0.20 | 6.28 ± 0.24 | -3.33 ±0.24 |
| 0.2 (Backward) | -0.91 ± 0.08 | 6.19 ± 0.26 | -3.51 ± 0.27 |
| 0.3 (Forward) | -0.84 ± 0.07 | 6.37 ± 0.18 | -3.32 ± 0.09 |
| 0.3 (Backward) | -0.99 ± 0.22 | 6.11 ± 0.16 | -3.63 ± 0.24 |

[a] Parameters are average and standard deviation from three trials for fits to eq 3.1 in Materials and Methods.

**Table 3.2.** Thermodynamic parameters from pH titration in 0.1 M NaCl at 25 ºC for the AcH73 variant of iso-1-cytochrome *c*.[a]

| [gdnHCl] (M) | p$K_{C1}$ | p$K_{H1}$ | p$K_{C2}$ |
|---|---|---|---|
| 0 | -0.41 ± 0.02 | 6.16 ± 0.14 | -2.58 ± 0.08 |
| 0.1 | -0.53 ± 0.17 | 6.25 ± 0.22 | -2.97 ± 0.44 |
| 0.2 | -0.81 ± 0.15 | 6.24± 0.24 | -3.40 ± 0.25 |
| 0.3 | -0.91 ± 0.17 | 6.24 ± 0.21 | -3.48 ± 0.23 |

[a] Parameters are average and standard deviation from both forward and backward trials at 0.1 to 0.3 M gdnHCl and for three trials at 0 M gdnHCl from fits of the data to eq 3.1 in Materials and Methods.

The value of p$K_{H1}$ at all gdnHCl concentrations is between 6 and 6.3, consistent with a histidine and is not strongly sensitive to gdnHCl concentration. The values of both p$K_{C1}$ (His 73-heme alkaline conformer) and p$K_{C2}$ (Lys79-heme alkaline conformer) become progressively more negative (i.e, more favorable) as the gdnHCl concentration increases, as expected. If a linear free energy relationship is assumed for this alkaline transition (eq 3.3); *m* values of 2.4 ± 0.3 and 4.2 ± 0.8 kcal/ (mol×M) (figure 3.5) are obtained for the His 73-heme and Lys 79-heme alkaline conformers, respectively.

**Equation 3.2**

$$\Delta G_u = \Delta G_u^{\circ}(H_2O) - m[gdnHCl]$$

The *m* value indicates that structural disruption for the higher pH phase is greater than that in the lower pH phase of the alkaline transition, as the *m*-value correlates strongly with the amount of protein surface exposed to solvent upon unfolding [129]. Calculations were also done using a p$K_{H2}$ of 9.4 and 11.7 (values obtained from pH jump data Table 3.3.). No significant changes were observed for the p$K_{H1}$ of His, p$K_{C1}$ and the *m*-value derived from the slope of $\Delta G^{o}_{u}(H_2O)$ versus gdnHCl concentration plots (with p$K_{H2}$ = 11.7, *m*-values obtained are 2.4 ± 0.3 and 4.5 ± 0.8; with p$K_{H2}$ as 9.4, *m*-values obtained

are 3.2 ± 0.9 and 5.3 ± 1.3). Thus, the choice of p$K_{H2}$ has minimal effect on the *m*-values obtained from these data.

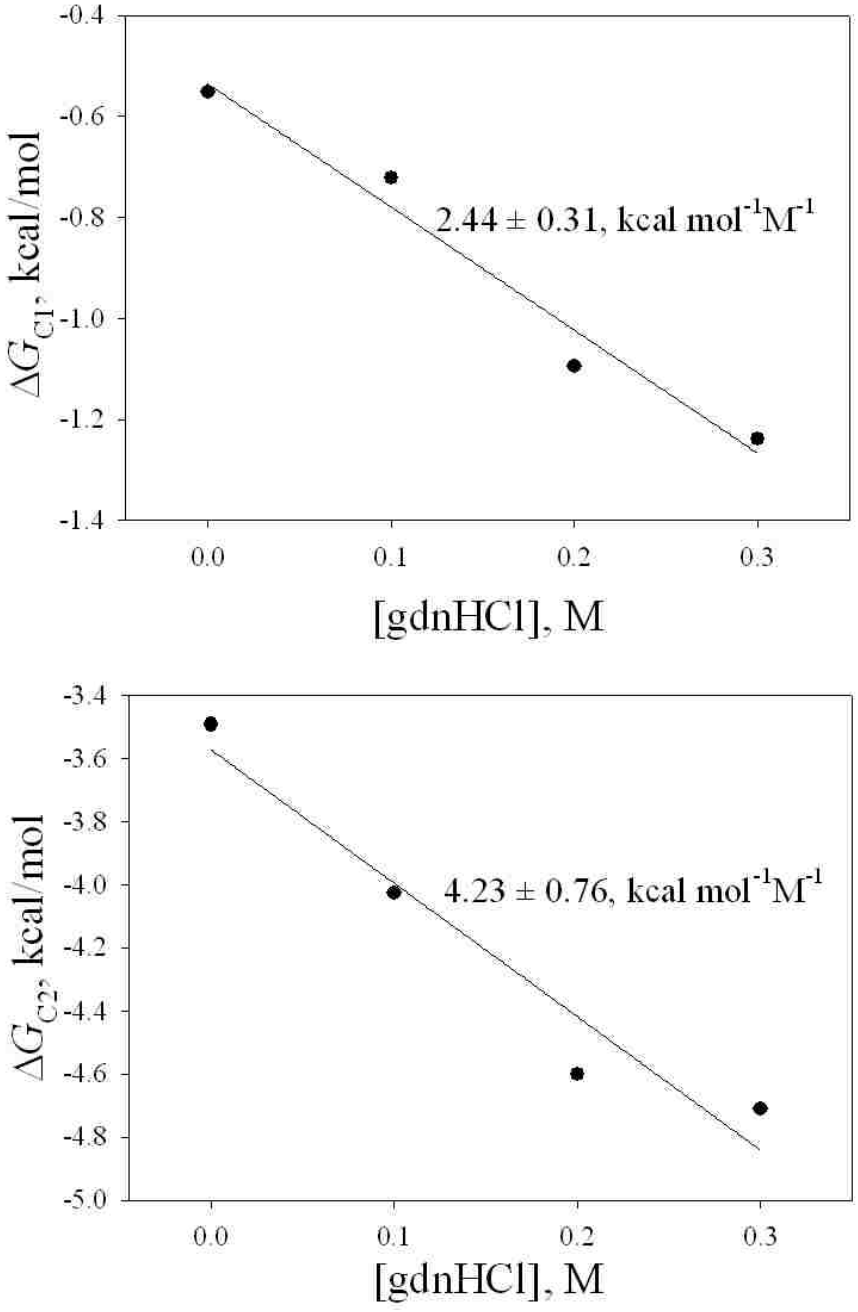


**Figure 3.5** Plots of Free Energy versus gdnHCl concentration for the AcH73 variant of iso-1-cyt *c*. The free energies, $\Delta G_{C1}$ and $\Delta G_{C2}$ represent formation of the His73-heme and Lys79-heme alkaline conformers, respectively. $\Delta G$ values were calculated as $\Delta G = 2.303RTpK$.

### *3.3.4 Alkaline transition monitored in the region from 350 to 450 nm wavelength.*

Monitoring absorbance in the region from 350 to 450 nm allows the alkaline transition to be measured at much lower protein concentration using the intense heme Soret band near 400 nm. The heme Soret band occurs in the 380-450 nm wavelength region [130, 131]. At lower protein concentration, we were able to observe spectral changes from pH 1.97 to 11.05 without problems with protein aggregation. Figures 3.6 (a) – (d) show the presence of four distinct isosbestic points suggesting that the acid transition is complicated. Figures 3.6 (e) and (f) shows that the alkaline region gives two sets of isosbestic points, suggesting that two different states are populated in this pH region. Two isosbestic points (~382 and 412 nm) are observed from pH 5.34 to 6.6 and one isosbestic point (~414 nm) is observed from pH 6.78 to 11.05. These data are comparable to the data obtained with the K73H variant of iso-1-cyt *c* as seen in *ref* [23]. For better insight into the acid and alkaline transitions [23, 100, 132] absorbance at 380 and 398 nm are plotted as a function of pH (figure 3.7). These were plotted separately for the acidic and basic region for simplicity for both absorbance at 380 and absorbance at 398 nm.

Figure 3.7 (a) and 3.7 (c) show the acid transition which is fitted to the Henderson-Hasselbalch equation (eq 3.3 [23, 132]).

**Equation 3.3**

$$A_{\lambda} = \frac{A_N + \left(A_{Acid}\left(10^{n[pK_{app} - pH]}\right)\right)}{1 + \left(10^{n[pK_{app} - pH]}\right)}$$

where $A_{\lambda}$, is the absorbance at 380 or 398 nm, $A_N$ is the absorbance of the native state (also considered to be the low spin state), $A_{acid}$ is the absorbance of the acid state (also considered to be the high spin state), $n$ is the number of protons involved in the transition,

p$K_{app}$ is the apparent p$K_a$ for the transition. The non-coincidence of the p$K_{app}$ at the two different wavelengths is consistent with the plots in figure 3.6 which indicate that the acid transition is not two-state.

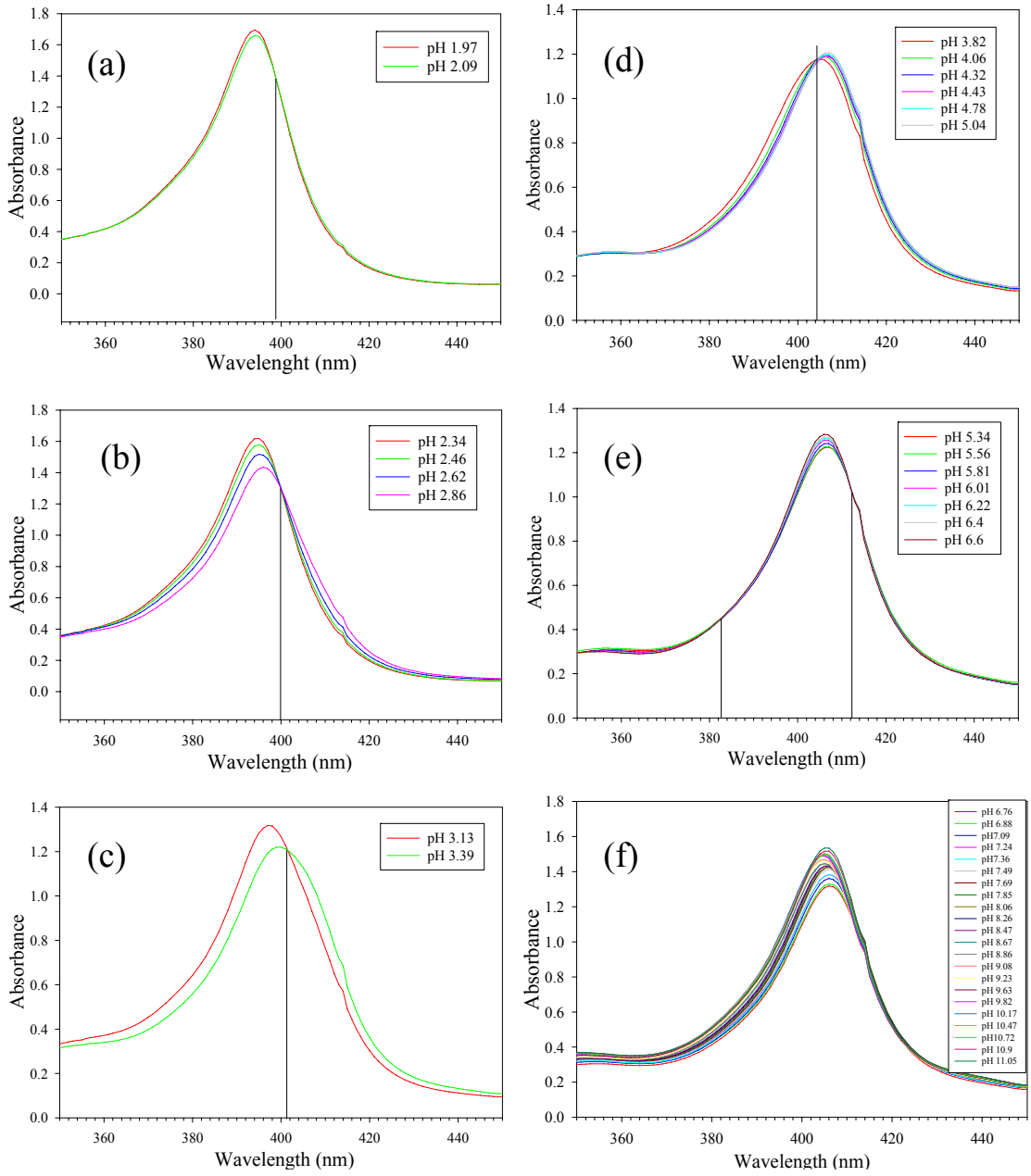


**Figure 3.6** Plot of absorbance spectra as a function of pH for the AcH73 variant of iso-1-cyt *c* at 22 ± 1 ºC in the presence of 0.1 M NaCl. (a) pH 1.97 – 2.09 (398 nm) (b) pH 2.34 – 2.86 (402 nm) (c) pH 3.13 – 3.39 (400 nm) (d) pH 3.82 – 5.04 (404 nm) (e) pH 5.34 – 6.6 (382 and 412 nm) and (f) pH 6.78 – 11.05 (414 nm). Isosbestic points are given in parentheses for each pH range.

The parameters from the fits are shown in Table 3.3 for both wavelengths ($A_{380}$ and $A_{398}$). The number of protons involved in the acid transition is more than 1, consistent with previous data showing that the acid transition is a multi-proton process [44].

Figure 3.7 (b) and (d) show the alkaline transition data fitted to eq 17 from *ref* [23], which is similar to equation 3.1 in the Materials and Methods. The values obtained from the fits for both the wavelengths ($A_{380}$ and $A_{398}$) are shown in Table 3.4. The parameters in Table 3.2 are more reliable because 695 nm monitors loss of Met80-heme ligation directly. At 380 and 398 nm the extinction coefficients may differ for the Lys-heme and His-heme conformers and the relative amplitudes of the two phases are unlikely to be directly related to the relative concentrations of the species.

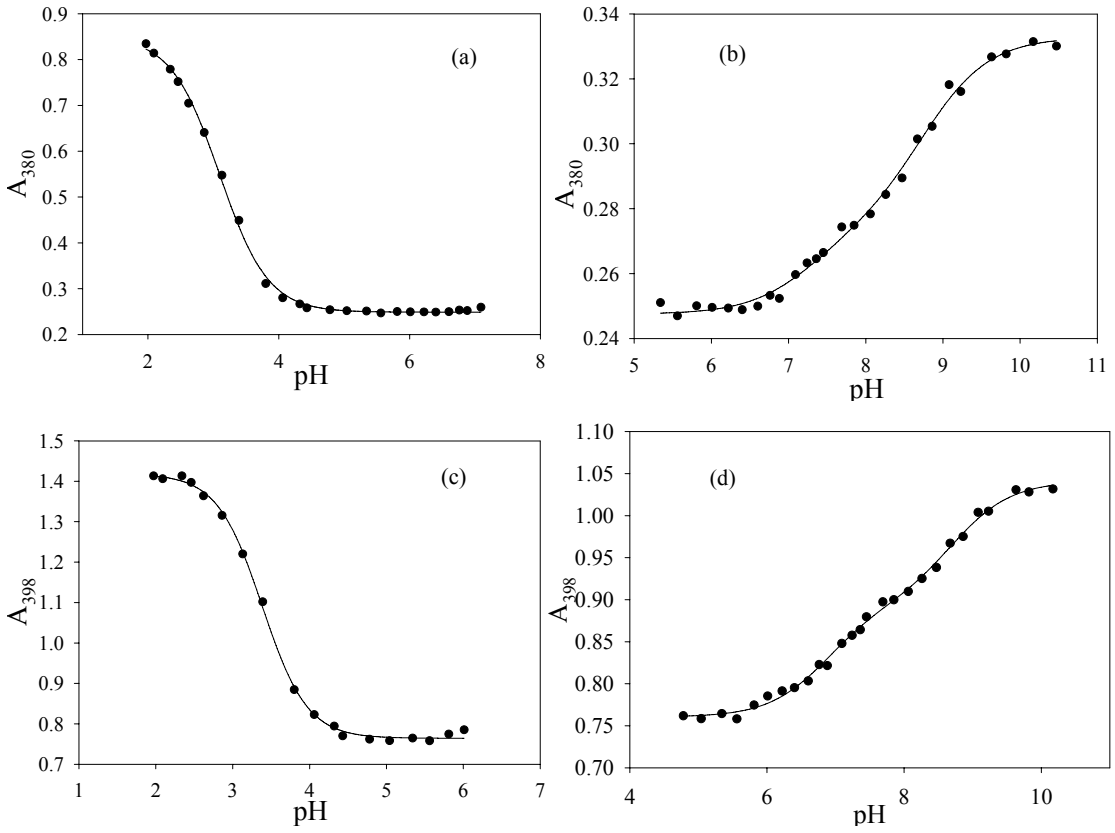


**Figure 3.7** Plots of absorbance in the (a) acid and (b) basic regions at 380 nm and in (c) acid and (d) basic regions at 398 nm as a function of pH for the AcH73 variant of iso-1-cyt *c* at 22 ± 1 ºC in the presence of 0.1 M NaCl.

**Table 3.3** Thermodynamic Parameters from pH titration of AcH73 on fitting the acidic region data from pH ~2 to ~7 for $A_{380}$ and pH ~2 to ~6 for $A_{398}$ to the Henderson-Hasselbalch equation.

| Absorbance wavelength | n | p$K_{app}$ |
|---|---|---|
| 380 nm | 1.43 ± 0.23 | 3.14 ± 0.04 |
| 398 nm | 1.96 ± 0.40 | 3.38 ± 0.02 |

**Table 3.4** Thermodynamic Parameters from pH titration of AcH73 on fitting the alkaline region data from to a model involving two ligands with different p$K_H$'s.

| Absorbance wavelength | p$K_{C1}$ | p$K_{H1}$ | p$K_{C2}$* |
|---|---|---|---|
| 380 nm | 0.44 ± 0.04 | 7.46 ± 0.20 | -1.91 ± 0.30 |
| 398 nm | 0.11 ± 0.04 | 7.09 ± 0.02 | -2.09 ± 0.30 |

*p$K_{H2}$ was set to 10.8 as in *ref* [23]

### *3.3.5 Stopped–Flow Kinetic Studies of the Alkaline Transition for the K79H Variant of Iso-1-cyt c.*

For upward pH jumps, an initial pH of 5 was used, since the population of the native state of the AcH73 is maximal near this pH. Data were collected from final pHs of 5.8 to 11.2. For downward pH jumps, the initial pH was set to 7.8 (to focus on the kinetics due to the His73-heme conformer, which is dominant in this pH region) and data were collected from pH 5 to 6.4. Representative traces of downward and upward pH jumps are shown in figure 3.8.

Two kinetic phases are observed; a fast and a slow phase. The pH dependence of these phases is shown in figures 3.9 and 3.10. The amplitude of the fast phase increases from pH 5.8 to 8 (figure 3.9b) as expected for the His73-heme alkaline conformer, based on equilibrium pH titrations. Similarly, the amplitude for the slow phase grows from pH

8 to 11 (figure 3.10 inset), as expected for formation of a lysine-heme alkaline conformer. However, the rise in the amplitude of the slow phase is not as smooth as would be expected for a process promoted by a single proton ionization.

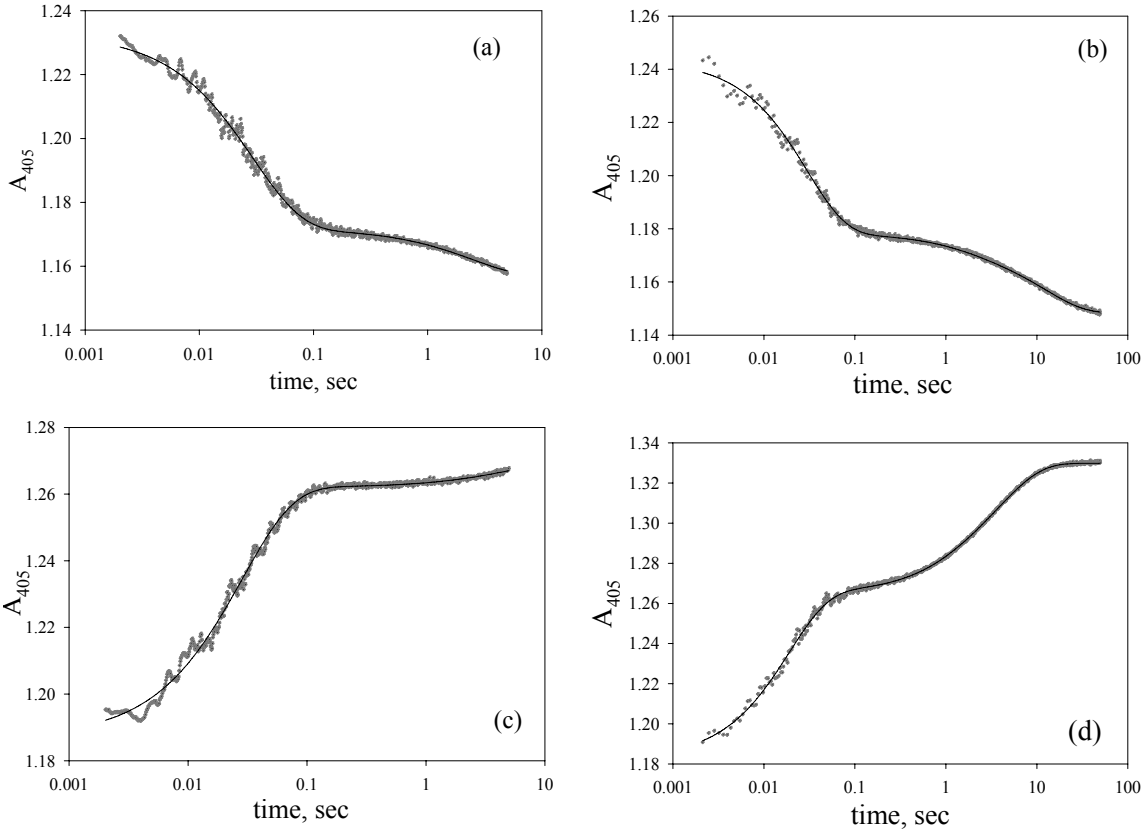


**Figure 3.8** Plots of absorbance at 405 nm as a function of time at 25 ºC for the AcH73 variant of iso-1-cyt *c*. (a) 5 s and (b) 50s time scale data for downward pH jump experiments ending at pH 5. (c) 5 s time scale data ending at pH 7.2 and (d) 50 s time scale data ending at pH 9 for upward pH jump experiments. Buffers all contain 0.1 M NaCl as described in the Materials and Methods. The time scale is logarithmic.

The rate constant and the amplitude data as a function of pH for both the fast and slow phases appear to be consistent with a single ionizable group triggering the alkaline transition [97]. Parameters from a fit to this model are shown in Table 3.5. A dramatic difference in the p$K_H$'s for the ionizable group is observed for the $k_{obs}$ and amplitude data

for the fast phase, yielding ~9.4 and ~6.4, respectively (see figure 3.9). The fit to the $k_{obs}$ data also indicates that $k_f$ is one half the magnitude of $k_b$. This is inconsistent with the thermodynamic data which indicate that $k_f$ should be about twice the magnitude of $k_b$ (p$K_{Cl}$ at 0 M gdnHCl is -0.41, see Tables 3.1 and 3.2). These results indicate that the kinetics is more complicated than the standard model for the alkaline conformational transition.

**Figure 3.9** On the next page are the plots of (a) rate constant and (b) amplitude data for the fast phase from 50 s data collected at 25 ºC as a function of pH in 10 mM buffer containing 0.1 M NaCl. Open circles are data from upward pH jump experiments and solid circles are data from downward pH jump experiments. The solid curve in panel A is a fit of upward and downward pH jump rate constants from pH 5 to 10.6 to eq 2.6 in the Materials and Methods, section 2.2.8 of Chapter 2. The solid curve in panel B is a fit of upward pH jump amplitudes from pH 5.8 to 10 to eq 2.7 in the Materials and Methods, section 2.2.8 of Chapter 2. Rate constants and amplitudes presented in this figure are collected in Tables B1, B3, and B5 in Appendix B.

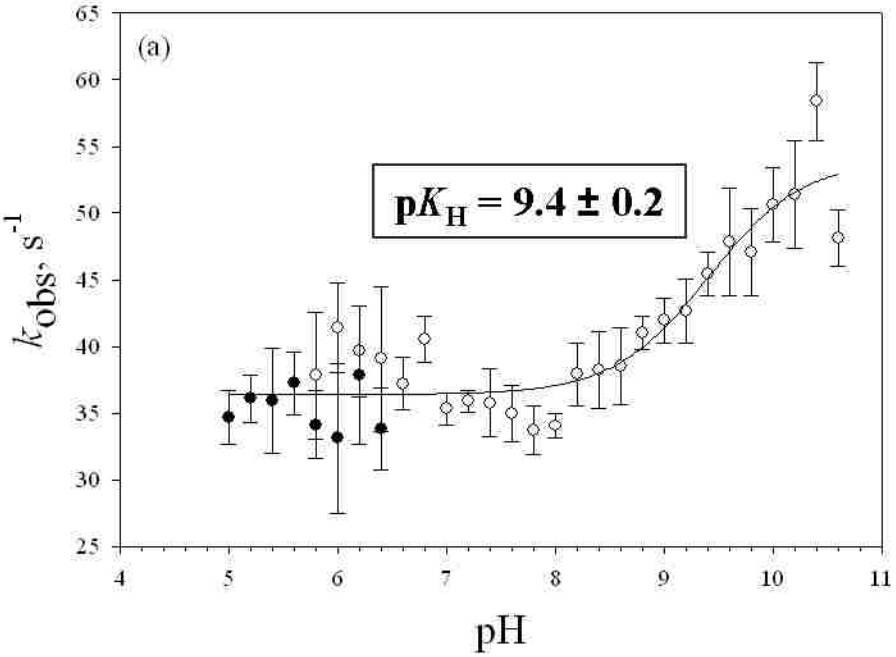


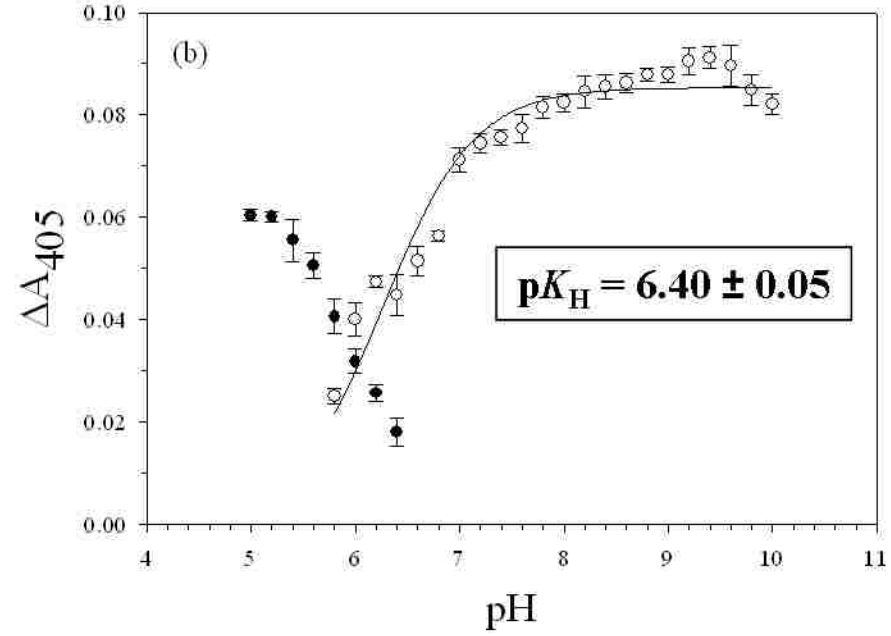


Fits of the slow phase $k_{obs}$ versus pH to the standard kinetic model, for the alkaline transition, (figure 3.10), yield a p$K_H$ for this ionization near 11.7. A range of values is observed for p$K_H$ for alkaline conformers involving lysine. In some variants of

iso-1-cyt *c*, p$K_H$ values observed are as low as 9 to 9.5 for lysine-heme alkaline conformers [59, 113]. In the WT protein, the p$K_H$ for Lys79 is 10.8, whereas p$K_H$ is 12 for Lys73 [48]. The amplitude versus pH data for the slow phase is not smooth. This behavior may result from an overlap in $k_{obs}$ for the Lys79 alkaline conformer at low pH with a proline isomerization phase associated with the His73-heme alkaline conformer (figure 3.10 inset).

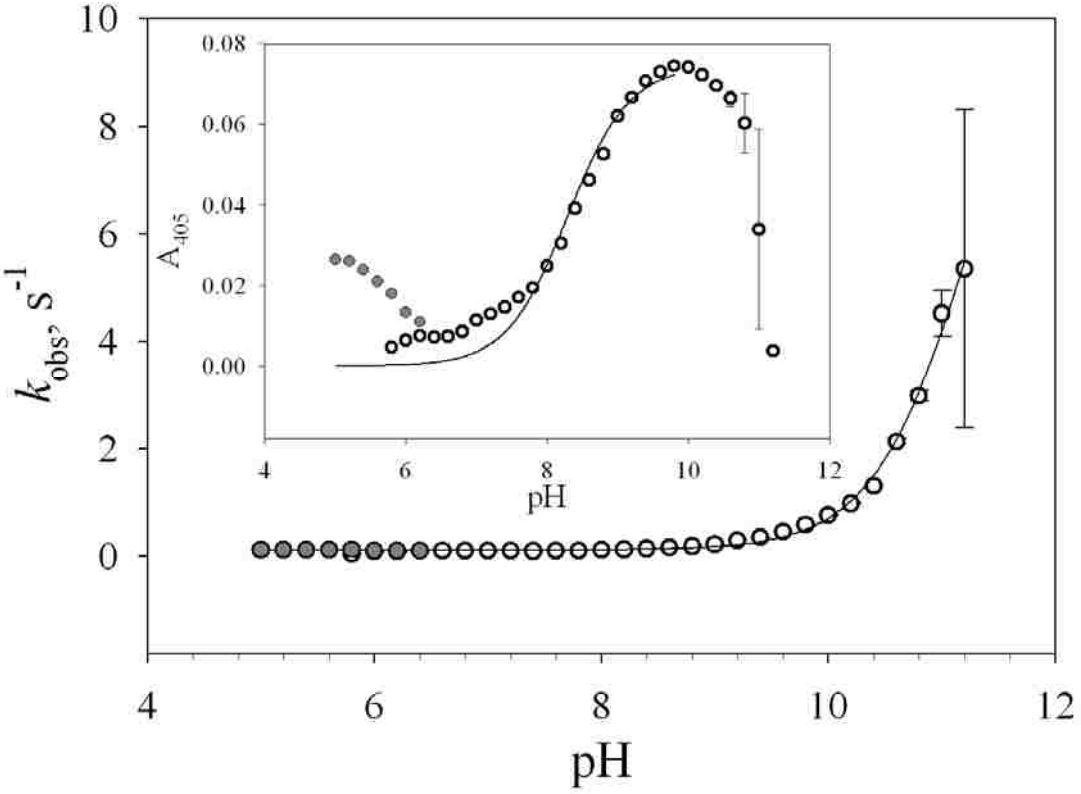


**Figure 3.10** Plots of rate constant and amplitude (inset) data for the slow phase from 50 s data collected at 25º C as a function of pH in 10 mM buffer containing 0.1 M NaCl. Open circles are data from upward pH jump experiments and filled circles are data from downward pH jump experiments. The solid curve is a fit of upward and downward pH jump rate constants from pH 5 to 11.2 to eq 2.6 in the Materials and Methods, section 2.2.8 of Chapter 2. Eq 2.7 from the Materials and Methods, section 2.2.8 of Chapter 2 is used to fit the amplitude data for upward pH jump experiments. The rate constants and amplitudes in this figure are collected in Tables B2, B4 and B6 in Appendix B.

**Table 3.5** Rate and ionization constants associated with the fast and slow phase of the alkaline transition of the AcH73 variant of iso-1-cyt *c*.

| Parameter | Fast phase[a] | Slow phase[b] |
|---|---|---|
| $k_{f1}$, $s^{-1}$ | 16.5 ± 1.8 | 11.7 ± 0.7 |
| $k_{b1}$, $s^{-1}$ | 35.5 ± 0.7 | 0.11 ± 0.01 |
| p$K_H$ ($k_{obs}$ data) | 9.4 ± 0.2 | 11.70 ± 0.04 |
| p$K_H$ (Amp. data) | 6.40 ± 0.05 | |

[a] Parameters are the average and standard deviation from three sets of $k_{obs}$ and amplitude versus pH data fit to eq 2.6 and 2.7, respectively, in the Materials and Methods, section 2.2.8 of Chapter 2. Two data sets were collected on a 5 s time scale and one on a 50 s time scale.

[b]Parameters are the average and standard deviation from the fits of $k_{obs}$ and amplitude versus pH data from two independent data sets to equations 2.6 and 2.7, respectively, in the Materials and Methods section 2.2.8 of Chapter 2. Both data sets were collected on a 50 s time scale

### *3.3.6 Anaerobic Stopped-Flow Kinetic Measurements.*

Electron transfer experiments were done at pH 5, 5.5, 6, 6.5, 7, 7.5, 8, 8.5 and 9. This covers the pH range of the His73-heme alkaline conformational transition observed in pH-jump kinetic studies and thermodynamic studies. Protein at each pH was mixed in a 1:1 ratio with six different concentrations of $a_6Ru^{2+}$, as described in the Materials and Methods. Reduction of the protein was followed via the increase in the absorbance at 550 nm as shown in figure 3.11. Fits to three and four exponential rise equations were done. The latter gave significantly improved residuals (Appendix B, figure B1).

The rate constant $k_1$ for the fastest phase was plotted as a function of $a_6Ru^{2+}$ concentration as shown in figure 3.12. The fast phase rate constant showed a linear dependence on $a_6Ru^{2+}$ concentration for all pH's ranging from 5 to 9.

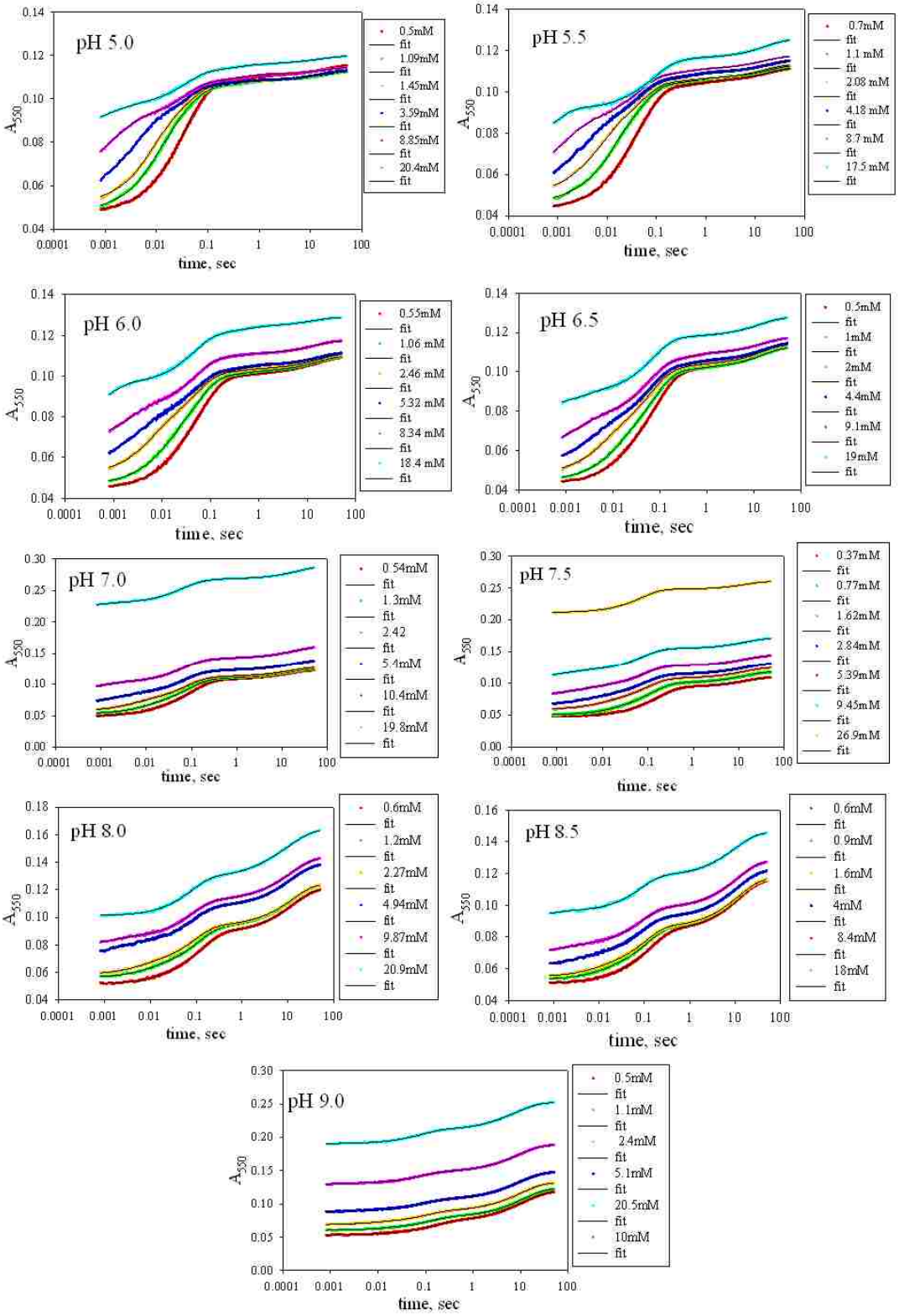


**Figure 3.11** Plots of absorbance at 550 nm versus time (on logarithmic scale) for reduction of the AcH73 variant of iso-1-cyt *c* with $a_6Ru^{2+}$ from pH 5 to pH 9, at different [$a_6Ru^{2+}$].

This phase is attributed to the bimolecular ET reaction of $a_6Ru^{2+}$ with the native Met80-heme ligation state of the native conformer and is used to determine the ET rate constant, $k_{ET}$, using equation 3.3 (see figure 3.14) as shown in figure 3.12. Values for the highest concentration i.e., 20 mM for fast phase are not included in the graphs in figure 3.12 due to the relatively large errors in $k_1$ at this concentration of $a_6Ru^{2+}$. At 20 mM $a_6Ru^{2+}$, most of the amplitude occurs in the mixing dead time, as can be seen from figure 3.11. An increase in the background absorbance due to $a_6Ru^{2+}$ is also apparent at 20 mM $a_6Ru^{2+}$ in figure 3.11.

**Equation 3.3**

$$k_{obs} = k_{ET}[a_6Ru^{2+}]$$

The ET rate constant shows a decrease in magnitude with increased pH (figure 3.13). It is unclear whether this is a real decrease or an artifact of the decreased amplitude of the fast phase at higher pH where the population of the native state is low.

**Figure 3.12** On the next page, are plots of observed rate constant $k_{obs}$ ($s^{-1}$) for the reaction of $a_6Ru^{2+}$ with the native conformer of the AcH73 variant (fast phase) at 25 ºC as a function of $[a_6Ru^{2+}]$ for pH 5, 5.5, 6, 6.5, 7, 7.5, 8, 8.5 and 9; Buffers are 10 mM and contain 0.1 M NaCl. The values for $k_{obs}$ represents the fast phase ($k_1$) obtained from the fits shown in figure 3.11 and the solid line is a fit to Eq. 3.3. The rate constants shown in this figure are collected in appendix B, Table B7.

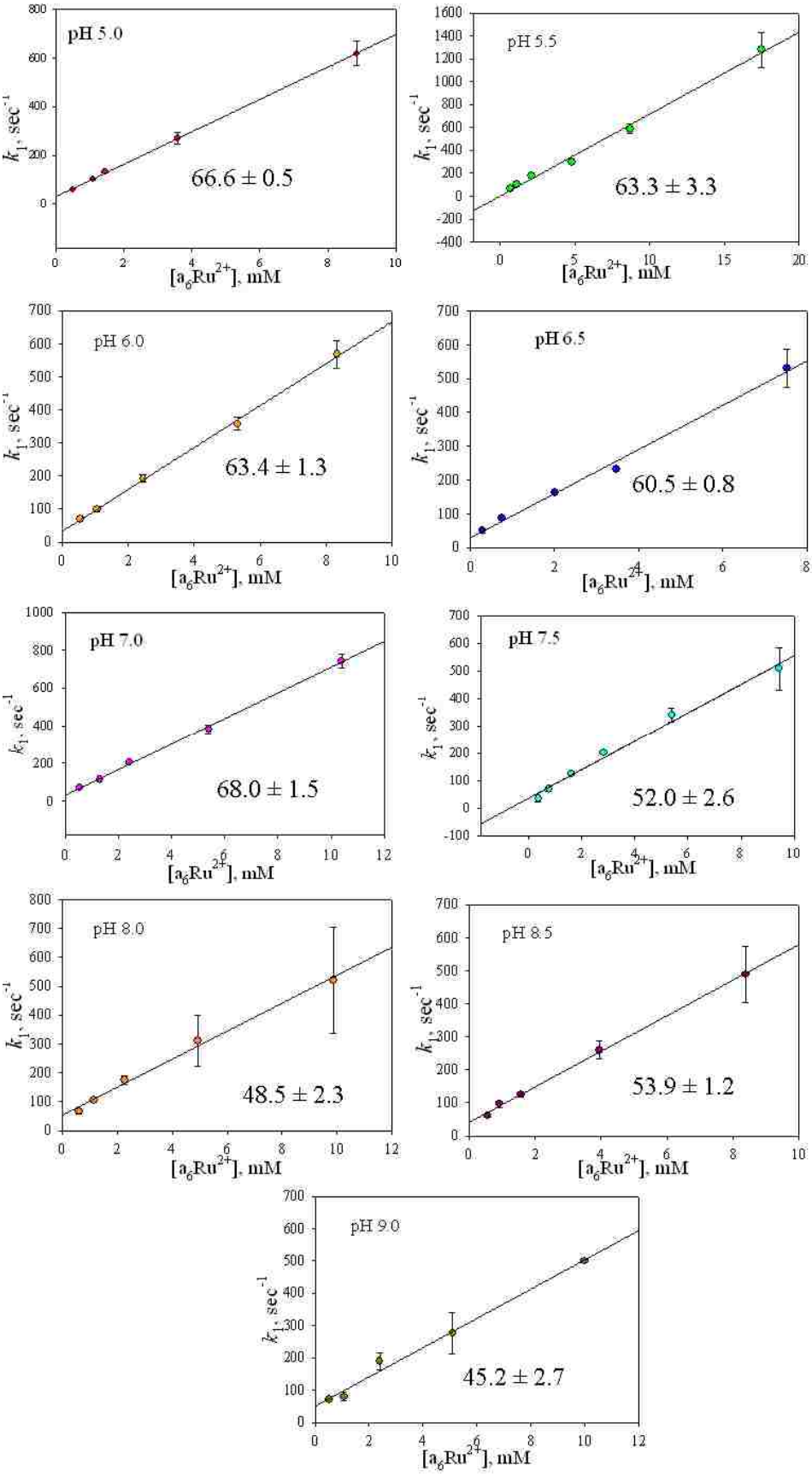
pH 5.0
66.6 ± 0.5
pH 5.5
63.3 ± 3.3
pH 6.0
63.4 ± 1.3
pH 6.5
60.5 ± 0.8
pH 7.0
68.0 ± 1.5
pH 7.5
52.0 ± 2.6
pH 8.0
48.5 ± 2.3
pH 8.5
53.9 ± 1.2
pH 9.0
45.2 ± 2.7
$k_1$, sec$^{-1}$
[$a_6Ru^{2+}$], mM

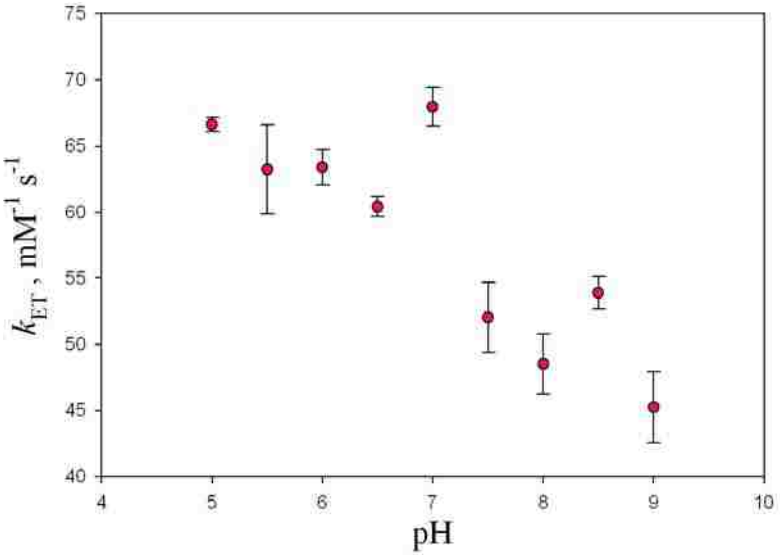


**Figure 3.13** Plot of ET rate constant, $k_{ET}$ ($mM^{-1}s^{-1}$), as a function of pH. The values for $k_{ET}$ are obtained from fits to eq. 3.3 as shown in figure 3.12.

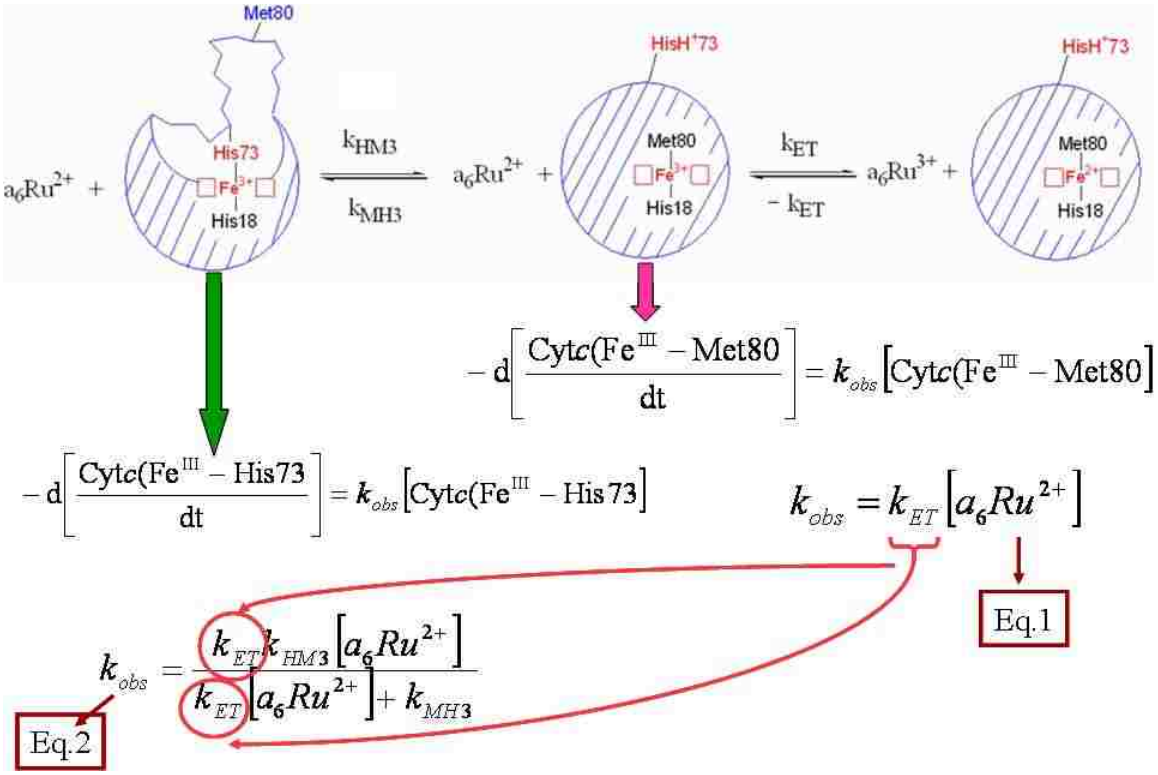


**Figure 3.14** Gated Electron Transfer Kinetic Mechanism.

The first intermediate phase $k_2$, showed saturation behavior as a function of $a_6Ru^{2+}$ concentration from pH 5 to pH 9 as shown in figure 3.15. The solid lines are fits to the eq 3.4 from figure 3.14,

**Equation 3.4**

$$k_{obs} = \frac{k_{ET} k_{HM3} [a_6 Ru^{2+}]}{k_{ET} [a_6 Ru^{2+}] + k_{MH3}}$$

where $k_{obs}$ is the observed rate constant for the reaction of $a_6Ru^{2+}$ with the native conformer of the AcH73 variant (first intermediate phase, $k_2$), $k_{HM3}$ is the rate for formation of Met80-heme ligated native state from the His73-heme ligated alkaline state and $k_{MH3}$ is the reverse rate of this reaction. These values for $k_{HM3}$ and $k_{MH3}$ are plotted as a function of pH as shown in figure 3.24 (values of micro-constant $k_{HM3}$ and $k_{MH3}$ are collected in Appendix B, Table B11).

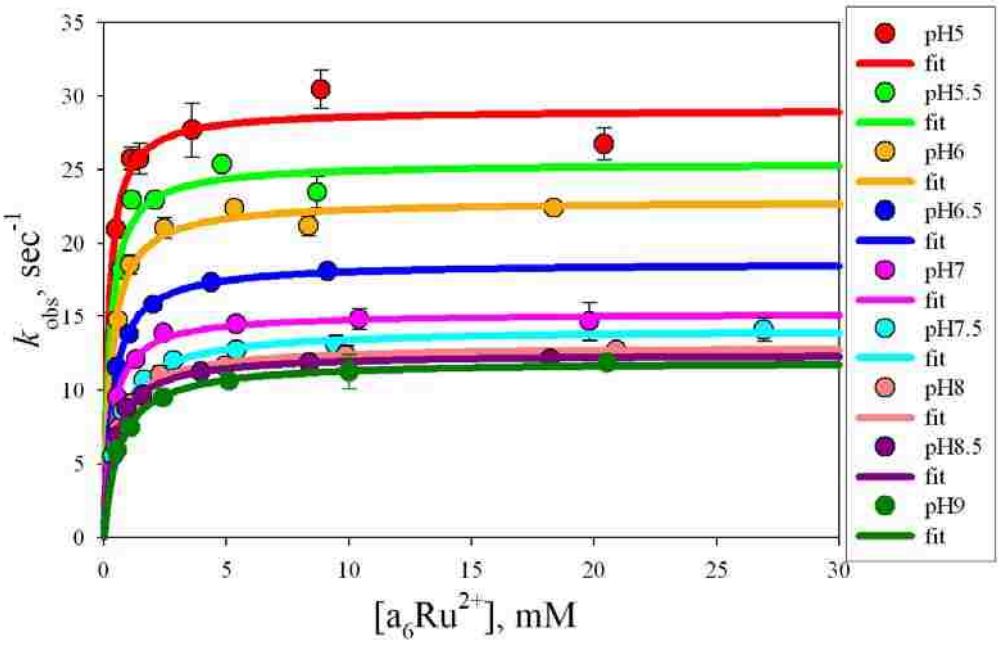


**Figure 3.15** Plots of observed rate constant $k_{obs}$ ($s^{-1}$) for the reaction of $a_6Ru^{2+}$ with the AcH73 variant (intermediate phase, $k_2$, values are collected in Appendix B, Table B8) as a function of [$a_6Ru^{2+}$] for pH 5 – 9 in 10 mM buffers containing 0.1 M NaCl, and at 25 ºC. The values for $k_{obs}$ represent the intermediate phase ($k_2$) obtained from fits shown in figure 3.11 and the solid lines are fits to eq 3.4 which gives values for $k_{HM3}$ and $k_{MH3}$ as shown in figure. 3.14.

The second intermediate phase, $k_3$, also demonstrates saturation behavior (Appendix B, Table B9). The plateau value shows little variation in magnitude from pH 5 to pH 7 (figure 3.16a). A decrease in plateau value of $k_3$ is seen above pH 7. The low amplitude of this phase leads to some irregularity in the pH dependence of the data (see figure 3.15a). This second intermediate phase may be due to a conformer of the AcH73 variant with a high spin heme state resulting from $H_2O/OH^-$ binding in the 6$^{th}$ coordination site. However, we could find no clear evidence of an absorbance band between 620 and 650 nm typical for a high spin heme. The inability to see this band could be due to the low population of this form of the protein (figure 3.17).

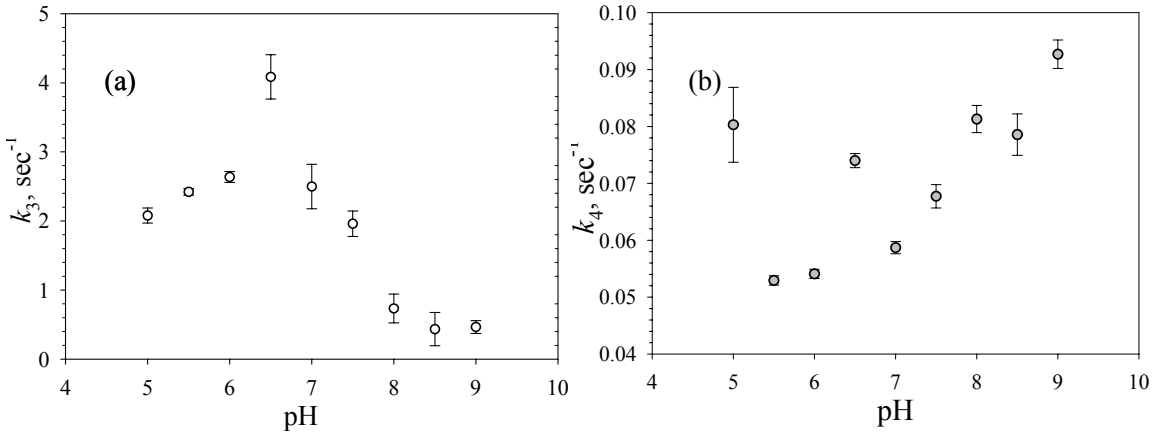


**Figure 3.16** Plots of (a) second intermediate phase ($k_3$) and (b) slowest phase ($k_4$) from fits to equation 3.2. for ~5 mM [$a_6Ru^{2+}$] as a function of pH.

The fourth phase with the smallest rate constant, $k_4$, increases from ~0.03 to ~0.1 $s^{-1}$ over the pH range 5 to 9 (Appendix B, Table B10). At pH's below 7.5, $k_4$ appears to be invariant with $a_6Ru^{2+}$ concentration. At these pH values, $k_4$ is likely due largely to the His73-heme alkaline conformer with a *cis*-peptidyl proline bond. There are irregularities in the magnitude of this phase due to the low amplitude of this phase from pH 5 to 6.5. At

higher pH, $k_4$ increases with $a_6Ru^{2+}$ concentration and grows in magnitude. Above pH 7.5, $k_4$ is likely due to the Lys79-heme alkaline conformer as indicated by the rapid increase in its amplitude (figure 3.17), similar to the behavior seen for formation of the Lys79-heme alkaline conformer in pH-jump studies (figure 3.11)

Fractional amplitude data are plotted for all four phases at 5 mM $a_6Ru^{2+}$ as shown in figure 3.17, to show the variation of species associated with each rate constant. The 5 mM $a_6Ru^{2+}$ data were selected for this comparison as all four phases were well separated and the fast phase amplitude could still be evaluated reliably (figure 3.11). Figure 3.17 clearly shows a decrease in the population of the fast phase associated with the bimolecular ET to the native state (red line, figure 3.17), as pH increases. The population of the slowest phase increases from pH 5 to 9 (pink line, figure 3.17). The slowest phase in the lower neutral pH range is attributed to proline isomerization associated with the His73-heme alkaline conformer, since its rate constant is in the 100 s time regime [133, 134]. Above pH 7.5, the Lys79-heme alkaline conformer likely contributes to this phase. The first intermediate phase is assigned to the His73-heme alkaline conformer. The fractional amplitude (green line in figure 3.17) shows a rise in its population to a plateau at pH 6.5, near the p$K_a$ for histidine ionization. A decrease in the population of the His-heme alkaline conformer is seen as it is replaced by the Lys79-heme alkaline conformer above pH 7 (pink line in figure 3.17). The fractional amplitude of the second intermediate phase (blue line in figure 13.7) decreases slightly from pH 5 to 8 and then shows a slight increase in population from 8 to 9. This phase could be due to a high spin heme state as discussed above. Interestingly, the data suggest that the protein is never fully native and

that there is a low population of a species that is neither the native state nor an alkaline conformer throughout the pH regime monitored.

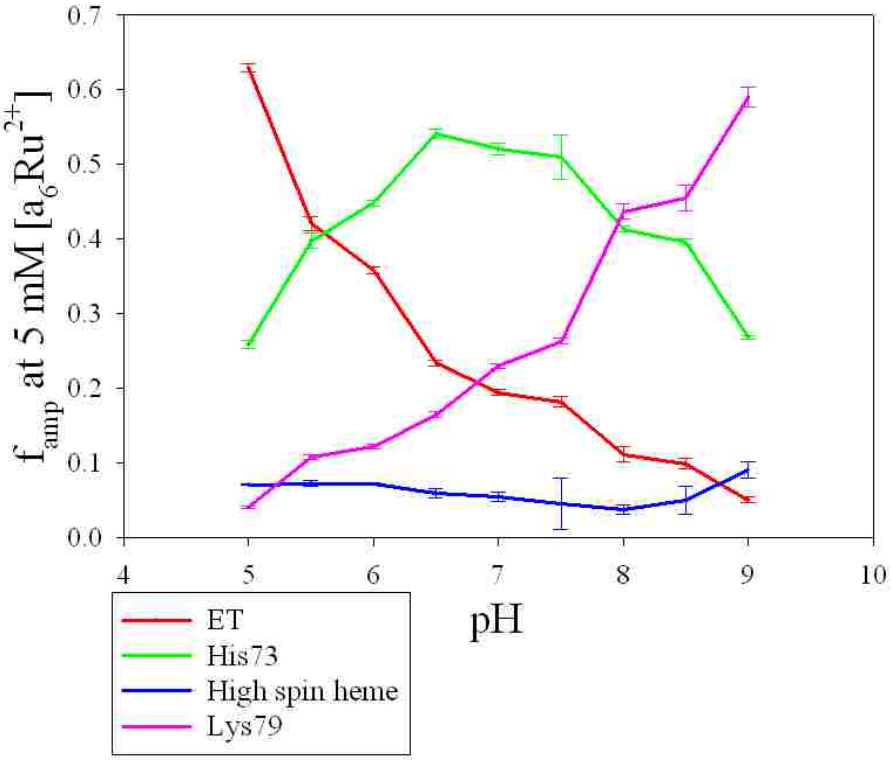


**Figure 3.17** Plots of fractional amplitude ($f_{amp}$) as a function of pH for the phases obtained from a fit to a four exponential rise to maximum equation at 5 mM $a_6Ru^{2+}$ concentration.

### *3.3.7 $^1$H NMR Spectroscopy.*

NMR studies were done to determine whether nonnative species of the AcH73 variant could be detected at pH 5 and to probe the nature of the alkaline conformer at higher pH. The NMR spectrum for the downfield region is shown in figure 3.18 (additional spectra are available in Appendix B, figures B2-B4). Figure is focused on the resonances due to heme methyl groups which responds to ligand changes in the alkaline transition. Assignment of the peaks was done on the basis of *references* [23, 48] for iso-1-cyt *c* and *ref* [135] for denatured and intermediate states of horse cyt *c*. The main points

from these studies are; (i) at low pH (5.06 and 6.3), the native state dominates based on the presence of native state heme-methyl peaks at 32 and 35 ppm, and the Met80 peak ~ -23 ppm and the Pro30 peak ~ -5.5 ppm in the upfield region (Appendix B, figures B2-B4); (ii) the presence of broad peaks at lower pH, at ~14 and 16 ppm may indicate residual His73 binding; (iii) near pH 7.5, broad peaks ~14 and 16 ppm are more prominent consistent with a higher population of the His73-heme alkaline state; (iv) at higher pH, peak ~19 is consistent with a Lys79 alkaline form, however the peak expected near 24 is broadened and other peaks between 18 and 26 ppm may reflect unfolded forms of protein with other lysines bound (this is consistent with the large *m*-value for the Lys79-driven alkaline transition, figure 3.5, section 3.3.3).

**Figure 3.18** On the next page are the NMR spectra of AcH73 variant at 600 MHz at 4 different pH's showing the downfield region from 12 to 40 ppm. Spectra were acquired at 25 ºC in 0.1 M NaCl, $D_2O$ solution.

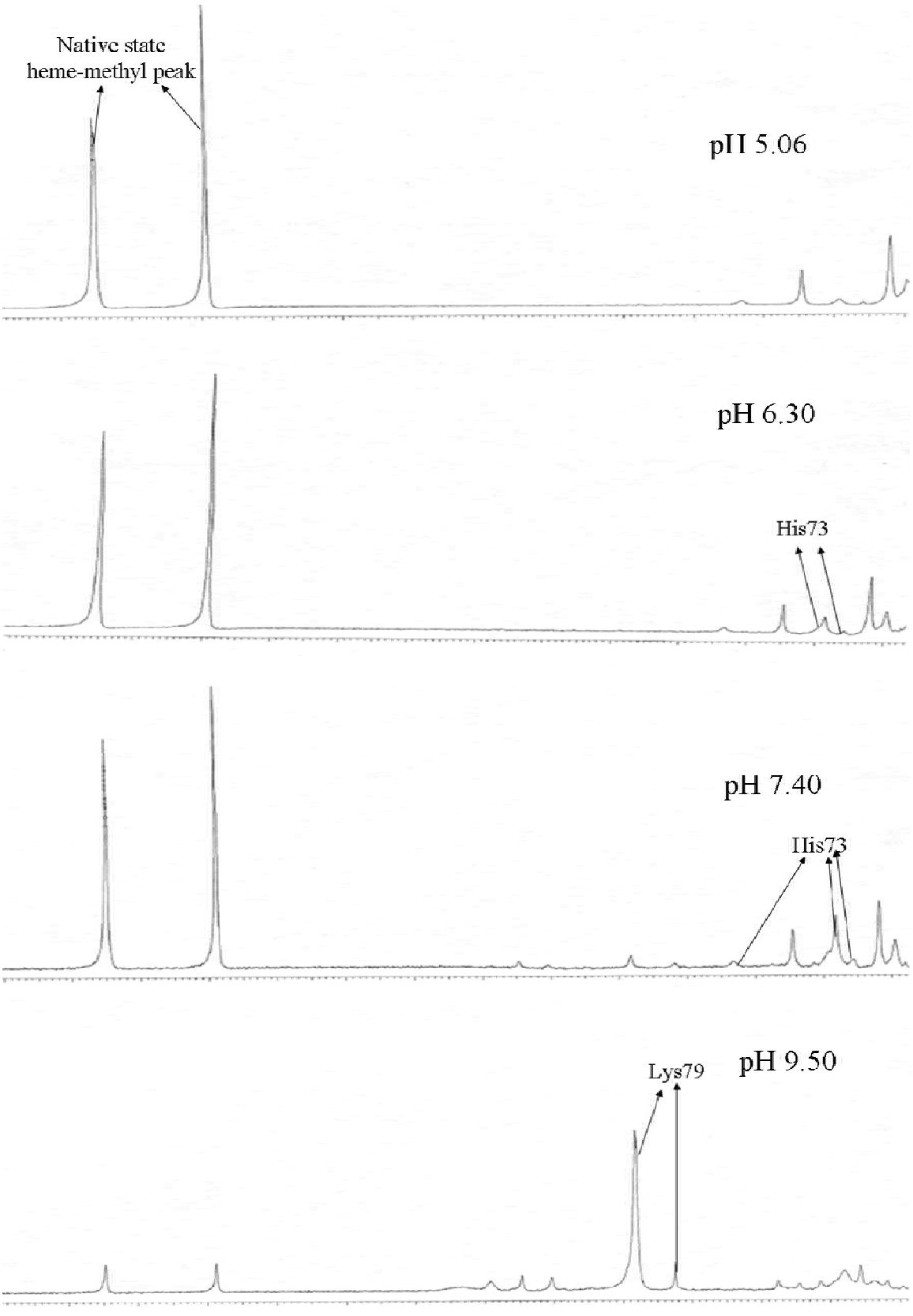
Native state
heme-methyl peak
pH 5.06
pH 6.30
His73
pH 7.40
His73
pH 9.50
Lys79
36
34
32
30
28
26
24
22
20
18
16
14
12
Chemical Shifts (ppm)

## 3.4 Discussion

### *3.4.1 Effect of Stability of the K73H Variant versus the AcH73 Variant of Iso-1-cyt c on the Thermodynamic Parameters of the Alkaline Conformational Transition.*

This study confirms that the global stability of the AcH73 variant is half that of the K73H variant. The *m*-value for global unfolding of the AcH73 variant is smaller than that of the K73H variant suggesting that global unfolding occurs from a more unfolded intermediate for the AcH73 variant than for the K73H variant. We attribute the loss in global stability to the His26Asn mutation in the AcH73 variant, which likely disrupts the bridging hydrogen bond between the green and gray surface loops (figure 3.1). A His26 to valine mutation showed similar destabilizing effects on the global unfolding of rat cytochrome *c* in urea solution [136].

The *m*-value for partial unfolding of the AcH73 variant (1.56 ±0.27 kcal $mol^{-1}$ $M^{-1}$) at pH 7.5 is similar to that for the K73H variant (~1.8 kcal $mol^{-1}$ $M^{-1}$ [100]) but $\Delta G^{o}_{u}(H_2O)$ is much more negative (-0.77 ± 0.01 kcal/mol) than for the K73H variant (0.37 ± 0.12 kcal/mol). Within error the *m*-value for partial denaturation cannot be distinguished, however, the $\Delta G^{o}_{u}(H_2O)$ values clearly show that AcH73 variant favors the His73-heme alkaline conformer more then the K73H variant.

pH titration studies shows similar biphasic behavior for both the AcH73 and the K73H variants of iso-1-cyt *c* at all gdnHCl concentrations studied (figure 3.3 and figure 6(a) in *ref* [23]). $pK_{C1}$ and $pK_{C2}$ values obtained from fits to these plots are more negative for AcH73 variant than for the K73H variant (Tables 1 and 2 in *ref* [23]). The *m*-values obtained for the AcH73 variant for the lower pH (2.4 ± 0.3 kcal $mol^{-1}$ $M^{-1}$) and higher pH (4.2 ± 0.8 kcal $mol^{-1}$ $M^{-1}$) phases are considerably larger then those for the K73H variant,

1.67 ± 0.08 and 1.1 ± 0.2 kcal $mol^{-1}$ $M^{-1}$, for lower and higher pH phases [23]. The *m*-value for the higher pH phase is similar to that for global unfolding of the WT protein [101], suggesting that the high pH "alkaline state" may be largely unfolded. The $\Delta G_{NI}$ (His-heme bound form) calculated from $pK_{C1}$ is -0.6 kcal/mol (Table 3.2 and figure 3.5), which is 1 kcal $mol^{-1}$ more negative than that of the K73H variant. These stability data are summarized in figure 3.19.

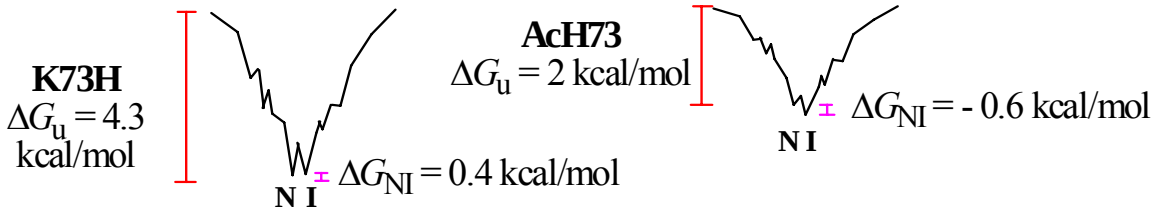


**Figure 3.19** Folding funnels for the K73H and AcH73 variants of iso-1-cyt *c* showing dual-well landscape for both proteins. Here N represents the native state (Met80-Heme bound) and I the intermediate state (His73-heme alkaline conformer).

The pH dependence of the heme Soret band shows a similarity in the $pK_{app}$ and the number of protons involved in the acid transition. For the acid transition $n = 1.9 \pm 0.1$, $pK_{app} = 3.31 \pm 0.04$ for K73H [96] and $n = 1.96 \pm 0.4$, $pK_{app} = 3.38 \pm 0.02$ for the AcH73 variant. Titrations in the heme Soret region also show biphasic behavior for the AcH73 and K73H variant in the alkaline region.

### *3.4.2 Kinetics of the Alkaline Conformational Transition of the AcH73 Variant of Iso-1-Cytochrome c from pH Jump Experiments.*

Striking differences are observed in the pH jump kinetics of the AcH73 variant when compared with the more stable K73H variant. The $k_{obs}$ for the fast phase of the K73H variant decreases from pH 5 to 6, is independent of pH form pH 6 to 8 and then

increases above pH 8, consistent with the involvement of three ionizable groups with p$K_a$'s of ~5.6, ~6.4 and ~8.7. For the AcH73 variant, the fast phase rate constant does not change in the pH range from 5 to 8 and then increases above pH 8. A fit of the data to a model involving a single ionizable triggering group (equation 2.6, Chapter 2) gives p$K_H$ of 9.4 ± 0.2 [64, 137]. The pH dependence of the amplitude of the fast phase gives a p$K_H$ of 6.40 ± 0.05 when fitted to the same model (equation 2.7, Chapter 2). Clearly the single ionization model cannot account for the data.

The slow phase rate constant data fitted to a model involving a single ionization is consistent with Lys79 as the ligand at higher alkaline pH. The amplitude data however seems to be more complicated than the single ionization model used to fit the data (figure 3.10). Closer inspection of the data suggests that three phases are involved. The first phase from pH 5 to 6.4, we attribute to proline isomerization. The rate constants in this region are similar to those observed for the A79H73 variant which has no Lys79 (see *ref* [62]). The second phase is seen from pH 6.4 to pH 8 where $k_{obs}$ appears to increase linearly with increasing pH. No similar phase is seen with the K73H and A79H73 variants. The third phase is seen from pH 8 onwards and is assigned to the Lys79 alkaline conformer.

### *3.4.3 Electron Transfer Method Provides Insight into the Alkaline Conformational Transition.*

Electron transfer experiments were developed in this study as a tool to extract microscopic forward and backward rate constants for the alkaline transition of the AcH73 variant. In particular, we test the hypothesis that the lack of change in $k_{obs}$ for the fast

phase from pH 5 to 8 is due to compensation of changes in the forward and backward rate constants.

The second phase from stopped flow ET data show hyperbolic plots similar to the saturation behavior observed in Michaels-Menten kinetics (figure 3.15). Equation 3.6 derived with the steady state approximation for the scheme in figure 3.14 predicts this behavior. Two limiting forms of this equation are, (1) when formation of the native sate is dominant and there is no back reaction at maximum $a_6Ru^{2+}$ concentration, then $k_{obs} = k_{HM3}$; and (2) when $k_{MH3} = k_{ET}\,[a_6Ru^{2+}]$, then $k_{obs} = (k_{HM3}/2)$. Thus, as $k_{ET}$ can be measured independently, both the forward, $k_{MH3}$, and backward, $k_{HM3}$, rate constants for the alkaline transition can be obtained.

As we know $k_{ET}$ from the fast phase data fitted to the pseudo-first-order equation 3.5, this value can be used in equation 3.6 (figure 3.14). The concentration of $a_6Ru^{2+}$ is known from experiment and so one can get the values for the forward and backward rate constants for the conformational transitions i.e., $k_{HM3}$ and $k_{MH3}$. $k_{HM3}$ in figure 3.14 corresponds to $k_b$ from pH jump studies (Table 3.5) and $k_{MH3}$ in figure 3.14 corresponds to $k_f$ from pH jump studies (Table 3.5).

The values of $k_{HM3}$ and $k_{MH3}$ from fitting the second phase data to eq 3.6 are summarized in figure 3.20. These data demonstrate that the constant magnitude of $k_{obs}$ in pH jump data from pH 5 to 8 is due to compensation between these conformational rate constants. An increase in the rate of formation of the His73-heme bound species ($k_{MH3}$) is matched with a decrease in the rate of formation of the Met80-heme bound species ($k_{HM3}$). The important point about these conformational rate constants is that these rate constants ($k_{HM3}$ and $k_{MH3}$) add up to the same value as $k_{obs}$ for fast phase obtained from pH

jump kinetic studies (figure 3.20). Thus, the ET data demonstrate the presence of a third ionizable group with p$K_a$ ~ 5.5 (see fig 3.20) which is not resolved in pH jump studies. Thus, the behavior observed for the His73-heme alkaline transition is identical for the K73H and A79H73 variants of iso-1-cyt *c* (see figure 3.20).

His26, which is involved in a hydrogen bond between two surface loops, was speculated to play role in the opening of the heme crevice during the alkaline transition. In AcH73, His26 has been mutated to Asn and thus cannot be responsible for the p$K_a$ at 5.5. The heme propionate D group (figure 1.8), which is supposed to have a p$K_a$ below 5 could be the group responsible for this p$K_a$ [137, 138], though it is not clear at this point.

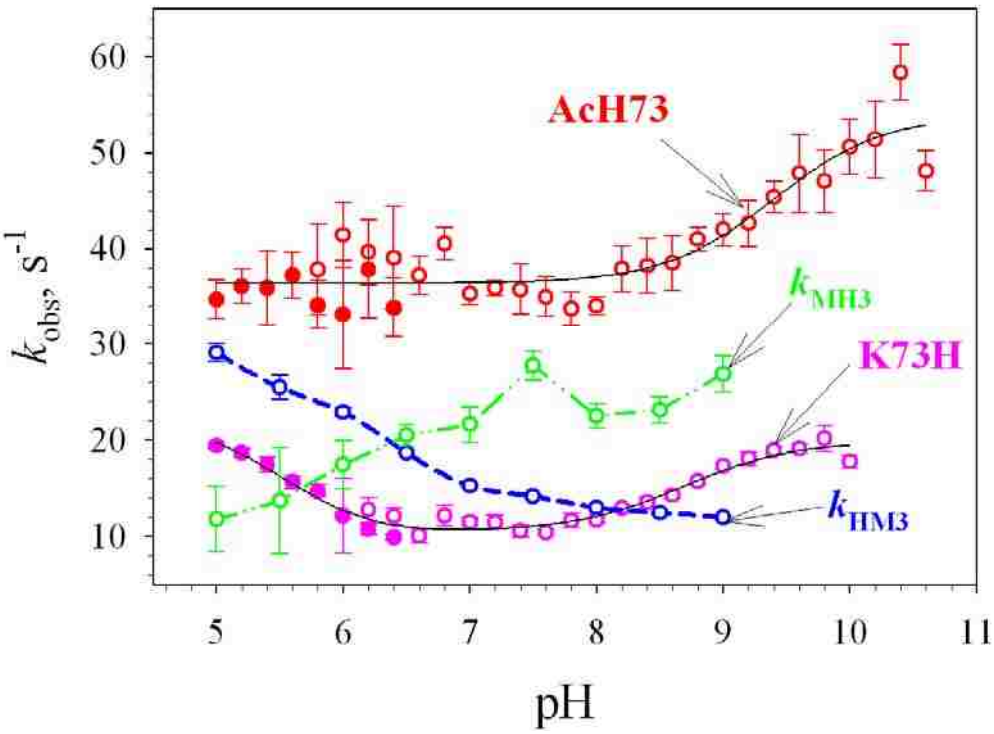


**Figure 3.20** Plots of $k_{HM3}$ (blue, same as $k_b$ in pH jump experiments) and $k_{MH3}$ (green, same as $k_f$ in pH jump experiments) rate constants with respect to pH jump kinetics data for the AcH73 (red) and K73H (purple) variants as a function of pH. The rate constants $k_{HM3}$ and $k_{MH3}$ are collected in Table B11 in Appendix B.

The third phase obtained from fitting ET data in figure 3.13 to a four exponential rise equation could be due to a high spin state however no direct spectroscopic data is available to support this assignment. The A79H73 variant data, which lacks Lys79 clearly populates a high spin state above pH 9 [62].

The fourth and slowest phase obtained from fitting ET data in figure 3.12 to a four exponential rise equation is analogous to the slow phase in pH jump studies; it is likely due to proline isomerization between pH 5 and 8. At higher pH this phase is assigned to the Lys79-heme alkaline conformers as the amplitude increases, consistent with thermodynamic, pH jump, NMR and K73H [61] data. In the case of the A79H73 variant where Lys79 was mutated to alanine no such increase in slow phase amplitude was observed [62] which further supports this assignment.

### *3.4.4 Effect of Global Destabilization on Kinetics at the Bottom of a Folding Funnel.*

At pH 7.5, the His73-heme bound form (intermediate state) is maximally populated (figure 3.17), Thermodynamic and kinetic data for the less stable AcH73 versus the more stable K73H variant is summarized in figure 3.21. At pH 7.5, $k_{NI} = 3.5 \pm 0.2\ s^{-1}$ and $k_{IN} = 7.0 \pm 0.4\ s^{-1}$ for the more stable K73H variant [61] and for the less stable AcH73 variant, $k_{NI} = 28 \pm 0.2\ s^{-1}$ and $k_{IN} = 14 \pm 0.2\ s^{-1}$ (Appendix B, Table B11). Thus, the kinetics of the interconversion of N and I for the less stable AcH73 variant is faster in both directions, consistent with the barriers at the bottom of a folding funnel decreasing as a protein becomes less stable. While glassy behavior might be expected at the bottom of the folding funnel, multi-exponential kinetics are not observed. Thus, I (His73-heme) and N (Met80-heme) dominate the bottom of the energy landscape of these proteins.

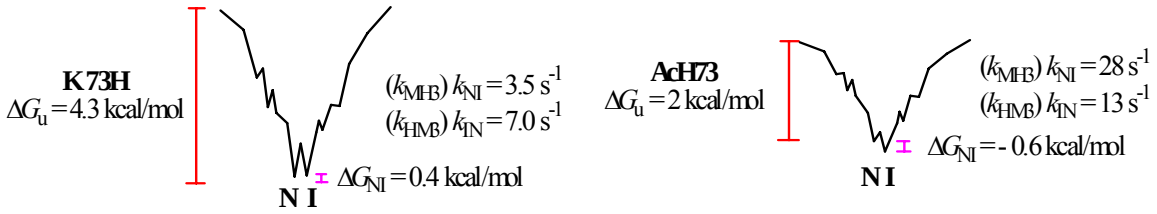


**Figure 3.21** Energy landscape for the K73H and AcH73 variants of iso-1-cyt *c*. Here N represents the native state (Met80-heme ligation) and I represent Intermediate state (His73-heme ligation). Rate constants, $k_{NI}$ ($k_{MH3}$) and $k_{IN}$ ($k_{HM3}$) at pH 7.5 are given.

## 3.5 Conclusions

These studies show that the absence of Asn31/His26/Glu44 hydrogen bond broadly affects the thermodynamic and kinetics of conformational changes in iso-1-cyt *c*. The present study also demonstrates the utility of ET methods as a tool to probe conformational changes. ET experiments not only resolve the presence of a third ionizable group but also provide direct evaluation of both the forward and backward conformational transition rate constants over a wide pH range. These studies support the modulation of the alkaline conformational transition by three ionizable groups, as seen with the more stable K73H and A79H73 variants of iso-1-cyt *c*. His26 has been speculated to be the third ionizable group but these studies demonstrate that it has no role in the alkaline transition. This study also provides a beautiful example of how lower stability decreases the barriers between conformations at the bottom of a folding funnel. This observation is analogous to the behavior of cold-adapted enzymes from psychrophilic organisms. The dynamics in these less stable enzymes are enhanced, allowing the catalytically active state to still be readily accessed at low temperature [139].

# CHAPTER 4

## *KINETICS OF PROLINE ISOMERIZATION MONITORED THROUGH CONFORMATIONALLY GATED ELECTRON TRANSFER WITH THE A79H73 VARIANT OF ISO-1-CYTOCHROME C*

### 4.1 Introduction

Proline (Pro) stands alone among all 20 amino acids because of its unique structure, as its side chain is bonded to both the nitrogen and the α-carbon. Proline has a remarkable influence on protein architecture because its ring structure makes it more conformationally restricted. Peptide bonds in proteins can occur in two isomeric states: *trans,* when ω dihedral angel is 180º, and *cis*, when ω is 0º (figure 4.1). In most peptide bonds the *trans* configuration is favored as the α-carbons are placed far away from each other as shown in figure 4.1. In X-Pro, where X is any of the other 19 amino acids, this distortion causes steric clashes between the α-carbons on X and both the $\alpha$ and the N bound $\delta$ carbons on Pro. As a result this increases the probability of occurrence of the *cis* configuration from 1:500 to 1:4 [140].

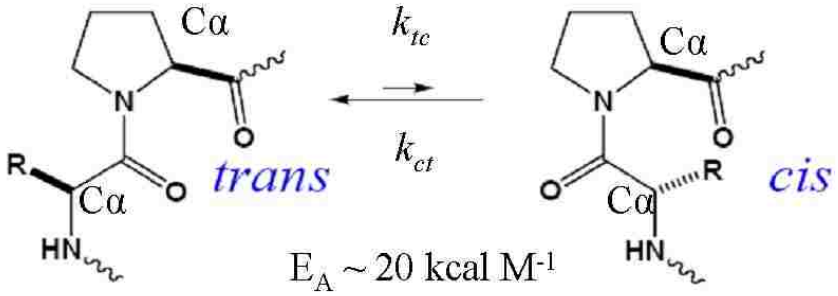


**Figure 4.1** Figure showing the *cis* and *trans* isomers of proline with an activation energy barrier of ~20 kcal $mol^{-1}$. $k_{tc}$ and $k_{ct}$ are the rate constants for proline isomerization on going from the *trans* to the *cis* form and vice versa.

The favorability of one isomer over the other depends on a number of factors, like the nature of the amino acid preceding Pro, the solvent in which the protein is present, and the conformation, folded versus unfolded states of the protein. Studies in *ref* [141] with pentapeptides have shown that the presence of an X-Pro peptide bond favors the *cis* isomer. Peptide bonds preceding proline are referred as a prolyl bond and those preceding residues other then Pro and referred as non-prolyl bonds. Among the amino acids other than Pro, tryptophan, tyrosine and phenylalanine favor the *cis* isomer in X-Pro bonds, while amino acids like isoleucine and valine due to steric hindrance favors the *trans* isomer in X-Pro bonds. In native folded proteins, non-prolyl *cis* peptide bonds are very rare. From 571 protein structures studies, only 43 *cis* non-prolyl peptides were found [142].

The *trans* form is favored for X-Pro peptide bonds in the unfolded protein molecule, but when proline is present in a *cis* form in the native state of protein then it slows down the folding process due to the intrinsically slow reaction of *cis-trans* isomerization. This condition is referred to as incorrect prolyl isomers. The activation barrier between the *cis* and *trans* form is ~20 kcal $mol^{-1}$ [143], causing proline isomerization to be a slow process. These isomers do not necessarily block the early folding steps, but slow down the overall folding process. Studies with single domain proteins have shown an increase in the folding time from milliseconds to minutes [144]. These incorrect prolyl isomers are referred to as traps in the protein folding mechanism. Prolyl isomerization is slow because of the CN partial double bond character of the peptide bond, which has to be overcome. When the resonance contribution to the CN double bond character is increased in the presence of solvents that donate hydrogen

bonds or a proton to the carbonyl group, then it slows down this isomerization process even further [145]. The process of isomerization is fast when the resonance is decreased by protonation of N in the amino group [144].

In the native protein, usually each prolyl peptide bond is in a defined conformation, either *cis* or *trans*, depending on the constraints dictated by the native state. After unfolding when constraints are removed, these bonds become free to isomerize slowly. This creates a mixture of species with correct prolyl isomers and, depending on the number of prolines, one or more unfolded species with incorrect prolyl isomers. The proteins with all correct isomers refold rapidly but those with incorrect isomers refold slowly. As a result, they create proline-limited steps in the folding kinetics for many small single domain proteins. When *cis* proline is present in the native state, then a larger amplitude is associated with this slow phase during refolding reactions. When unfolding into the equilibrium region, a large amplitude slow phase is observed, as *cis* to *trans* isomerization pulls the equilibrium to the unfolded form. But in proteins with all *trans* proline, smaller amplitudes associated with the slow phase are seen, which is expected since proline in the *trans* state is favored over proline in *cis* state for unfolded proteins. Studies with large proteins show smaller amplitudes and a 5-10 times faster reaction for *cis* →*trans* than for *trans* →*cis* isomerization. When direct folding is much faster than rate limiting proline isomerization, then the relative amplitude of these slow refolding reactions depends only on the relative population of the unfolded species and it is independent of the final folding conditions, the probe used to monitor refolding, the denaturant used (as a result it will not depend on the initial conditions of unfolding), pH and temperature [144]. Proline isomerization studies of pentapeptides [141] with Tyr and

His as the preceding amino acid showed some dependency on pH due to side chain ionization. His-Pro showed an increase in the isomerization rate below pH 5 while Tyr-Pro showed decrease in isomerization rate near its p$K_a$.

All prolines in mitochondrial cytochromes *c* are in the *trans* form [146] and so the amplitude associated with proline isomerization is small. Iso-1-cytochrome *c* (iso-1-cyt *c*) has four prolines at positions 25, 30, 71 and 76. Prolines 71 and 76 are present in Ω- loop D (red loop) (figure 4.2), which participates in the alkaline conformational transition. Met80 which is also present in this loop is bound to the heme in the native state of the protein near pH 5.

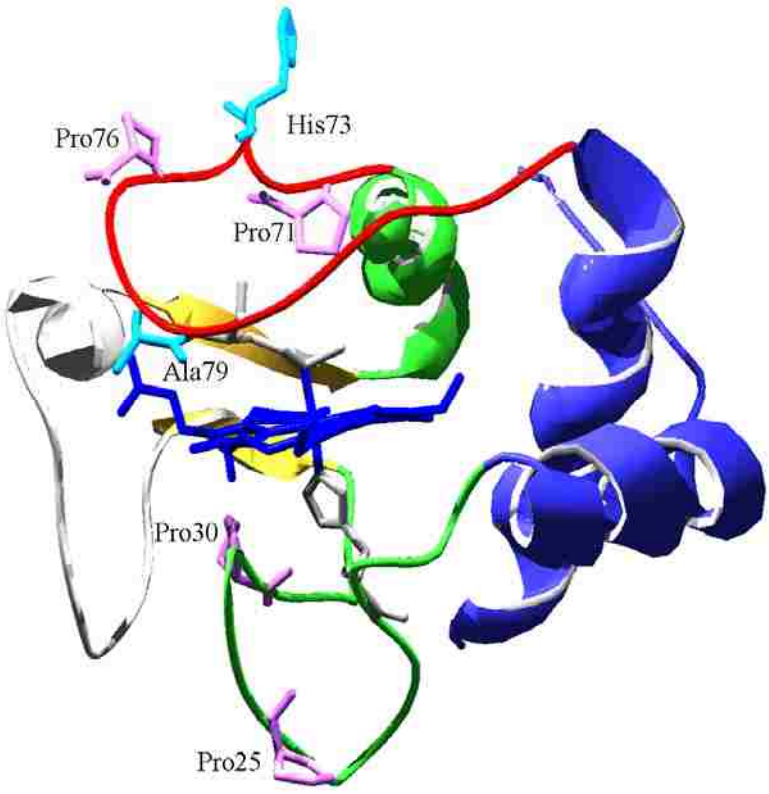


**Figure 4.2** Iso-1-cyt *c* showing the side chains of His73 and Ala79 colored in cyan. Prolines 25, 30, 71 and 76 are colored lavender. The heme cofactor is shown in blue with the heme ligands Met80 and His18 colored in grey. The substructures of cytochrome *c*, as defined by Englander and co-workers are shown from least to most stable in the colors gray, red, yellow, green, and blue [79].

Lysines present at positions 73 and 79 in this loop are known to replace Met80 in the alkaline state. The alkaline state is a partially unfolded form of iso-1-cyt *c*. This alkaline conformational transition may play an important role in the biological process mediated by cytochrome *c* such as, cellular respiration and apoptosis. Studies have been done with lysines 73 and 79 replaced with histidine in our laboratory [23, 24, 96, 100]. These studies have demonstrated that His variants at these positions lead to a partially unfolded form of iso-1-cyt *c*, which is analogous to the alkaline conformational transition, but occurs near physiological pH. While His73 variants have been useful, the presence of Lys79 complicates analysis of partially unfolding caused by His73-heme ligation. In particular, the kinetics due to Lys79 ligation and of proline isomerization linked to the His73–heme conformer occurs on a similar time scale at some pHs. This makes the assignment of this phase difficult. To simplify the partial unfolding of the His73 variant, Lys79 was replaced by Ala in the K73H variant, producing an A79H73 variant of iso-1-cyt *c* [62]. This A79H73 variant showed differences in behavior as compared to the K73H variant, including a salt dependent alkaline transition and an acid transition with ~ 1 proton uptake (~2.5 protons for the wild type protein, [96]). It also showed the presence of a slow phase which increased in amplitude from pH 6 to 7.5 followed by leveling off to pH 9 and then finally showing a decrease up to pH 10. This behavior was particularly interesting as the rate constants for proline isomerization were also pH dependent [62].

Electron transfer (ET) studies done in our lab as a function of pH and at different concentrations of hexaaminеruthenium(II) chloride complex ($a_6Ru^{2+}$) [24, 64, 73, 81] have been successfully used to pull out information about the conformational dynamics

of iso-1-cyt *c* taking place in the physiological and alkaline pH regions. We know from studies with K73H [61] and A79H73 [62] that this slow phase can be observed in these ET experiments. Figure 4.2, shows how proline isomerization acts as a conformational gate that must precede ET. Iso-1-cyt *c* in the alkaline state with a *cis* proline, $Alk^{ox}$ (*cis* Pro); must convert into the alkaline state with a *trans* Pro, $Alk^{ox}$ (*trans* Pro), before formation of the native state. ET can only take place from the native state as the alkaline form has too low a redox potential ($E^o$ ~41 mV vs. NHE) to be reduced by reagents such as $a_6Ru^{2+}$ ($E^o$ ~60 mV vs. NHE) [49].

If the pseudo-first order rate constant for direct ET, $k_{ET}[a_6Ru^{2+}]$, is much greater than $k_{HM3}$, and $k_{tc} \ll k_{MH3}$ then ET to $Alk^{ox}$ (*trans* Pro) is limited by $k_{HM3}$ and ET to $Alk^{ox}$ (*cis* Pro) is limited by $k_{ct}$. In the case of the A79H73 variant of iso-1-cyt *c*, His73-heme bound (redox inactive, alkaline state) will have to equilibrate to form the Met80-heme bound form (redox active, native state). This Met80-heme bound form then reacts with $a_6Ru^{2+}$, which can be monitored at 550 nm. The difference in millimolar extinction coefficient of oxidized and reduced cytochrome *c* is ~18.5 x $10^3$ at 550 nm [74] and as a result an increase in absorbance is observed (see figure 1.15 in Chapter 1) at this wavelength in ET experiments. Depending on pH, three ET phases are expected, a fast phase associated with direct ET to the native state, an intermediate phase for the conformational change from $Alk^{ox}$ (*trans* Pro) as seen in previous studies [24, 64, 81], and a slow phase attributable to proline isomerization. In the present study, the A79H73 variant of iso-1-cyt *c* is studied over a wider pH range from pH 5.5 to 9, to have a better understanding for the process of proline isomerization and the effect of pH on the process.

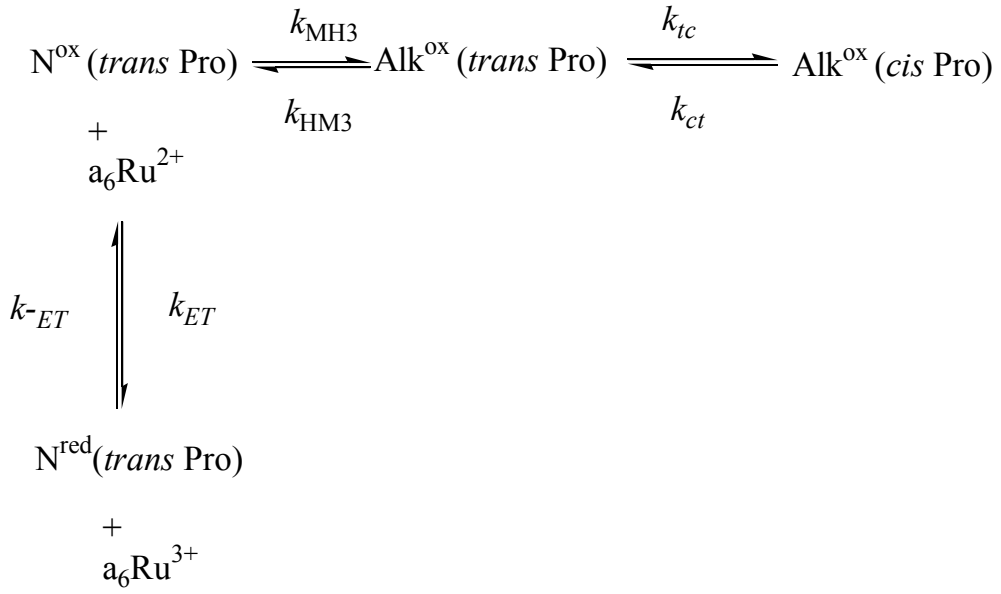


**Figure 4.3** Rate constant determination for *cis* to *trans* isomerization of Pro, $k_{ct,}$ using electron transfer from hexaminеruthenium(II) chloride, $a_6Ru^{2+}$.

## 4.2 Materials and Methods

### *4.2.1 Isolation and Purification of Proteins*

The A79H73 variant was isolated and purified, from *Saccharomyces cerevisiae* using techniques described previously in the Materials and Methods section 2.2.1 of Chapter 2 for the H79 variant.

### *4.2.2 Molecular Weight Determination by MALDI-TOF Mass Spectroscopy.*

Molecular weight was determined for the A79H73 variant as described previously in the materials and methods section of Chapter 2. The main peak gave m/z = 12,640.33 ± 5 (average and standard deviation of two independent spectra, consistent with the expected molecular mass of 12,646.19 g/mol for the A79H73 variant. All experiments were carried out with this material.

### *4.2.3 Electron Transfer Experiments by the Stopped Flow Method*

Experiments were done using hexaammineruthenium(II) chloride ($a_6Ru^{2+}$) with an Applied Photophysics SX20 stopped flow spectrophotometer, as described previously in Chapter 2. The buffers used for these experiments were acetic acid (pH 5.5), MES (pH 6 & 6.5), $NaH_2PO_4$ (pH 7 & 7.5), Tris (pH 8 & 8.5) and $H_3BO_3$ (pH 9 & 9.5). The protein concentration after mixing with $a_6Ru^{2+}$ was ~5 μM. Three different concentrations of $a_6Ru^{2+}$, 1.25, 2.5, and 5 mM were used for these experiments. Selection of these three concentrations was done on the basis of previous studies with the A79H73 variant [62]. The concentration of $a_6Ru^{2+}$ was determined as described in the Materials and Method section 3.2.9 of Chapter 3. At each concentration of $a_6Ru^{2+}$, five kinetic traces were collected. For all traces, 5000 points were collected logarithmically on 100 sec time scale. Analysis of the data was done using the curve fitting program, Sigma Plot (v.7.0). The data were fit to a quadruple exponential rise to maximum equation for 100 sec time scale data as shown in figure 4.1.

## 4.3 Results

### *4.3.1 Anaerobic Stopped-Flow Kinetic Measurements.*

Initial studies done with the A79H73 variant of iso-1-cyt *c* indicated that gated ET is independent of $a_6Ru^{2+}$ concentration. pH-jump studies showed the presence of a distinct slow phase which was dependent on pH. Based on the preliminary ET results done at pH 6, 6.5 and 7.5 [81] and also pH jump studies [62], ET experiments were carried out from pH 5.5 to 9.5 to cover a broader pH range coincident with the pH jump studies. The same $a_6Ru^{2+}$ concentrations (i.e., 1.25, 2.5 and 5 mM) were used. The kinetic

traces obtained on reaction of oxidized A79H73 with $a_6Ru^{2+}$ are shown in figure 4.4 for the pH range of 5.5 to 9.5. An increase in absorbance was seen at 550 nm as expected. Also, an increase in background absorbance was seen with increased $a_6Ru^{2+}$ concentration as was observed with the AcH73 variant (Chapter 3). These data were fitted to both three and four exponential rise to maximum equations but based on better residuals, the quadruple exponential fits were used (figure C1 in Appendix C). The general trend seen from pH 5 to 9.5 is that the fast phase amplitude decreases with pH and the slower phase amplitudes increase with pH as the alkaline state populates.

**Figure 4.4** On the next page are plots of absorbance at 550 nm versus time (on logarithmic scale) for reduction of the A79H73 variant of iso-1-cyt *c* with $a_6Ru^{2+}$ from pH 5.5 to pH 9.5, at three different concentrations of $a_6Ru^{2+}$(red trace for ~1.25, green for ~2.5 and blue for ~5 mM $a_6Ru^{2+}$). The solid lines are fits to the four exponential eq.

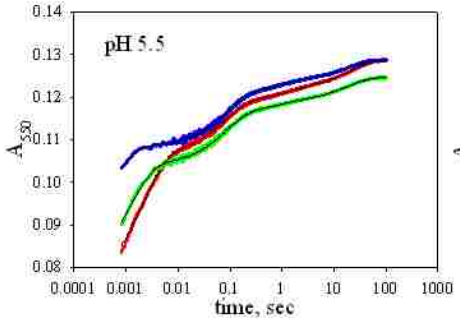
pH 5.5
A550
time, sec

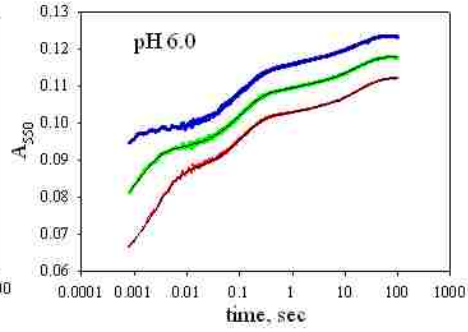
pH 6.0
A550
time, sec

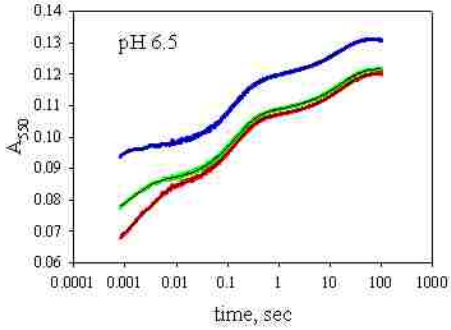
pH 6.5
A550
time, sec

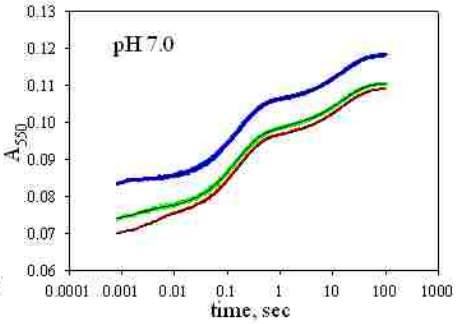
pH 7.0
A550
time, sec

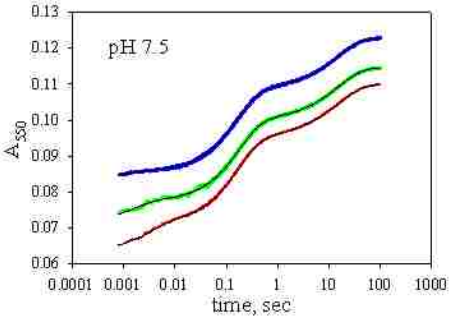
pH 7.5
A550
time, sec

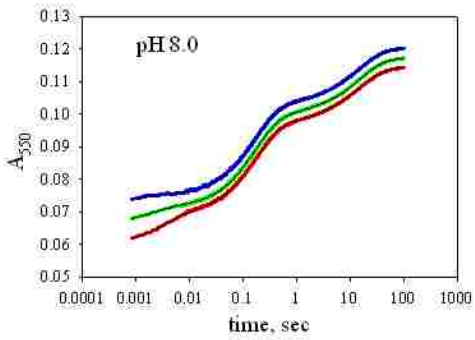
pH 8.0
A550
time, sec

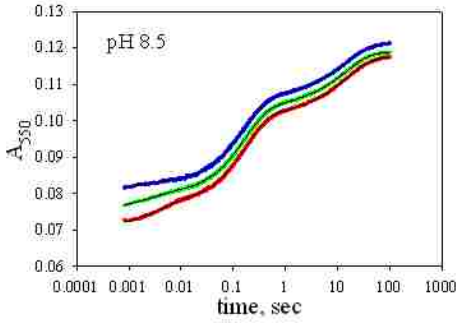
pH 8.5
A550
time, sec

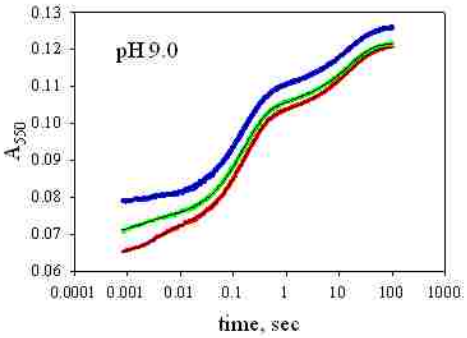
pH 9.0
A550
time, sec

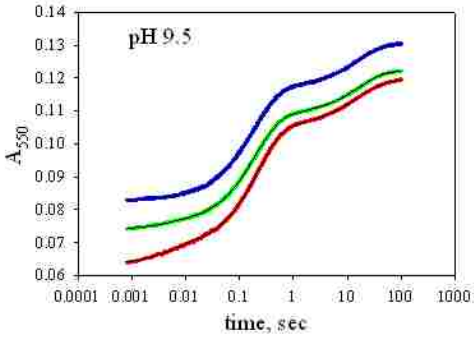
pH 9.5
A550
time, sec

The fastest phase ($k_1$) obtained from these fits is plotted as a function of $a_6Ru^{2+}$ concentration as shown in figure 4.5 (also see appendix C, Table C1) for the pH range of 5.5 to 9.5. $k_1$ increases linearly with $a_6Ru^{2+}$ concentration for all pH's ranging from 5.5 to 9.5 (figures 4.5, and appendix C, Table C1). This phase is attributed to direct ET of the Met80-heme ligated native conformer with the ruthenium complex. The plots in figure 4.5 were used to determine the ET rate constant, $k_{ET}$, using equation 3.3 (Chapter 3). The $k_{ET}$ are plotted as a function of pH in figure 4.6. $k_{ET}$ at pH 6 and 6.5 are consistent with previously reported values [81], but at pH 7.5 $k_{ET}$ is larger then previously reported (133 ± 9 $mM^{-1}s^{-1}$) in *ref* [81]. At pH ≥ 8, $k_{ET}$ appears to decrease; this could be an artifact of low amplitude of the fast phase in this pH region.

The second phase, $k_2$ obtained from quadruple exponential fits of the kinetic traces shown in figure 4.3 is plotted as a function of [$a_6Ru^{2+}$] for all pHs in figure 4.7 (also in appendix C, Table C2). The rate constant for this phase does not change significantly with increased [$a_6Ru^{2+}$]. It does however decrease with increased pH (figure 4.7). Thus, we have used the average value of $k_2$ for all [$a_6Ru^{2+}$] for $k_{HM3}$. The values obtained for $k_{HM3}$ are shown in appendix C, Table C5 and figure 4.11.

**Figure 4.5** On the next page are plots of observed rate constant $k_{obs}$ ($s^{-1}$) for the reaction of $a_6Ru^{2+}$ with the native conformer of the A79H73 variant as a function of $a_6Ru^{2+}$ concentration at 25 ºC for pH 5.5-9.5; Buffers were 10 mM concentration in 0.1 M NaCl. The values for $k_{obs}$ represent the fast phase ($k_1$) obtained from the fits shown in figure 4.4 and the solid line is a fit to eq. 3.3 (Chapter 3).

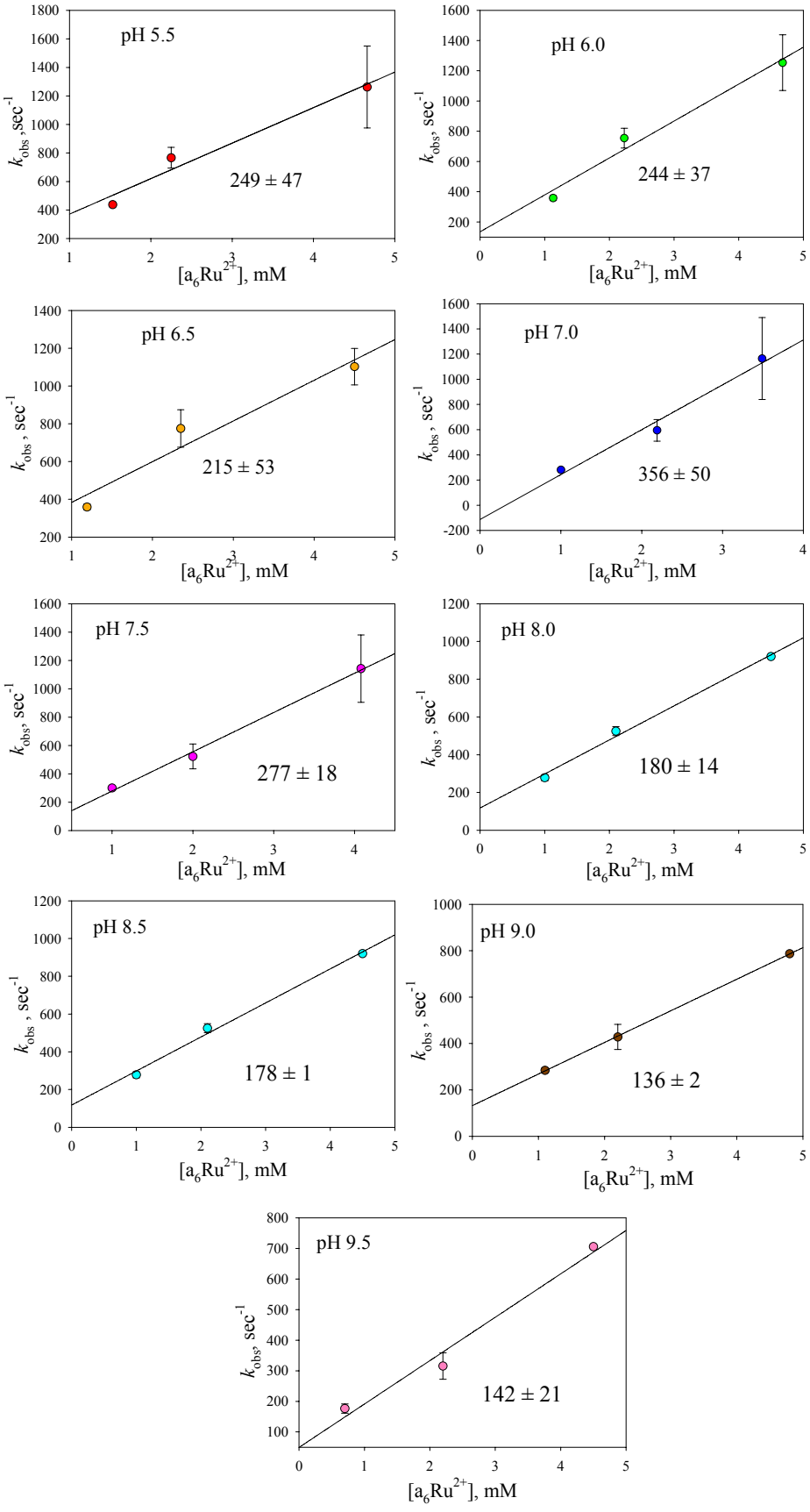
pH 5.5
249 ± 47
pH 6.0
244 ± 37
pH 6.5
215 ± 53
pH 7.0
356 ± 50
pH 7.5
277 ± 18
pH 8.0
180 ± 14
pH 8.5
178 ± 1
pH 9.0
136 ± 2
pH 9.5
142 ± 21
$k_{obs}$, sec$^{-1}$
[$a_6Ru^{2+}$], mM

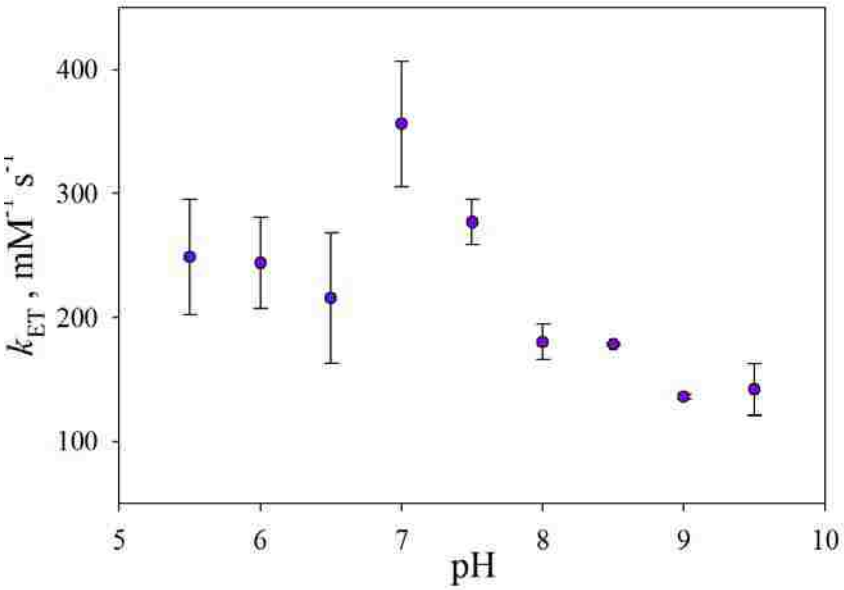


**Figure 4.6** Plot of ET rate constant, $k_{ET}$ ($mM^{-1}s^{-1}$), as a function of pH. The values for $k_{ET}$ are obtained from the fits to eq. 3.3 as shown in figure 4.5.

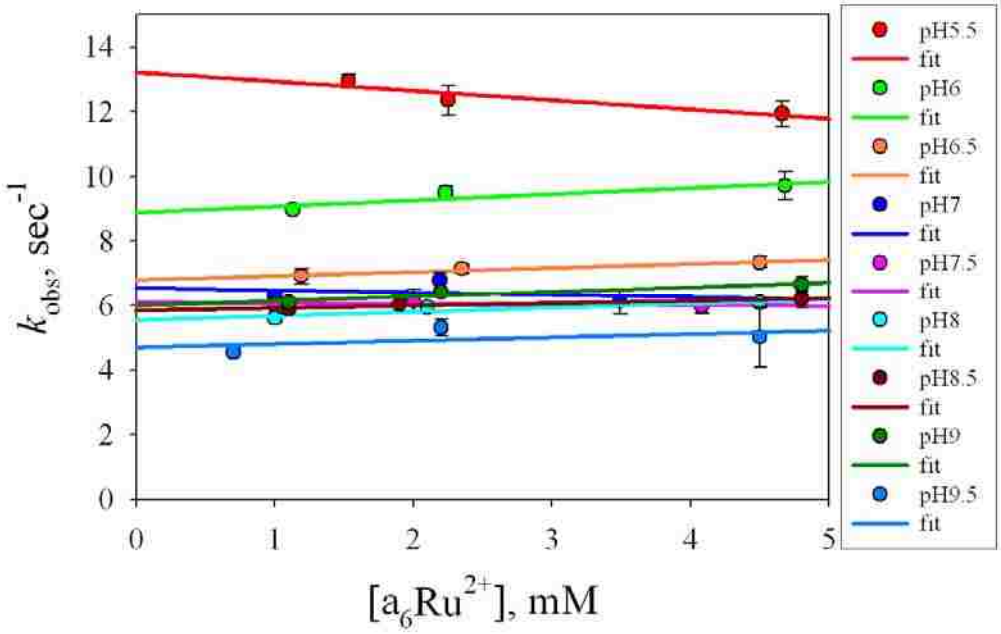


**Figure 4.7** Plots of the faster intermediate rate constant, $k_2$ ($s^{-1}$), for the reaction of $a_6Ru^{2+}$ with the A79H73 variant as a function of $a_6Ru^{2+}$ concentration at 25 ºC for pH 5.5 – 9.5, Buffers used are at 10 mM concentration in 0.1 M NaCl. The values of $k_2$ were obtained from the fits shown in figures 4.4 and the solid lines are fits to a linear equation, showing modest to no dependence of $k_2$ on $[a_6Ru^{2+}]$ The values for $k_2$ are collected in Appendix C, Table C2.

The slower intermediate phase, $k_3$, obtained from fitting the redox kinetic traces (as shown in figure 4.3) is plotted as a function of pH for three concentrations of $a_6Ru^{2+}$, figure 4.8 (also appendix C, Table C3). This phase is more or less similar, within error, at all three concentrations, except at pH 9.5.

In general $k_3$ is near 1.0 $s^{-1}$ at all pHs, except at pH 9.5. At pH 9.5 $k_2$ and $k_3$ are closest in magnitude. The change in $k_3$ with $[a_6Ru^{2+}]$ may be an artifact of the difficulty in distributing amplitude between these two closely spaced phases. It is also apparent that even the quadruple exponential fit is imperfect at pH 9.5 (Appendix C, figure C1). Previous data for the 100 sec time scale [81], was fitted to a two exponential rise equation were fast phase was missing due to the glitch in the logarithmic collection of data in the instrument and also this third (slower intermediate) phase was missing. The previous data were refitted to triple exponential equation and the values obtained are shown in parentheses in Appendix C, Table C3.

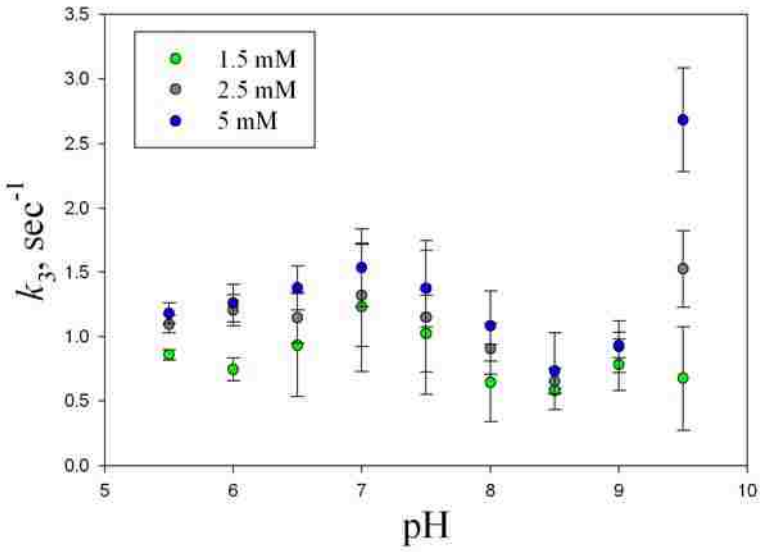


**Figure 4.8** Plots of the slower intermediate rate constant, $k_3$, from fits to a quadruple rise to maximum equation for ~1.25, ~2.5 and ~5 mM $a_6Ru^{2+}$ concentration as a function of pH. Rate constants are given in Appendix C, Table C3.

The fourth and slowest, $k_4$, phase obtained from fitting the ET kinetic traces (figure 4.3) is plotted as a function of pH for three concentrations of $a_6Ru^{2+}$ in figure 4.8. Observed rate constants varied from 0.042 - 0.065 $s^{-1}$. Thus, this rate constant is consistent with proline isomerization. This phase shows little dependence on pH, perhaps a slight increase in rates from pH 5 to 7, then $k_4$ is more or less constant up to pH 9 and then undergoes a slight decrease at pH 9.5 (figure 4.9). The values for 5 mM $a_6Ru^{2+}$ are a bit higher from pH 5.5 to 6.5. The cause of [$a_6Ru^{2+}$] dependence in this pH region is unclear. The values obtained from triple exponential fits to the previous A79H73 data are shown in parenthesis in Appendix C, Table C4. Values from the two data sets are similar.

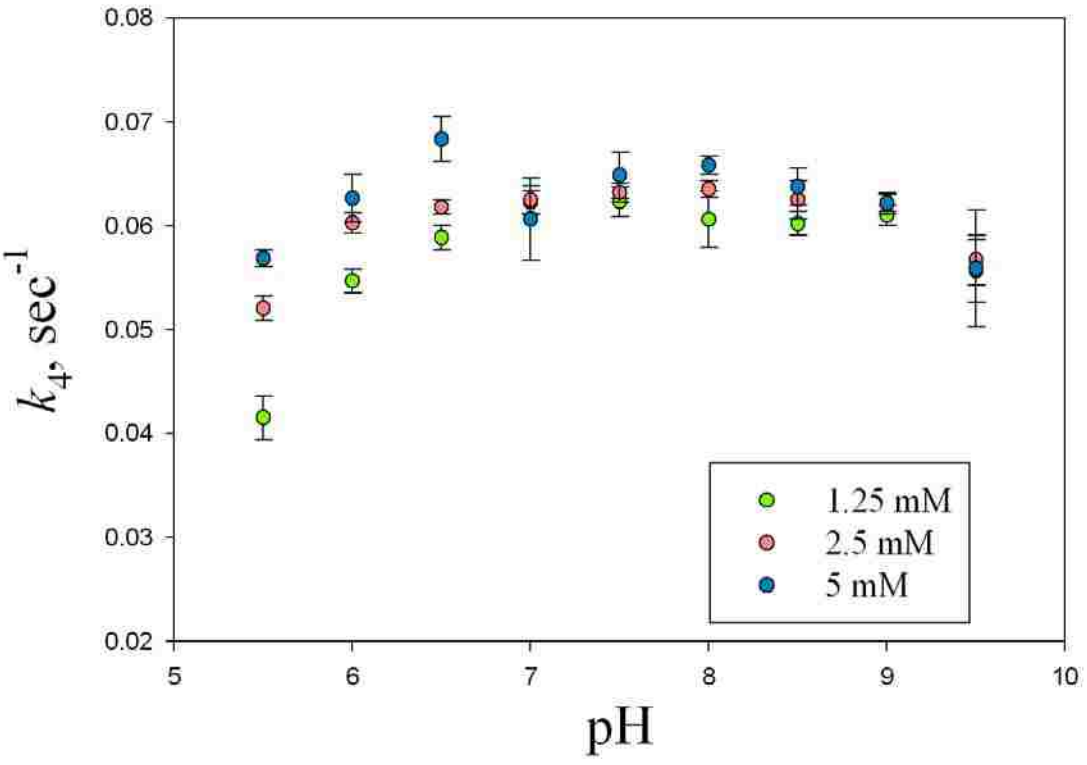


**Figure 4.9** Plots of the slowest rate constant, $k_4$, from fits to a quadruple rise to maximum equation for ~1.25, ~2.5 and ~5 mM $a_6Ru^{2+}$ concentration as a function of pH. Rate constant values are shown in Appendix C, Table C4.

Fractional amplitudes of the ET phase were determined at all the three $a_6Ru^{2+}$concentrations for the data obtained from triple and quadruple exponential rise to maximum equations to observe the variation of the population of species associated with each rate constant. Average and standard deviation for 1.25 and 2.5 mM $a_6Ru^{2+}$ fractional amplitude data is shown in figure 4.10 as a function of pH. At 5 mM $a_6Ru^{2+}$ concentration much of the amplitude of the direct ET phase, $k_1$, occurs in the dead time of mixing, thus the 5 mM data provides less reliable fractional amplitudes. Figure 4.9 for both 1.25 and 2.5 mM $a_6Ru^{2+}$ concentrations, clearly shows the decrease in the population of the native state, which is responsible for the fastest phase associated with direct ET (red line). The populations of the species responsible for second and the fourth phases, attributed to the His73-heme to native conformational change and proline isomerization, respectively, increase from pH 5.5 to 7 and then level off. At pH 9.5 the fractional amplitude for the fourth phase shows a decrease relative to the second phase.

The population of the third phase, $k_3$, (blue line in figure 4.9 (b) and (d)) from the quadruple exponential fit is more or less invariant at both 1.25 and 2.5 mM $a_6Ru^{2+}$ concentrations for the pH range of 5.5 to 9.5. There may be a slight increase in the population of the species responsible for this phase above pH 8.0.

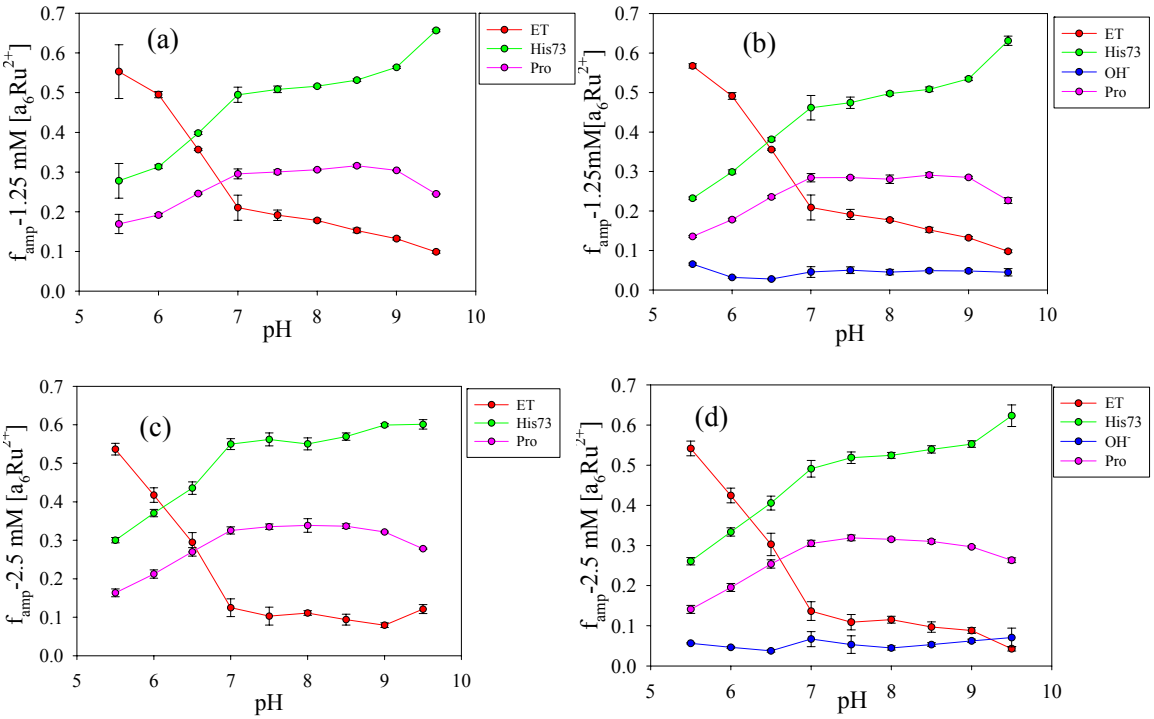


**Figure 4.10** Plots of fractional amplitude ($f_{amp}$) as a function of pH obtained from fits to three (a and c) and four (b and d) exponential rise to maximum equations for 1.25 and 2.5 mM [$a_6Ru^{2+}$].

## 4.4 Discussion

### *4.4.1 Population of Conformers of the A79H73 Variant as a Function of pH*

The four phases obtained from the quadruple exponential fit of the kinetic traces represent four distinct conformers of iso-1-cyt *c* in the pH region 5.5 to 9.5. The fractional amplitude associated with the fast phase rate constant decreases with an increase in pH suggesting that it is associated with the native state. The amplitude at pH 5.5 is around 60%. The intermediate phase increases and then levels off at higher pH, consisted with the His73-heme alkaline conformer. This intermediate phase shows compensatory behavior to the fast ET phase reaching ~60% population at pH 9.5. The slowest phase increases from pH 5.5 to pH 7, then levels off up to pH 9, and then

decreases at pH 9.5. This phase is attributed to proline isomerization as Lys79 is not present in A79H73 variant. Less than 10% population is observed for the slower intermediate phase from the quadruple exponential fit throughout the pH range of 5.5 to 9.5. Looking at the residuals in figure C1, Appendix C shows improvement in the residuals from pH 5.5 to pH 7.5 but above pH 8 there is not as much of a difference between the quadruple and triple exponential fits. The species responsible for this phase is unclear; it could be due to a high spin state, although spectroscopic data suggest that its amplitude is too small for this assignment, since a substantial absorbance peak is evident at 620 nm by pH 9.5 [62]. Overall, the behavior of the fractional amplitude data is similar to that seen with the ET data for the AcH73 variant (Chapter 3).

### *4.4.2 Effect of pH on the ET reaction, the Alkaline Conformational Transition and the High Spin State.*

Our anaerobic stopped flow data are consistent with results for the ET reaction as a function of pH seen in the preliminary studies with the A79H73 variant of iso-1-cyt *c* [81] over a narrower pH range. The $k_{ET}$ obtained from the fast phase data is three to four times the $k_{ET}$ obtained for AcH73 variant (Chapter 3) and the K73H variant [73]. This suggests that removal of the Lys at position 79 enhances the rate of electron transfer to the native state. The variation with pH is similar to that observed for the AcH73 variant i.e., a decrease in the $k_{ET}$ from pH 7 - 9.5, which may be an artifact of the low population of the native conformer at higher pH, and thus the low amplitude of the fast phase.

The second phase which is assigned to the conformational change from the His73-heme alkaline conformer to the native state, based on the pH dependence of its fractional

amplitude, shows no dependence on the concentration of the $a_6Ru^{2+}$. This type of behavior is seen for AcH73 at higher concentrations of $a_6Ru^{2+}$, where $k_{ET}[a_6Ru^{2+}] \gg k_{MH3}$. In other words at the concentration of $a_6Ru^{2+}$ in our experiments, the rate of the ET reaction is so fast that formation of the redox active Met80-heme bound conformer becomes rate limiting. Thus, $k_{obs}$ equals $k_{HM3}$ for the faster intermediate phase. The magnitude of $k_{HM3}$ decreases as pH increases (figure 4.11). The value of $k_{HM3}$ obtained from the fits are subtracted from $k_{obs}$, obtained from pH jump data from *ref* [62], to obtain $k_{MH3}$, (as $k_{obs}$ from pH jump studies is the sum of the forward and the backward rate constants for the conformational transitions occurring at alkaline pH). In pH jump studies, the forward rate constant ($k_f$) is the same as $k_{MH3}$ and the backward rate constant ($k_b$) is the same as $k_{HM3}$. We have used the best fit line of the pH jump $k_{obs}$ data to eq 4.1, to calculate $k_{MH3}$ from our $k_{HM3}$ values obtained directly from ET data. The $k_{HM3}$ values are shown in figure 4.11 (red circles, see Appendix C, Table C5).

**Equation 4.1**

$$k_{obs} = \underbrace{\left(\frac{K_{HL}}{K_{HL}+[H^+]}\right)\left(\frac{k_{f1}[H^+]^2 + k_{f2}K_{H1}[H^+] + k_{f3}K_{H1}K_{H2}}{K_{H1}K_{H2} + K_{H1}[H^+] + [H^+]^2}\right)}_{k_f\,(k_{MH3})} + \underbrace{\left(\frac{k_{b1}[H^+]^2 + k_{b2}K_{H1}[H^+] + k_{b3}K_{H1}K_{H2}}{K_{H1}K_{H2} + K_{H1}[H^+] + [H^+]^2}\right)}_{k_b\,(k_{HM3})}$$

The common feature between the K73H, AcH73 and A79H73 variants is the mutation of Lys73 to His. Comparison of the pH jump data for the K73H [61] and A79H73 [62] variants, and also the ET data for the AcH73 variant (Chapter 3) indicates the presence of an ionizable group with p$K_a$ ~5 to 5.5 modulating $k_b$ for the His73-heme alkaline transition below pH 6. This result is further supported by the ET data for A79H73, which allows the direct evaluation of $k_{HM3}$ ($k_b$). $k_{MH3}$ increases from pH 5.5 to

6.5, and levels out near pH 7, consistent with the ionization of His73 controlling the formation of the His73-heme alkaline conformer. $k_{MH3}$ increases again above pH 8, which is consistent with the third ionizable group modulating the alkaline transition.

In fitting pH jump data in *ref* [62], the assumption was made that the equilibrium constants are constant throughout the pH range of 5 to 10. To check the validity of this assumption $k_{HM3}$ ($k_b$) and $k_{MH3}$ ($k_f$) were calculated separately from equation 4.1, which is based on three ionizable triggering mechanism for the alkaline conformational transition as described in *ref* [62]. The parameters were taken directly from Table 2 of *ref* [62], values obtained from these calculations are shown in figure 4.11 as squares and triangles.

This assumption works well for acidic and neutral pH regions, but not so well above pH 8. However the ET data suggests that the population of native state decreases as alkalinity increases, thus, the earlier assumption that the equilibrium constant for the His73-heme alkaline transition of the A79H73 variant is invariant with pH appears not to be true.

The second intermediate phase, $k_3$, could be due to a high spin heme state resulting from a hydroxyl-heme bound form ($OH^-$-heme). The fractional population is similar to that seen with the AcH73 variant data (Chapter 3). Thermodynamic studies with the A79H73 variant indicate the presence of a high-spin heme state, which starts to populate above pH 8 [62]. However, lack of a strong increase in the fractional amplitude of this phase above pH 8, casts doubt on its assignment to a high-spin state.

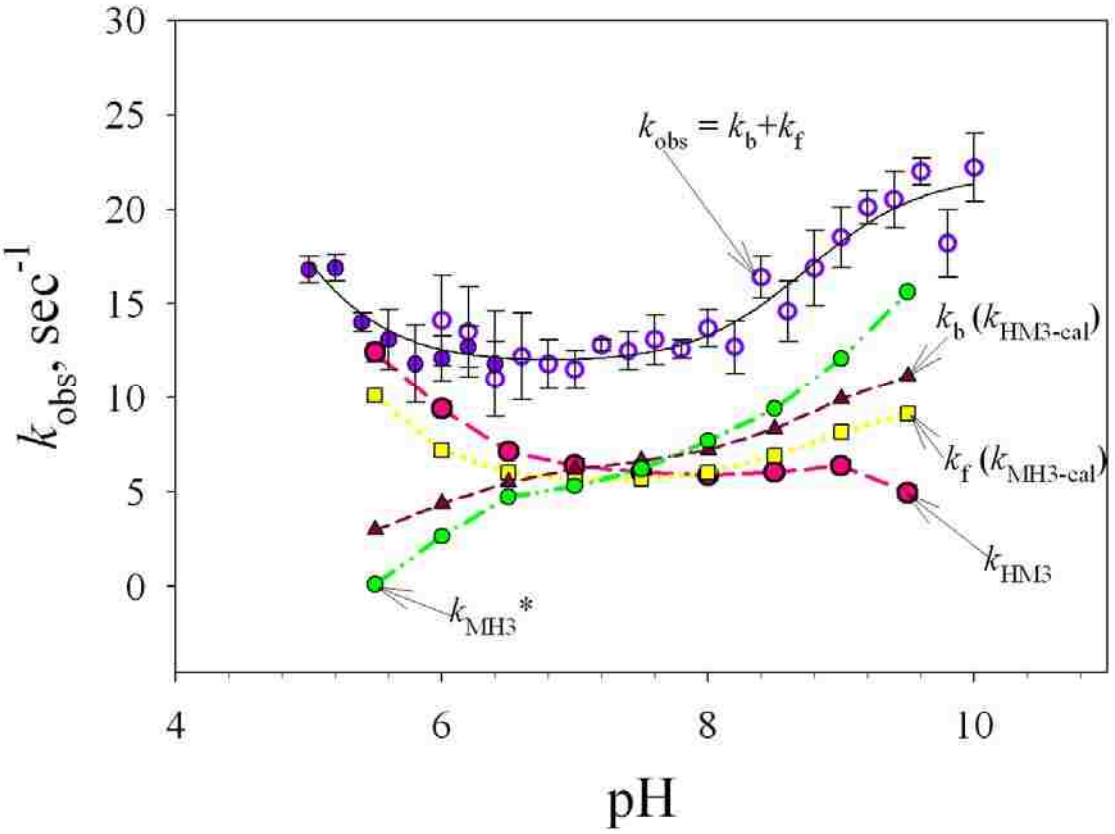


**Figure 4.11** Plots of $k_{HM3}$ (forward) and $k_{MH3}$ (backward) rate constants with respect to pH-jump kinetics data for the A79H73 variant as a function of pH. pH jump data ($k_{obs} = k_b + k_f$) for A79H73 from *ref* [62] are shown in purple (closed circles for downward pH jump data and open circles for upward pH jump data). The solid line is the fit to the eq 4.1. Values for $k_{HM3}$ were obtained from the ET data in figure 4.7. $k_{MH3}$* values are obtained from subtracting $k_{HM3}$ from $k_{obs}$ (from the fit to the pH jump data, eq 4.1, *ref* [62]). The values for $k_{HM3}$ and $k_{MH3}$ are collected in Appendix C, Table C5. $k_f$ ($k_{MH3\text{-}cal}$) and $k_b$ ($k_{HM3\text{-}cal}$) are calculated directly from eq 4.1 based on the pH jump data form *ref* [62].

### *4.4.1 Effect of pH on cis- trans Proline Isomerization.*

The fourth phase or the slowest phase, $k_4$, (occurring on a 10 - 25 s time scale) obtained from fits to the redox kinetic traces from figure 4.4, is attributed to proline isomerization as discussed above. Figure 4.12 shows $k_{ct}$ obtained from $k_4$ at 5 mM [$a_6Ru^{2+}$]. This slow phase matches well with the slow phase obtained from the downward

pH jump data in *ref* [62] near pH 5.5, as can be seen from figure 4.11 and also appendix C, Tables C4 and C6. In figure 4.12 open green circles are from upward pH jump and close green circles are from downward pH jump slow phase kinetic data. The slowest phase observed from ET experiments is assumed to be due to *cis* to *trans* proline isomerization ($k_{ct}$, see figure 4.2, red triangles, and Appendix C, Table C6).

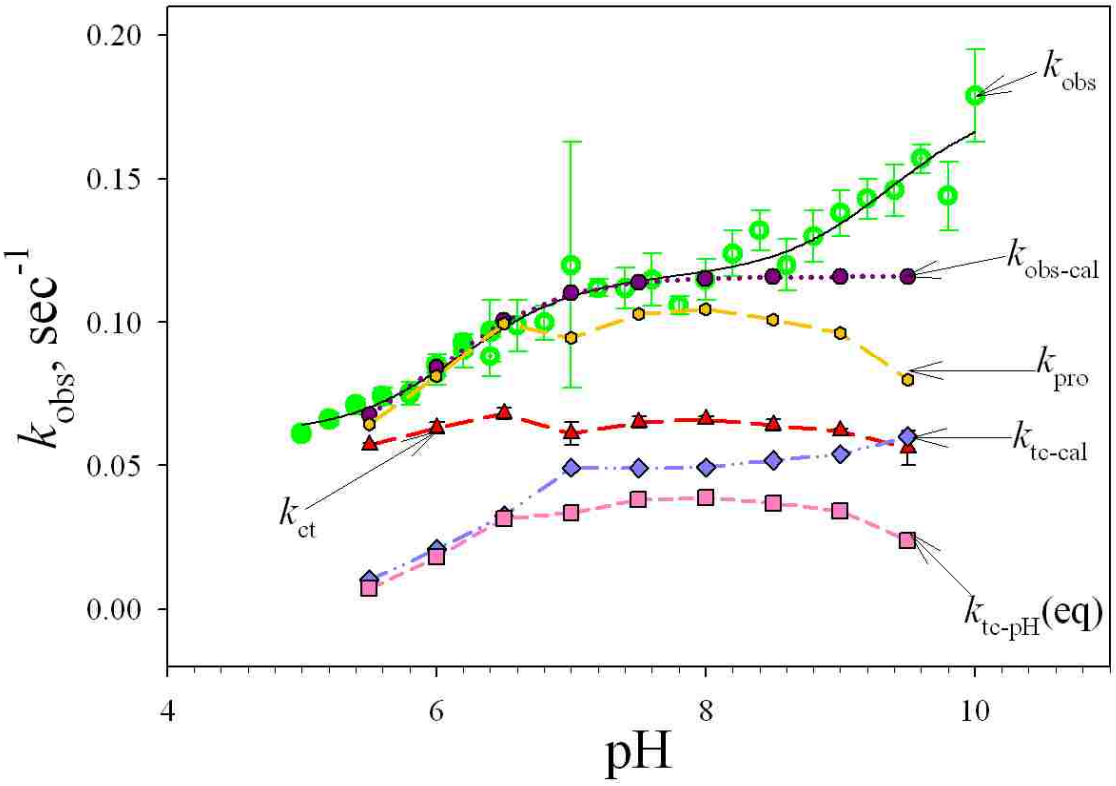


**Figure 4.12** Plots of $k_{tc}$ (forward) and $k_{ct}$ (backward) rate constants with respect to the slow phase from pH-jump kinetics for A79H73 as a function of pH. pH jump data ($k_{obs} = k_{tc} + k_{ct}$) for the A79H73 variant are from *ref* [62] and are shown in green (closed green circles for downward and open green circles for upward pH jump data). The solid line is the fit to the eq 8 in *ref* [62]. Values for $k_{ct}$ are from $k_4$ at 5 mM $a_6Ru^{2+}$ concentration from fits of the ET data to a quadruple exponential rise to maximum equation as shown in figure 4.4. $k_{tc\text{-}pH}$ (eq) values are obtained from eq 4.5. $k_{pro}$ is the sum of $k_{tc\text{-}pH}$ (eq) and $k_{ct}$. The values for $k_{obs\text{-}cal}$ were calculated from eq 4.3, using the parameters for slow phase from [62] in Table 2.

If we assume that $k_{obs}$ from pH jump data represents the sum of the forward ($k_{tc}$) and backward ($k_{ct}$) proline isomerization, then $k_{tc}$ can be calculated by subtracting $k_{ct}$ (obtained from ET data) from $k_{obs}$ ($k_{tc\text{-}cal}$ in figure 4.11, see also, Appendix C, Table C6). In figure 4.11 $k_{tc\text{-}cal}$ increases and then levels out above pH 7. This rate constant is expected to increase as the His73-heme alkaline conformation populates.

Interestingly, $k_{tc\text{-}cal}$ is larger in magnitude than $k_{ct}$ from ET data at pH 9. However amplitude data in figure 4.13 is inconsistent with $k_{tc\text{-}cal}$ being larger than $k_{ct}$. The amplitude for fast intermediate phase ($A_f$), is proportional to the concentration of the alkaline His73-heme conformer with a *trans* proline (native proline isomer) and the amplitude for slow phase ($A_s$) is proportional to the concentration of the alkaline His73-heme conformer with a *cis* proline. The ratio of these amplitude yields the equilibrium constant $K_{iso}$ ($A_s/A_f$) (eq 4.2) which is ~0.5 for the pH range of 5.5 to 9.5 (figure 4.12 and Appendix C, Table C6). Thus the ratio of $k_{ct}$ and $k_{tc}$ should be 2:1.

On the basis of amplitude data from figure 4.13 we can calculate $k_{tc}$ versus pH, such that it is consistent with $K_{iso}$. We first hypothesize that an ionizable group is coupled to $k_{tc}$ in such a way that $k_{tc}$ increases as the His73-heme alkaline conformer populates ($k_{tc\text{-}pH}$ equation 4.3). To calculate $k_{tc\text{-}pH}$ that is consistent with $K_{iso}$ from amplitude data, $k_{tc\text{-}pH}$(eq), we substitute for $k_{tc}$ in eq 4.4 using eq 4.2 to obtain eq 4.5.

**Equation 4.2**

$$K_{iso} = \frac{k_{tc}}{k_{ct}} = \frac{A_s}{A_f}$$

**Equation 4.3**

$$k_{obs} = k_{tc}\left(\frac{K_{HL}}{K_{HL} + [H^+]}\right) + k_{ct}$$

**Equation 4.4**

$$k_{tc-pH} = k_{tc}\left(\frac{K_{HL}}{K_{HL} + [H^+]}\right)$$

**Equation 4.5**

$$k_{tc-pH}(eq) = K_{iso}k_{ct}\left(\frac{K_{HL}}{K_{HL} + [H^+]}\right)$$

In the above equations, $K_{HL}$ is the ionization constant of the ionizable group coupled to $k_{tc}$. Its value is taken from slow phase fits in Table 2 *ref* [62] ($pK_{HL}$= 6). $k_{ct}$ was taken directly from ET data at 5 mM $a_6Ru^{2+}$ as given in Appendix C, Table C6. The $k_{tc\text{-}pH}$(eq) values obtained from eq 4.5 for the pH range 5.5-9.5 are given in Appendix C, Table C6 and are also shown in figure 4.12 (pink squares). $k_{pro}$ in figure 4.5 was obtained by summation of $k_{ct}$ and $k_{tc\text{-}pH}$(eq). $k_{pro}$ (yellow circles) in figure 4.12 shows the effect of an ionizable group on proline isomerization. The ET data match the pH jump data reasonably well up to pH 8. The ET data indicates that the increase in $k_{obs}$ for the slow pH jump phase at higher pH is not attributable to proline isomerization.

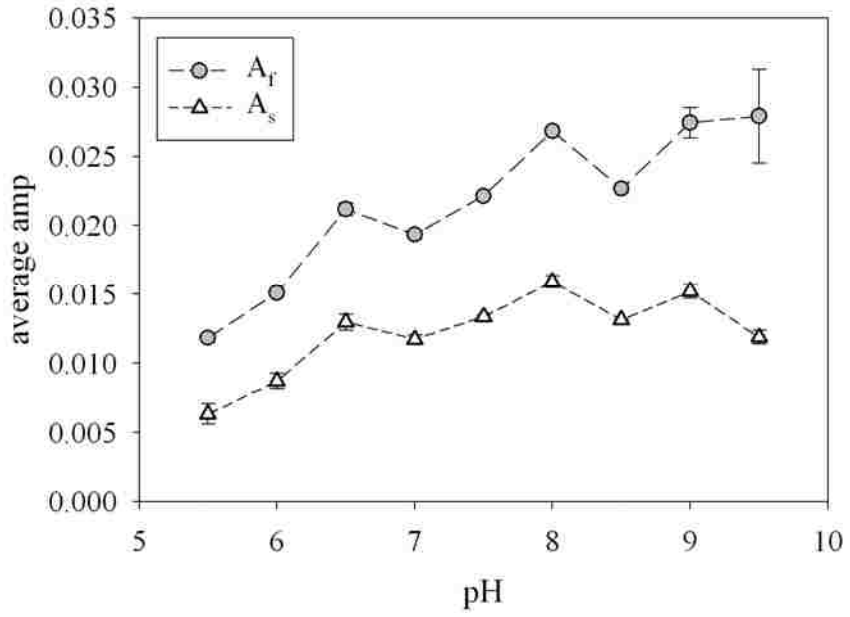


**Figure 4.13** Plots of amplitude for the faster intermediate ($A_f$) and the slowest phase ($A_s$) are from average amplitudes at all three $a_6Ru^{2+}$ concentrations from ET experiment data.

The proline at position 76 is believed to be responsible for the slow kinetic phase of the A79H73 based on work on the folding of iso-2 cyt *c*, where Pro76 was mutated to Gly, eliminating the slow phase of the folding kinetics [111]. This Pro76 is present in all mitochondrial cytochromes *c* and X-ray crystallography has shown that Pro76 occurs as the *trans* imide isomer near the protein surface and is the second amino acid in a type II reverse turn as shown in figure 4.2 [111, 147-149]. The turn is positioned between a short segment of helix (residues 70-75) and the native heme ligand Met80 (figure 4.2). Isoleucine is present at position 75 which increases the propensity of Pro76 to be in the *trans* form as mentioned in the Introduction (% cis ~12.0%, $K_{iso}$ ~12.0/88.0 = ~0.14). As His is present at position 73 in A79H73 and predominantly binds to heme at physiological pH, this appears to lead to some constraints on Pro76 to which promote the *cis* isomer, since $K_{iso}$ ~ 0.5 and % cis ~33% in the His73-heme alkaline conformer. This slow phase is not seen with H79 variant. Thus, the His79-heme alkaline conformer presumably does not permit proline isomerization [64].

This *cis-trans* isomerization of Pro76 slows down the Met80 binding to the heme. This effect can be seen in the ET experiments where Met80 binding to heme becomes the rate limiting step leading to Gated ET. Thus, this *cis-trans* isomerization acts as a conformational switch and indirectly affects the electron transfer mechanism. Proline *cis-trans* isomerization is known to act as a backbone and thus conformational switch. Studies with the Pro8 residue present between the second and third transmembrane helices of 5-Hydroxytryptamine type 3 (5-$HT_3$) have shown the molecular rearrangement at Pro8 gate the neurotransmitter ion channel [150]. Recent studies have also pointed towards prolyl *cis-trans* isomerization as a novel molecular timer to help control the

amplitude and duration of cellular processes, and possibly as a new target for therapeutic interventions [151].

## 4.5 Conclusions

Proline *cis-trans* isomerization reactions and amplitudes are typically independent of pH. However, studies on the A79H73 variant showed variation in this slow phase attributable to Pro76 *cis-trans* isomerization in previous pH jump studies. ET experiments monitored using $a_6Ru^{2+}$ for reduction of the A79H73 variant of iso-1-cyt *c* over the pH range of 5.5 to 9.5 allows $k_{ct}$ to be measured directly and $K_{iso}$ to be obtained from amplitude data over a broad pH range. The data shows that above pH 8 the slow phase observed in pH jump experiments likely has contributions from other sources beside proline isomerization or that prolines other then Pro76 are able to isomerize.

These studies also show the utility of the ET methods to probe not only conformational dynamics, but also the equilibria associated with them, i.e., proline isomerization. The information about $k_{ct}$ obtained directly from these ET methods shows that the interpretation in previous studies with the A79H73 variant dealing with pH jump are correct up to pH 8. Present studies also indicates that the slow phase at pH higher then 8 is not due to the proline isomerization. Direct measurement of His73-heme to native state conformational change i.e. $k_{HM3}$, provides the evidence for the involvement of an ionizable group with p$K_a$ near 5.5, similar to that observed with K73H and AcH73 variants previously. Finally, these studies also demonstrate that the A79H73 variant is not fully native near pH 5.

# CHAPTER 5

## *MODIFICATION OF THE DYNAMICS OF THE ALKALINE TRANSFORMATION BY MUTATIONS IN AN Ω- LOOP OF ISO-1-CYTOCHROME C*

### 5.1 Introduction

Protein secondary structure is classified as regular and nonregular secondary structure. Regular secondary structures are easily identified as α-helix and β-strand with repeating backbone dihedral angles and hydrogen bonding [152, 153]. Nonregular structures lack such patterns and are often lumped together as random coil, coil or loops. Loops were first described by Leszczynski and Rose in 1986 as a continuous chain segment of six or more amino acids that adopts a "loop-shaped" conformation in three-dimensional space, with a small distance between its segment termini [154]. Though this definition was related to the Ω-loop, it holds true for loops in general also. On average, 4-5 loops are found in a protein. Loops were classified in 1992 [155] based on the proximity of the end points of peptide segments rather than on the specific conformation of the peptide backbone. In general omega (Ω) loops have two ends close to each other and a planar nonlinear backbone; zeta (ζ) loops have two ends close to each other, but a nonplanar nonlinear backbone and lastly strap-loops are linear loops in which the segment end points are not close in space. Ω-loops are generally found on the surface of proteins and because of this disposition, changes in amino acid sequence and loop length were considered to be less disruptive than changes made in the core of the protein. However, studies have shown the importance of Ω-loops in protein function, stability and also in protein folding. Some of the studies that supported the role of Ω-loops in protein function include: deletion of one Ω-loop, which converts the mammalian pancreatic

phospholipase into a snake venom protein [156]; studies showing that they are an important part of immunoglobulins, participating in antigen binding [157]; studies showing that they are essential for catalytic activity in tryptophan synthase as binding of the substrate leads to conformational changes in the loop [158]; and studies showing that they participate in the active site for various other enzymes with involvement of conformational changes in the loop [159]. Single and multiple deletions in Ω-loops have been shown to affect protein stability drastically, both stabilizing and destabilizing a protein. Dihydrofolate reductase [160] and human superoxide dismutase [161] are common enzymes used in these studies. Some loops bind metal ions. Studies have shown a stabilizing effect when the metal is bound to the loop. These studies include the effect of calcium binding on the stability of *Bacillus subtilis* neutral protease and subtilisin BPN, and with the thermostable proteins, thermolysin and thermitase [162]. Loops bury a large amount of hydrophobic surface area within their structures, they are compact and contain a substantial number of intra-loop hydrogen bonds suggesting that loops are autonomous folding units and play an active role in protein folding [159]. This has led to studies with loops isolated from proteins in various solutions and different conditions [159, 163]. Studies with interleukin-1β [164] have suggested a role of loops in aggregate formation and with human lysozymes [165] as a component of amyloid fibrils. These studies have suggested that some loops may maintain independent structure in solution but that some loops are not independent folding units [159]. Despite these studies, the relation between loop structure, and loop stability and function, is still not clear [159].

With the ease of working with cytochrome *c* and its very well known electron transfer function, various studies pertaining to loops have been done. Cytochrome *c* has

three conserved helices, one at the amino terminus and one at the carboxyl terminus (blue colored helices in figure 5.1), and one running from residues 60-70, (green colored helix in figure 5.1), which are joined by three or four Ω-loops. The position of these loops is conserved, although there is some variation in the composition between family members from different species [166]. As *Saccharomyces cerevisiae* requires a functional cytochrome *c*, it provides an advantage in studying the effects of mutation on protein structure and function, which can be distinguished *in vivo*. Iso-1-cytochrome *c* is known to have four loops, loop A (residues 18-32), B (residues 34-43) C (residues 40-54) and D (residues 70-85) as shown in figure 5.1. Deletions in loops B and C have been shown to have no effect on the folded protein but deletions in loops A and D have led to a complete deficiency of holocytochrome *c* [166].

The focus of this chapter is on Ω-loop D, which has a highly conserved sequence among different species of cytochrome *c* (cyt *c*). Various studies with eukaryotic cyt *c* have hypothesized its involvement at a step in the bioprocessing of apocytochrome *c*, such as mitochondrial recognition or import, heme lyase recognition or reactivity, and heme binding or folding [167]. This Ω-loop D consists of Methionine at position 80 which serves as the sixth ligand for binding to the heme and three lysines at positions 72, 73 and 79. Ω-loop D is known to control the alkaline transition in ferricytochrome *c* [77] and lysines at positions 73 and 79 in yeast iso-1-cyt *c* are identified as the ligands replacing Met80 and binding to the heme in this base-induced conformational change [48, 60]. The alkaline conformational transition is suggested to participate in the electron transfer function of cyt *c* [168], and plays an important role in apoptosis [55].

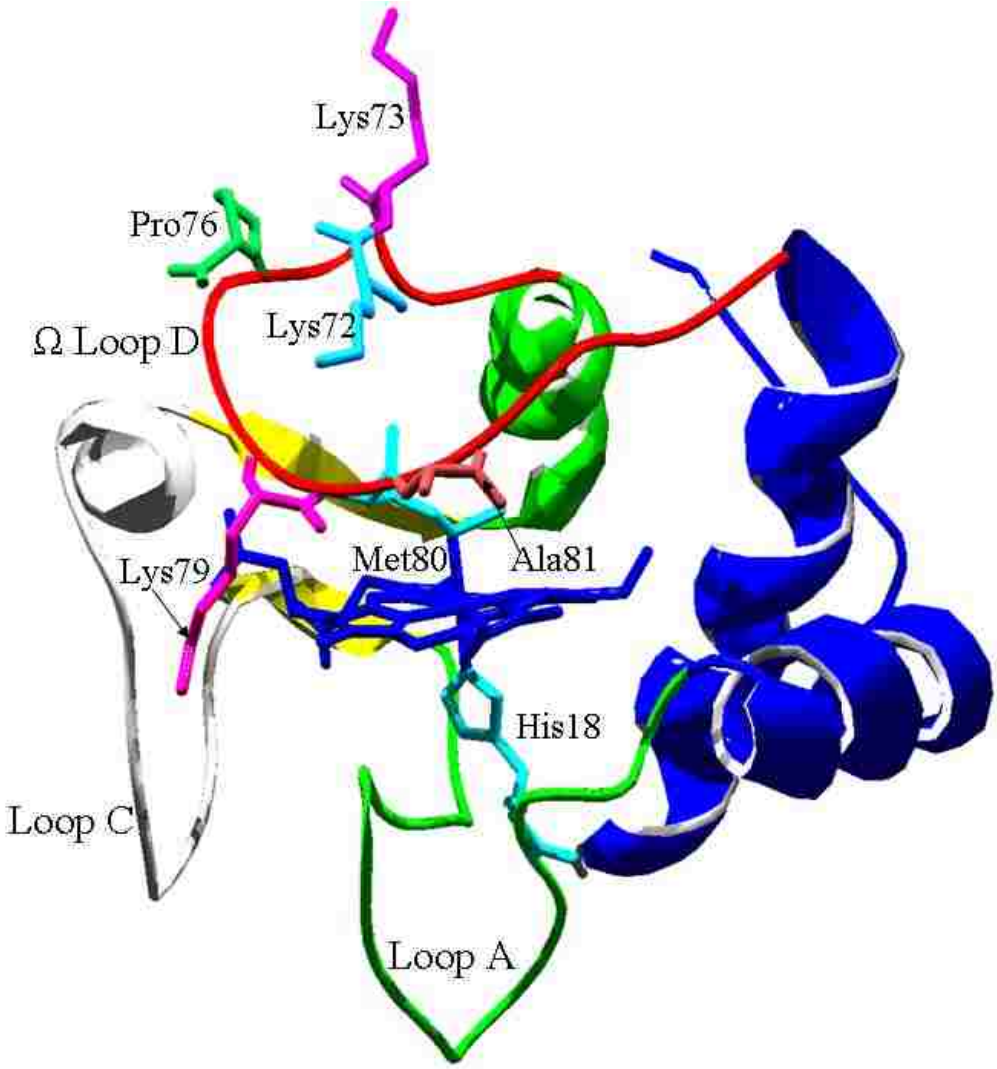


**Figure 5.1** Iso-1-cyt *c* showing the side chains of Lys72 (blue) Lys73 (pink), Pro76 (green), Lys79 (pink) and Ala81 (brick red) The heme cofactor is shown in blue with the heme ligands Met80 (cyan) and His18 (cyan). The substructures of cytochrome *c* as defined by Englander and co-workers are shown from least to most stable in the colors gray, red, yellow, green, and blue [24].

Previous studies have dealt with the mutation of Tyr74, Ile75, Pro76, Gly77, Thr78 and Lys79 to various amino acids including alanine, valine and glycine. Studies from our lab with mutations at positions 73 and 79 to histidine and alanine have shown modifications in the alkaline transition [23, 59, 61, 62, 64, 73, 81]. These studies have

suggested the presence of an intermediate state with a His-heme bound conformer before lysine binds to the heme and also the alteration in the gated electron transfer rate and thus modulation of its function. In the present study, we aim further to understand the effect on the alkaline conformational transition of varying the position of histidine in the loop. The effect of such mutations will be evaluated using thermodynamic and kinetic approaches.

Solvent accessible surface area (SASA) calculations were used to propose new mutations in the Ω-loop D region (positions 70-85). Ala 81 was found to have 100% and Pro76, 87% solvent exposed surface area. Highly solvent-exposed side chains normally cause only minor changes in protein stability [169, 170]. Two other mutants H73G76 and H73G76A79 were prepared to study proline isomerization effects on the alkaline transition. Proline 76 is believed to undergo isomerization during partial unfolding to the alkaline conformer as mentioned in Chapter 4 and also in *ref* [111].

## 5.2 Materials and Methods

### *5.2.1 Preparation of the Variants.*

#### *5.2.1.1 Evaluation of Solvent-exposed Surface Area*

Cartesian coordinates of atoms in PDB format for iso-1 cytochrome *c* (2ycc) were obtained from the Protein Data Bank. This file was then submitted to the GETAREA web service provided by the Sealy Center for Structural Biology at the University of Texas Medical Branch (http://www.scsb.utmb.edu/cgi-bin/get_a_form.tcl) for SASA determination. Residues are considered to be exposed if the ratio of side chain surface area exposed relative to the side chain area exposed in a random coil exceeds 50%. If the

ratio is less than 20% the side chain is considered to be buried. Based on this analysis Ala81 and Pro76 were chosen as sites from replacement with histidine.

*5.2.1.2 Preparation in Saccharomyces cerevisiae (yeast)*

The H81 (A81H) , P76H, H73G76 (K73H, P76G), H73G76A79 (K73H, P76G, K79A) and A73H79 (K73A, K79H) variants were prepared by the unique restriction site elimination sitedirected mutagenesis method [82] using the pRS/C7.8 phagemid vector as described previously [84]. For the H81 and P76H variants single stranded (ss) DNA template for pseudo wild type (pWT, C102S) was used. For the H73G76 variant, ssDNA for H73 (K73H, C102S) was used as template. For the H73G76A79 variant ssDNA template carrying the A79H73 [62] variant was used and ssDNA template with the K79H variant was used to produce the A73H79 variant of iso-1-cyt *c*. All of these variants (including pWT) contain the mutation, Cys102→Ser. ssDNA was prepared from TG-1 *Escherichia coli* cells infected with the R408 helper phage [171], using phenol extraction methods [172] to remove the protein coat. The selection oligonucleotide primer *Sac*I$^-$II$^+$ [84] was used to eliminate the unique *Sac*I restriction site upstream from the iso-1-cyt *c* gene (*CYC1*) and restore the *Sac*II restriction site. The selection oligonucleotide, *Sac*I$^+$II$^-$, was used when the ssDNA template contain the *Sac*II restriction site. The mutagenic oligonucleotide primers (Table 5.1) were purchased from Operon Biotechnologies, Inc. (Huntsville, Alabama). The sequence of individual clones was analyzed to confirm the mutation using a Beckman CEQ 8000 capillary electrophoresis autosequencer.

Phagemid DNA carrying the desired *CYC1* variant genes was transformed into the GM-3C-2 strain. Growth, isolation and purification of the variant proteins were done as described in Chapter 2, Materials and Methods section 2.2.1. The variants P76H,

H73G76 and H73G76A79 in yeast showed slow growth and very low yields compared to H81 and other variants grown in lab. Also, their purification yielded multiple chromatographic peaks. To solve these problems the same variants were expressed in *E. coli*, which does not require iso-1-cyt *c* to be functional.

*5.2.1.3 Preparation of Variants in E. coli*

Lys72 was mutated to Ala for variants prepared for expression in *E. coli* as Lys72 in yeast cyt *c* is trimethylated and hence does not participate in the alkaline transition. The Lys72→ Ala (A72 variant) variant was prepared by the unique restriction site elimination site-directed mutagenesis method as described above. *Eco*RV$^{+}$*Aat*II$^{-}$ 5'-d(GTGCCACCTGACGTCTAAGAAACC)-3' was used as the selection primer for its preparation. The vector used was pBTR1 [56, 109] carrying the TM variant (native His 26, 33 and 39 mutated to Asn, Asn and Gln respectively; to avoid interference in the denatured state). The pBTR1(TM) (5.6 kb) vector carries the heme lyase gene in addition to *CYC1* to provide for heme insertion into apocytochrome *c* in the cytoplasm of *E. coli*. The P76H and H73G76 variants were prepared using the QuikChange II site-directed mutagenesis kit (Stratagene) and the pBTR1(TM) vector carrying the K72A mutation was used as the DNA template. The A72H73G76A79 variant was prepared using the A72H73G76 dsDNA as template. The mutagenic primers used for these preparations are shown in Table 5.1 and the variants generated are named, A72H76, A72H73G76 and A72H73G76A79.

These variants were expressed and isolated from BL21-DE3 *E. coli* cells (Novagen) using the pBTR1 vector as described previously [21]. Purification and

concentration determination were done as described in Chapter 2, Materials and Methods, section 2.2.2.

**Table 5.1.** Oligonucleotide primers used for site directed mutagenesis.

| Variant | Oligonucleotide primers from 5'-3' |
|---|---|
| H81 | CCCACCAAA**GTG**CATCTTGGTAC |
| P76H | CATCTTGGTACC**CAT**GAATATATTTC |
| H73G76 | CATCTTGGTACC**ACC**AATATA**GTG**C |
| H73G76A79 | CAT**AGC**GGTACC**ACC**AATATA**GTG**C |
| K72A | CAGGAATATATTT**GGC**TGGGTTAGT |
| A72H76 | TAACCCAGCCAAATATATT**CAT**GGTACCAAGATGGCC |
| A72H76-R | GGCCATCTTGGTACC**ATG**AATATATTTGGCTGGGTTA |
| A72H73G76 | ACTTGACTAACCCA**GCC**CAC TATATT**GGT**GGTACCAAGATGG |
| A72H73G76-R | CCATCTTGGTACC**ACC**AATATA**GTG**GGC TGGGTTAGTCAAGT |
| A72H73G76A79 | **C**CAC TATATT**GGT**GGTACC**GCG**ATGGCCTTTGGTGGGTTG |
| A72H73G76A79-R | CAACCCACCAAAGGCCAT**CGC**GGTACC**ACC**AATATA**GTG**G |

Anti-codons (top 4 and R primers) and Codons (all others) in blue represent that for alanine at position 72, green is for histidine, red is for glycine and magenta is for alanine at position 79 in iso-1-cyt *c*.
R represents the reverse template used in QuikChange mutagenesis.

### *5.2.2 Molecular Weight Determination by MALDI-TOF Mass Spectroscopy.*

Molecular weight was determined for all variants as described previously in Materials and Methods, section 2.2.2 and 3.2.2. of Chapters 2 and 3, respectively. The main peak gave m/z consistent with the expected molecular weight for all the variants as shown in

Table 5.2 (average and standard deviation of 4 to 5 independent spectra). All experiments were carried out with this material.

**Table 5.2.** Calculated and determined m/z for the main peak from HPLC.

| Variants | Expected Mass (g/mol) | m/z from MALDI |
|---|---|---|
| H81 | 12760.37 | 12776.1 ± 2.2 |
| A72H76 | 12571.55 | 12578.4 ± 2.5 |
| A72H73G76 | 12555.52 | 12558.1 ± 3.2 |
| A72H73G76A79 | 12498.46 | 12500.7 ± 2.2 |

### *5.2.3 Oxidation of Protein.*

Protein was oxidized and separated from oxidizing agent as described previously in Chapter 2. The concentration and degree of oxidation of the protein were determined, as described previously in Materials and Methods, section 2.2.2 of Chapter 2.

### *5.2.4 GdnHCl Denaturation Monitored by Circular Dichroism Spectroscopy.*

Global stability of the protein was determined as described previously in Materials and Methods, section 2.2.4 of Chapter 2.

### *5.2.5 Partial Unfolding by GdnHCl Monitored at 695 nm.*

Partial unfolding of protein was monitored at 695 nm, $A_{695}$, as a function of gdnHCl concentration using a Beckman DU 800 spectrophotometer as described previously in Materials and Methods section 2.2.5 of Chapter 2.

### *5.2.6 pH Titration Experiments.*

The alkaline conformational transition caused by His81 was monitored as a function of pH at 0, 0.2, 0.3, 0.4 and 0.6 M gdnHCl concentration with 0.1 M NaCl and at 0 M gdnHCl concentration with 0.5 M NaCl, as described previously, in Materials and Methods, section 2.2.6 of Chapter 2. Equation 5.1 was used to fit the data.

**Equation5.1**

$$\varepsilon_{695corr} = \varepsilon_{alk} + \frac{(\varepsilon_A - \varepsilon_{Alk}) + \left(\frac{10^{-pK_{C1}}}{1+10^{n(pK_{H1}-pH)}}\right)(\varepsilon_N - \varepsilon_{Alk})}{1+\left[\frac{10^{-pK_{C1}}}{1+10^{n(pK_{H1}-pH)}}\left(1+\frac{10^{-pK_{C2}}}{1+10^{(pK_{H2}-pH)}}+\frac{10^{-pK_{C3}}}{1+10^{(pK_{H3}-pH)}}\right)\right]}$$

In eq 5.1, $\varepsilon_N$ is the extinction coefficient at 695 nm of the Met80–heme bound native state, $\varepsilon_{Alk}$ is the extinction coefficient at 695 nm of the alkaline state, $\varepsilon_A$ is the extinction coefficient at 695 nm of the acid state, A. The ($\varepsilon_N$ - $\varepsilon_{Alk}$) was set to the difference of $\varepsilon_N$ - $\varepsilon_{Alk}$ from 0 M gdnHCl (0.6 $mM^{-1}cm^{-1}$). The parameters p$K_{C1}$ and p$K_{H1}$ are equilibrium and ionization constants respectively, corresponding to the acid unfolding. p$K_{H1}$ was arbitrarily set to 5 for this transition. p$K_{C2}$ and p$K_{H2}$ correspond to the His81 heme alkaline conformational transition and p$K_{C3}$ and p$K_{H3}$ correspond to the alkaline transitions due to Lys(73/79). p$K_{H3}$ was set to 10.8 as in *ref* [48] .

A rearranged form of the Henderson-Hasselbalch equation, equation 5.2, was used to fit the acid and alkaline pH-titration data in some cases *ref* [23].

**Equation 5.2**

$$\varepsilon_{695} = \frac{\varepsilon_N + \varepsilon_{alk/acid}\left(10^{n[pK_a(app)-pH]}\right)}{1+10^{n(pK_a(app)-pH)}}$$

In eq 5.2, all the parameters are the same as described for equation 5.1. p$K_a$(app) is the apparent p$K_a$ described by Davis et al. [97]

### *5.2.7 pH Jump Stopped-flow Experiments.*

All pH jump experiments were carried out at 25 $^oC$ as described previously in the Materials and Methods section 2.2.8 of Chapter 2 and in *ref* [61]. Data were collected on

different time scales ranging from 50 to 500 s depending upon the completion of the reaction. Data for the upward and downward pH jump experiments were fit to triple or quadruple exponential equations. The $k_{obs}$ and amplitude data as a function of pH for the fast, intermediate and slow phase were fit to the equation involving two and three ionizable groups for triggering the alkaline conformational transition as mentioned in *ref* [61, 62, 64].

### *5.2.8 Electron Transfer Experiments by the Stopped Flow Method.*

Experiments were done using hexaammineruthenium(II) chloride ($a_6Ru^{2+}$) and bis(2,2',2"-terpyridyl)cobalt(II) triflate, $[Co(terpy)_2](CF_3SO_3)_2$ ($[Co(terpy)_2]^{2+}$), at pH 7.5 (10 mM phosphate buffer, 0.1 M NaCl) under anerobic conditions with an Applied Photophysics SX20 stopped flow spectrophotometer, as described previously in Materials and Methods, section 2.2.9 of Chapter 2 and section 3.2.9 of Chapter 3. The cobalt complex was synthesized from commercially available cobalt(II) chloride hexahydrate ($CoCl_2.6H_2O$; from Fisher Scientific); 2,2':6',2"-terpyridine (Aldrich); and sodium triflate ($NaCF_3SO_3$); from Acros Organics, as described in *ref* [173]. Structural characterization of the $[Co(terpy)_2]^{2+}$ complex was done using 400 MHz $^1H$ NMR spectroscopy as described in *ref* [174]. The concentration of the cobalt complex was determined spectrophotometrically before and after each experiment at 316 nm ($\varepsilon$ = $3.34x10^4$ $M^{-1}cm^{-1}$) and 505 nm ($\varepsilon$ = 1404 $M^{-1}cm^{-1}$) [174]. For higher concentrations of cobalt complex, dilutions were prepared due to the higher absorbance of the cobalt complex. Reduction of the heme was monitored at 550 nm and a minimum of five traces were collected. For all traces, 5000 points were collected logarithmically on 100 to 500

sec time scales. For higher concentrations (>5 mM, after mixing) of the cobalt(II) complex, a shorter pathlength (2 mm) was used, due to the strong absorbance of the Co(II) complex. We were not able to do experiments above 5 mM cobalt complex concentration due to solubility issues. Analysis of the data was done using the curve fitting program, Sigma Plot (v.7.0). The data were fit to double, triple or quadruple exponential rise to maximum equations.

## 5.3 Results

### *5.3.1 Global Unfolding by GdnHCl Denaturation.*

Global unfolding of all variants as a function of gdnHCl was monitored by CD spectroscopy. The ellipticity measured at 222 nm is plotted against gdnHCl concentration for all four variants as shown in figure 5.2. Thermodynamic parameters obtained from a fit of the data to eq 2.1 (Chapter 2, Material and Methods, section 2.2.4) are shown in Table 5.3. All these variants were found to be less stable than the wild type protein ($\Delta G_u^o(H_2O)$ = 5.77 ± 0.4 kcal/mol) [101]. The low *m*-value relative to wild type (*m* = 5.11 ± 0.36 kcal/mol·M) [101]) indicates that for variants containing the K73H and K81H mutations, global unfolding occurs from a partially unfolded form of the protein.

The H81 variant is slightly more stable than the K73H {($\Delta G^o_u(H_2O)$ = 4.32 ± 0.11 kcal/mol, *m* = 3.59 ± 0.01 kcal/(mol×M) and a titration midpoint, $C_m$ = 1.15 ± 0.01 M) and H79 ($\Delta G^o_u(H_2O)$ = 4.45 ± 0.30 kcal/mol, *m* = 3.53 ± 0.25 kcal/(mol×M) and $C_m$ = 1.26 ± 0.01 M) variants of iso-1-cyt *c*, whereas the A72H76 is the least stable variant among these four variants. Both the H81 and A72H76 variants have similar *m*-values to the K73H and H79 variants, suggesting that these variants unfold from a similar partially

unfolded form of the protein. $\Delta G^{o}_{u}(H_2O)$ for the A72H73G76 and A72H73G76A79 variants are slightly lower than that of the K73H and H79 variants. The *m*-values are significantly lower, suggesting that the P76G mutation leads to a more unfolded partially unfolded form of the protein. The A72H76, A72H73G76 and A72H73G76A79 variants can further be compared to the TM variant ($\Delta G^{o}_{u}(H_2O)$ = 4.02 ± 0.17 kcal/mol, *m* = 3.99 ± 0.17 kcal/(mol×M) and $C_m$ = 1.008 ± 0.0003 M *ref* [175]), which serves as the base protein for these variants. Both variants have comparable stability within error to the TM variant. A72H76 is less stable as compared to the TM variant, suggesting a destabilizing effect of histidine at position 76. All these variants have lower *m*-values than the TM variant suggesting they unfold from a partially unfolded form. The degree of unfolding of the partially unfolded form appears to be largest for the A72H73G76 and A72H73G76A79 variants.

**Figure 5.2** On the next page is the plot of ellipticity observed at 222 nm as a function of gdnHCl concentration for the H81 (green circles), A72H76 (pink squares), A72H73G76 (blue triangles) and A72H73G76A79 (grey hexagons) variants of iso-1-cytochrome *c*. Data were acquired at 25 ºC in 20 mM Tris, pH 7.5, 40 mM NaCl and at 4 μM protein concentration. The solid curves are fits of the data to eq 2.1 in Materials and Methods, section 2.2.4 of Chapter 2.

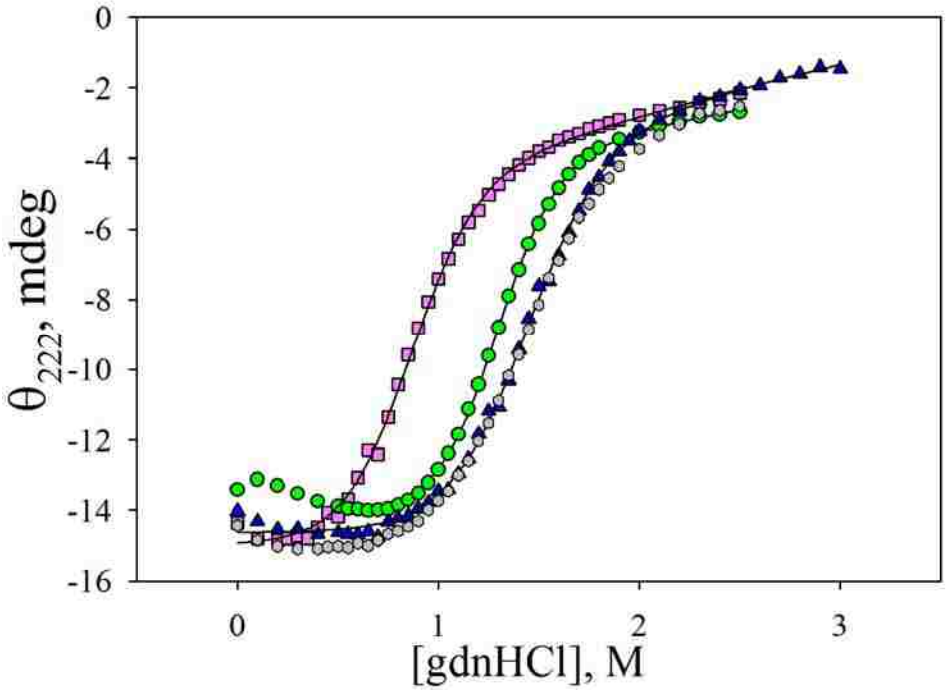


**Table 5.3.** Thermodynamic parameters for gdnHCl unfolding of variants of iso-1-cyt *c* monitored by ellipticity at 222 nm at pH 7.5 and 25 ºC.

| Variants | $\Delta G_u^o(H_2O)$ (kcal/mol) | *m* (kcal / mol·M) | $C_m$ (M) |
|---|---|---|---|
| H81 | 4.89 ± 0.40 | 3.85 ± 0.20 | 1.27 ± 0.05 |
| A72H76 | 3.01 ± 0.10 | 3.56 ± 0.10 | 0.85 ± 0.02 |
| A72H73G76 | 4.21 ± 0.20 | 3.16 ± 0.07 | 1.33 ± 0.03 |
| A72H73G76A79 | 3.94 ± 0.08 | 2.89 ± 0.05 | 1.37 ± 0.04 |

### *5.3.3 Partial Unfolding by GdnHCl.*

Partial denaturation studies were done for the H81 variant at pH 7.5 as a function of gdnHCl. The loss of the Met80-heme conformer was monitored at 695 nm. A plot of absorbance as a function of gdnHCl concentration is shown in figure 5.3. The fit of the data to eq 2.2 from Chapter 2 gives $\Delta G^o_u(H_2O)$ = 1.87 ± 0.02 kcal/mol, and *m* = 2.65 ± 0.05 kcal/(mol×M). A more positive $\Delta G^o_u(H_2O)$ value suggests that partial unfolding

mediated by His81 binding to the heme is not as favorable compared to His73 and His79 binding to heme in the K73H [23] and H79 [64] variants.

Partial denaturation studies were done for the A72H76 variant at pH 7.5 but the absorbance at 695 nm was very low (figure F1 in Appendix F) suggesting that the native conformer for this variant is drastically affected by the mutation of Pro76 to histidine. This supports the studies done in *ref* [167], where His at position 76 showed zero preference in a genetic selection assay and leads to production of non-functional cytochrome *c*. Partial unfolding studies cannot be done with the A72H73G76 and A72H73G76A79 variants as pH titration studies showed very weak absorbance at 695 nm even at pH 5.

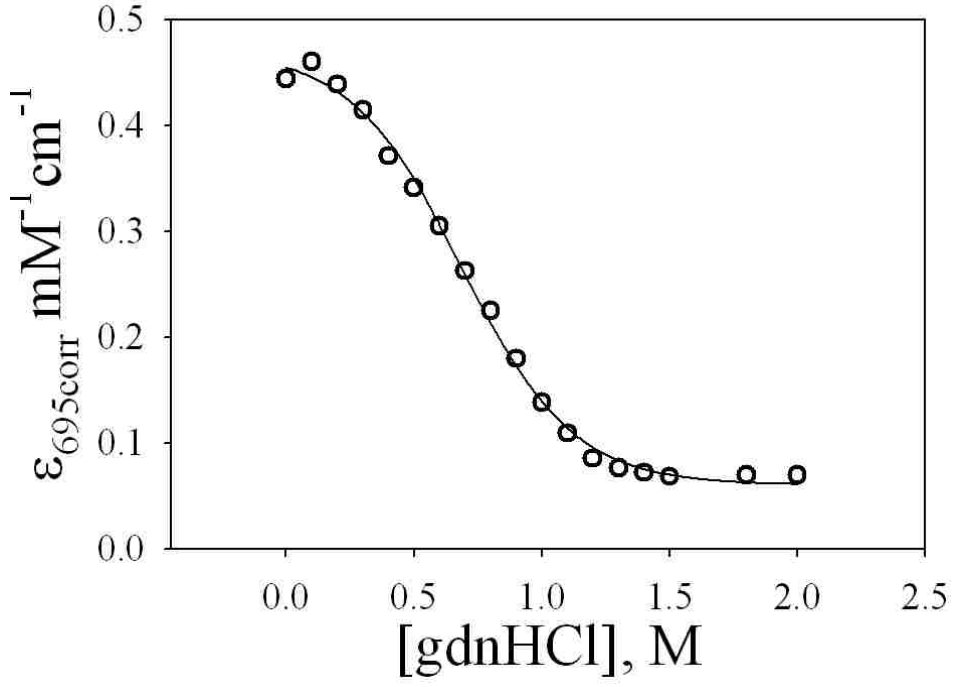


**Figure 5.3** Plot of $\varepsilon_{695corr}$ versus gdnHCl concentration for H81 iso-1-cyt *c*. Data were acquired at room temperature (22 ± 1 ºC) in the presence of 20 mM Tris, pH 7.5, 40 mM NaCl (○). The solid curves are fits of the data to eq 2.2 in Materials and Methods, section 2.2.5 of Chapter 2.

### *5.3.3 pH Dependence of the Native Heme-Met 80 Conformer Stability.*

*5.3.3.1 pH Dependence of 695 nm Absorbance for the H81 Variant*

The conformational stability for the H81 variant was monitored through the acid and alkaline transitions at different gdnHCl concentrations. Changes in the band at 695 nm characteristic of Met80-heme ligation were followed from pH 2 to 11. An increase in the absorbance band at 695 nm was seen near pH 5 followed by a decrease in the alkaline region. Figure 5.4 shows the data at different gdnHCl concentration, fitted to equation 5.1. The thermodynamic parameters obtained from fits are shown in Table 5.4 for both 0.1 and 0.5 M NaCl concentration.

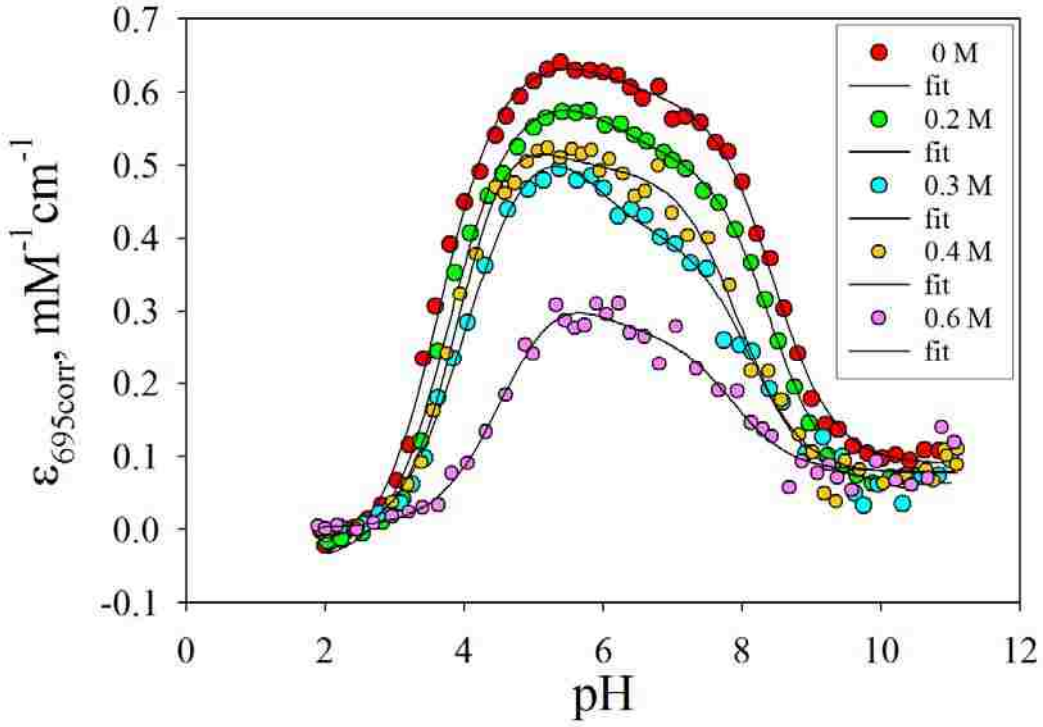


**Figure 5.4** Plot of $\varepsilon_{695corr}$ ($mM^{-1}cm^{-1}$) versus pH for H81 iso-1-cytochrome *c* at different concentrations of gdnHCl. Data were collected at room temperature (22 ± 1 ºC) in 0.1 M NaCl with 0, 0.2, 0.3, 0.4 and 0.6 M gdnHCl. The solid curves are fits to eq 5.1 as described in Materials and Methods.

The value of p$K_{H2}$ is in the range of 5.9 to 6.2, which is consistent with the p$K_a$ of histidine and is not sensitive to gdnHCl concentration. The value of p$K_{C1}$ becomes progressively less negative as the gdnHCl concentration is increased, suggesting destabilization of the native state at higher gdnHCl concentration. The values of both p$K_{C2}$ (His81 binding to heme) and p$K_{C3}$ (Lys73/79 binding to heme) become progressively more negative (i.e. more favorable) as the gdnHCl concentration is increased. pH titrations were also done at 0.5 M NaCl concentration (Appendix F1. figures F2 and F3) to observe the effect of salt. The effect of salt concentration appears to be minor.

**Table 5.4.** Thermodynamic parameters from pH titration in 0.1 M NaCl at 25 ºC for the H81 variant of iso-1-cytochrome *c*.[a]

| [gdnHCl] (M) | p$K_{C1}$ | *n* | p$K_{C2}$ | p$K_{H2}$ | p$K_{C3}$ |
|---|---|---|---|---|---|
| 0 | -1.48 ± 0.24 | 1.02 ± 0.14 | 0.85 ± 0.17 | 5.9 ± 0.3 | -2.41 ± 0.04 |
| 0[b] | -1.32 ± 0.02 | 0.89 ± 0.04 | 0.99 ± 0.23 | 6.6 ± 0.3 | -2.34 ± 0.02 |
| 0.2 | -1.25 ± 0.07 | 0.99 ± 0.01 | 0.69 ± 0.02 | 6.2 ± 0.1 | -2.53 ± 0.04 |
| 0.3 | -0.90 ± 0.07 | 0.96 ± 0.05 | 0.31 ± 0.05 | 5.8 ± 0.2 | -2.91 ± 0.07 |
| 0.4 | -1.10 ± 0.13 | 1.1 ± 0.1 | 0.47 ± 0.07 | 5.8 ± 0.6 | -2.79 ± 0.17 |
| 0.6 | -0.06 ± 0.08 | 0.83 ± 0.06 | -0.13 ± 0.26 | 6.1 ± 0.9 | -3.37 ± 0.14 |

[a] Parameters are from fits of the data to eq 5.1 in Materials and Methods.

[b] Data acquired in the presence of 0.5 M NaCl.

A linear free energy relation is assumed for these transitions and the free energy calculated from respective p$K_C$'s are fitted to eq 3.3 from Chapter 3, Results section 3.3.3 as shown in figure 5.5. The *m*-value for the His81 conformational transition (p$K_{C2}$) is similar to that seen with the K73H variant suggesting a similarity in structural disruption for both variants. The *m*-value for Lys (73/79) conformational transition (p$K_{C3}$) is larger

then that seen with K73H variant for the Lys79 conformational transition suggesting that Lys73 may be the dominant ligand in the higher pH alkaline transition. The number of protons involved in the acid transition is ~1, which is lower than usual. The plots in figure 5.6 show one isosbestic point in the pH region 4-8 consistent with His81 heme ligation and another isosbestic point for the pH range 8.2-11, consistent with the Lys-heme conformer. The presence of multiple isosbestic points from pH 2 to 4 suggests that the acid transition phase is a complicated process compared to the alkaline transitions.

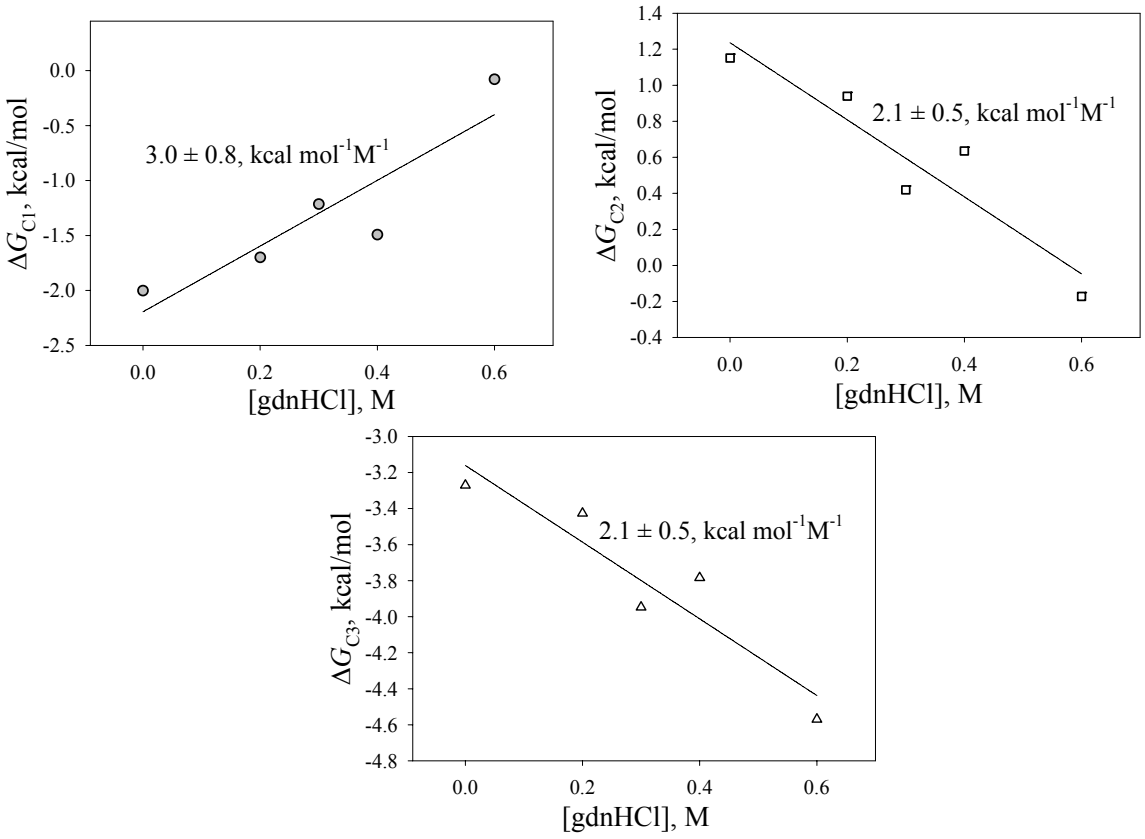


**Figure 5.5** Plots of Free Energy versus gdnHCl concentration for the H81 variant of iso-1 cyt *c*. The Free Energies, $\Delta G_{C1}$ (○), $\Delta G_{C2}$ (□) and $\Delta G_{C3}$ (Δ), represent the acid ionization, His81-heme and Lys(73/79)-heme alkaline conformers, respectively.

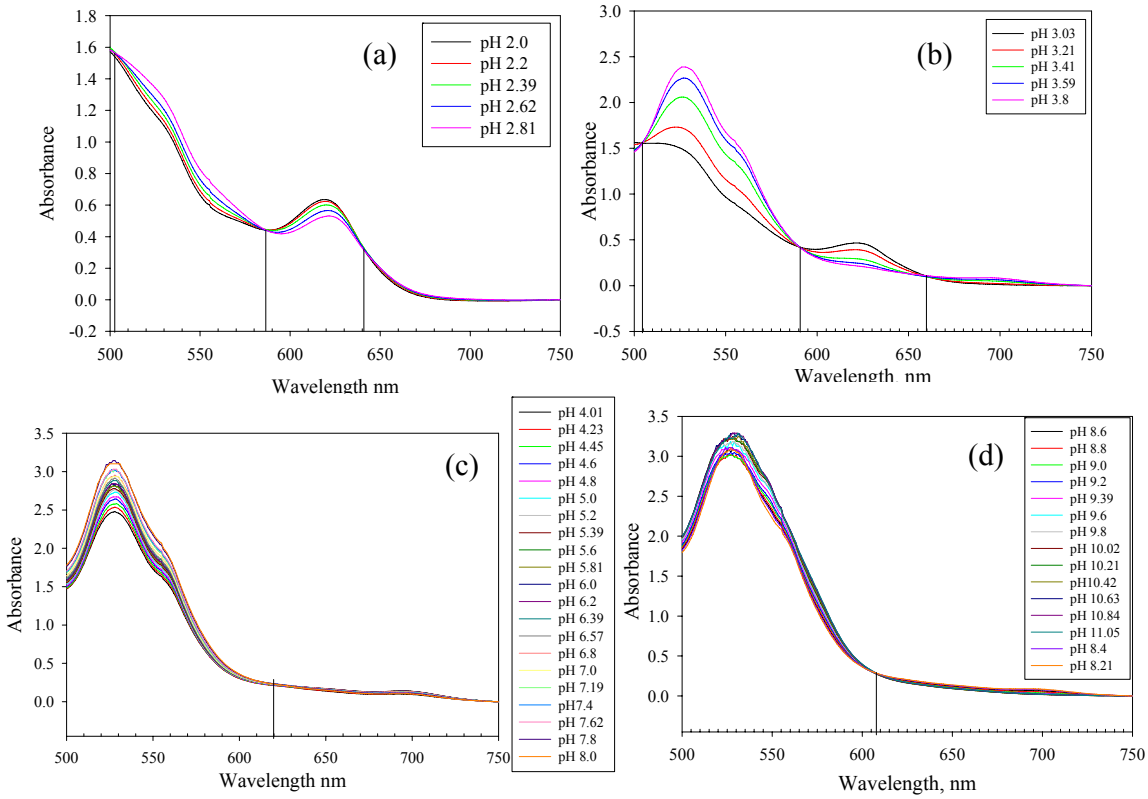


**Figure 5.6** Plot of absorbance spectra as a function of pH for the H81 variant of iso-1-cyt *c* at 22 ± 1 ºC in the presence of 0.1 M NaCl. (a) pH 2.0 – 2.81 (~503 nm, ~586 nm and ~641 nm) (b) pH 3.03 – 3.8 (~504 nm, ~591 nm and ~659) (c) pH 4.01 – 8.0 (~620 nm) and (d) pH 8.21 – 11.05 (~608 nm). Isosbestic points are given in parentheses.

The fractional population of each state of the H81 variant as a function of pH was calculated from the equation used to obtain the thermodynamic parameters, to determine the variation in the population of acid, native and alkaline forms of the protein (figure 5.7). This plot clearly shows that the decrease in the acid state is compensated by an increase of the native state near physiological pH. At alkaline pH, the Lys-heme bound state is dominant and the His81-heme conformer is ~10% populated near pH 7.5.

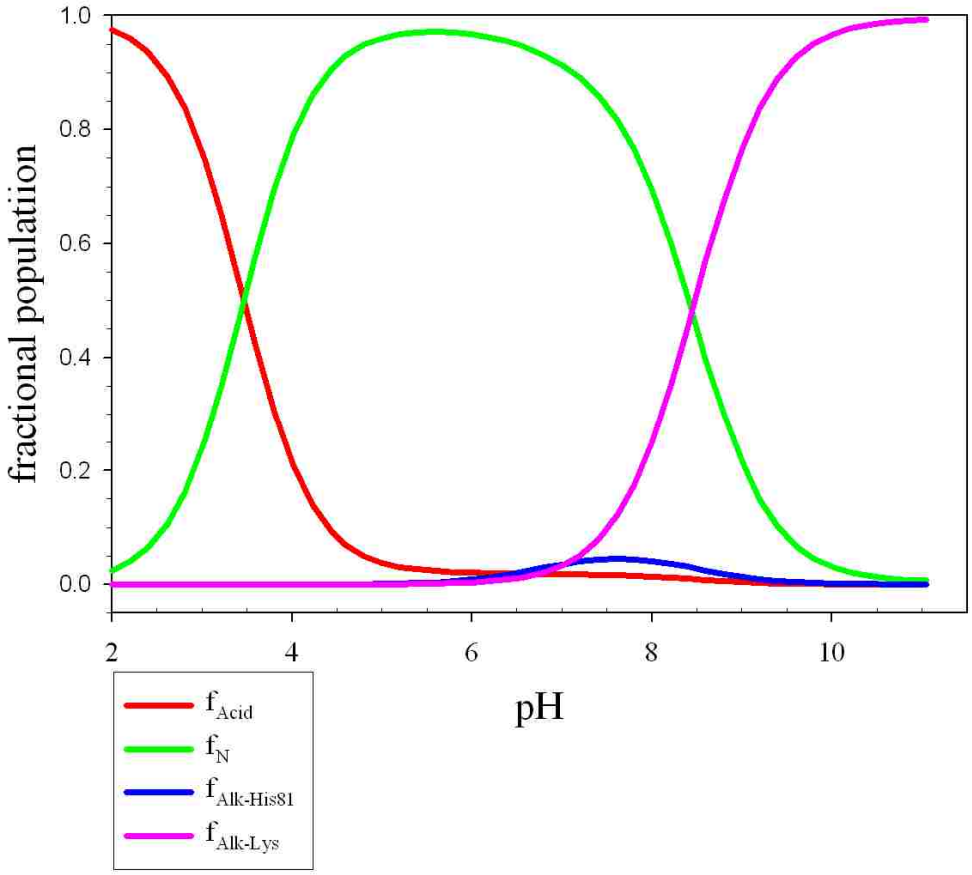


**Figure 5.7** Plot of fractional population versus pH for H81 iso-1-cytochrome *c* at 0 M gdnHCl. Data were collected at room temperature (22 ± 1 ºC) in 0.1 M NaCl.

*5.3.3.2 pH Dependence of Absorbance at 695 for the A72H76 Variant*

Spectrophotometric pH titrations at 695 nm were carried out for A72H76 variant from pH 2 to 11 as for the H81variant. The absorbance band at 695 nm is sensitive to Met80 as the sixth ligand for heme and so it decreases in the acid or alkaline regions reflecting the displacement of the Met80 ligand as shown in figure 5.8. The data points were divided into two sets (acid and alkaline transition pH ranges) for ease of fitting and extracting thermodynamic parameters using the Henderson-Hesselbalch equation (eq 5.2 in Materials and Methods). Thermodynamic parameters from the fits are shown in Table 5.5. The acid transition phase yields a p$K_a$(app) of 3.74 which is believed to be associated

with protonation of His18 (the fifth ligand for the heme see *ref* [176]). It is a multiple proton process as expected for the acid transition. The alkaline transition phase associated with a p$K_a$(app) of 6.34 is likely due to His76-heme ligation, however involvement of Lys binding to the heme cannot be ruled out. This alkaline transition is associated with release of one proton as expected. The plots of absorbance spectra as a function of pH (figure 5.9) show multiple isosbestic points in the acid region similar to the H81 variant, suggestive that this process is more complicated than the alkaline transition which yields a single isosbestic point from pH 5 to 8.

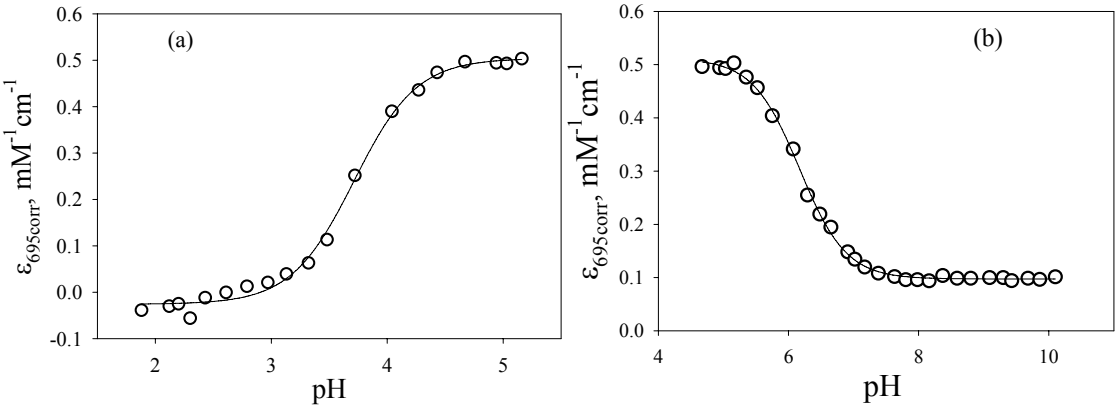


**Figure 5.8** Plot of $\varepsilon_{695corr}$ $mM^{-1}cm^{-1}$ versus pH (a) acidic region (pH 1.9-5) and (b) basic region (pH 5-10) for A72H76 iso-1-cytochrome *c*. Data were collected at room temperature (22 ± 1 ºC) in 0.1 M NaCl. The solid curves are fits to eq 5.2 as described in Materials and Methods.

**Table 5.5.** Thermodynamic parameters from pH titration in 0.1 M NaCl at 22 ± 1 ºC for the A72H76 variant of iso-1-cytochrome *c*.[a]

| **0M [gdnHCl]** | ***n*** | **p$K_H$(app)** |
|---|---|---|
| Acidic region | 1.7 ± 0.2 | 3.74 ± 0.02 |
| Basic region | 1.0 ± 0.2 | 6.34 ± 0.15 |

[a] Parameters are from fits of the data to eq 5.2 in Materials and Methods.

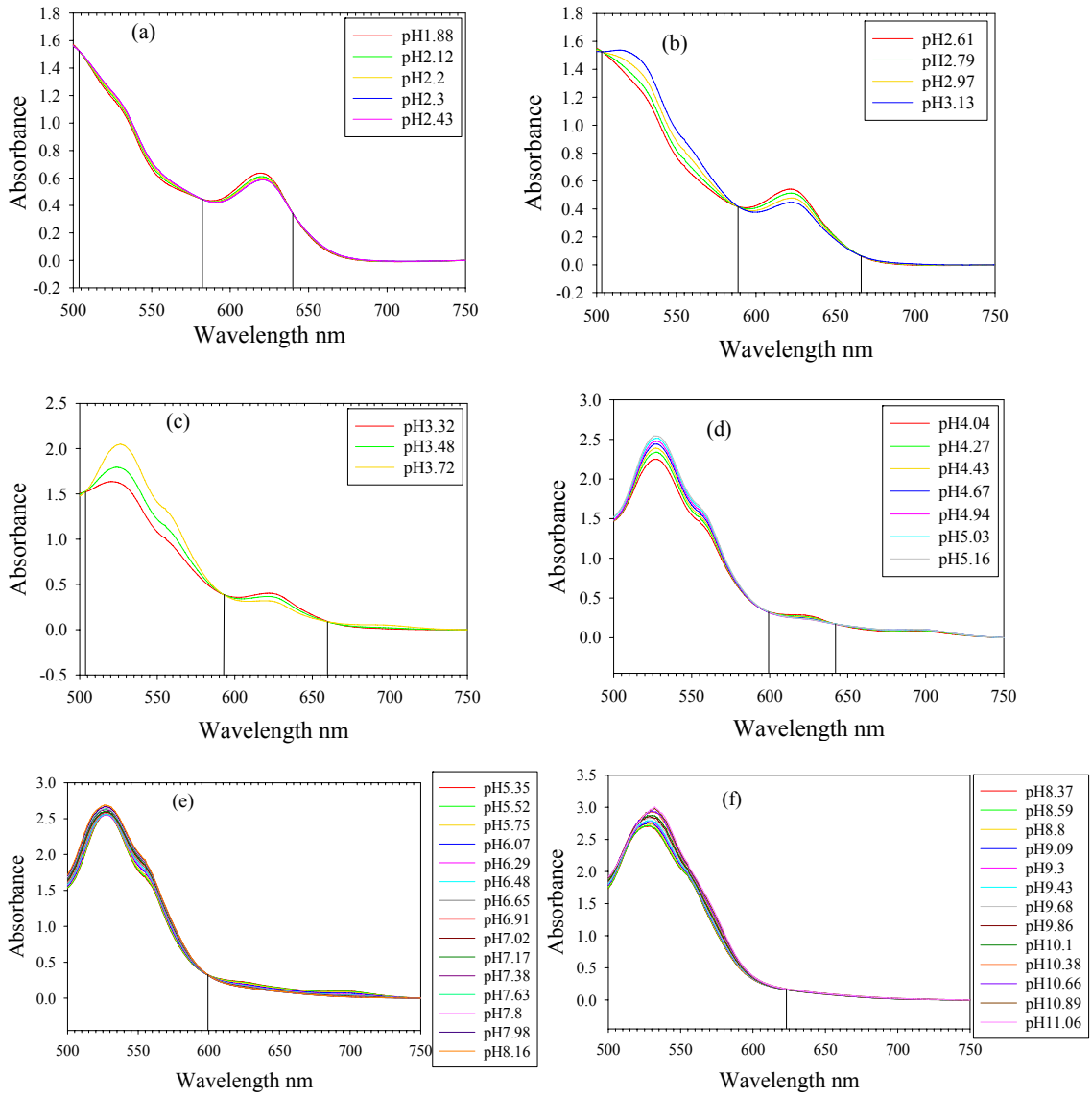


**Figure 5.9** Plot of absorbance spectra as a function of pH for the A72H76 variant of iso-1-cyt *c* at 22 ± 1 ºC in the presence of 0.1 M NaCl. (a) pH 1.88 – 2.33 (504, 583 and 645 nm) (b) pH 2.61 – 3.13 (503, 589 and 666 nm) (c) pH 3.32 – 3.72 (504, 593 and 660 nm) (d) pH 4.04 – 5.16 (599 and 643 nm) (e) pH 5.35 – 8.16 (599 nm) and (f) pH 9.37-11.06 (623nm). Isosbestic points are given in parentheses.

*5.3.3.3 pH Dependence of Absorbance at 695 for the A72H73G76 and A72H73G76A79 variants.*

pH titrations done with the A72H73G76 and A72H73G76A79 variants showed very weak extinction coefficients at 695 nm in the range of 0.1 $mM^{-1}cm^{-1}$(figures F4 and F5 in Appendix F), which is $1/5^{th}$ the extinction coefficient seen with the H81 variant as shown in figure 5.4. These data could not be fitted to any thermodynamic model. This result suggests that these variants do not significantly populate the native state, due to the absence of the characteristic band at 695 nm for Met80-heme ligation.

### *5.3.4 Stopped–Flow Kinetic Studies of the Alkaline Transition as a Function of pH.*

*5.3.4.1 pH Jump Kinetics of the H81 Variant.*

pH-jump kinetics for the H81 variant was monitored at 405 nm, which is the wavelength of maximum change in absorbance for the conversion between the native and His-heme ligated alkaline states as described in Chapters 2 and 3. Representative kinetic traces are shown in Appendix F, figure F6. Triple and quadruple exponential fits to the data suggested the presence of three distinct phases from pH 5 to 8.8 and pH 11 to 11.2, and four distinct phases from pH 9 to 10.8. The values of rate constants and amplitudes from both upward and downward pH jump data are shown in Appendix D, Tables D1 – D9. For simplicity the data from pH 5 to 9.8 were taken into consideration for fitting to double and triple ionization mechanism schemes described previously in *references* [61, 62, 64]. Above pH 9.8, alkaline denaturation appears to occur.

In the fast phase kinetics data shown in figure 5.10, $k_{obs}$ and amplitude data from pH 5 to 8.8 are taken from triple exponential fits, while from pH 9 to 9.8 they are taken

from quadruple exponential fits, due to the better residuals as compared to triple exponential fits and the presence of a distinct fourth phase. A triple ionization scheme was used to fit the $k_{obs}$ versus pH data, which provided inadequate parameters associated with large errors, suggesting there might be a fourth ionizable group. The amplitude data (figure 5.10b) also showed unusual behavior which was not seen with the K73H or H79 variants. No leveling out of the amplitude near pH 7.5 is observed. Instead the amplitude continues to increase.

**Figure 5.10** On the next page are plots of (a) rate constant and (b) amplitude data for the fast phase collected at 25 ºC as a function of pH in 10 mM buffer containing 0.1 M NaCl. Open circles are data from upward pH jump experiments and solid circles are data from downward pH jump experiments. The $k_{obs}$ and amplitude data from pH 5 to 8.8 are taken from triple exponential fits, while from pH 9 to 9.8 they are taken from quadruple exponential fits due to better residuals as compared to triple exponential fits and the clear presence of a fourth phase. The solid curves in panels (a) and (b) are just meant to follow the general trend in the fast phase kinetics. Rate constants and amplitudes presented in this figure are collected in Tables D1, D5 and D7 in Appendix D.

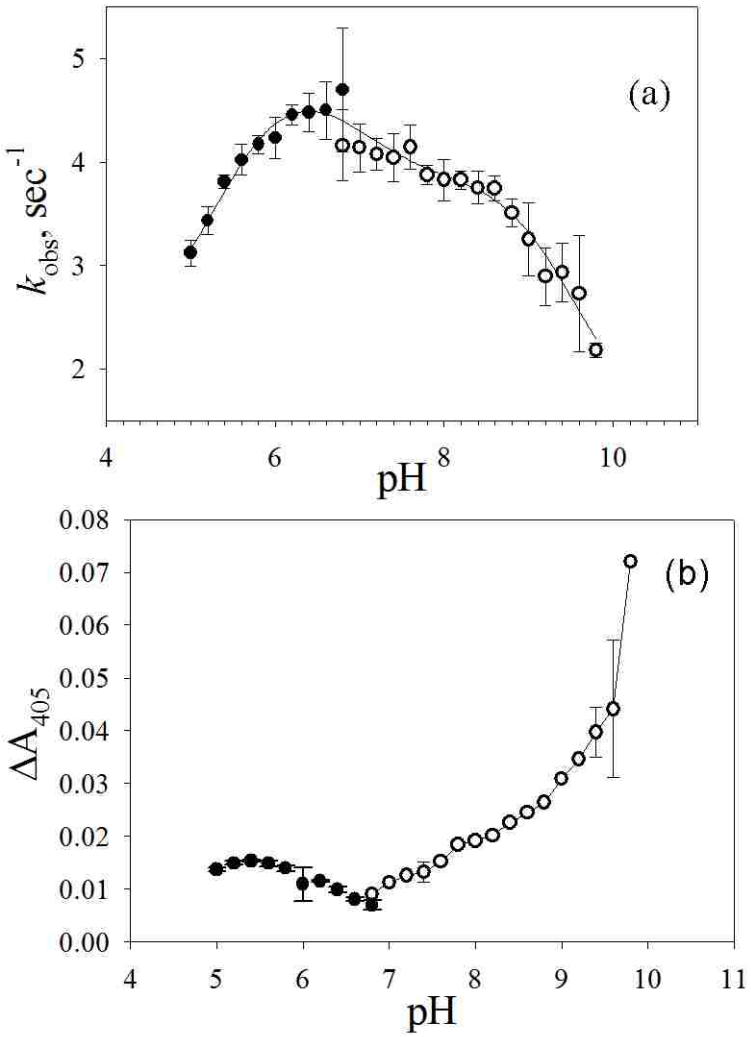


The intermediate phase was pulled out from a three exponential equation for the pH range 7 to 8.8 and from a four exponential equation for the pH range of 9 to 9.6. Data from pH 9.4 started showing larger errors as seen in figure 5.11. At pH 9.8 and 10 this phase appears to merge with the fast phase in figure 5.10. The decrease in the amplitude of the intermediate phase seems to be inconsistent with the increase in the rate constant data. This phase was fitted to a single ionization scheme for the rate constant. However, large errors associated with the values indicate an inadequate fit to a single ionization scheme.

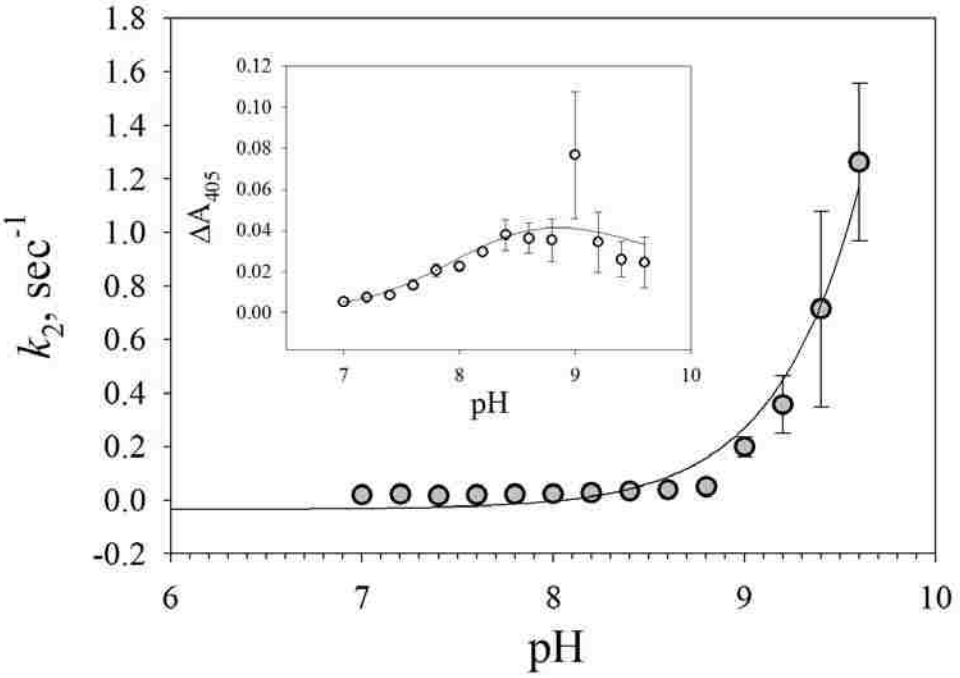


**Figure 5.11** Plots of rate constant and amplitude (inset) data for the first intermediate phase collected at 25º C as a function of pH in 10 mM buffer containing 0.1 M NaCl. Filled circles are rate constant data from upward pH jump experiments. The solid line is a fit from pH 7 to 9.6 to eq 2.6 in the Materials and Methods, section 2.2.8 of Chapter 2. The solid line through the amplitude data is only intended to show the trend of change in amplitude associated with this intermediate phase. The errors in the parameters are larger than the magnitude of the parameters for the fit to the rate constant versus pH data. Thus, they are not reported. The rate constants and amplitudes in this figure are collected in Table D2 and D8 (for down ward pH jump data, which is not shown in this graph) in Appendix D.

The slow phase rate constant and amplitude data is relatively simple and was fitted well to the single ionization scheme, equations 2.6 for rate constant and 2.7 for amplitude data, from the Materials and Methods, section 2.28 of Chapter 2. The kinetic parameters from the fits are shown in Table 5.6. Based on the p$K_H$ from $k_{obs}$ and amplitude data this phase can be assigned to a lysine-heme alkaline conformer.

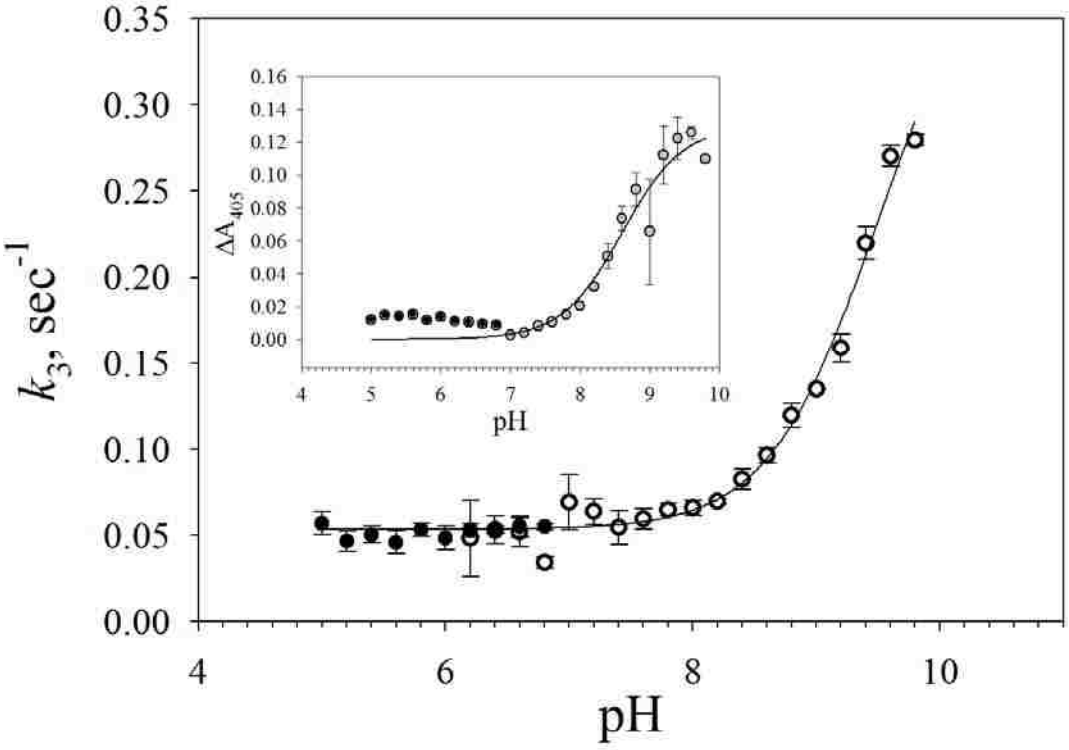


**Figure 5.12** Plots of rate constant for the slow phase collected at 25 ºC as a function of pH in 10 mM buffer containing 0.1 M NaCl. Open circles are data from upward pH jump experiments and solid black circles are data from downward pH jump experiments. The solid curve is a fit of upward and downward pH jump rate constants from pH 5 to 9.8 to eq 2.6 in the Materials and Methods, section 2.2.8 in Chapter 2. Eq 2.7 from the Materials and Methods, section 2.2.8 from Chapter 2 is used to fit the amplitude data in the inset for upward pH jump experiments from pH 7 to 9.8. Rate constants and amplitudes presented in this figure are collected in Tables D3, D6 and D9 in Appendix D.

**Table 5.6.** Rate and ionization constants associated with the slow phase of the alkaline transition of H81 iso-1-cyt *c*.

| Parameters | Slow Phase |
|---|---|
| $k_f$, s$^{-1}$ | 0.35 ± 0.03 |
| $k_b$, s$^{-1}$ | 0.053 ± 0.003 |
| p$K_H$ ($k_{obs}$ data) | 9.4 ± 0.1 |
| p$K_H$ (Amp. data) | 9.5 ± 0.1 |

A quadruple exponential fit was used from pH 9 to 10.8. A very fast phase was observed, occurring in the range of 50 - 200 $s^{-1}$ for the pH range 9 to 11.2. Though its presence is consistent and shows an increase in amplitude from pH 9 to 11.2, relative errors are higher than for other phases, especially at pH 9.8 and pH 10. We believe this phase may be associated with alkaline denaturation. Values for these rate constants and amplitudes are given in Table D4 in Appendix D.

*5.3.4.2 pH jump Kinetics of the A72H76 Variant.*

Kinetic studies were carried out to gain further insight into the alkaline transition caused by His76-heme ligation using pH jump stopped flow methods. Representative kinetic traces are shown in Appendix F, figure F7. Kinetic traces were fitted to triple exponential rise and decay equations as discussed in the Materials and Methods. The values for the rate constants and amplitudes are given in Appendix E, Tables E1-E10. The rate constants and amplitudes for the fast phase from pH 5 to 9.8 were considered and fit to a double ionization mechanism to get information about the changes in kinetics with pH. Parameters from the fits are shown in Table 5.7. The rate constant and amplitude data fits yield p$K_{HL}$= 6.4 and 6.5, which is consistent with ionization of a histidine suggesting its association with His76-heme ligation.

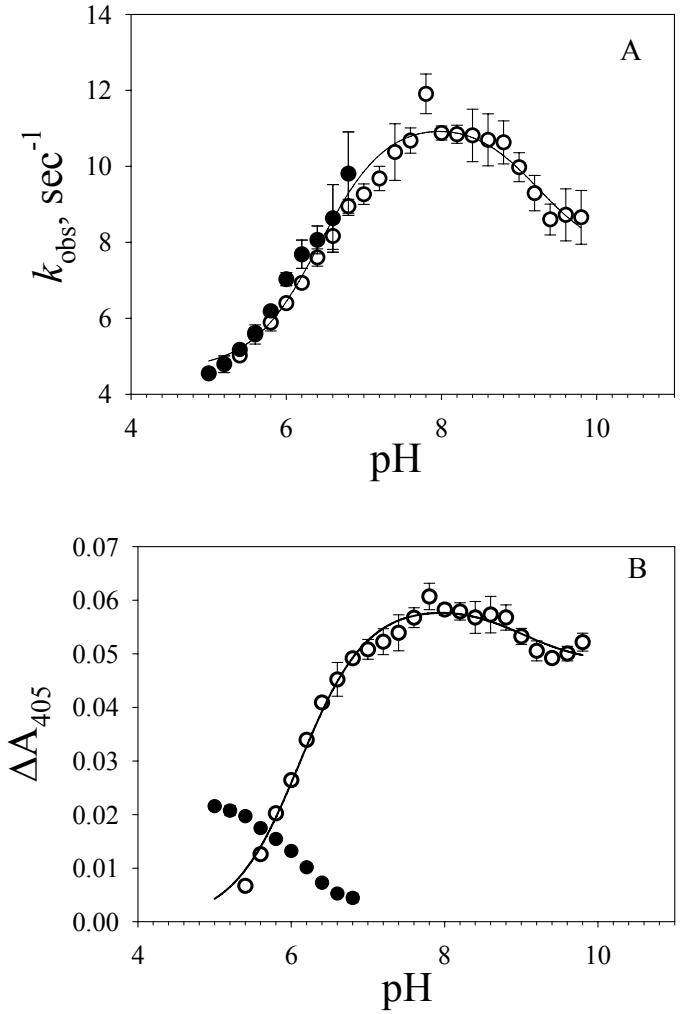


**Figure 5.13** Plots of (a) rate constant and (b) amplitude data for the fast phase collected at 25 ºC as a function of pH in 10 mM buffer containing 0.1 M NaCl. Open circles are data from upward pH jump experiments and solid circles are data from downward pH jump experiments. The solid curve in panel A is a fit of upward and downward pH jump rate constants from pH 5 to 9.8 to eq 2.8 and in panel B fitted to eq 2.9 from the Materials and Methods, section 2.2.8 of Chapter 2. Rate constants and amplitudes presented in this figure are collected in Tables E1, E6 and E8 in Appendix E.

The slow phase rate constant and amplitude data were fitted to a single ionization triggering mechanism (figure 5.14). The parameters obtained from fits are shown in Table 5.7. The p$K_{H2}$ associated with the rate constant is near 9, low for ionization of lysine, but consistent with same values reported for lysine-heme alkaline conformers [61,

62, 64]. As can be seen from figure 5.14, a single ionization mechanism does not fit well to the amplitude data. Above pH 9.8, the slow phase becomes faster, though the amplitude drops. Another slow phase is seen from pH 10.2, increasing in magnitude up to pH 11.2 (Appendix E, Table E4).

Other than these two phases, an intermediate phase is also seen from pH 5 to 7.8, with a magnitude of 0.03 to 1.0 $sec^{-1}$ (Appendix E, Tables E2 and E9). From pH 8 onwards this phase is missing and taken over by a very fast phase growing from 100's to 3000 $s^{-1}$ and associated with an increase in amplitude. This type of behavior was also seen with the H81 variant of iso-1-cyt *c*. The values are shown in Table E5, Appendix E. These results suggest complicated kinetic behavior at higher alkaline pH.

**Figure 5.14** On the next page is the plot of rate constant for the slow phase collected at 25 ºC as a function of pH in 10 mM buffer containing 0.1 M NaCl. Open circles are data from upward pH jump experiments and solid black circles are data from downward pH jump experiments. The solid curve is a fit of upward and downward pH jump rate constants from pH 5 to 9.8 to eq 2.6 in the Materials and Methods, section 2.2.8 of Chapter 2. Eq 2.7, Materials and Methods, section 2.2.8 of Chapter 2 is used to fit the amplitude data in the inset for upward pH jump experiments from pH 5 to 9.8. Rate constants and amplitudes presented in this figure are collected in Tables E3, E7 and E10 in Appendix E.

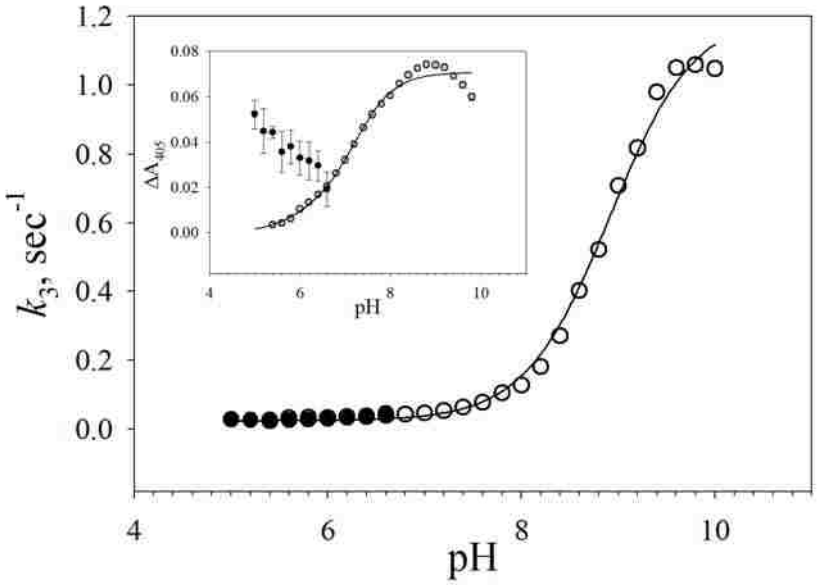


**Table 5.7.** Rate and ionization constants associated with the fast and slow phase of the alkaline transition of A72H76 variant of iso-1-cyt *c*.

| Parameter | Fast phase [a] | Slow phase [b] |
|---|---|---|
| $k_{f1}$, s$^{-1}$ | 6.6 ± 0.2 | 1.20 ± 0.02 |
| $k_{b1}$, s$^{-1}$ | 4.6 ± 0.2 | 0.030 ± 0.004 |
| $k_{f2}$, s$^{-1}$ | 3.6 ± 0.4 | |
| $k_{b2}$, s$^{-1a}$ | 4.0 ± 0.4 | |
| p$K_{HL}$ ($k_{obs}$ data) | 6.4 ± 0.1 | |
| p$K_{HL}$ (Amp. data) | 6.50± 0.03 | |
| p$K_{H2}$ ($k_{obs}$ data) | 9.2 ± 0.3 | 9.00 ± 0.02 |
| p$K_{H2}$ (Amp. data) | 8.8 ± 0.3 | 8.8 ± 0.1 |

[a] The values for $k_b$ and $k_f$ were calculated iteratively. To fit $k_{obs}$ versus pH data to eq 2.8, the $k_{f2}/k_{b2}$ ratio was set to 1.4 (arbitrarily guessed) to get the initial kinetic parameters. Amplitude data for the fast phase was fitted to eq 2.9; $k_{b2}$ was allowed to vary to obtain the best fit. The values of $k_{f1}$, $k_{f2}$ and $k_{b2}$ were taken from fits of $k_{obs}$ data to constrain the parameters. The new $k_{f2}/k_{b2}$ ratio was used to refit the $k_{obs}$ versus pH data. The values of $k_{f1}$, kb1, kf2 and kf2 obtained from this fit were used to construct a final fit of the amplitude data.

[b] Parameters are obtained from fits to eq 2.6 and 2.7 from Chapter2. The ratio of $k_f/k_b$ in eq 2.7 was constrained using $k_f$ and $k_b$ obtained from the $k_{obs}$ versus pH data.

### *5.3.5 Anaerobic Stopped-flow Kinetic Studies for H81 and A72H76 Variants.*

The alkaline transition can lead to conformationally gated ET processes as discussed in earlier chapters. These studies provide complementary means of extracting information about not only rates of the ET reaction but also the conformational change and proline isomerization process associated with ET. To have better insight into the kinetics of alkaline conformational transition, ET experiments were carried out for both the H81 and A72H76 variants. For these studies along with a ruthenium complex, $a_6Ru^{2+}$, cobalt complex, $[Co(terpy)_2]^{2+}$, was also used to slow down the ET process in an attempt to directly extract the forward and backward rates of the conformational transitions. The kinetic traces obtained on reaction of oxidized H81 and A72H76 with $a_6Ru^{2+}$ and the cobalt complex are shown in figures F8-F11, Appendix F. These all showed an increase in absorbance at 550 nm as expected for reduction of iso-1-cyt *c*.

#### *5.3.5.1 Anaerobic ET stopped flow kinetics of the H81 variant.*

The fastest phase ($k_1$) obtained from the fits to a triple exponential equation are plotted as a function of $a_6Ru^{2+}$ concentration as shown in figure 5.15 (also in Table G1, Appendix G) for the pH 7.5. This phase shows a linear dependency on the $a_6Ru^{2+}$ concentration and is assigned to the ET reaction of the native Met80-heme conformer with $a_6Ru^{2+}$. The data give a value of $k_{ET} = 27.1 \pm 1.3$ $mM^{-1}cm^{-1}$ on fitting to equation 3.5 from Chapter 3. This value is 3 to 4 times lower than that of the K73H and H79 variants suggesting a decrease in ET efficiency with a His mutation at position 81. The intermediate phase showed no dependence on $a_6Ru^{2+}$ as shown in figure 5.16, although a dramatic decrease in the rate constant is seen after 5 mM $a_6Ru^{2+}$ concentration. This

effect could be due to an interaction of the metal complex with the protein. A slight decrease in the intermediate phase has been seen with other mutants near 20 mM $a_6Ru^{2+}$ concentration but the effect was never so drastic. As a result, data up to 5 mM $a_6Ru^{2+}$ concentration were considered to be reliable. These data were fitted to a linear equation (figure 5.16), demonstrating the lack of dependence on [$a_6Ru^{2+}$] in this concentration range. The third phase showed constant behavior up to 5 mM $a_6Ru^{2+}$ concentration and then a slight inclination towards increasing values (figure 5.17). This phase could be a mixed effect of proline isomerization and a Lys-heme alkaline conformer as has been seen previously with other variants. The values of the kinetic parameters obtained are shown in Table 5.8.

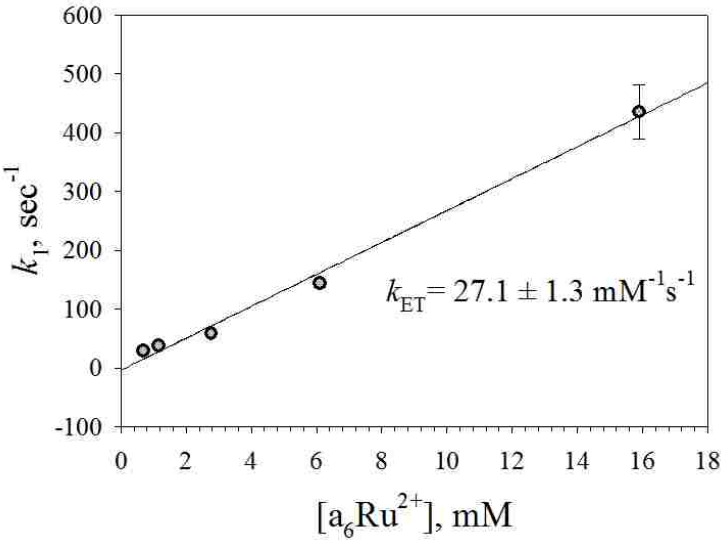


**Figure 5.15** Plot of observed rate constant $k_{obs}$ ($s^{-1}$) for the reaction of $a_6Ru^{2+}$ with the native conformer of the H81 variant (fast phase) as a function of $a_6Ru^{2+}$ concentration at pH 7.5; 10 mM $NaH_2PO_4$ buffer in 0.1 M NaCl, and 25 ºC. The values for $k_{obs}$ represent the fast phase ($k_1$) obtained from the fits shown in figure F8, Appendix F and the solid line is a fit to Eq. 3.5 (Chapter 3). The values for the rate constants and amplitudes are given in Table G1, Appendix G.

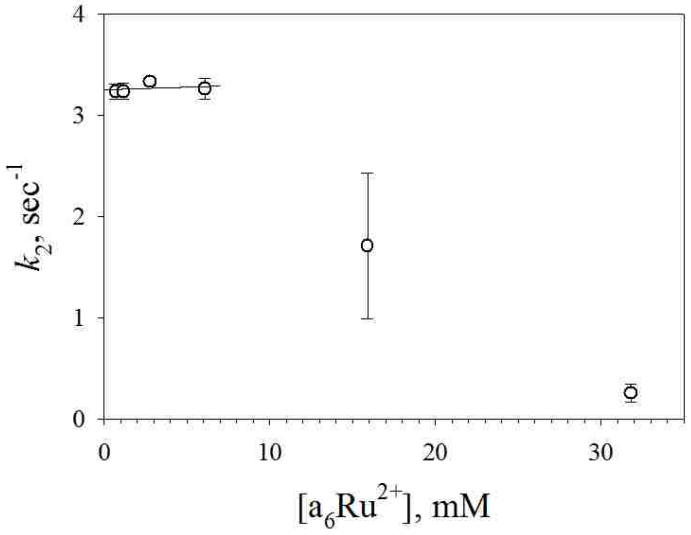


**Figure 5.16** Plot of observed rate constant $k_{obs}$ ($s^{-1}$) for the reaction of $a_6Ru^{2+}$ with the native conformer of the H81 variant (intermediate phase) as a function of $a_6Ru^{2+}$ concentration for pH 7.5; 10 mM $NaH_2PO_4$ buffer in 0.1 M NaCl, and 25 ºC. The values for $k_{obs}$ represent the intermediate phase ($k_2$) obtained from fits as shown in figure F8, Appendix F and the solid line is a fit to a linear equation. The values for the rate constants and amplitudes are given in Table G2, Appendix G.

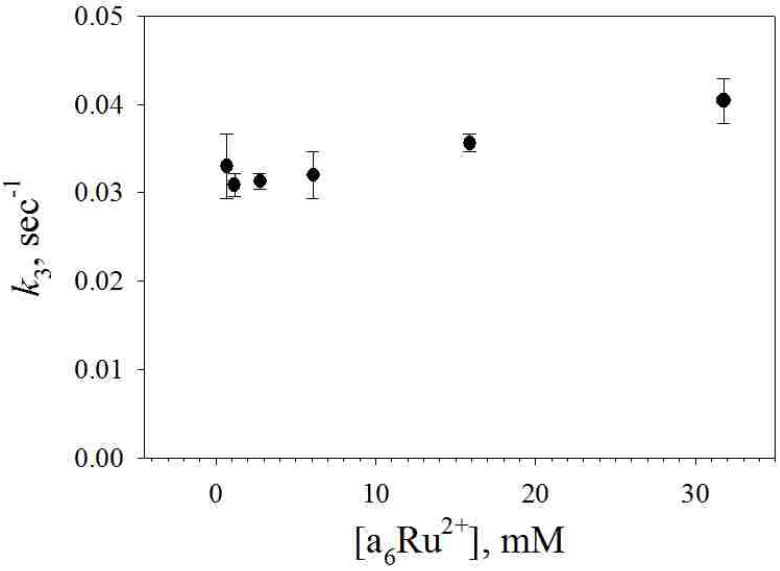


**Figure 5.17** Plots of slowest phase ($k_3$) from fits to a triple exponential rise equation as shown in figure F8, Appendix F. The values for the rate constants and amplitudes are given in Table G3, Appendix G.

The kinetic traces from anaerobic reaction of oxidized H81 with the cobalt complex are shown in figure F9, Appendix F. The ET reaction of H81 with the cobalt complex showed similar behavior as seen with the ruthenium complex, although the fast phase attributed to the ET reaction is almost 10 times slower. The fast phase was fitted to eq 3.5 from Chapter 3 and showed linear dependency on the cobalt complex concentration. The slope from the fit, $k_{ET}$, was also 10 times slower as compared to reaction with the ruthenium complex as shown in figure 5.18 and Table 5.8. The intermediate phase is plotted as a function of cobalt complex concentration in figure 5.19. The $k_{ET}$ was used in eq 3.6 to obtain the values of forward and backward rate constants related to conformational changes as discussed in Chapter 3. The value of $k_{HM3}$ obtained is smaller than that obtained from the ET reaction with the ruthenium complex; this could be due to absence of upper limit data points (data higher then 5 mM $[Co(terpy)_2]^{2+}$ was not collected as mentioned in Materials and Methods). The magnitude of $k_1$ and $k_2$ are similar below 0.6 mM cobalt complex concentration. Thus, the separation of these rate constants may not be reliable (see Appendix H, Table H1 and H2). The slowest phase is plotted as a function of cobalt complex concentration as shown in figure 5.20. This phase was also fitted to eq 3.6 from Chapter 3 using the value of $k_{ET}$ obtained from figure 5.18 in eq 3.6 to determine the forward and backward rate constants related to these slow conformational changes. The values of the kinetic parameters obtained are shown in Table 5.8.

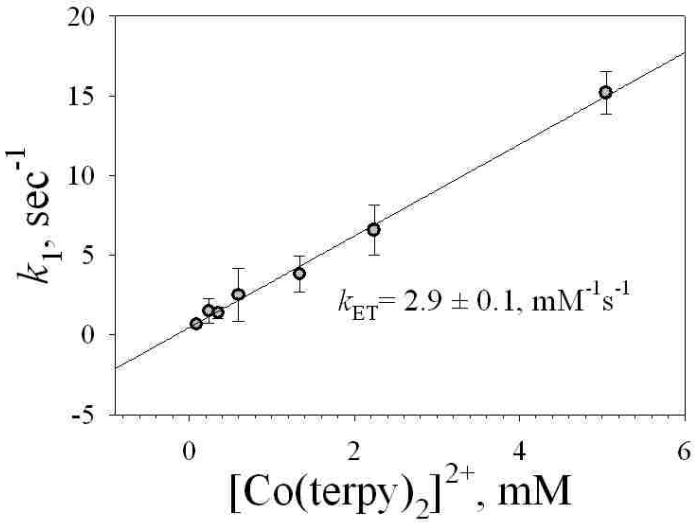


**Figure 5.18** Plot of the observed rate constant $k_{obs}$ ($s^{-1}$) for the reaction of $[Co(terpy)_2]^{2+}$ with the native conformer of the H81 variant (fast phase) as a function of $[Co(terpy)_2]^{2+}$ concentration for pH 7.5; 10 mM $NaH_2PO_4$ buffer in 0.1 M NaCl, and 25 ºC. The values for $k_{obs}$ represent the fast phase ($k_1$) obtained from the fits shown in figure F9, Appendix F and the solid line is a fit to Eq. 3.5 (Chapter 3). The values for the rate constants and amplitudes are given in Table H1, Appendix H.

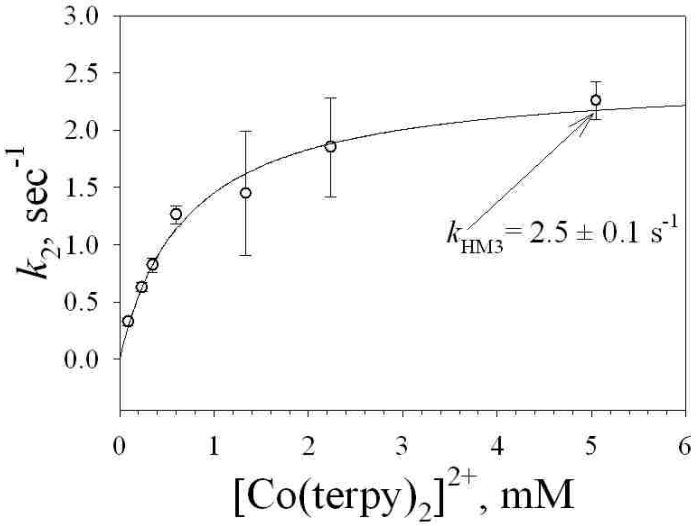


**Figure 5.19** Plot of observed rate constant $k_{obs}$ ($s^{-1}$) for the reaction of $[Co(terpy)_2]^{2+}$ with the native conformer of the H81 variant (intermediate phase) as a function of $a_6Ru^{2+}$ concentration for pH 7.5; 10 mM $NaH_2PO_4$ buffer in 0.1 M NaCl, and 25 ºC. The values for $k_{obs}$ represent the intermediate phase ($k_2$) obtained from fits as shown in figure F9, Appendix F and the solid line is a fit to eq 3.6 in Chapter 3, which gives values for $k_{HM3}$ and $k_{MH3}$. The values for the rate constants and amplitudes are given in Table H2, Appendix H.

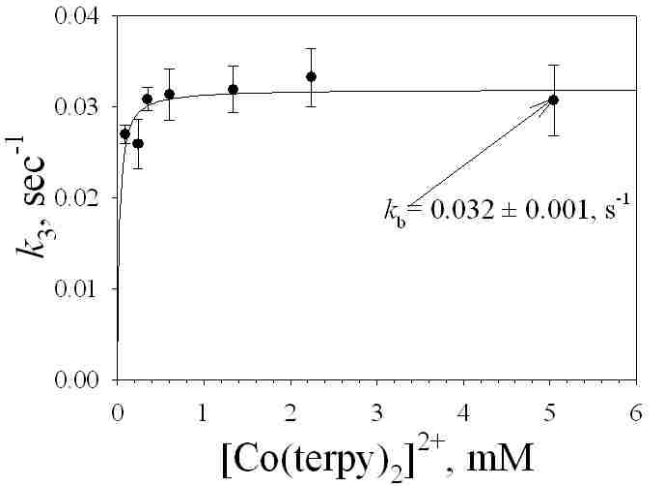


**Figure 5.20** Plots of the slowest phase ($k_3$) from fits to a triple exponential rise equation as shown in figure F9, Appendix F. The solid line is fit to eq 3.6 in Chapter 3, which gives values for $k_b$ and $k_f$ controlling the slow conformational change associated with the alkaline conformational change. The values for the rate constants and amplitudes are given in Table H3, Appendix H.

*5.3.5.2 Anaerobic ET stopped flow kinetics of A72H76 variant.*

The kinetic traces obtained on reaction of the oxidized A72H76 variant with ruthenium are shown in figure F10, Appendix F. A fast phase obtained from a triple exponential fit showed a linear dependency on $a_6Ru^{2+}$ concentration (figure 5.21), which was then fitted to eq 3.6 as mentioned in Chapter 3. These values are in the same range as that seen with the H81 variant. The slope of the graph gave $k_{ET} = 24.7$ mM$^{-1}$s$^{-1}$ similar but a bit less than that seen with the H81 variant. The intermediate phase showed saturation behavior as a function of $a_6Ru^{2+}$ concentration (figure 5.22). Eq 3.6 from Chapter 3 was used to fit intermediate phase data, along with the value of $k_{ET}$ obtained from fitting the fast phase, to obtain information about $k_{MH3}$, the forward and $k_{HM3}$, the backward rate constants for the alkaline conformational change associated with His76-heme binding. The values obtained from the fits are shown in Table 5.8. The slow phase as shown in

figure 5.23 increases somewhat as [$a_6Ru^{2+}$] increases, but the value at ~13 mM $a_6Ru^{2+}$ concentration seems to be an outlier.

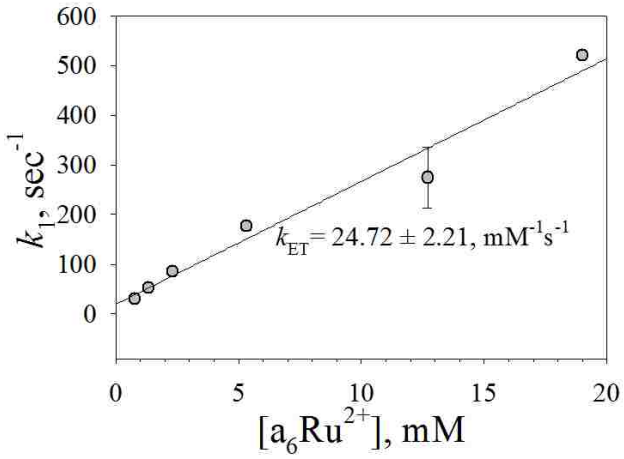


**Figure 5.21** Plots of observed rate constant $k_{obs}$ ($s^{-1}$) for the reaction of $a_6Ru^{2+}$ with the native conformer of the A72H76 variant (fast phase) as a function of $a_6Ru^{2+}$ concentration for pH 7.5; 10 mM $NaH_2PO_4$ buffer in 0.1 M NaCl, and 25 ºC. The values for $k_{obs}$ represent the fast phase ($k_1$) obtained from the fits shown in figure F10, Appendix F and the solid line is a fit to Eq. 3.5 (Chapter 3). The values for the rate constants and amplitudes are given in Table I1, Appendix I.

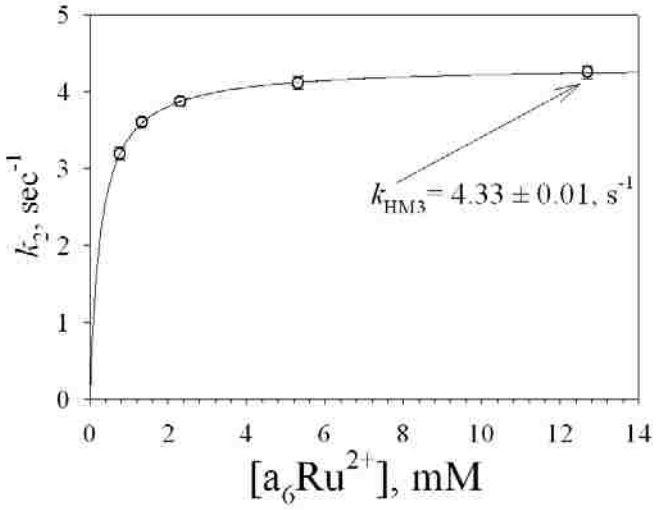


**Figure 5.22** Plot of the observed rate constant $k_{obs}$ ($s^{-1}$) for the reaction of $a_6Ru^{2+}$ with the native conformer of the A72H76 variant (intermediate phase) as a function of $a_6Ru^{2+}$ concentration for pH 7.5; 10 mM $NaH_2PO_4$ buffer in 0.1 M NaCl, and 25 ºC. The values for $k_{obs}$ represent the intermediate phase ($k_2$) obtained from fits as shown in figure F10, Appendix F and the solid line is fit to eq 3.6 (Chapter 3), which gives values for $k_{HM3}$ and $k_{MH3}$. The values for the rate constants and amplitudes are given in Table I2, Appendix I.

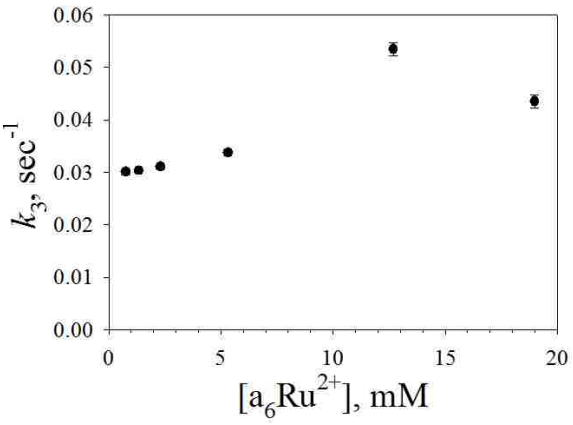


**Figure 5.23** Plots of slowest phase ($k_3$) from fits to a triple exponential rise equation as shown in figure F10, Appendix F. The values for the rate constants and amplitudes are given in Table I3, Appendix I.

The kinetic traces from the ET reaction of oxidized A72H76 at different concentrations of $[Co(terpy)_2]^{2+}$ are shown in figure F11, Appendix F. These kinetic traces fit well to a double exponential rise equation. No substantial fast phase was obtained with this reaction. The faster phase obtained from this reaction was of similar magnitude as that of the intermediate phase obtained for the H81 reaction with $[Co(terpy)_2]^{2+}$ and showed similar saturation behavior (figure 5.24). Based on this observation and the H81 and A72H76 reactions with $a_6Ru^{2+}$, the value of $k_{ET}$ for H81 was used in eq 3.6 from chapter 3 to fit the $[Co(terpy)_2]^{2+}$ concentration dependence of the faster phase. Since $k_{ET}$ was not visible for the reaction of A72H76 with $[Co(terpy)_2]^{2+}$ it suggests the possibility of a less favorable ET reaction which could be due to a lower E°' for the A72H76 variant. The values obtained are shown in Table 5.8. The slowest phase was similar to that seen with the H81 reaction with $[Co(terpy)_2]^{2+}$ (figure 5.25). This phase also showed saturation behavior and was fitted to eq 3.6 from chapter 3 to determine the forward and backward conformational rate constants. The values obtained from the fits are shown in Table 5.8.

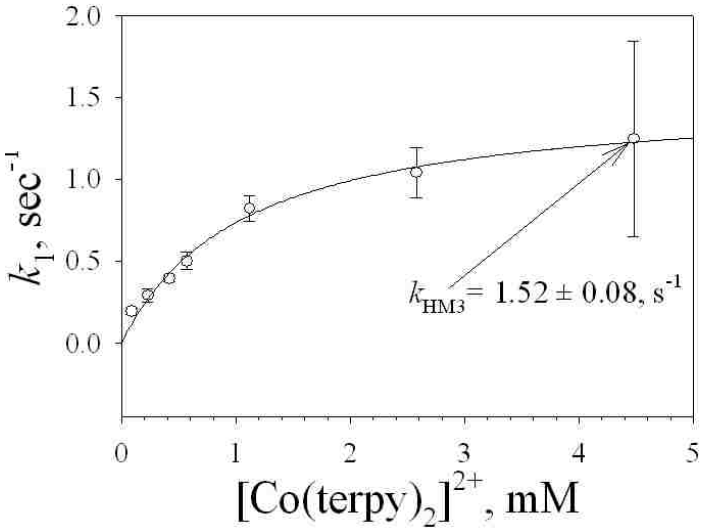


**Figure 5.24** Plot of the observed rate constant $k_{obs}$ ($s^{-1}$) for the reaction of $[Co(terpy)_2]^{2+}$ with the native conformer of the A72H76 variant (fast phase) as a function of $[Co(terpy)_2]^{2+}$ concentration for pH 7.5; 10 mM $NaH_2PO_4$ buffer in 0.1 M NaCl, and at 25 ºC. The values for $k_{obs}$ represent the fast phase ($k_1$) obtained from fits as shown in figure F11, Appendix F. The values for the rate constants and amplitudes are given in Table J1, Appendix J.

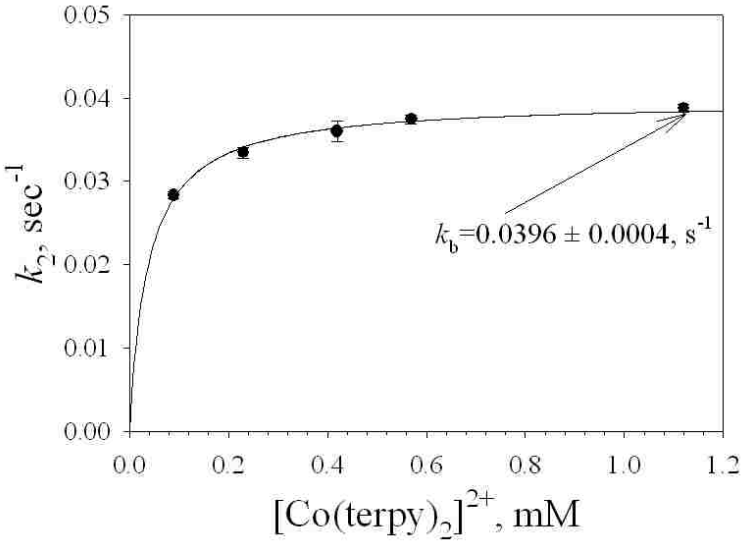


**Figure 5.25** Plot of observed rate constant $k_{obs}$ ($s^{-1}$) for the reaction of $[Co(terpy)_2]^{2+}$ with the native conformer of the A72H76 variant (slow phase) as a function of $[Co(terpy)_2]^{2+}$ concentration for pH 7.5; 10 mM $NaH_2PO_4$ buffer in 0.1 M NaCl, and at 25 ºC. The values for $k_{obs}$ represent the slow phase ($k_2$) obtained from fits as shown in figure F11, Appendix F. The values for the rate constants and amplitudes are given in Table J2, Appendix J.

**Table 5.8.** Parameters from ET data for the H81 and A72H76 variants with $a_6Ru^{2+}$ and $[Co(terpy)_2]^{2+}$.

| | Rate constants | H81 | A72H76 |
|---|---|---|---|
| $[a_6Ru^{2+}]$ | $k_{ET}$ ($mM^{-1}s^{-1}$) | 27.0 ± 1.3 | 25.0 ± 2.2 |
| | $k_{HM3}$ ($s^{-1}$) | 3.3 ± 0.1 [a] | 4.30 ± 0.01 |
| | $k_{MH3}$ ($s^{-1}$) | | 6.8 ± 0.1 |
| $[Co(terpy)_2]^{2+}$ | $k_{ET}$ ($mM^{-1}s^{-1}$) | 2.9 ± 0.1 | 2.7[b] |
| | $k_{HM3}$ ($s^{-1}$) | 2.5 ± 0.1 | 1.5 ± 0.1 |
| | $k_{MH3}$ ($s^{-1}$) | 2.1 ± 0.3 | 2.9 ± 0.4 |
| | $k_f$ ($s^{-1}$) | 0.06 ± 0.03 | 0.10 ± 0.01 |
| | $k_b$ ($s^{-1}$) | 0.032 ± 0.001 | 0.0400 ± 0.0004 |

[a] This value is average of $k_2$ from 0.7 to 6.1 mM $[a_6Ru^{2+}]$.

[b] This value is assumed based on the $k_{ET}$ for H81 with $[Co(terpy)_2]^{2+}$, the fractional difference between the H81 and A72H76 reaction with $a_6Ru^{2+}$ was used to adjust $k_{ET}$ for reaction of A72H76 with $[Co(terpy)_2]^{2+}$.

## 5.4 Discussion

### *5.4.1 Effect of the Position of Alternate Heme Ligands on the Thermodynamics and Kinetics of the Alkaline Transition of Iso-1-cyt c*

The goal of this project was to study the effects on the alkaline conformational transition caused by variation of the position of the histidine in Ω-loop D. The variants used for these studies can be divided into two sets based on the spatial position of the histidine in Ω-loop D. The H81 variant has the histidine on the C-terminal side and the A72H76, A72H73G76 and A72H73G76A79 variants have histidine on the N-terminal side of Ω-loop D (figure 5.1). The percentage solvent exposed surface area for the amino acids in the wild type protein are: H81, 100%; Pro76, 87%; Lys73, 89.8%; and Lys79, 54.7%. Among these variants, H81 has less effect on the global stability, while the other

three variants are relatively more destabilized. As the alkaline conformer is stabilized over the native state, pH jump kinetic studies reactions were not possible for the A72H73G76 and A72H73G76A79 variants of iso-1-cyt *c*.

### *5.4.2 Properties of Previous Histidine Variants in the Ω-Loop D of Iso-1-cyt c*

In previous work in our lab with the K73H [23, 61, 100] and H79 [64] variants, the mutation site was on the N-terminal side of the native Met80 ligand. In these variants, lysine at positions 73 and 79 (native ligands replacing Met80 in the alkaline conformational transition) were replaced by histidines. Studies with these K73H and H79 variants showed that though both variants had similar stability, the His79–heme alkaline conformer was more stable than the His73-heme alkaline conformer. Kinetic studies showed that the rate of formation of the His-heme alkaline conformer ($k_f$) is the same for both variants ($3.3 \pm 0.2\ s^{-1}$ for the H79 variant [64] and $3.5 \pm 0.2\ s^{-1}$ for the K73H variant [61]). However the back rate of formation of the native conformer (Met80-heme ligation, $k_b$) is 10 times slower for the H79 ($0.7 \pm 0.1\ s^{-1}$) [64] than for the K73H variant ($7.0 \pm 0.4\ s^{-1}$) [61]. These studies suggested that the K79H mutation acts primarily by stabilization of the alkaline state and not destabilization of the native state.

Another striking difference between the K73H and H79 variants is the overall kinetic behavior over the pH range 5 to 10. With His73, an inverted bell shaped curve is seen for $k_{obs}$ versus pH. $k_{obs}$ decreases from pH 5 to 6, is constant from pH 6 to 8 and again increases from pH 8 to 10. On the other hand the H79 variant has a bell or a dome shaped curve for $k_{obs}$ versus pH, where an increase in $k_{obs}$ is seen from pH 5 to 7.5, reaching its maximum at pH 8 followed by a decrease from pH 8.4 to 10. Curve fitting

for both variants gave p$K_{HL}$ consistent with the His (6.75 ± 0.04 for H79 [64] and 6.4 ± 0.5 for K73H [61]) as the ionizable group triggering the alkaline conformational transition associated with the fast phase. Both variants also showed the presence of an auxiliary ionizable group with p$K_a$ ~9. The K73H variant data requires the presence of a third ionizable group with an ionization constant of ~5.5 which affects the kinetics. The latter ionizable group is not observed for the H79 variant.

The amplitude associated with the fast phase for the K73H and H79 variants also showed a difference in behavior as a function of pH. For the K73H variant, an increase in amplitude was observed from pH 5 to 8. The amplitude then remained constant up to pH10. While for the H79 variant, amplitude data as a function of pH showed an increase from pH 5 to pH 8 and followed by a decrease up to pH 10. Curve fitting of the amplitude data for both the K73H and H79 variants yielded similar values of p$K_{HL}$ (6.8 ± 0.2 for H79 [64] and 7.2 ± 0.1 for K73H [61]) consistent with the thermodynamic data and suggestive of His as the primary ionizable group triggering the conformation changes.

### *5.4.3 Comparison of the Thermodynamics and pH Jump Kinetic Studies of the H81 and A72H76 Variants to the K73H and H79 Variants*

The histidine in the H81 variant is on the opposite side of the Met80 heme ligand compared to the histidines in the A72H76, K73H and H79 variants. The H81 variant has comparable stability to the K73H and H79 variants while the A72H76 variant is the least stable variant. pH dependent stability studies provides a p$K_C$ (equilibrium for conformation change) for the His-heme alkaline conformer of 0.85 ± 0.17 for H81 as compared to -0.63 to -1.2 for the H79 variant [64] and 0.28 ± 0.01 for the K73H variant

[23]. This supports partial unfolding studies by gdnHCl which also show His-heme binding to be less favorable for the H81 variant as compared to the K73H and H79 variants. The surprising point from the thermodynamics of partial unfolding is that positions 79 and 81 are just one amino acid from Met80 and yet one position stabilizes His-heme ligation and the other does not. Interestingly a F82H variant of iso-1-cyt *c* strongly favors His82 binding to heme [177, 178]. A monophasic pH-titration curve is obtained for the A72H76 variant, associated with a p$K_a$(app) of 6.34 consistent with His-heme ligation at relatively low pH. This observation suggests high favorability for His76 binding to the heme, although an exact p$K_C$ cannot be obtained from the monophasic transition from the A72H76 native state. Previous studies with a P76A variant [179] and also in the present study with mutation of Pro76 to Gly also large decreases in the stability of the native state relative to alkaline conformers. Thus, based on these thermodynamic studies, we can say that the effect of the amino acid position in the loop position on stability towards alkaline isomerization cannot be predicted readily.

Qualitatively, kinetics for both H81 and A72H76 resemble the behavior of the H79 variant rather than the K73H variant. The kinetics for A72H76 variant is simpler. The $k_{obs}$ and amplitude data fit well to a double ionization mechanism scheme as for the H79 variant. Both proteins show the presence of two ionization constants of ~6.5 and 9 that affect the alkaline transition. The third ionization constant near a p$K_a$ of 5.5 is missing. Also, the forward rate for formation of the His76-heme conformer is two times faster and the back rate for formation of native state is four times faster as compared to the H79 variant. Interestingly, this is consistent with the result observed for the AcH73

versus the K73H variant. Again, the less stable variant has faster kinetics for interconversion between the native and partially unfolded states.

The slow phase for the A72H76 variant has a back reaction that occurs at a similar rate as compared to the H79 variant but the forward rate is faster by 5-fold. This result suggests that at higher pH the lysine-heme alkaline state is stabilized and favored much more over the native state for the A72H76 variant. Despite these similarities between the A72H76 and H79 variants, some phenomenal differences were also observed. The presence of three distinct intermediate states from the upward pH jump kinetics in different pH regions and one intermediate phase for downward pH jump kinetics were observed with the A72H76 variant, while no such intermediate phases were observed with the H79 variant in pH jump studies.

The kinetics of the H81 variant, showed complex behavior as compared to the H79 and A72H76 variants. The $k_{obs}$ for the fast phase decreases, while the amplitude continually increases. A closer look at the intermediate phase suggests that it might be affecting the amplitude of the fast phase, as the rate constant for the fast phase and the intermediate phase approach each other closer near pH 10. Like the A72H76 variant, the H81 variant also showed two intermediate phases for upward pH jumps and one intermediate phase for the downward pH jump kinetics. The slow phase is simple and similar to the H79 variant. The $k_f$ and $k_b$ from the slow phase for the H81 variant are slightly higher but of the same magnitude as that of the H79 variant. These studies suggest that solvent exposed side chains in the loop at different positions affect the dynamics of the proteins distinctly.

### *5.4.4 Comparison of the Conformationally Gated ET Kinetics of the H81 and A72H76 Variants*

ET reactions have been used in our lab to resolve the microscopic rate constants, especially for the histidine–heme alkaline transitions as discussed in Chapters 2, 3, and 4 and also in *ref* [24, 64, 73, 81]. For the present study, along with the ruthenium complex, $a_6Ru^{2+}$, ET studies were also carried out with a cobalt complex, $[Co(terpy)_2]^{2+}$, to attempt to probe slower conformational dynamics. The $k_{ET}$ for $a_6Ru^{2+}$ with cyt *c* is ~5.0 x$10^4$ $M^{-1}s^{-1}$ (see Chapter 2-4) and that for $[Co(terpy)_2]^{2+}$ is expected to be ~1.0 x$10^3$ $M^{-1}s^{-1}$ [180]. Thus, an order of magnitude difference in $k_{ET}$ will be observed for the reaction of cyt *c* with $a_6Ru^{2+}$ versus $[Co(terpy)_2]^{2+}$. The expectation with slower ET kinetics was that we could resolve much slower $k_{MH3}$ rate constants directly from ET studies (see Chapter 2) [61]. The $k_{ET}$ obtained for the H81 variant reaction with $[Co(terpy)_2]^{2+}$ is indeed smaller by an of order magnitude compared to that with $a_6Ru^{2+}$ (Table 5.8). Unfortunately, $k_{obs}$ for direct ET and for the conformational gated ET rate constant, $k_{HM3}$, are close enough in magnitude that they are difficult to resolve.

For the H81 variant, the intermediate phase is constant up to 6 mM with $a_6Ru^{2+}$. This phase is assigned to $k_{HM3,}$ as the conformation change is independent of reagent concentration. The average of this intermediate phase from 0.7 to 6.1 mM [$a_6Ru^{2+}$], $k_{HM3}$ = 3.33 ± 0.05 $s^{-1}$. The value for $k_{MH3}$ cannot be obtained from the ET data for the intermediate phase, as the saturation level was seen even for the lowest concentration of the $a_6Ru^{2+}$ reagent used for these studies. The value for $k_{MH3}$ can be calculated by subtracting $k_{HM3}$ from $k_{obs}$ (average of $k_{obs}$ at pH 7.4 and 7.6, obtained from pH jump data as given in Table D1, Appendix D) yielding $k_{MH3}$ = 0.8 $sec^{-1}$ (Table 5.9).

For the A72H76 variant, $k_{HM3}$ and $k_{MH3}$ were determined directly from fitting the intermediate phase to eq 3.6 from Chapter 3 as shown in figure 5.22 and Tables 5.8 and 5.9. The sum of these rate constants (11.1 $s^{-1}$) is near to the $k_{obs}$ at pH 7.6 (10.7 $s^{-1}$) in pH jump studies. The similarity of $k_{MH3}$ ($k_f$) and $k_{HM3}$ ($k_b$) obtained from ET studies and pH jump data for these variants suggests the validity of the kinetic model used for these studies.

### *5.4.5 Comparison of the Conformational ET Gate for Variants of Iso-1cytochrome c*

The forward and the backward conformational rates are summarized in Table 5.9. For comparison, variants are arranged in the ascending order in which they occur in Ω-loop D (figure 5.1). At first glance, it looks like that there is a trend of decreasing $k_{HM3}$ as the position of the histidine moves from 73 to 81, however the H81 variant breaks this trend. $k_{MH3}$ for the K73H and H79 variants is of the same order, $k_{MH3}$ is fastest for the A72H76 variant and the H81 variant seems to disfavor the alkaline state. In this case of the H79 variant, His-heme ligation is more favored due to the smaller structural disruption involved. The H81 variant which also places histidine next to Met80 (native ligand) on the other hand, shows very different behavior. This might be associated with constraints on the amino acid at this position, being highly solvent exposed (Ala 81 in WT is 100% solvent exposed surface), which may cause more structural disruption than might be expected based on its position adjacent to Met80.

**Table 5.9.** Forward and backward conformational rate constants for variants of iso-1-cytochrome *c* obtained on reaction with $a_6Ru^{2+}$ at pH 7.5 (10 mM $NaH_2PO_4$ buffer 0.1 M NaCl) and 25 ºC.

| Variants | $k_{HM3,}$ $s^{-1}$ | $k_{MH3,}$ $s^{-1}$ [a] |
|---|---|---|
| K73H | 7.0 ± 0.2 [b] | 3.5 ± 0.2 |
| A72H76 | 4.30 ± 0.01 [c] | 6.80 ± 0.07 [c] |
| H79 | 0.63 ± 0.02 [d] | 2.80 ± 0.02 |
| H81 | 3.30 ± 0.05 [e] | 0.80 ± 0.05 |

[a] Unless otherwise indicated these values are calculated by subtracting $k_{HM3}$ from $k_{obs}$, which is the average value of $k_{obs}$ from pH 7.4 and 7.6 in pH jump data.

[b] This value is the average of the slow phase from ET data *ref* [73].

[c] These values are directly obtained from ET data for the A72H76 variant.

[d] This value is the average of the slow ET phase from *ref* [64].

[e] This values is directly obtained from ET data for the H81 variant.

Previous work from our lab has shown that the His73-heme ET gate operates on a ~143 ms [73] and the His79-heme ET gate on a ~1.58 s [64] time scale near physiological pH. Present work with the A72H76 variant shows that the His76-heme ET gate operates on a ~233 ms and for the H81 variant, His81-heme ET gate operates on a ~ 307 ms time scale, i.e., in between the K73H and H79 variants. Lysine-heme ET gates operate on a 15-30 s time scale [81]. This suggests that we can significantly modulate the rate of the His-heme ET gate near physiological pH by changing the position of the histidine ligand in Ω-loop D used in the alkaline state.

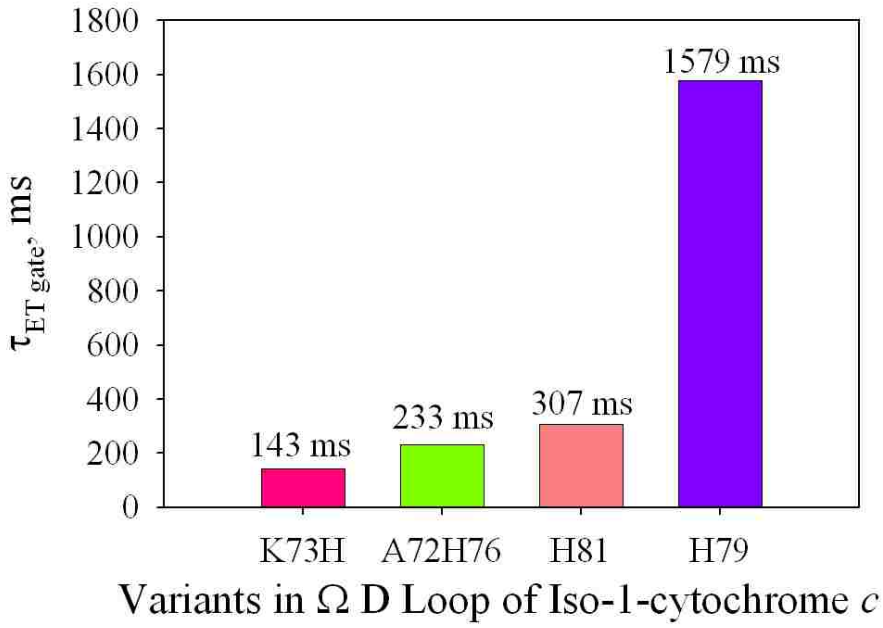


**Figure 5.26** Summary of the ET Gate lifetimes at pH 7.5 for the variants of iso-1-cytochrome *c*.

Based on these thermodynamic and kinetic studies for the H81, A72H76, H79 and K73H variants, the effects on the energy landscapes of this conformational change can be summarized in figure 3.27:

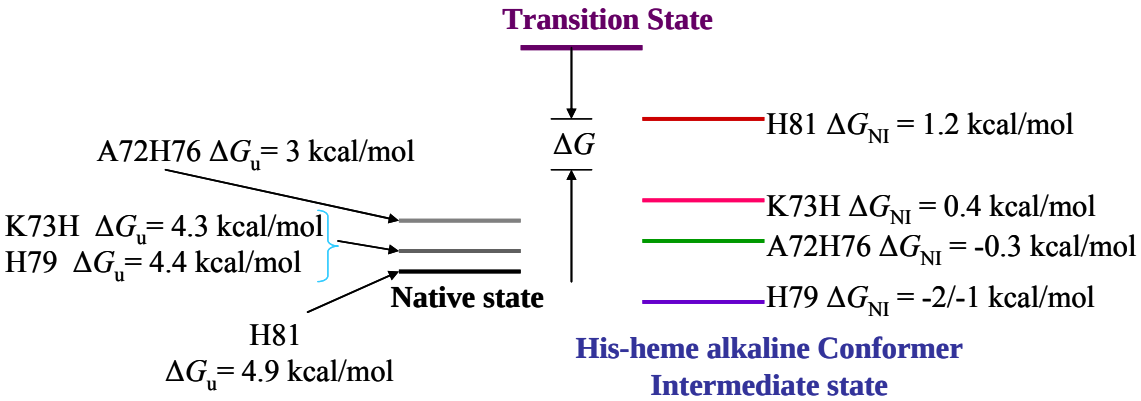


**Figure 5.27** Summary of the energy states (native and intermediate) for the variants of iso-1-cytochrome *c* based on the thermodynamic and kinetic studies at pH 7.5.

## 5.5 Conclusions

We have demonstrated that histidine position in Ω-loop D significantly affects the alkaline transition. The histidine-heme alkaline conformer is destabilized for the H81 variant, while it is stabilized for the A72H76 variant. The alkaline conformation stabilization appears to be even greater for A72H73G76 and A72H73G76A79 variants. As a result thermodynamic and kinetic studies were not possible with them. The A72H76 variant shows the presence of two ionizable groups participating in the alkaline transition similar to what is seen with the His79 variant, while the kinetics are more complex for H81. The similarity of the rate constants obtained from pH jump data and ET data suggests the validity of the kinetic model used for these studies. Conformationally gated ET kinetics were fast with $a_6Ru^{2+}$ complex, such that rate of loss of the native conformer ($k_f$ or $k_{MH3}$) could only be followed with the A72H76 variant. With $[Co(terpy)_2]^{2+}$ the kinetics were so slow that it was difficult to resolve direct ET rates from the rate of the conformational changes. This indicates that an inorganic reagent with $k_{ET}$ in between the rate constant of $a_6Ru^{2+}$ and $[Co(terpy)_2]^{2+}$ will be helpful to get direct information on $k_{MH3}$ ($k_f$) from ET studies. The current study also shows that by modulating the nature and position of the alternate ligand in Ω-loop D of iso-1-cytochrome *c*, the thermodynamic and kinetic properties can be tuned at physiological pH and provide ET gates with variable rates.

# CHAPTER 6

## *CONFORMATIONALLY GATED ELECTRON TRANSFER STUDIES BY FLASH PHOTOLYSIS*

### 6.1 Introduction

So far in the previous chapters the focus was mainly on intermolecular electron transfer (ET) reactions, in which the ET takes place between two molecules not connected by any linkage or bridge (i.e. reaction between iso-1-cyt *c* and hexaaminеruthenium(II) chloride or the cobalt terpyridine complex). In the present Chapter emphasis is on intramolecular ET reactions, where a semisynthetic approach is used, as described previously [181, 182]. In this approach, redox-active inorganic reagents are bound covalently to specific residues in the polypeptide chain of a structurally well-characterized ET metalloprotein [181].

As mentioned in chapter 1, equation 1.1, the rate of electron transfer ($k_{ET}$) depends on $H_{AB}$, the electronic coupling between the donor and the acceptor at the transition state [65]. This term mainly depends on the distance between the donor and the acceptor [67]. It has been demonstrated that intramolecular rates of electron transfer can be significantly altered when donor and acceptor are separated by different peptide units [183]. It is also known that the secondary structure (α-helix, β sheet) content of a protein and its tertiary structure defines the distance dependence of electronic coupling in a protein [184]. Depending on the coupling distance from the heme center (redox center), different sites in cytochrome *c* have been characterized as hot spots (represents strong coupling to heme), cold spots (weak coupling with heme) and average spots as shown in figure 6.1 [184].

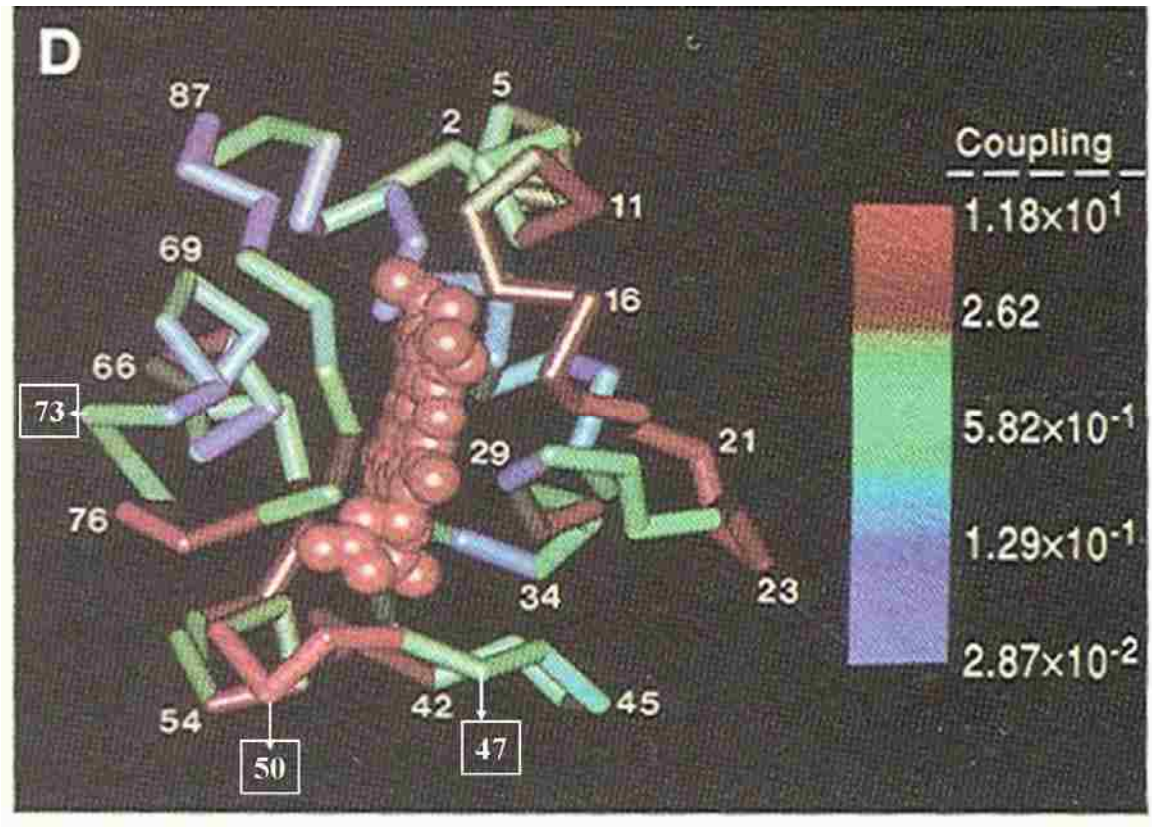


**Figure 6.1** Figure of cytochrome *c* showing the extent of the electronic coupling with the heme center (red color represents a hot spot of strong coupling, green an average spot and blue a cold spot, or weak coupling). The mutations designed for this project are represented with the position number in a square {47 and 73 in an average spot (green color), and 50 in a hot spot (red color)}. This figure is modified from *ref* [184].

Cytochrome *c* has been used by various groups for the semisynthetic approach to understand the role of redox-site separation distance on metalloprotein electron-transfer rates, using pulse radiolysis [183] and flash photolysis [181, 182]. Various ruthenium compounds have been used in these studies because of the kinetic inertness of Ru(II), its selectivity for binding to nitrogen and sulfur ligands and also the ease of characterization with NMR and other physical techniques. These studies have shown selective binding of a pentaammineruthenium(II) moiety ($a_5Ru^{2+}$) to His33 in horse cyt *c*. The reduction of

this protein complex was initiated by excitation of $Ru(bpy)_3^{2+}$ (bpy = 2,2'-bipyridine) as shown in figure 6.2. The main features of these studies are: oxidized cyt *c* ($PFe^{III}$) covalently bound to $a_5Ru^{3+}$ ($PFe^{III}$-$Ru^{III}$) is three times faster quencher for $Ru^{2+}(bpy)_3$* than $PFe^{III}$; electron transfer from $PFe^{III}$-$Ru^{II}$ to $PFe^{III}$ heme center is slower than the back ET reaction to $Ru^{3+}(bpy)_3$, thus, to prevent this back reaction EDTA was used as a scavenger for $Ru^{3+}(bpy)_3$; $PFe^{III}$-$Ru^{II}$ is formed in five fold excess compared to the thermodynamic product $PFe^{II}$-$Ru^{III}$. $PFe^{III}$-$Ru^{II}$→ $PFe^{II}$-$Ru^{III}$ is independent of protein concentration suggesting a simple intramolecular ET reaction [181].

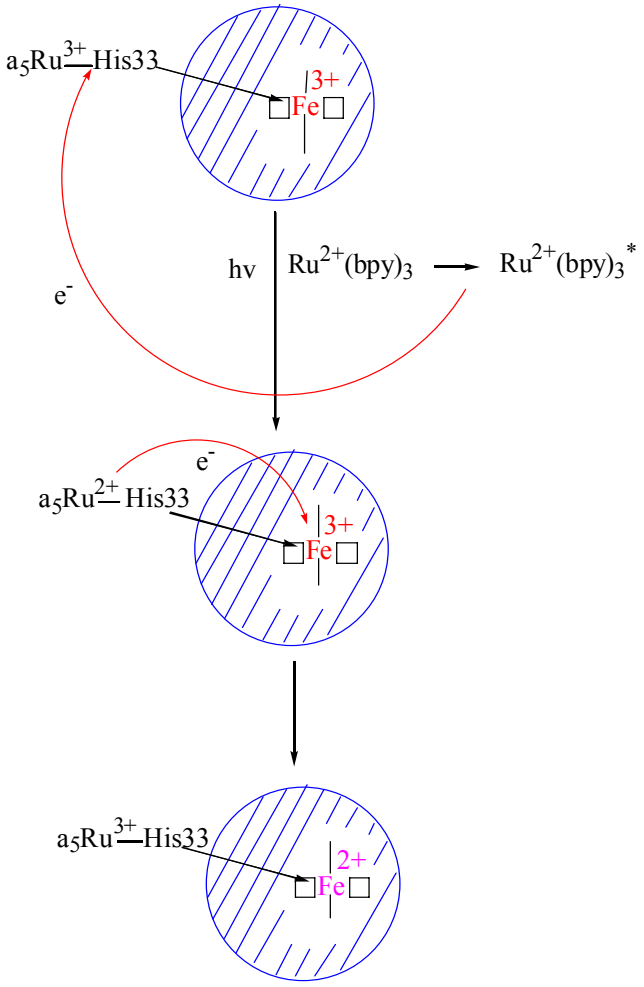


**Figure 6.2 R**eaction scheme for intramolecular ET using $Ru(bpy)_3^{2+}$ and pentaammineruthenium(III) complexed with cytochrome *c*. Based on *ref* [181, 182].

It was also indicated that the redox potential of the heme center in $PFe^{III}$-$Ru^{III}$ will be perturbed upon the loss of the native state Met80-heme coordination, with the possibility of $PFe^{II}$-$Ru^{III}$ being both the thermodynamic and kinetic product. Lysines at positions 73 and 79 are known to replace Met80-heme ligation at alkaline pH [48, 60]. The decrease in the reduction potential for iso-1cyt *c* has been reported from pH 5 (290 mV) to pH 10.03 (230 mV) [48].

With the incorporation of the above mentioned ideas, a series of mutants i.e., AcH50, AcH50H73, AcH47, AcH47H73 have been designed to develop a photo-inducible gated ET reaction. The base template for all these variants (AcTM) lacks surface histidines at position 26, 33 and 39 and the N terminal amino group is acetylated. Thus selective binding of an $a_5Ru^{2+}$ moiety to iso-1-cyt *c* at the desired position (His 47 or 50) can be achieved. Aspartate is present at position 50 (hot spot), serine is present at position 47 (average spot) and a position 73 ligand will provide a conformational switching mechanism.

In our lab lysine at position 73 has been mutated to histidine [100] to populate a His-heme conformer near physiological pH. This serves as the intermediate state before lysine heme ligation is attained under more alkaline conditions [61, 100]. With the use of the above mentioned variants, the flash photolysis technique can be used along with the semisynthetic approach to study photo-inducible gated ET. We expect that ET from the $a_5Ru^{2+}$-modified histidine to the heme will only be possible from the native conformer. Thus, ET from the His73-heme conformer will be conformationally gated (see figure 6.3).

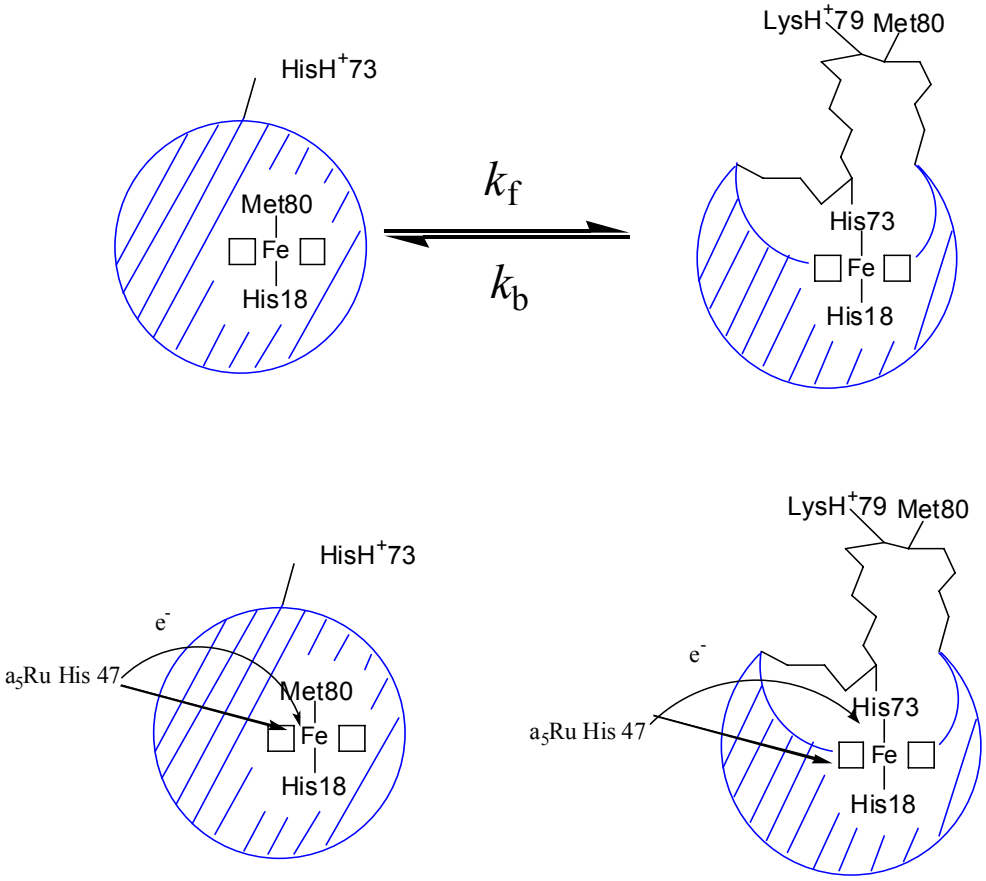


**Figure 6.3** Representative figures showing the reaction scheme of intramolecular ET reaction during the alkaline conformational transition ($k_f$ and $k_b$ are the conformational rate constant).

## 6.2 Materials and Methods

### *6.2.1 Preparation of the Variants.*

*Preparation in Saccharomyces cerevisiae (yeast)*

The AcH47 (S47H), AcH50 (D50H), AcH47H73 (S47H, K73H) and AcH50H73 (D50H, K73H) variants were prepared by the unique restriction site elimination, site directed mutagenesis method [82] using the pRS/C7.8 phagemid vector as described previously [84]. AcTM ssDNA was used for preparation of the AcH47 and AcH50 variants, while AcH73 ssDNA template was used for the preparation of the AcH47H73 and AcH50H73 variants. For preparation of AcH73 variant K73H mutation was

introduced to AcTm ssDNA template using the method mentioned above. Single stranded DNA was prepared from TG-1 *Escherichia coli* cells with the R408 helper phage [171], using the phenol extraction method [172] as described previously in Chapter 5, Materials and Methods, section 5.2.1. The selection primers used for preparation of the AcH73, AcH47 and AcH50 variants was $SacI^{-}II^{+}$, as described in Materials and Methods, section 2.2.1 of Chapter 2. The mutagenic oligonucleotide primers Table 6.1 were purchased from Biosynthesis, Inc for D50H, and from Qiagen for the S47H and K73H primers.

Sequence analysis, phagemid DNA preparation, transformation into the GM-3C-2 strain, growth isolation and purification of the variant proteins was done as described in Chapter 2 Materials and Methods section 2.2.1. Because of the low yield, multiple peaks in HPLC and low stability of these variants, the same set of variants was prepared in an *E coli* expression plasmid.

*Preparation in E coli*

Lysine 72 was first mutated to alanine by the unique restriction site elimination site directed mutagenesis method as described in Chapter 5, Materials and Methods section 5.2.1. $EcoRV^{-}AatII^{+}$ is used as the selection primer for this mutation. The vector used was pRbs-BTR1 carrying the TM variant (native His 26, 33 and 39 mutated to Asn, Asn and Gln) and the canonical AT rich ribosomal binding site. This vector is similar to the pBTR1 vector described in Materials and Methods, section 5.2.1 of Chapter 5 but short produces higher yields of cytochrome *c* [185, 186]. K72A ssDNA was used for the preparation of the H47A72 (S47H, K72A) and H50A72 (D50H, K72A) variants. The mutagenic primers used for these preparations are shown in Table 6.1. and the procedure

used for mutagenesis is the unique restriction site elimination method. For the H47A72H73 and A50A72H73 variants, ssDNA was prepared from the H47A72 and H50A72 variants by the procedure described in Chapter 5. These variants were expressed and isolated from BL21-DE3 *Escherichia coli* cells (Novagen) using the pRbs-BTR1 vector as described previously [21]. Purification and concentration determination was done as described in Chapter 2, Materials and Methods, section 2.2.2.

**Table 6.1.** Oligonucleotide primers used for site directed mutagenesis.

| Mutants | Oligonucleotide primers from 5'-3' |
|---|---|
| K73H | d(CAGGAATATA**GTG**CTTTGGGTTA) |
| S47H | d(GCATCTGTG**TAG**TGATACCCTTCAG) |
| D50H | d(GATATTGGC**ATG**TGTGTACGAATAC) |
| K72A | d(CAGGAATATATTT**GGC**TGGGTTAGT) |
| H73A72 | d(AGGAATATA**GTGGGC**TGGGTTAGTC) |

Anti-codons underlined are for the mutation of the specific site.

### *6.2.2 Molecular Weight Determination by MALDI-TOF Mass Spectroscopy.*

Molecular weight was determined for all the variants as described previously in Materials and Methods, section 2.2.2 and 3.2.2 of Chapters 2 and 3. The main peak gave m/z for all variants as shown in Table 6.2 (average and standard deviation of two independent spectra), which are consistent with the expected molecular mass of each variant. All experiments were carried out with this material for AcH47. For AcH50 six peaks were obtained from HPLC, out of which the m/z for the main peak is given in Table 6.2. No experiments were done with this protein.

**Table 6.2.** Calculated and determined m/z for the main peak from HPLC.

| Variants | Expected Mass (g/mol) | M/z from MALDI |
|---|---|---|
| AcH47 | 12702.29 | 12703 ± 1 |
| AcH50 | 12674.28 | 12662.6 ± 2.2 |

### *6.2.3 Oxidation of Protein.*

Protein was oxidized and separated from oxidizing agent as described previously in Chapter 2. The concentration and degree of oxidation of the protein were determined, as described previously in Materials and Methods, section 2.2.2 of Chapter 2.

### *6.2.4 GdnHCl Denaturation Monitored by Circular Dichroism Spectroscopy.*

Global stability of the protein was determined in the same manner as described previously in Materials and Methods, section 2.2.4 of Chapter 2.

## 6.3 Results and Discussions

### *6.3.1 Global Unfolding by GdnHCl Denaturation.*

The stability of each of these variants was determined by the guanidine HCl denaturation method assuming a two state unfolding transition as described previously. The denaturation curves for these variants are shown in figures 6.4 and 6.5. The thermodynamic parameters for each of the variants are collected in Table 6.2.

The AcH47 variant shows low stability and the *m*-value is smaller to that of the AcTM variant. The same variant when expressed in *E coli* is more stable but has a similar *m*-value as shown in Table 6.3. The main difference between these two variants is acetylation of the N terminal amino group in AcH47 and mutation of lysine at position 72

to alanine in H47H72 which should have minor effects on stability and yet they differ dramatically. Interestingly replacement of Lysine at position 73 by histidine in the same variant i.e. H47A72H73 decreases its stability and lowers the *m*-value suggesting that unfolding occurs from a partially unfolded state as for K73H variants discussed in earlier Chapters.

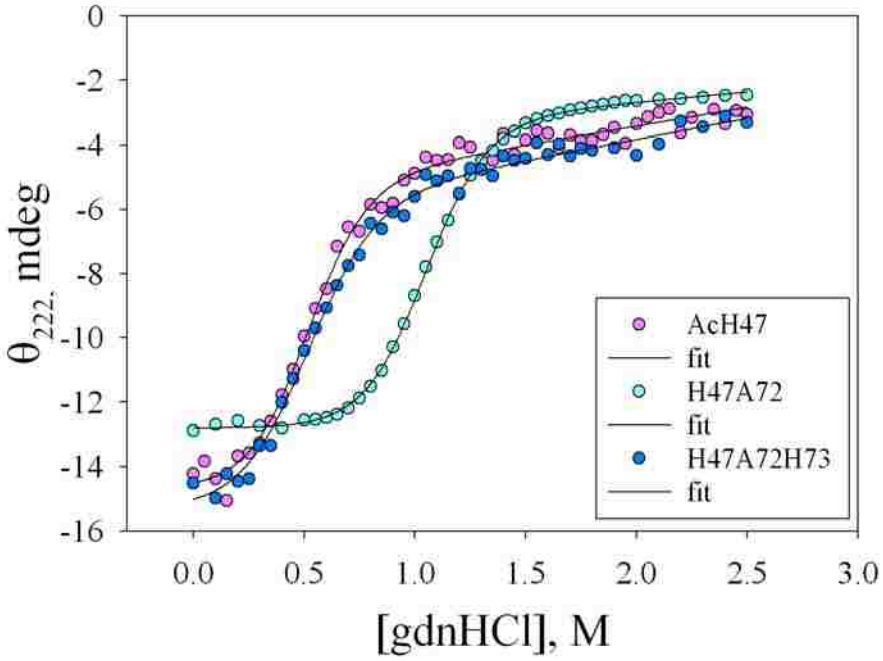


**Figure 6.4** Plot of ellipticity observed at 222 nm as a function of gdnHCl concentration for the AcH47 (pink circles), H47A72 (cyan circles) and H47A72H73 (blue circles) variants of iso-1-cytochrome *c*. Data were acquired at 25 ºC in 20 mM Tris, pH 7.5, 40 mM NaCl and at 4 μM protein concentration. The solid curve is a fit of the data to eq 2.1 in Materials and Methods, section 2.2.4 of Chapter 2.

The gdnHCl denaturation curves of the variants involving mutation at position 50 are shown in figure 6.5. The native state in AcH50H73 variant from yeast has the lowest $\Delta G_u^o$ and *m*-value as shown in Table 6.3. Its $\Delta G_u^o$ and *m*-value are half that of AcH73 variant suggesting a strong destabilizing effect of the mutation at position 50 from

aspartate to histidine. The H50A72H73 variant expressed in *E coli* shows improved stability and a higher *m*-value than for the AcH50H73 variant. H50A72H73 seems to be more stable than H47A72H73 but with a comparable *m*-value. H50A72 is less stable than the TM variant but more stable than H50A72H73 variant. The *m*-value is similar to that of the TM variant.

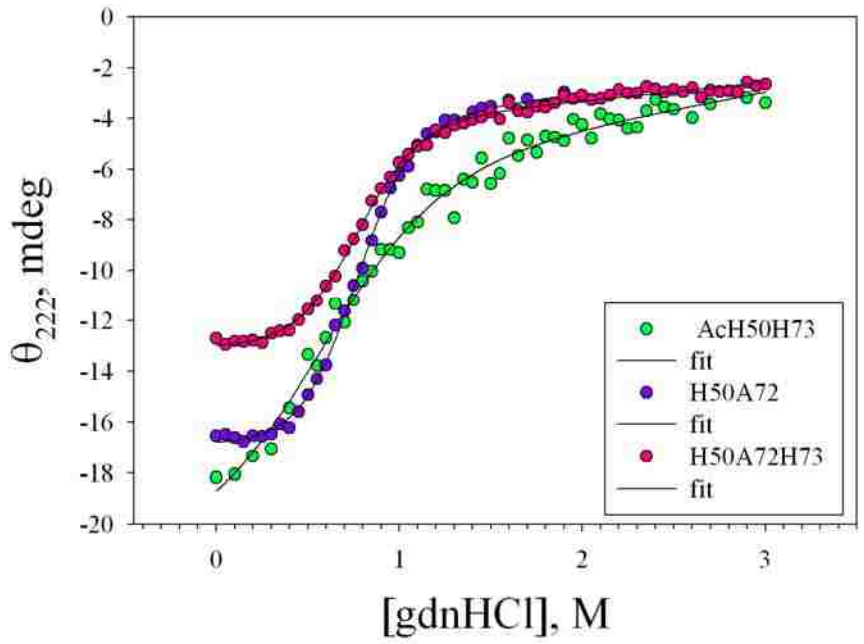


**Figure 6.5** Plot of ellipticity observed at 222 nm as a function of gdnHCl concentration for the AcH50H73 (green circles), H50A72 (purple circles) and H50A72H73 (dark pink circles) variants of iso-1-cytochrome *c*. Data were acquired at 25 ºC in 20 mM Tris, pH 7.5, 40 mM NaCl and at 4 µM protein concentration. The solid curve is a fit of the data to eq 2.1 in Materials and Methods, section 2.2.4 of Chapter 2.

**Table 6.3.** Thermodynamic parameters for gdnHCl unfolding of variants of iso-1-cyt *c* monitored by ellipticity at 222 nm at pH 7.5.

| Variants | $\Delta G_u^o(H_2O)$(kcal/mol) | *m* (kcal / mol·M) | $C_m$ (M) |
|---|---|---|---|
| AcH47* | 2.21 ± 0.11 | 4.22 ± 0.31 | 0.51 ± 0.01 |
| H47A72 | 4.32 ± 0.09 | 4.58 ± 0.11 | 1.06 ± 0.02 |
| H47A72H73 | 2.01 ± 0.08 | 3.68 ± 0.27 | 0.53 ± 0.03 |
| AcH50H73* | 0.95 ± 0.03 | 1.83 ± 0.16 | 0.52 ± 0.03 |
| H50A72 | 3.16 ± 0.29 | 4.03 ± 0.26 | 1.27 ± 0.04 |
| H50A72H73 | 2.95 ± 0.30 | 3.84 ± 0.33 | 1.30 ± 0.02 |
| AcTm [a] | 3.93 ± 0.15 | 3.71 ± 0.18 | 1.06 ± 0.04 |
| AcH73 [b] | 2.02 ± 0.15 | 2.68 ± 0.21 | 0.75 ± 0.05 |
| Tm [c] | 4.02 ± 0.17 | 3.99 ± 0.17 | 1.008 ± 0.0003 |

*These variants are expressed in Yeast.

[a] This value is taken from *ref* [75].

[b] This value is taken from *ref* [24].

[c] This value is taken from *ref* [175].

## 6.4 Conclusions

The results of this chapter are preliminary, providing data for the global stability of the variants expressed in yeast and bacteria. The lower value of $\Delta Gu^o(H_2O)$ and the *m*-value suggests that the native state is destabilized in these variants, which significantly affected the functionality of iso-1-cyt *c*, so much so that they could not be expressed in yeast. In most of these variants partially unfolded states seems to be more unfolded (lower *m*-value for global unfolding) with the exception of the H47A72 and H50A72 variants, suggesting that His at position 73 is populating a partially unfolded form.

Preliminary electron transfer experiments were carried out using $Ru(bpy)_3^{2+}$ and the wild type and AcH47 variants of iso-1cytochrome *c*. EDTA was used as quencher and the change in absorbance at 550 nm was monitored by flash photolysis as described in

*references* [181, 182]. No success was obtained with initial trials in this experiment as no change in the absorbance signal was observed.

Future work for this project will involve basic thermodynamic and kinetic experiments as described in earlier chapters for the characterization of the variants of iso-1-cyt *c* mentioned in this chapter. For the intramolecular ET reactions the binding of $a_5Ru^{2+}$ moiety to the iso-1-cyt *c* variant has to be optimized before actual flash photolysis experiments can be carried out.

## Bibliography


1. Pietzsch, J., *The Importance of Protein Folding.* http://www.nature.com/horizon/proteinfolding/background.html, 2002.

2. Kendrew, J.C., et al., *A three-dimensional model of the myoglobin molecule obtained by x-ray analysis.* Nature, 1958. **181**(4610): p. 662-6.

3. Anfinsen, C.B., *Principles that govern the folding of protein chains.* Science, 1973. **181**(96): p. 223-30.

4. Levinthal, C., in Mossbauer Spectroscopy in Biological Systems, Proceedings of a Meeting held at Allerton House, Monticello, IL, eds. Debrunner, P., Tsibris, J. C. M. & Munck, E. (University of Illinois Press, Urbana), 1969: p. 22-24.

5. Ptitsyn, O.B., *Stages in the mechanism of self-organization of protein molecules.* Dokl Akad Nauk SSSR, 1973. **210**(5): p. 1213-5.

6. Fersht, A.R., *From the first protein structures to our current knowledge of protein folding: delights and scepticisms.* Nature Reviews: Molecular Cell Biology, 2008. **9**(8): p. 650-654.

7. Dill, K.A., Ozkan, S. B., Shell, M. S., Weikl, T. R., *The protein folding problem.* Annu Rev Biophys, 2008. **37**: p. 289-316.

8. Tripp, K.W., Barrick, D., *Rerouting the folding pathway of the Notch ankyrin domain by reshaping the energy landscape.* Journal American Chemical Society, 2008. **130**(17): p. 5681-8.

9. Cheung, M.S., Chavez, L.L., Onuchic,J.N., *The energy landscape for protein folding and possible connections to function.* Polymer 2004. **45** p. 547–555.

10. Onuchic, J.N., Z. Luthey-Schulten, and P.G. Wolynes, *Theory of protein folding: the energy landscape perspective.* Annual Rev Phys Chem, 1997. **48**: p. 545-600.

11. Montgomery, J.A., et al., *Effects of Translation-Rotation Coupling on Hydrodynamic Diffusion Tensors.* Journal of Chemical Physics, 1977. **67**(12): p. 5971-5972.

12. Onuchic, J.N., *Contacting the protein folding funnel with NMR.* Proc Natl Acad Sci U S America, 1997. **94**(14): p. 7129-31.

13. Hosseinkhani, S. and M. Nemat-Gorgani, *Partial unfolding of carbonic anhydrase provides a method for its immobilization on hydrophobic adsorbents and protects it against irreversible thermoinactivation.* Enzyme and Microbial Technology, 2003. **33**(2-3): p. 179-184.

14. Krishna, M.M., et al., *Order of steps in the cytochrome C folding pathway: evidence for a sequential stabilization mechanism.* Journal of Molecular Biology, 2006. **359**(5): p. 1410-9.

15. Raschke, T.M. and S. Marqusee, *The kinetic folding intermediate of ribonuclease H resembles the acid molten globule and partially unfolded molecules detected under native conditions.* Nature Structure Biol, 1997. **4**(4): p. 298-304.

16. Cellitti, J., R. Bernstein, and S. Marqusee, *Exploring subdomain cooperativity in T4 lysozyme II: uncovering the C-terminal subdomain as a hidden intermediate in the kinetic folding pathway.* Protein Science, 2007. **16**(5): p. 852-62.

17. Guijarro, J.I., et al., *Amyloid fibril formation by an SH3 domain.* Proc Natl Acad Sci U S A, 1998. **95**(8): p. 4224-8.

18. Dobson, C.M., *Protein misfolding, evolution and disease.* Trends Biochem Sci, 1999. **24**(9): p. 329-32.

19. Losi, A., *Flavin-based Blue-Light photosensors: a photobiophysics update.* Photochem Photobiol, 2007. **83**(6): p. 1283-300.

20. Milstein, S.J., et al., *Partially unfolded proteins efficiently penetrate cell membranes--implications for oral drug delivery.* J Control Release, 1998. **53**(1-3): p. 259-67.

21. Kurchan, E., H. Roder, and B.E. Bowler, *Kinetics of loop formation and breakage in the denatured state of iso-1-cytochrome c.* J Mol Biol, 2005. **353**(3): p. 730-43.

22. Nelson, C.J., M.J. LaConte, and B.E. Bowler, *Direct detection of heat and cold denaturation for partial unfolding of a protein.* Journal of American Chemical Society, 2001. **123**(30): p. 7453-4.

23. Nelson, C.J. and B.E. Bowler, *pH dependence of formation of a partially unfolded state of a Lys 73 --> His variant of iso-1-cytochrome c: implications for the alkaline conformational transition of cytochrome c.* Biochemistry, 2000. **39**(44): p. 13584-94.

24. Bandi, S. and B.E. Bowler, *Probing the bottom of a folding funnel using conformationally gated electron transfer reactions.* Journal of the American Chemical Society, 2008. **130**(24): p. 7540-7541.

25. Ruf, R.A., et al., *Alpha-Synuclein conformation affects its tyrosine-dependent oxidative aggregation.* Biochemistry, 2008. **47**(51): p. 13604-9.

26. Bertini, I., G. Cavallaro, and A. Rosato, *Cytochrome c: occurrence and functions.* Chem Rev, 2006. **106**(1): p. 90-115.

27. Ow, Y.P., et al., *Cytochrome c: functions beyond respiration.* Nat Rev Mol Cell Biol, 2008. **9**(7): p. 532-42.

28. MacMunn, C.A., Phil. Tr. Roy. Soc. London, 1886. **167**: p. 267.

29. Keilin, D., Proc. Roy. Soc. London, Series B, 1926. **100**: p. 129.

30. Keilin, D., Proc. Roy. Soc. London, Series B, 1929. **104**: p. 206.

31. Keilin, D., Proc. Roy. Soc. London, Series B, 1930. **106**: p. 418.

32. Margoliash, E. and A. Schejter, *How does a small protein become so popular?: A succinct account of the developement of our understanding of cytochrome c* in *Cytochrome c: A Multidisciplinary Approach (Scott, R.A., and Mauk, A.G., Eds) University Science Books, Sausilito, CA*. 1996 p. 4-5.

33. Perroud, T.D., M.P. Bokoch, and R.N. Zare, *Cytochrome c conformations resolved by the photon counting histogram: watching the alkaline transition with single-molecule sensitivity.* Proc Natl Acad Sci U S A, 2005. **102**(49): p. 17570-5.

34. Keilin, D., *The History of Cell Respiration and Cytochrome.* Cambridge Univ. Press, Cambridge, 1966.

35. Sherman, F. and J.W. Stewart, *Genetics and biosynthesis of cytochrome c.* Annu Rev Genet, 1971. **5**: p. 257-96.

36. Ambler, R.P., *Sequence variability in bacterial cytochromes c.* Biochim Biophys Acta, 1991. **1058**(1): p. 42-7.

37. Ambler, R.P. and M. Daniel, *Rattlesnake cytochrome c. A re-appraisal of the reported amino acid sequence.* Biochem J, 1991. **274 ( Pt 3)**: p. 825-31.

38. Meyer, T.E., *Evolution and Classifcation of c-Type Cytochromes, in Cytochrome c: A Multidisciplinary Approach (Scott, R.A., and Mauk, A.G., Eds)* University Science Books, Sausilito, CA, 1996: p. 33-40.

39. Hoang, L.M., H.; Krishna, M. M.; Lin, Y.; Englander, S. W., *Folding units govern the cytochrome c alkaline transition.* J Mol Biol, 2003. **331**(1): p. 37-43.

40. Stevens, J.M., et al., *C-type cytochrome formation: chemical and biological enigmas.* Acc Chem Res, 2004. **37**(12): p. 999-1007.

41. Moore, G.R. and G.W. Pettigrew, *Cytochrome c: Evolutionary, Structural and Physicochemical Aspects.* Springer-Verlag, New York, 1990: p. 50-51.

42. Krishna, M.M.G., et al., *Branching in the sequential folding pathway of cytochrome c.* Protein Science 2007. **16**(9): p. 1946–1956.

43. Theorell, H. and A. Åkesson, Journal of the American Chemical Society, 1941. **63**: p. 1812-1818.

44. Wilson, M.T., *Evolution and Classifcation of c-Type Cytochromes, in Cytochrome c: A Multidisciplinary Approach (Scott, R.A., and Mauk, A.G., Eds)* University Science Books, Sausilito, CA. 1996. 33-40., 1996: p. 611-634.

45. Bhuyan, A.K. and J.B. Udgaonkar, *Folding of horse cytochrome c in the reduced state.* J Mol Biol, 2001. **312**(5): p. 1135-60.

46. Moore, G.R. and G.W. Pettigrew, *Cytochrome c: Evolutionary, Structural and Physicochemical Aspects.* Springer-Verlag, New York, 1990: p. 69-70.

47. Dopner, S., et al., *The structural and functional role of lysine residues in the binding domain of cytochrome c in the electron transfer to cytochrome c oxidase.* European Journal of Biochemistry, 1999. **261**(2): p. 379-91.

48. Rosell, F.I., J.C. Ferrer, and A.G. Mauk, *Proton-linked protein conformational switching: Definition of the alkaline conformational transition of yeast iso-1-ferricytochrome c.* Journal of the American Chemical Society, 1998. **120**(44): p. 11234-11245.

49. Raphael, A.L. and H.B. Gray, *Semisynthesis of Axial-Ligand (Position-80) Mutants of Cytochrome-C.* Journal of the American Chemical Society, 1991. **113**(3): p. 1038-1040.

50. Davidson, V.L., *Chemically gated electron transfer. A means of accelerating and regulating rates of biological electron transfer.* Biochemistry, 2002. **41**(50): p. 14633-6.

51. Davidson, V.L., *Effects of kinetic coupling on experimentally determined electron transfer parameters.* Biochemistry, 2000. **39**(16): p. 4924-8.

52. Greenwood, C. and G. Palmer, *Evidence for the existence of two functionally distinct forms cytochrome c manomer at alkaline pH.* J Biol Chem, 1965. **240**(9): p. 3660-3.

53. Wilson, M.T. and C. Greenwood, *Studies on ferricytochrome c. 2. A correlation between reducibility and the possession of the 695mm absorption band of ferricytochrome c.* Eur J Biochem, 1971. **22**(1): p. 11-8.

54. Hodges, H.L., R.A. Holwerda, and H.B. Gray, *Kinetic Studies of Reduction of Ferricytochrome-C by Fe(Edta)2-.* Journal of the American Chemical Society, 1974. **96**(10): p. 3132-3137.

55. Jemmerson, R., et al., *A conformational change in cytochrome c of apoptotic and necrotic cells is detected by monoclonal antibody binding and mimicked by association of the native antigen with synthetic phospholipid vesicles.* Biochemistry, 1999. **38**(12): p. 3599-609.

56. Pollock, W.B., et al., *Bacterial expression of a mitochondrial cytochrome c. Trimethylation of lys72 in yeast iso-1-cytochrome c and the alkaline conformational transition.* Biochemistry, 1998. **37**(17): p. 6124-31.

57. Battistuzzi, G., et al., *Free energy of transition for the individual alkaline conformers of yeast iso-1-cytochrome c.* Biochemistry, 2007. **46**(6): p. 1694-702.

58. Assfalg, M., et al., *Structural model for an alkaline form of ferricytochrome c.* Journal of the American Chemical Society, 2003. **125**(10): p. 2913-22.

59. Baddam, S. and B.E. Bowler, *Mutation of asparagine 52 to glycine promotes the alkaline form of iso-1-cytochrome c and causes loss of cooperativity in acid unfolding.* Biochemistry, 2006. **45**(14): p. 4611-9.

60. Ferrer, J.C., et al., *Identification of Lys79 as an Iron Ligand in One Form of Alkaline Yeast Iso-1-Ferricytochrome-C.* Journal of the American Chemical Society, 1993. **115**(16): p. 7507-7508.

61. Martinez, R.E. and B.E. Bowler, *Proton-mediated dynamics of the alkaline conformational transition of yeast iso-1-cytochrome c.* Journal of American Chemical Society, 2004. **126**(21): p. 6751-8.

62. Baddam, S. and B.E. Bowler, *Thermodynamics and kinetics of formation of the alkaline state of a Lys 79-->Ala/Lys 73-->His variant of iso-1-cytochrome c.* Biochemistry, 2005. **44**(45): p. 14956-68.

63. Kristinsson, R. and B.E. Bowler, *Communication of stabilizing energy between substructures of a protein.* Biochemistry, 2005. **44**(7): p. 2349-59.

64. Bandi, S., S. Baddam, and B.E. Bowler, *Alkaline Conformational Transition and Gated Electron Transfer with a Lys 79 --> His Variant of Iso-1-cytochrome c.* Biochemistry, 2007. **46**(37): p. 10643-54.

65. Marcus, R.A. and N. Sutin, *Electron Transfers in Chemistry and Biology.* Biochimica Et Biophysica Acta, 1985. **811**(3): p. 265-322.

66. Hopfield, J.J., *Electron Transfer Between Biological Molecules by Thermally Activated Tunneling.* Proc Natl Acad Sci U S A, 1974. **71**(9): p. 3640-3644.

67. Gray, H.B. and J.E.R. Walther, *Electron Transfer.* Bioinorganic Chemistry (Bertini,I; Gray, H.B;Lippard, S.J and Valentine, J.S., Eds) University Books, Mill Valley, California, 1994: p. 315-363.

68. Davidson, V.L., *Protein Control of True, Gated, and Coupled Electron Transfer Reactions.* Acc Chem Res, 2008.

69. Guss, J.M., et al., *Crystal structure analyses of reduced (CuI) poplar plastocyanin at six pH values.* J Mol Biol, 1986. **192**(2): p. 361-87.

70. Holzman, T.F., et al., *pH-induced conformational states of bovine growth hormone.* Biochemistry, 1990. **29**(5): p. 1255-61.

71. Tatulian, S.A. and L.K. Tamm, *Reversible pH-dependent conformational change of reconstituted influenza hemagglutinin.* J Mol Biol, 1996. **260**(3): p. 312-6.

72. Weber, C., B. Michel, and H.R. Bosshard, *Spectroscopic analysis of the cytochrome c oxidase-cytochrome c complex: circular dichroism and magnetic circular dichroism measurements reveal change of cytochrome c heme geometry imposed by complex formation.* Proc Natl Acad Sci U S A, 1987. **84**(19): p. 6687-91.

73. Baddam, S. and B.E. Bowler, *Conformationally gated electron transfer in iso-1-cytochrome c: engineering the rate of a conformational switch.* Journal of the American Chemical Society, 2005. **127**(27): p. 9702-3.

74. Margoliash, E. and N. Frohwirt, *Spectrum of horse-heart cytochrome c.* Biochem J, 1959. **71**(3): p. 570-2.

75. Wandschneider, E., B.N. Hammack, and B.E. Bowler, *Evaluation of cooperative interactions between substructures of iso-1-cytochrome c using double mutant cycles.* Biochemistry, 2003. **42**(36): p. 10659-66.

76. Meyer, T.E., *Evolution and Classifcation of c-Type Cytochromes* Cytochrome c: A Multidisciplinary Approach (Scott, R.A., and Mauk, A.G., Eds) University Science Books, Sausilito, CA, 1996: p. 33-99.

77. Maity, H., J.N. Rumbley, and S.W. Englander, *Functional role of a protein foldon--an Omega-loop foldon controls the alkaline transition in ferricytochrome c.* Proteins, 2006. **63**(2): p. 349-55.

78. Bai, Y., et al., *Protein folding intermediates: native-state hydrogen exchange.* Science, 1995. **269**(5221): p. 192-7.

79. Krishna, M.M., et al., *Cooperative omega loops in cytochrome c: role in folding and function.* J Mol Biol, 2003. **331**(1): p. 29-36.

80. Dopner, S., et al., *Alkaline conformational transitions of ferricytochrome c studied by resonance Raman spectroscopy.* Journal of the American Chemical Society, 1998. **120**(44): p. 11246-11255.

81. Baddam, S. and B.E. Bowler, *Tuning the rate and pH accessibility of a conformational electron transfer gate.* Inorganic Chemistry, 2006. **45**(16): p. 6338-46.

82. Deng, W.P. and J.A. Nickoloff, *Site-directed mutagenesis of virtually any plasmid by eliminating a unique site.* Anal Biochem, 1992. **200**(1): p. 81-8.

83. Hammack, B.N., C.R. Smith, and B.E. Bowler, *Denatured state thermodynamics: residual structure, chain stiffness and scaling factors.* J Mol Biol, 2001. **311**(5): p. 1091-104.

84. Smith, C.R., N. Mateljevic, and B.E. Bowler, *Effects of topology and excluded volume on protein denatured state conformational properties.* Biochemistry, 2002. **41**(31): p. 10173-81.

85. Montgomery, D.L., et al., *Identification and isolation of the yeast cytochrome c gene.* Cell, 1978. **14**(3): p. 673-80.

86. Smith, M., et al., *Sequence of the gene for iso-1-cytochrome c in Saccharomyces cerevisiae.* Cell, 1979. **16**(4): p. 753-61.

87. Faye, G., et al., *Deletion mapping of sequences essential for in vivo transcription of the iso-1-cytochrome c gene.* Proc Natl Acad Sci U S A, 1981. **78**(4): p. 2258-62.

88. Ito, H., et al., *Transformation of intact yeast cells treated with alkali cations.* J Bacteriol, 1983. **153**(1): p. 163-8.

89. Bowler, B.E., et al., *Destabilizing effects of replacing a surface lysine of cytochrome c with aromatic amino acids: implications for the denatured state.* Biochemistry, 1993. **32**(1): p. 183-90.

90. Bowler, B.E., A. Dong, and W.S. Caughey, *Characterization of the guanidine hydrochloride-denatured state of iso-1-cytochrome c by infrared spectroscopy.* Biochemistry, 1994. **33**(9): p. 2402-8.

91. Redzic, J.S. and B.E. Bowler, *Role of hydrogen bond networks and dynamics in positive and negative cooperative stabilization of a protein.* Biochemistry, 2005. **44**(8): p. 2900-8.

92. Pace, C.N., *Determination and analysis of urea and guanidine hydrochloride denaturation curves.* Methods in Enzymology, 1986. **131**: p. 266-80.

93. Schellman, J.A., *Solvent denaturation.* Biopolymers, 1978. **17**(5): p. 1305-1322.

94. Moore, G.R. and G.W. Pettigrew, *Cytochrome c: Evolutionary, Structural and Physicochemical Aspects. Springer-Verlag, New York* 1990: p. 69-70 and 184-196.

95. Margoliash, E., and Frowhirt, N, *Spectrum of horse-heart cytochrome c.* Biochem. J, 1959. **71**: p. 570-572.

96. Godbole, S. and B.E. Bowler, *Effect of pH on formation of a nativelike intermediate on the unfolding pathway of a Lys 73 --> His variant of yeast iso-1-cytochrome c.* Biochemistry, 1999. **38**(1): p. 487-95.

97. Davis, L.A., A. Schejter, and G.P. Hess, *Alkaline isomerization of oxidized cytochrome c. Equilibrium and kinetic measurements.* J Biol Chem, 1974. **249**(8): p. 2624-32.

98. Fergusson, J.E. and J.L. Love, *Ruthenium ammines.* Inorganic Synthesis, 1972. **13**: p. 208-213.

99. Allen, A.D. and C.V. Senoff, *Preparation and infrared spectra of some ammine complexes of ruthenium (II) and ruthenium (III).* Can.. J. Chem, 1967. **45**: p. 1337-1341.

100. Godbole, S., et al., *A lysine 73-->histidine variant of yeast iso-1-cytochrome c: evidence for a native-like intermediate in the unfolding pathway and implications for m value effects.* Biochemistry, 1997. **36**(1): p. 119-26.

101. Godbole, S., B. Hammack, and B.E. Bowler, *Measuring denatured state energetics: deviations from random coil behavior and implications for the folding of iso-1-cytochrome c.* J Mol Biol, 2000. **296**(1): p. 217-28.

102. Stellwagen, E. and J. Babul, *Stabilization of the globular structure of ferricytochrome c by chloride in acidic solvents.* Biochemistry, 1975. **14**(23): p. 5135-40.

103. Greenwood, C. and M.T. Wilson, *Studies on ferricytochrome c. I. Effect of pH, ionic strength and protein denaturants on the spectra of ferricytochrome c.* Eur J Biochem, 1971. **22**(1): p. 5-10.

104. Dyson, H.J. and J.K. Beattie, *Spin state and unfolding equilibria of ferricytochrome c in acidic solutions.* J Biol Chem, 1982. **257**(5): p. 2267-73.

105. Robinson, J.B., Jr., J.M. Strottmann, and E. Stellwagen, *A globular high spin form of ferricytochrome c.* J Biol Chem, 1983. **258**(11): p. 6772-6.

106. Drew, H.R. and R.E. Dickerson, *The unfolding of the cytochromes c in methanol and acid.* J Biol Chem, 1978. **253**(23): p. 8420-7.

107. Myer, Y.P., et al., *Urea denaturation of horse heart ferricytochrome c. Equilibrium studies and characterization of intermediate forms.* Biochemistry, 1980. **19**(1): p. 199-207.

108. Angstrom, J., G.R. Moore, and R.J.P. Williams, *The Magnetic-Susceptibility of Ferricytochrome-C.* Biochimica Et Biophysica Acta, 1982. **703**(1): p. 87-94.

109. Rosell, F.I. and A.G. Mauk, *Spectroscopic properties of a mitochondrial cytochrome C with a single thioether bond to the heme prosthetic group.* Biochemistry, 2002. **41**(24): p. 7811-8.

110. Feinberg, B.A., et al., *Direct voltammetric observation of redox driven changes in axial coordination and intramolecular rearrangement of the phenylalanine-82-histidine variant of yeast iso-1-cytochrome c.* Biochemistry, 1998. **37**(38): p. 13091-13101.

111. Wood, L.C., et al., *Replacement of a conserved proline eliminates the absorbance-detected slow folding phase of iso-2-cytochrome c.* Biochemistry, 1988. **27**(23): p. 8562-8.

112. Berghuis, A.M. and G.D. Brayer, *Oxidation state-dependent conformational changes in cytochrome c.* J Mol Biol, 1992. **223**(4): p. 959-76.

113. Pearce, L.L., et al., *Mutation-induced perturbation of the cytochrome c alkaline transition.* Biochemistry, 1989. **28**(8): p. 3152-6.

114. Rosell, F.I., et al., *Characterization of an alkaline transition intermediate stabilized in the Phe82Trp variant of yeast iso-1-cytochrome c.* Biochemistry, 2000. **39**(30): p. 9047-54.

115. Hartshorn, R.T. and G.R. Moore, *A denaturation-induced proton-uptake study of horse ferricytochrome c.* Biochem J, 1989. **258**(2): p. 595-8.

116. Tonge, P., G.R. Moore, and C.W. Wharton, *Fourier-transform infra-red studies of the alkaline isomerization of mitochondrial cytochrome c and the ionization of carboxylic acids.* Biochem J, 1989. **258**(2): p. 599-605.

117. Telford, J.R., et al., *Protein folding triggered by electron transfer.* Acc Chem Res, 1998. **31**(11): p. 755-763.

118. Di Bilio, A.J., et al., *Electron transfer in ruthenium-modified plastocyanin.* Journal of the American Chemical Society, 1998. **120**(30): p. 7551-7556.

119. Bryngelson, J.D., et al., *Funnels, Pathways, and the Energy Landscape of Protein-Folding - a Synthesis.* Proteins-Structure Function and Genetics, 1995. **21**(3): p. 167-195.

120. Wolynes, P.G., *Energy landscapes and solved protein-folding problems.* Philosophical Transactions of the Royal Society of London Series a-Mathematical Physical and Engineering Sciences, 2005. **363**(1827): p. 453-464.

121. Mines, G.A., et al., *Cytochrome c folding triggered by electron transfer.* Chemistry & Biology, 1996. **3**(6): p. 491-497.

122. Oliveberg, M. and P.G. Wolynes, *The experimental survey of protein-folding energy landscapes.* Quarterly Reviews of Biophysics, 2005. **38**(3): p. 245-288.

123. Mines, G.A., et al., *Protein folding triggered by electron transfer.* Abstracts of Papers of the American Chemical Society, 1996. **212**: p. 152-PHYS.

124. Tonomura, B., et al., *Test reactions for a stopped-flow apparatus. Reduction of 2,6-dichlorophenolindophenol and potassium ferricyanide by L-ascorbic acid.* Anal Biochem, 1978. **84**(2): p. 370-83.

125. Rao, K.S., et al., *Kinetic mechanism of glutaryl-CoA dehydrogenase.* Biochemistry, 2006. **45**(51): p. 15853-61.

126. Ford, P.C., J.R. Kuempel, and H. Taube, *The Acid-Catalyzed Aquation of Hexaaminеruthenium(II) and Pentaaminepyridinenium(II) Complex Ions.* Inorganic Chemistry, 1968. **7**(10): p. 1976-1983.

127. Matsubara, T. and P.C. Ford, *Photochemistry of Ruthenium(Ii)-Saturated Amine Complexes Ru(Nh3)62+, Ru(Nh3)5h2o2+, and Ru(En)32+ in Aqueous-Solution.* Inorganic Chemistry, 1978. **17**(7): p. 1747-1752.

128. Meyer, T.J. and H. Taube, *Electron Transfer Reactions of Ruthenium Ammines.* Inorganic Chemistry, 1968. **7**(11): p. 2369-2370.

129. Myers, J.K., C.N. Pace, and J.M. Scholtz, *Denaturant m values and heat capacity changes: relation to changes in accessible surface areas of protein unfolding.* Protein Science, 1995. **4**(10): p. 2138-48.

130. Fee, J.A., et al., *Integrity of thermus thermophilus cytochrome c552 synthesized by Escherichia coli cells expressing the host-specific cytochrome c maturation genes, ccmABCDEFGH: biochemical, spectral, and structural characterization of the recombinant protein.* Protein Science, 2000. **9**(11): p. 2074-84.

131. Blauer, G., N. Sreerama, and R.W. Woody, *Optical activity of hemoproteins in the Soret region. Circular dichroism of the heme undecapeptide of cytochrome c in aqueous solution.* Biochemistry, 1993. **32**(26): p. 6674-9.

132. Smith, C.R., E. Wandschneider, and B.E. Bowler, *Effect of pH on the iso-1-cytochrome c denatured state: changing constraints due to heme ligation.* Biochemistry, 2003. **42**(7): p. 2174-84.

133. Mayr, L.M., et al., *Kinetic analysis of the unfolding and refolding of ribonuclease Tl by a stopped-flow double-mixing technique.* Biochemistry, 1996. **35**(17): p. 5550-5561.

134. Odefey, C., L.M. Mayr, and F.X. Schmid, *Non-Prolyl Cis-Trans Peptide-Bond Isomerization as a Rate-Determining Step in Protein Unfolding and Refolding.* J Mol Biol, 1995. **245**(1): p. 69-78.

135. Russell, B.S. and K.L. Bren, *Denaturant dependence of equilibrium unfolding intermediates and denatured state structure of horse ferricytochrome c.* J Biol Inorg Chem, 2002. **7**(7-8): p. 909-16.

136. Qin, W., et al., *The role of histidines 26 and 33 in the structural stabilization of cytochrome c.* Biochim Biophys Acta, 1995. **1252**(1): p. 87-94.

137. Pielak, G.K., et al., *Nuclear Magnetic Resonance Stdies of Class I Cytochromes c, in Cytochrome c: A Multidisciplinary Approach (Scott, R.A., and Mauk, A.G., Eds)* University Science Books, Sausilito, CA. 1996. 33-40., 1996: p. 203-284.

138. Aviram, I. and Y. Krauss, *The structure of the heme crevice of ferric cytochrome c alkylated at methionine-80.* J Biol Chem, 1974. **249**(8): p. 2575-8.

139. D'Amico, S., et al., *Activity-stability relationships in extremophilic enzymes.* J Biol Chem, 2003. **278**(10): p. 7891-6.

140. Pielak, G.J., *Woes of proline: a cautionary kinetic tale.* Protein Sci, 2006. **15**(3): p. 393-4.

141. Reimer, U., et al., *Side-chain effects on peptidyl-prolyl cis/trans isomerisation.* J Mol Biol, 1998. **279**(2): p. 449-60.

142. Jabs, A., M.S. Weiss, and R. Hilgenfeld, *Non-proline cis peptide bonds in proteins.* J Mol Biol, 1999. **286**(1): p. 291-304.

143. Pauling, L., *The Nature of the Chemical Bond.* 2nd ed, cornell Unversity Press, Ithaca, New York, N.Y, 1948: p. 207.

144. Schmid, F., *Prolyl Isomerization in Protein Folding:Protein Folding Handbook (Buchner,J and Kiefhaber, T., Eds).* 2005. **2**(Wiley-VCH Verlag GmbH & Co. KGaA): p. 916-945.

145. Steinberg, I.Z., et al., *The Configurational Changes of Poly-L-proline in Solution.* Journal of the American Chemical Society, 1960. **82**(20): p. 5263-5279.

146. Pierce, M.M. and B.T. Nall, *Coupled kinetic traps in cytochrome c folding: His-heme misligation and proline isomerization.* J Mol Biol, 2000. **298**(5): p. 955-69.

147. Takano, T., et al., *Tuna cytochrome c at 2.0 A resolution. II. Ferrocytochrome structure analysis.* J Biol Chem, 1977. **252**(2): p. 776-85.

148. Takano, T. and R.E. Dickerson, *Conformation change of cytochrome c. I. Ferrocytochrome c structure refined at 1.5 A resolution.* J Mol Biol, 1981. **153**(1): p. 79-94.

149. Takano, T. and R.E. Dickerson, *Conformation change of cytochrome c. II. Ferricytochrome c refinement at 1.8 A and comparison with the ferrocytochrome structure.* J Mol Biol, 1981. **153**(1): p. 95-115.

150. Lummis, S.C., et al., *Cis-trans isomerization at a proline opens the pore of a neurotransmitter-gated ion channel.* Nature, 2005. **438**(7065): p. 248-52.

151. Lu, K.P., et al., *Prolyl cis-trans isomerization as a molecular timer.* Nat Chem Biol, 2007. **3**(10): p. 619-29.

152. Pauling, L. and R.B. Corey, *Configurations of Polypeptide Chains With Favored Orientations Around Single Bonds: Two New Pleated Sheets.* Proc Natl Acad Sci U S A, 1951. **37**(11): p. 729-40.

153. Pauling, L., R.B. Corey, and H.R. Branson, *The structure of proteins; two hydrogen-bonded helical configurations of the polypeptide chain.* Proc Natl Acad Sci U S A, 1951. **37**(4): p. 205-11.

154. Leszczynski, J.F. and G.D. Rose, *Loops in globular proteins: a novel category of secondary structure.* Science, 1986. **234**(4778): p. 849-55.

155. Ring, C.S., et al., *Taxonomy and conformational analysis of loops in proteins.* J Mol Biol, 1992. **224**(3): p. 685-99.

156. Kuipers, O.P., et al., *Enhanced activity and altered specificity of phospholipase A2 by deletion of a surface loop.* Science, 1989. **244**(4900): p. 82-5.

157. Chothia, C. and A.M. Lesk, *Canonical structures for the hypervariable regions of immunoglobulins.* J Mol Biol, 1987. **196**(4): p. 901-17.

158. Brzovic, P.S., et al., *Characterization of the functional role of a flexible loop in the alpha-subunit of tryptophan synthase from Salmonella typhimurium by rapid-*

*scanning, stopped-flow spectroscopy and site-directed mutagenesis.* Biochemistry, 1993. **32**(39): p. 10404-13.

159. Fetrow, J.S., *Omega loops: nonregular secondary structures significant in protein function and stability.* Faseb J, 1995. **9**(9): p. 708-17.

160. Gekko, K., et al., *Effects of point mutation in a flexible loop on the stability and enzymatic function of Escherichia coli dihydrofolate reductase.* J Biochem, 1993. **113**(1): p. 74-80.

161. Parge, H.E., R.A. Hallewell, and J.A. Tainer, *Atomic structures of wild-type and thermostable mutant recombinant human Cu,Zn superoxide dismutase.* Proc Natl Acad Sci U S A, 1992. **89**(13): p. 6109-13.

162. Toma, S., et al., *Grafting of a calcium-binding loop of thermolysin to Bacillus subtilis neutral protease.* Biochemistry, 1991. **30**(1): p. 97-106.

163. Jimenez, M.A., et al., *CD and 1H-NMR studies on the conformational properties of peptide fragments from the C-terminal domain of thermolysin.* Eur J Biochem, 1993. **211**(3): p. 569-81.

164. Chrunyk, B.A. and R. Wetzel, *Breakdown in the relationship between thermal and thermodynamic stability in an interleukin-1 beta point mutant modified in a surface loop.* Protein Eng, 1993. **6**(7): p. 733-8.

165. Pepys, M.B., et al., *Human lysozyme gene mutations cause hereditary systemic amyloidosis.* Nature, 1993. **362**(6420): p. 553-7.

166. Fetrow, J.S., T.S. Cardillo, and F. Sherman, *Deletions and replacements of omega loops in yeast iso-1-cytochrome c.* Proteins, 1989. **6**(4): p. 372-81.

167. Mulligan-Pullyblank, P., et al., *Loop replacement and random mutagenesis of omega-loop D, residues 70-84, in iso-1-cytochrome c.* J Biol Chem, 1996. **271**(15): p. 8633-45.

168. Wilson, M.T., *The Alkaline Transition in Ferricytochrome c, in Cytochrome c: A Multidisciplinary Approach (Scott, R.A., and Mauk, A.G., Eds) University Science Books, Sausilito, CA. .* 1996: p. 33-40 and 611-634.

169. Perutz, M.F. and H. Lehmann, *Molecular pathology of human haemoglobin.* Nature, 1968. **219**(5157): p. 902-9.

170. Alber, T., et al., *Temperature-sensitive mutations of bacteriophage T4 lysozyme occur at sites with low mobility and low solvent accessibility in the folded protein.* Biochemistry, 1987. **26**(13): p. 3754-8.

171. Russel, M., S. Kidd, and M.R. Kelley, *An improved filamentous helper phage for generating single-stranded plasmid DNA.* Gene, 1986. **45**(3): p. 333-8.

172. Sambrook, J. and D.W. Russell, *Molecular Cloning: A Laboratory Manual.* Cold Spring Harbor Laboratory Press, Cold Spring Harbor, NY, 2001: p. 3.26-3.29.

173. Stanbury, D.M. and L.A. Lednicky, *Outer-Sphere Electron-Transfer Reactions Involving the Chlorite Chlorine Dioxide Couple - Activation Barriers for Bent Triatomic Species.* Journal of the American Chemical Society, 1984. **106**(10): p. 2847-2853.

174. Constable, E.C., et al., *Structural characterisation of a 1 : 1 cobalt(II)-2,2 ': 6 ',2 ''-Terpyridine complex.* Inorganic Chemistry Communications, 2006. **9**(5): p. 504-506.

175. Godbole, S. and B.E. Bowler, *A histidine variant of yeast iso-1-cytochrome c that strongly affects the energetics of the denatured state.* J Mol Biol, 1997. **268**(5): p. 816-21.

176. Moore, G.R. and G.W. Pettigrew, *Cytochrome c: Evolutionary, Structural and Physicochemical Aspects* Springer-Verlag, New York 1990: p. 1-25.

177. Feinberg, B.A., et al., *Direct voltammetric observation of redox driven changes in axial coordination and intramolecular rearrangement of the phenylalanine-82-histidine variant of yeast iso-1-cytochrome c.* Biochemistry, 1998. **37**(38): p. 13091-101.

178. Hawkins, B.K., et al., *Novel Axial Ligand Interchange in Cytochrome-C - Incorporation of a Histidine at Position-82 Leads to Displacement of the Wild-Type Methionine-80 Ligand.* Journal of the American Chemical Society, 1994. **116**(7): p. 3111-3112.

179. Black, K.M. and C.J. Wallace, *Probing the role of the conserved beta-II turn Pro-76/Gly-77 of mitochondrial cytochrome c.* Biochem Cell Biol, 2007. **85**(3): p. 366-74.

180. Drake, P.L., et al., *Ph-Dependence of Rate Constants for Reactions of Cytochrome-C with Inorganic Redox Partners and Mechanistic Implications.* Inorganic Chemistry, 1989. **28**(7): p. 1361-1366.

181. Nocera, D.G., et al., *Kinetics of Intramolecular Electron-Transfer from Ru-Ii to Fe-Iii in Ruthenium-Modified Cytochrome-C.* Journal of the American Chemical Society, 1984. **106**(18): p. 5145-5150.

182. Winkler, J.R., et al., *Electron-Transfer Kinetics of Pentaammineruthenium(Iii)(Histidine-33)-Ferricytochrome-C - Measurement of the Rate of Intramolecular Electron-Transfer between Redox Centers Separated by 15-a in a Protein.* Journal of the American Chemical Society, 1982. **104**(21): p. 5798-5800.

183. Isied, S.S., G. Worosila, and S.J. Atherton, *Electron-Transfer across Polypeptides .4. Intramolecular Electron-Transfer from Ruthenium(Ii) to Iron(Iii) in Histidine-33 Modified Horse Heart Cytochrome-C.* Journal of the American Chemical Society, 1982. **104**(26): p. 7659-7661.

184. Beratan, D.N., J.N. Betts, and J.N. Onuchic, *Protein electron transfer rates set by the bridging secondary and tertiary structure.* Science, 1991. **252**(5010): p. 1285-8.

185. Rumbley, J.N., L. Hoang, and S.W. Englander, *Recombinant equine cytochrome c in Escherichia coli: high-level expression, characterization, and folding and assembly mutants.* Biochemistry, 2002. **41**(47): p. 13894-901.

186. Duncan, M.G., M.D. Williams, and B.E. Bowler, *Compressing the Free Energy Range of Substructure Stabilities in Iso-1- cytochrome c.* Protein Science, 2009. **In Press**.

APPENDICES

# A. Tables of Rate Constants and Amplitudes for the K79H Variant

**Parameters in 0.1 M NaCl and at 25 $^{o}$C.**

**Table A1.** $k_{obs}$ average data for fast kinetic phase from upward pH jumps experiments.[a,b]

| pH | $k_{obs}$, $s^{-1}$ | pH | $k_{obs}$, $s^{-1}$ | pH | $k_{obs}$, $s^{-1}$ |
|---|---|---|---|---|---|
| 5.6 | 1.0 ± 0.3 | 7.6 | 3.5 ± 0.4 | 9.6 | 2.2 ± 0.3 |
| 5.8 | 1.0 ± 0.2 | 7.8 | 3.7 ± 0.4 | 9.8 | 2.1 ± 0.1 |
| 6.0 | 1.2 ± 0.2 | 8.0 | 3.8 ± 0.4 | 10.0 | 1.9 ± 0.1 |
| 6.2 | 1.4 ± 0.1 | 8.2 | 3.6 ± 0.1 | 10.2 | 2.3 ± 0.4 |
| 6.4 | 1.7 ± 0.2 | 8.4 | 3.5 ± 0.1 | 10.4 | 2.1 ± 0.2 |
| 6.6 | 2.0 ± 0.2 | 8.6 | 3.5 ± 0.1 | 10.6 | 2.4 ± 0.1 |
| 6.8 | 2.6 ± 0.3 | 8.8 | 3.3 ± 0.1 | 10.8 | 3.3 ± 0.3 |
| 7.0 | 2.9 ± 0.3 | 9.0 | 3.2 ± 0.2 | 11.0 | 5.1 ± 1.1 |
| 7.2 | 3.0 ± 0.4 | 9.2 | 2.9 ± 0.2 | 11.2 | 8.3 ± 1.4 |
| 7.4 | 3.4 ± 0.4 | 9.4 | 2.5 ± 0.1 | | |

[a] Data from pH 5.6 to 8.0 are the average of three data sets, two with data collected on a 5 s time scale and one with data collected on a 50 s timescale. From pH 8.2 to 11.2 the data is the average of two data sets, one with data collected on a 5 s time scale and one with data collected on a 50 s timescale. Each data set was composed of at least 3 to 5 kinetic traces at each pH.

[b] Data collected on a 5 s time scale were fit to a single exponential equation up to pH 8.4 and with a double exponential equation above that pH. Data collected on a 50 second time were fit to a single exponential equation up to pH 6.6 and with a double exponential equation above that pH.

**Table A2.** $k_{obs}$ average data for slow kinetic phase from upward pH jump experiments.[a]

| pH | $k_{obs}$, $s^{-1}$ | pH | $k_{obs}$, $s^{-1}$ | pH | $k_{obs}$, $s^{-1}$ |
|---|---|---|---|---|---|
| 6.8 | 0.052 ± 0.016 | 8.4 | 0.045 ± 0.003 | 10.0 | 0.195 ± 0.008 |
| 7.0 | 0.045 ± 0.023 | 8.6 | 0.053 ± 0.004 | 10.2 | 0.228 ± 0.005 |
| 7.2 | 0.065 ± 0.038 | 8.8 | 0.062 ± 0.003 | 10.4 | 0.241 ± 0.005 |
| 7.4 | 0.035 ± 0.009 | 9.0 | 0.079 ± 0.007 | 10.6 | 0.247 ± 0.003 |
| 7.6 | 0.037 ± 0.006 | 9.2 | 0.096 ± 0.007 | 10.8 | 0.284 ± 0.006 |
| 7.8 | 0.042 ± 0.009 | 9.4 | 0.120 ± 0.008 | 11.0 | 0.403 ± 0.011 |
| 8.0 | 0.039 ± 0.002 | 9.6 | 0.158 ± 0.013 | 11.2 | 0.629 ± 0.017 |
| 8.2 | 0.041 ± 0.003 | 9.8 | 0.172 ± 0.003 | | |

[a] These values are the average and standard deviation from two independent data sets of pH jump experiments for data from pH 6.8 to 10.0. Each data set was composed of at least 3 to 5 kinetic traces at each pH. Above pH 10.0, the values are from a single data set composed of 5 kinetic traces at each pH.

**Table A3.** Amplitude average data for fast kinetic phase from upward pH jumps.[a,b]

| pH | Amplitude (absorbance units) | pH | Amplitude (absorbance units) | pH | Amplitude (absorbance units) |
|---|---|---|---|---|---|
| 5.6 | 0.015 ± 0.003 | 7.6 | 0.060 ± 0.003 | 9.6 | 0.035 ± 0.001 |
| 5.8 | 0.021 ± 0.002 | 7.8 | 0.061 ± 0.002 | 9.8 | 0.034 ± 0.002 |
| 6.0 | 0.029 ± 0.005 | 8.0 | 0.062 ± 0.004 | 10.0 | 0.036 ± 0.002 |
| 6.2 | 0.039 ± 0.005 | 8.2 | 0.059 ± 0.001 | 10.2 | 0.038 ± 0.004 |
| 6.4 | 0.045 ± 0.004 | 8.4 | 0.056 ± 0.001 | 10.4 | 0.045 ± 0.003 |
| 6.6 | 0.052 ± 0.004 | 8.6 | 0.053 ± 0.001 | 10.6 | 0.052 ± 0.002 |
| 6.8 | 0.056 ± 0.004 | 8.8 | 0.049 ± 0.001 | 10.8 | 0.055 ± 0.003 |
| 7.0 | 0.057 ± 0.003 | 9.0 | 0.047 ± 0.001 | 11.0 | 0.058 ± 0.003 |
| 7.2 | 0.058 ± 0.004 | 9.2 | 0.042 ± 0.001 | 11.2 | 0.062 ± 0.007 |
| 7.4 | 0.059 ± 0.003 | 9.4 | 0.038 ± 0.001 | | |

[a] Data from pH 5.6 to 8.0 are the average of three data sets, two with data collected on a 5 s time scale and one with data collected on a 50 s timescale. From pH 8.2 to 11.2 the data are the average of two data sets, one with data collected on a 5 s time scale and one with data collected on a 50 s timescale. Each data set was composed of at least 3 to 5 kinetic traces at each pH.

[b] Data collected on a 5 second time were fit to a single exponential equation up to pH 8.4 and with a double exponential equation above that pH. Data collected on a 50 second time were fit to a single exponential equation up to pH 6.6 and with a double exponential equation above that pH.

**Table A4.** Amplitude average data for slow kinetic phase from upward pH jump experiments.[a]

| pH | Amplitude (absorbance units) | pH | Amplitude (absorbance units) | pH | Amplitude (absorbance units) |
|---|---|---|---|---|---|
| 6.8 | 0.0018 ± 0.0005 | 8.4 | 0.032 ± 0.002 | 10.0 | 0.079 ± 0.003 |
| 7.0 | 0.0028 ± 0.0006 | 8.6 | 0.044 ± 0.005 | 10.2 | 0.083 ± 0.002 |
| 7.2 | 0.0033 ± 0.0009 | 8.8 | 0.051 ± 0.001 | 10.4 | 0.084 ± 0.001 |
| 7.4 | 0.0063 ± 0.0008 | 9.0 | 0.060 ± 0.002 | 10.6 | 0.084 ± 0.002 |
| 7.6 | 0.009 ± 0.002 | 9.2 | 0.068 ± 0.002 | 10.8 | 0.086 ± 0.001 |
| 7.8 | 0.012 ± 0.002 | 9.4 | 0.074 ± 0.002 | 11.0 | 0.089 ± 0.001 |
| 8.0 | 0.018 ± 0.002 | 9.6 | 0.079 ± 0.002 | 11.2 | 0.094 ± 0.003 |
| 8.2 | 0.026 ± 0.002 | 9.8 | 0.079 ± 0.002 | | |

[a] These values are the average and standard deviation from two independent data sets collected on a 50 s time scale for data from pH 6.8 to 10.0. Each data set was composed of at least 3 to 5 kinetic traces at each pH. Above pH 10.0, the values are from a single 50 s data set composed of 5 kinetic traces at each pH.

**Table A5.** $k_{obs}$ and amplitude average data for fast kinetic phase from downward pH jump experiments.[a]

| pH | $k_{obs}$, $s^{-1}$ | Amplitude (absorbance units) |
|---|---|---|
| 5.0 | 0.7 ± 0.1 | 0.048 ± 0.006 |
| 5.2 | 0.8 ± 0.1 | 0.041 ± 0.004 |
| 5.4 | 0.9 ± 0.2 | 0.041 ± 0.005 |
| 5.6 | 1.0 ± 0.2 | 0.038 ± 0.003 |
| 5.8 | 1.0 ± 0.2 | 0.034 ± 0.004 |
| 6.0 | 1.3 ± 0.3 | 0.029 ± 0.004 |
| 6.2 | 1.4 ± 0.4 | 0.021 ± 0.003 |
| 6.4 | 1.9 ± 0.6 | 0.016 ± 0.002 |
| 6.6 | 2.1 ± 1.0 | 0.010 ± 0.002 |

[a] Data are the average of three data sets, two with data collected on a 5 s time scale and one with data collected on a 50 s timescale. Each data set was composed of at least 5 kinetic traces at each pH.

**Table A6.** $k_{obs}$ and amplitude average data for slow kinetic phase from downward pH jump experiments.[a]

| pH | $k_{obs}$, $s^{-1}$ | Amplitude (absorbance units) |
|---|---|---|
| 5.0 | 0.039 ± 0.007 | 0.014 ± 0.002 |
| 5.2 | 0.036 ± 0.004 | 0.015 ± 0.002 |
| 5.4 | 0.031 ± 0.003 | 0.015 ± 0.002 |
| 5.6 | 0.033 ± 0.009 | 0.013 ± 0.001 |
| 5.8 | 0.034 ± 0.008 | 0.011 ± 0.002 |
| 6.0 | 0.034 ± 0.003 | 0.011 ± 0.002 |
| 6.2 | 0.03 ± 0.01 | 0.009 ± 0.002 |
| 6.4 | 0.03 ± 0.01 | 0.008 ± 0.003 |
| 6.6 | 0.03 ± 0.01 | 0.009 ± 0.001 |

[a] These values are the average and standard deviation from two independent data sets collected on a 50 s time scale. Each data set was composed of at least 3 to 5 kinetic traces at each pH.

## B. Tables of Rate Constants and Amplitudes for the AcH73 Variant in 0.1 M NaCl and at 25 °C.

**Table B1.** $k_{obs}$ data for the fast kinetic phase from upward pH jumps experiments.[a,b]

| pH | $k_{obs}$, $s^{-1}$ | pH | $k_{obs}$, $s^{-1}$ | pH | $k_{obs}$, $s^{-1}$ |
|---|---|---|---|---|---|
| 5.8 | 36.9 ± 0.8 | 7.8 | 32.5 ± 1.0 | 9.8 | 46.3 ± 3.6 |
| 6.0 | 39.4 ± 2.2 | 8.0 | 33.4 ± 0.7 | 10.0 | 47.7 ± 2.8 |
| 6.2 | 39.0 ± 0.8 | 8.2 | 37.0 ± 1.1 | 10.2 | 49.7 ± 3.2 |
| 6.4 | 38.2 ± 0.7 | 8.4 | 36.1 ± 1.8 | 10.4 | 52.4 ± 5.2 |
| 6.6 | 37.8 ± 2.1 | 8.6 | 36.6 ± 1.5 | 10.6 | 44.4 ± 4.8 |
| 6.8 | 39.4 ± 0.9 | 8.8 | 39.3 ± 1.6 | 10.8 | 37.8 ± 8.9 |
| 7.0 | 33.6 ± 1.6 | 9.0 | 41.7 ± 2.9 | 11.0 | 22.1 ± 7.2 |
| 7.2 | 35.8 ± 0.8 | 9.2 | 42.8 ± 3.7 | 11.2 | 20.0 ± 0.2 |
| 7.4 | 34.4 ± 1.1 | 9.4 | 44.9 ± 3.3 | | |
| 7.6 | 34.6 ± 1.1 | 9.6 | 47.6 ± 4.1 | | |

[a] Data from pH 5.8 to 11.2 are the average of three data sets, two with data collected on a 5 s time scale and one with data collected on a 50 s timescale. Each data set was composed of at least 5 kinetic traces at each pH.

[b] Data collected on a 5 s time scale were fit to a single exponential equation and with a double exponential equation at each pH. Data collected on a 50 second time were fit to a double exponential equation at each pH.

**Table B2.** $k_{obs}$ data for the slow kinetic phase from upward pH jump experiments.[a]

| pH | $k_{obs}$, $s^{-1}$ | pH | $k_{obs}$, $s^{-1}$ | pH | $k_{obs}$, $s^{-1}$ |
|---|---|---|---|---|---|
| 5.8 | 0.045 ± 0.008 | 7.8 | 0.119 ± 0.001 | 9.8 | 0.76 ± 0.01 |
| 6.0 | 0.084 ± 0.008 | 8.0 | 0.124 ± 0.002 | 10.0 | 0.98 ± 0.02 |
| 6.2 | 0.085 ± 0.007 | 8.2 | 0.139 ± 0.008 | 10.2 | 1.31 ± 0.02 |
| 6.4 | 0.099 ± 0.009 | 8.4 | 0.157 ± 0.001 | 10.4 | 2.130 ± 0.003 |
| 6.6 | 0.106 ± 0.004 | 8.6 | 0.182 ± 0.002 | 10.6 | 3.0 ± 0.1 |
| 6.8 | 0.102 ± 0.010 | 8.8 | 0.214 ± 0.001 | 10.8 | 4.5 ± 0.4 |
| 7.0 | 0.101 ± 0.003 | 9.0 | 0.287 ± 0.001 | 11.0 | 5 ± 3 |
| 7.2 | 0.096 ± 0.002 | 9.2 | 0.350 ± 0.008 | 11.2 | 0.21 ± 0.05 |
| 7.4 | 0.098 ± 0.002 | 9.4 | 0.450 ± 0.006 | | |
| 7.6 | 0.107 ± 0.004 | 9.6 | 0.586 ± 0.007 | | |

[a] These values are the average and standard deviation from a single data set of pH jump experiments. Each data set was composed of at least 5 kinetic traces at each pH.

**Table B3.** Amplitude data for the fast kinetic phase from upward pH jump experiments. [a,b]

| pH | Amplitude (absorbance units) | pH | Amplitude (absorbance units) | pH | Amplitude (absorbance units) |
|---|---|---|---|---|---|
| 5.8 | 0.029 ± 0.006 | 7.8 | 0.084 ± 0.004 | 9.8 | 0.086 ± 0.003 |
| 6.0 | 0.041 ± 0.001 | 8.0 | 0.083 ± 0.001 | 10.0 | 0.084 ± 0.003 |
| 6.2 | 0.0470 ± 0.0004 | 8.2 | 0.083 ± 0.004 | 10.2 | 0.080 ± 0.003 |
| 6.4 | 0.043 ± 0.003 | 8.4 | 0.088 ± 0.004 | 10.4 | 0.073 ± 0.005 |
| 6.6 | 0.055 ± 0.005 | 8.6 | 0.086 ± 0.001 | 10.6 | 0.064 ± 0.009 |
| 6.8 | 0.055 ± 0.003 | 8.8 | 0.089 ± 0.002 | 10.8 | 0.061 ± 0.014 |
| 7.0 | 0.074 ± 0.004 | 9.0 | 0.088 ± 0.002 | 11.0 | 0.081 ± 0.018 |
| 7.2 | 0.071 ± 0.005 | 9.2 | 0.090 ± 0.004 | 11.2 | 0.105 ± 0.001 |
| 7.4 | 0.075 ± 0.001 | 9.4 | 0.093 ± 0.001 | | |
| 7.6 | 0.074 ± 0.006 | 9.6 | 0.089 ± 0.004 | | |

[a] Data from pH 5.8 to 11.2 are the average of three data sets, two with data collected on a 5 s time scale and one with data collected on a 50 s timescale. Each data set was composed of at least 5 kinetic traces at each pH.

[b] Data collected on a 5 s time scale were fit to a single exponential equation and with a double exponential equation at each pH. Data collected on a 50 second time were fit to a a double exponential equation at each pH.

**Table B4.** Amplitude data for the slow kinetic phase from upward pH jump experiments.[a]

| pH | Amplitude (absorbance units) | pH | Amplitude (absorbance units) | pH | Amplitude (absorbance units) |
|---|---|---|---|---|---|
| 5.8 | 0.0047 ± 0.0005 | 7.8 | 0.0195 ± 0.0003 | 9.8 | 0.0744 ± 0.0005 |
| 6.0 | 0.0064 ± 0.0002 | 8.0 | 0.0248 ± 0.0002 | 10.0 | 0.0741 ± 0.0004 |
| 6.2 | 0.0076 ± 0.0003 | 8.2 | 0.0305 ± 0.0002 | 10.2 | 0.0722 ± 0.0007 |
| 6.4 | 0.0073 ± 0.0003 | 8.4 | 0.0391 ± 0.0007 | 10.4 | 0.0695 ± 0.001 |
| 6.6 | 0.0075 ± 0.0007 | 8.6 | 0.0461 ± 0.0005 | 10.6 | 0.0664 ± 0.001 |
| 6.8 | 0.0086 ± 0.0008 | 8.8 | 0.0526 ± 0.0002 | 10.8 | 0.0602 ± 0.007 |
| 7.0 | 0.0114 ± 0.0003 | 9.0 | 0.0620 ± 0.0002 | 11.0 | 0.0340 ± 0.025 |
| 7.2 | 0.0130 ± 0.0003 | 9.2 | 0.067 ± 0.001 | 11.2 | 0.0038 ± 0.0006 |
| 7.4 | 0.0147 ± 0.0003 | 9.4 | 0.0707 ± 0.0005 | | |
| 7.6 | 0.0171 ± 0.0001 | 9.6 | 0.0729 ± 0.0007 | | |

[a] These values are the average and standard deviation from a single data set of pH jump experiments. Each data set was composed of at least 5 kinetic traces at each pH.

**Table B5.** $k_{obs}$ and amplitude data for the fast kinetic phase from downward pH jump experiments.[a]

| pH | $k_{obs}$, $s^{-1}$ | Amplitude (absorbance units) |
|---|---|---|
| 5.0 | 33.0 ± 1.5 | 0.067 ± 0.009 |
| 5.2 | 35.1 ± 1.1 | 0.060 ± 0.001 |
| 5.4 | 35.6 ± 0.3 | 0.056 ± 0.001 |
| 5.6 | 35.3 ± 1.6 | 0.051 ± 0.001 |
| 5.8 | 35.4 ± 4.3 | 0.040 ± 0.002 |
| 6.0 | 33.9 ± 1.3 | 0.035 ± 0.005 |
| 6.2 | 36.0 ± 1.6 | 0.027 ± 0.001 |
| 6.4 | 35.0 ± 1.0 | 0.019 ± 0.001 |

[a] Data are the average of three data sets, two with data collected on a 5 s time scale and one with data collected on a 50 s timescale. Each data set was composed of at least 5 kinetic traces at each pH.

**Table B6.** $k_{obs}$ and amplitude data for the slow kinetic phase from downward pH jump experiments.[a]

| pH | $k_{obs}$, $s^{-1}$ | Amplitude (absorbance units) |
|---|---|---|
| 5.0 | 0.113 ± 0.002 | 0.0270 ± 0.0004 |
| 5.2 | 0.115 ± 0.001 | 0.0260 ± 0.0003 |
| 5.4 | 0.112 ± 0.001 | 0.0240 ± 0.0006 |
| 5.6 | 0.115 ± 0.002 | 0.0210 ± 0.0003 |
| 5.8 | 0.116 ± 0.003 | 0.0180 ± 0.0005 |
| 6.0 | 0.107 ± 0.013 | 0.0130 ± 0.0007 |
| 6.2 | 0.106 ± 0.015 | 0.0110 ± 0.0003 |
| 6.4 | 0.103 ± 0.021 | 0.0007 ± 0.0007 |

[a] These values are the average and standard deviation from a single data set of pH jump experiments. Each data set was composed of at least 5 kinetic traces at each pH.

**Table B7.** Fast rate constant, $k_1$, and its amplitude for the reduction of AcH73 iso-1-cytochrome *c* by $a_6Ru^{2+}$ as a function of pH and [$a_6Ru^{2+}$] from four exponential fits to the data in figure 3.11.

| pH | [$a_6Ru^{2+}$], mM | $k_{obs}$, $s^{-1}$ | Amplitude |
|---|---|---|---|
| **5.0** | 0.5 ± 0.1 | 60 ± 3 | 0.015 ± 0.002 |
| | 1.2 ± 0.1 | 102 ± 2 | 0.030 ± 0.001 |
| | 1.5 ± 0.1 | 132 ± 5 | 0.0312 ± 0.0010 |
| | 3.6 ± 0.4 | 271 ± 22 | 0.0286 ± 0.0004 |
| | 9.0 ± 0.4 | 619 ± 50 | 0.0225 ± 0.0010 |
| | 20.4 ± 0.8 | 1215 ± 346 | 0.0148 ± 0.0050 |
| **5.5** | 0.7 ± 0.1 | 63.4 ± 4 | 0.0130 ± 0.0008 |
| | 1.1 ± 0.1 | 102 ± 2 | 0.0233 ± 0.0007 |
| | 2.1 ± 0.1 | 175 ± 3 | 0.0262 ± 0.0002 |
| | 4.2 ± 0.2 | 298 ± 11 | 0.0251 ± 0.0006 |
| | 8.7 ± 0.3 | 587 ± 42 | 0.0221 ± 0.0010 |
| | 17.5 ± 0.7 | 1280 ± 152 | 0.0182 ± 0.0030 |
| **6.0** | 0.6 ± 0.1 | 69 ± 4 | 0.0107 ± 0.0007 |
| | 1.1 ± 0.1 | 99 ± 7 | 0.0174 ± 0.0009 |
| | 2.5 ± 0.1 | 192 ± 12 | 0.0235 ± 0.0040 |
| | 5.3 ± 0.1 | 357 ± 20 | 0.0195 ± 0.0003 |
| | 8.3 ± 0.3 | 568 ± 41 | 0.0177 ± 0.0010 |
| | 18.4 ± 0.4 | 1284 ± 390 | 0.0154 ± 0.0080 |
| **6.5** | 0.52 ± 0.02 | 69 ± 2 | 0.0114 ± 0.0003 |
| | 1.02 ± 0.03 | 99 ± 2 | 0.0162 ± 0.0002 |
| | 2.0 ± 0.1 | 168 ± 6 | 0.0188 ± 0.0003 |
| | 4.4 ± 0.2 | 299 ± 12 | 0.0181 ± 0.0005 |
| | 9.1 ± 0.3 | 592 ± 52 | 0.0155 ± 0.0010 |
| | 19.1 ± 0.9 | 1037 ± 273 | 0.0107 ± 0.0030 |
| **7.0** | 0.54 ± 0.02 | 69 ± 6 | 0.0870 ± 0.0002 |
| | 1.30 ± 0.04 | 113 ± 3 | 0.0127 ± 0.0002 |
| | 2.4 ± 0.2 | 206 ± 9 | 0.0145 ± 0.0004 |
| | 5.4 ± 0.4 | 382 ± 24 | 0.0132 ± 0.0004 |
| | 10.4 ± 0.3 | 742 ± 35 | 0.0123 ± 0.0010 |
| | 19.8 ± 0.6 | 1497 ± 428 | 0.0101 ± 0.0050 |
| **7.5** | 0.37 ± 0.04 | 34 ± 11 | 0.0038 ± 0.0008 |
| | 0.77 ± 0.06 | 68 ± 8 | 0.0069 ± 0.0008 |
| | 1.62 ± 0.04 | 125 ± 8 | 0.0161 ± 0.0100 |
| | 2.8 ± 0.2 | 201 ± 3 | 0.0116 ± 0.0002 |
| | 5.4 ± 0.1 | 339 ± 25 | 0.0119 ± 0.0003 |
| | 9.6 ± 0.3 | 509 ± 77 | 0.0100 ± 0.0007 |
| | 27 ± 1 | 1765 ± 137 | 0.0058 ± 0.0010 |

| | | | |
|---|---|---|---|
| **8.0** | 0.61 ± 0.04 | 67 ± 9 | 0.0040 ± 0.0002 |
| | 1.17 ± 0.03 | 106 ± 5 | 0.006 ± 0.001 |
| | 2.3 ± 0.1 | 175 ± 14 | 0.007 ± 0.001 |
| | 5.0 ± 0.1 | 312 ± 88 | 0.007 ± 0.001 |
| | 9.9 ± 0.3 | 521 ± 184 | 0.006 ± 0.001 |
| | 20.9 ± 0.6 | 1175 ± 480 | 0.002 ± 0.002 |
| **8.5** | 0.57 ± 0.03 | 61 ± 5 | 0.0037 ± 0.0002 |
| | 0.92 ± 0.11 | 96 ± 10 | 0.0052 ± 0.0002 |
| | 1.6 ± 0.1 | 126 ± 8 | 0.0057 ± 0.0004 |
| | 4.0 ± 0.1 | 259 ± 27 | 0.0058 ± 0.0002 |
| | 8.4 ± 0.3 | 489 ± 86 | 0.005 ± 0.001 |
| | 18.2 ± 0.5 | 1555 ± 127[a] | 0.007 ± 0.010 [a] |
| **9.0** | 0.53 ± 0.03 | 71 ± 13 | 0.0020 ± 0.0002 |
| | 1.07 ± 0.03 | 80 ± 13 | 0.0029 ± 0.0001 |
| | 2.4 ± 0.1 | 189 ± 26 | 0.0033 ± 0.0001 |
| | 5.1 ± 0.1 | 277 ± 64 | 0.0031 ± 0.0003 |
| | 10.0 ± 0.3 | 500 ± 6 | 0.003 ± 0.002 |
| | 20.5 ± 0.5 | 1511 ± 555[a] | 0.0012 ± 0.0007 [a] |

[a] This rate constant value is taken from one trial of experiment as values from the other trials showed variation due to very less amplitude at highest concentration of $a_6Ru^{2+}$.

**Table B8.** First intermediate rate constant, $k_2$, and its amplitude for the reduction of AcH73 iso-1-cytochrome *c* by $a_6Ru^{2+}$ as a function of pH and $[a_6Ru^{2+}]$ from four exponential fits to the data in figure 3.11.

| pH | $[a_6Ru^{2+}]$, mM | $k_{obs}$, $s^{-1}$ | Amplitude |
|---|---|---|---|
| **5.0** | 0.5 ± 0.1 | 21.0 ± 0.3 | 0.0456 ± 0.0020 |
| | 1.2 ± 0.1 | 26 ± 1 | 0.0265 ± 0.0010 |
| | 1.5 ± 0.1 | 26 ± 1 | 0.0234 ± 0.0010 |
| | 3.6 ± 0.4 | 28 ± 2 | 0.0193 ± 0.0010 |
| | 9.0 ± 0.4 | 31 ± 1 | 0.0173 ± 0.0004 |
| | 20.4 ± 0.8 | 27 ± 1 | 0.0166 ± 0.0004 |
| **5.5** | 0.7 ± 0.1 | 18 ± 0.2 | 0.0454 ± 0.0009 |
| | 1.1 ± 0.1 | 23.0 ± 0.5 | 0.0333 ± 0.0008 |
| | 2.1 ± 0.1 | 23.0 ± 0.5 | 0.0268 ± 0.0003 |
| | 4.2 ± 0.2 | 25.4 ± 0.2 | 0.0237 ± 0.0006 |
| | 8.7 ± 0.3 | 24 ± 1 | 0.0227 ± 0.0004 |
| | 17.5 ± 0.7 | 12 ± 1 | 0.0199 ± 0.001 |
| **6.0** | 0.6 ± 0.1 | 15 ± 0.4 | 0.0431 ± 0.0006 |
| | 1.1 ± 0.1 | 19 ± 1 | 0.0348 ± 0.0010 |
| | 2.5 ± 0.1 | 21 ± 1 | 0.0277 ± 0.0007 |
| | 5.3 ± 0.1 | 22.0 ± 0.4 | 0.0245 ± 0.0005 |
| | 8.3 ± 0.3 | 21 ± 1 | 0.0243 ± 0.0006 |
| | 18.4 ± 0.4 | 22.0 ± 0.3 | 0.0234 ± 0.0005 |
| **6.5** | 0.52 ± 0.02 | 12.0 ± 0.1 | 0.0444 ± 0.0010 |
| | 1.02 ± 0.03 | 14.0 ± 0.2 | 0.0386 ± 0.0005 |
| | 2.0 ± 0.1 | 16.0 ± 0.4 | 0.0333 ± 0.0002 |
| | 4.4 ± 0.2 | 17.4 ± 0.1 | 0.0302 ± 0.0006 |
| | 9.1 ± 0.3 | 18.2 ± 0.2 | 0.0288 ± 0.0004 |
| | 19.1 ± 0.9 | 15.0 ± 0.4 | 0.0286 ± 0.0005 |
| **7.0** | 0.54 ± 0.02 | 9.5 ± 0.1 | 0.0467 ± 0.0009 |
| | 1.30 ± 0.04 | 12.1 ± 0.1 | 0.0412 ± 0.0003 |
| | 2.4 ± 0.2 | 14.0 ± 0.3 | 0.0368 ± 0.0004 |
| | 5.4 ± 0.4 | 14.5 ± 0.3 | 0.0354 ± 0.0007 |
| | 10.4 ± 0.3 | 15 ± 1 | 0.0356 ± 0.0010 |
| | 19.8 ± 0.6 | 15.0 ± 1.3 | 0.0378 ± 0.0020 |
| **7.5** | 0.37 ± 0.04 | 5.6 ± 0.4 | 0.0420 ± 0.0050 |
| | 0.77 ± 0.06 | 8.6 ± 0.5 | 0.0410 ± 0.0010 |
| | 1.62 ± 0.04 | 11.0± 0.4 | 0.0375 ± 0.0003 |
| | 2.8 ± 0.2 | 12.0 ± 0.1 | 0.0352 ± 0.0003 |
| | 5.4 ± 0.1 | 13.0 ± 0.6 | 0.0341 ± 0.0010 |
| | 9.6 ± 0.3 | 13.1 ± 0.6 | 0.0337 ± 0.0010 |
| | 27 ± 1 | 14.1 ± 0.7 | 0.0343 ± 0.0020 |

| | | | |
|---|---|---|---|
| **8.0** | 0.61 ± 0.04 | 7.4 ± 0.1 | 0.0324 ± 0.0006 |
| | 1.17 ± 0.03 | 9.0 ± 0.3 | 0.0298 ± 0.0004 |
| | 2.3 ± 0.1 | 11.0 ± 0.6 | 0.0276 ± 0.0002 |
| | 5.0 ± 0.1 | 11.7 ± 0.5 | 0.0269 ± 0.0003 |
| | 9.9 ± 0.3 | 12.4 ± 0.6 | 0.0268 ± 0.0005 |
| | 20.9 ± 0.6 | 13.0 ± 0.5 | 0.0269 ± 0.0010 |
| **8.5** | 0.57 ± 0.03 | 7.0 ± 0.1 | 0.0294 ± 0.0003 |
| | 0.92 ± 0.11 | 9.9 ± 0.2 | 0.0269 ± 0.0005 |
| | 1.6 ± 0.1 | 10.0 ± 0.2 | 0.0255 ± 0.0002 |
| | 4.0 ± 0.1 | 11.0 ± 0.3 | 0.0241 ± 0.0003 |
| | 8.4 ± 0.3 | 12.0 ± 0.2 | 0.0233 ± 0.0003 |
| | 18.2 ± 0.5 | 12.0 ± 0.5 | 0.0215 ± 0.0005 |
| **9.0** | 0.53 ± 0.03 | 5.9 ± 0.1 | 0.0189 ± 0.0003 |
| | 1.07 ± 0.03 | 7.5 ± 0.1 | 0.0172 ± 0.0001 |
| | 2.4 ± 0.1 | 9.5 ± 0.2 | 0.0175 ± 0.0004 |
| | 5.1 ± 0.1 | 10.6 ± 0.4 | 0.0163 ± 0.0003 |
| | 10.0 ± 0.3 | 11.2 ± 1.2 | 0.0165 ± 0.0020 |
| | 20.5 ± 0.5 | 11.8 ± 0.3 | 0.0192 ± 0.0007 |

**Table B9**. Second intermediate rate constant, $k_3$, and its amplitude for the reduction of AcH73 iso-1-cytochrome *c* by $a_6Ru^{2+}$ as a function of pH and [$a_6Ru^{2+}$] from four exponential fits to the data in figure 3.11.

| pH | [$a_6Ru^{2+}$], mM | $k_{obs}$, $s^{-1}$ | Amplitude |
|---|---|---|---|
| **5.0** | 0.5 ± 0.1 | 1.5 ± 0.1 | 0.0027 ± 0.0001 |
| | 1.2 ± 0.1 | 1.8 ± 0.1 | 0.0032 ± 0.0001 |
| | 1.5 ± 0.1 | 2.7 ± 0.4 | 0.0020 ± 0.0002 |
| | 3.6 ± 0.4 | 3.2 ± 0.5 | 0.0022 ± 0.0003 |
| | 9.0 ± 0.4 | 2.6 ± 0.3 | 0.0040 ± 0.0003 |
| | 20.4 ± 0.8 | 2.8 ± 0.5 | 0.0029 ± 0.0006 |
| **5.5** | 0.7 ± 0.1 | 1.4 ± 0.1 | 0.0030 ± 0.0002 |
| | 1.1 ± 0.1 | 1.6 ± 0.1 | 0.0038 ± 0.0002 |
| | 2.1 ± 0.1 | 2.5 ± 0.2 | 0.0028 ± 0.0002 |
| | 4.2 ± 0.2 | 2.4 ± 0.05 | 0.0043 ± 0.0003 |
| | 8.7 ± 0.3 | 3.0 ± 0.3 | 0.0037 ± 0.0001 |
| | 17.5 ± 0.7 | 3.5 ± 0.8 | 0.0042 ± 0.0020 |
| **6.0** | 0.6 ± 0.1 | 2.0 ± 0.2 | 0.0026 ± 0.0003 |
| | 1.1 ± 0.1 | 2.1 ± 0.2 | 0.0029 ± 0.0003 |
| | 2.5 ± 0.1 | 2.8 ± 0.2 | 0.0029 ± 0.0003 |
| | 5.3 ± 0.1 | 2.6 ± 0.1 | 0.0039 ± 0.0001 |
| | 8.3 ± 0.3 | 3.4 ± 0.2 | 0.0027 ± 0.0004 |
| | 18.4 ± 0.4 | 2.2 ± 0.1 | 0.0044 ± 0.0002 |
| **6.5** | 0.52 ± 0.02 | 1.5 ± 0.1 | 0.0026 ± 0.0002 |
| | 1.02 ± 0.03 | 1.9 ± 0.2 | 0.0023 ± 0.0004 |
| | 2.0 ± 0.1 | 2.4 ± 0.3 | 0.0029 ± 0.0004 |
| | 4.4 ± 0.2 | 2.4 ± 0.2 | 0.0041 ± 0.0002 |
| | 9.1 ± 0.3 | 2.2 ± 0.1 | 0.0047 ± 0.0002 |
| | 19.1 ± 0.9 | 2.6 ± 0.9 | 0.0015 ± 0.0004 |
| **7.0** | 0.54 ± 0.02 | 1.8 ± 0.3 | 0.0031 ± 0.0004 |
| | 1.30 ± 0.04 | 2.3 ± 0.2 | 0.0036 ± 0.0002 |
| | 2.4 ± 0.2 | 2.6 ± 0.2 | 0.0039 ± 0.0004 |
| | 5.4 ± 0.4 | 2.5 ± 0.3 | 0.0037 ± 0.0004 |
| | 10.4 ± 0.3 | 2.4 ± 0.7 | 0.0034 ± 0.0010 |
| | 19.8 ± 0.6 | 2.8 ± 1.0 | 0.0016 ± 0.0002 |
| **7.5** | 0.37 ± 0.04 | 2.1 ± 1.5 | 0.0046 ± 0.0030 |
| | 0.77 ± 0.06 | 1.8 ± 1.3 | 0.0027 ± 0.0020 |
| | 1.62 ± 0.04 | 1.5 ± 1.1 | 0.0019 ± 0.0005 |
| | 2.8 ± 0.2 | 2.1 ± 0.3 | 0.0018 ± 0.0002 |
| | 5.4 ± 0.1 | 1.9 ± 1.4 | 0.0020 ± 0.0008 |
| | 9.6 ± 0.3 | 2.3 ± 2.6 | 0.0020 ± 0.0010 |
| | 27 ± 1 | 3.7 ± 1.5 | 0.0016 ± 0.0008 |

| | | | |
|---|---|---|---|
| **8.0** | 0.61 ± 0.04 | 0.46 ± 0.1 | 0.0020 ± 0.0003 |
| | 1.17 ± 0.03 | 0.74 ± 0.4 | 0.0020 ± 0.0001 |
| | 2.3 ± 0.1 | 1.3 ± 1.0 | 0.0030 ± 0.0003 |
| | 5.0 ± 0.1 | 0.7 ± 0.2 | 0.0020 ± 0.0004 |
| | 9.9 ± 0.3 | 0.6 ± 0.4 | 0.0040 ± 0.0007 |
| | 20.9 ± 0.6 | 0.6 ± 0.1 | 0.0070 ± 0.0005 |
| **8.5** | 0.57 ± 0.03 | 0.40 ± 0.02 | 0.0029 ± 0.0001 |
| | 0.92 ± 0.11 | 0.4 ± 0.1 | 0.0032 ± 0.0005 |
| | 1.6 ± 0.1 | 0.34 ± 0.05 | 0.0025 ± 0.0007 |
| | 4.0 ± 0.1 | 0.4 ± 0.1 | 0.0030 ± 0.0006 |
| | 8.4 ± 0.3 | 0.35 ± 0.05 | 0.0034 ± 0.0005 |
| | 18.2 ± 0.5 | 0.5 ± 0.2 | 0.0034 ± 0.0004 |
| **9.0** | 0.53 ± 0.03 | 0.30 ± 0.01 | 0.0066 ± 0.0003 |
| | 1.07 ± 0.03 | 0.30 ± 0.03 | 0.0057 ± 0.0010 |
| | 2.4 ± 0.1 | 0.50 ± 0.04 | 0.0054 ± 0.0004 |
| | 5.1 ± 0.1 | 0.5 ± 0.1 | 0.0055 ± 0.0007 |
| | 10.0 ± 0.3 | 0.4 ± 0.1 | 0.0069 ± 0.0030 |
| | 20.5 ± 0.5 | 0.4 ± 0.1 | 0.0098 ± 0.0020 |

**Table B10**. Slow rate constant, $k_4$, and its amplitude for the reduction of AcH73 iso-1-cytochrome *c* by $a_6Ru^{2+}$ as a function of pH and $[a_6Ru^{2+}]$ from four exponential fits to the data in figure 3.11.

| pH | $[a_6Ru^{2+}]$, mM | $k_{obs}$, $s^{-1}$ | Amplitude |
|---|---|---|---|
| **5.0** | 0.5 ± 0.1 | 0.045 ± 0.001 | 0.0054 ± 0.0001 |
| | 1.2 ± 0.1 | 0.038 ± 0.002 | 0.0050 ± 0.0001 |
| | 1.5 ± 0.1 | 0.057 ± 0.001 | 0.0053 ± 0.0001 |
| | 3.6 ± 0.4 | 0.062 ± 0.002 | 0.0052 ± 0.0003 |
| | 9.0 ± 0.4 | 0.062 ± 0.004 | 0.0036 ± 0.0002 |
| | 20.4 ± 0.8 | 0.067 ± 0.004 | 0.0043 ± 0.0005 |
| **5.5** | 0.7 ± 0.1 | 0.054 ± 0.002 | 0.0069 ± 0.0001 |
| | 1.1 ± 0.1 | 0.045 ± 0.001 | 0.0064 ± 0.0003 |
| | 2.1 ± 0.1 | 0.061 ± 0.001 | 0.0072 ± 0.0001 |
| | 4.2 ± 0.2 | 0.053 ± 0.001 | 0.0064 ± 0.0002 |
| | 8.7 ± 0.3 | 0.064 ± 0.001 | 0.0068 ± 0.0003 |
| | 17.5 ± 0.7 | 0.058 ± 0.003 | 0.0099 ± 0.0004 |
| **6.0** | 0.6 ± 0.1 | 0.062 ± 0.001 | 0.0082 ± 0.0001 |
| | 1.1 ± 0.1 | 0.059 ± 0.003 | 0.0079 ± 0.0001 |
| | 2.5 ± 0.1 | 0.058 ± 0.001 | 0.0076 ± 0.0001 |
| | 5.3 ± 0.1 | 0.054 ± 0.001 | 0.0067 ± 0.0001 |
| | 8.3 ± 0.3 | 0.069 ± 0.002 | 0.0070 ± 0.0002 |
| | 18.4 ± 0.4 | 0.066 ± 0.005 | 0.0053 ± 0.0005 |
| **6.5** | 0.52 ± 0.02 | 0.066 ± 0.001 | 0.0110 ± 0.0001 |
| | 1.02 ± 0.03 | 0.067 ± 0.001 | 0.0110 ± 0.0001 |
| | 2.0 ± 0.1 | 0.066 ± 0.001 | 0.0110 ± 0.0001 |
| | 4.4 ± 0.2 | 0.061 ± 0.001 | 0.0095 ± 0.0001 |
| | 9.1 ± 0.3 | 0.063 ± 0.001 | 0.0085 ± 0.0002 |
| | 19.1 ± 0.9 | 0.076 ± 0.001 | 0.0095 ± 0.0002 |
| **7.0** | 0.54 ± 0.02 | 0.068 ± 0.002 | 0.0150 ± 0.0001 |
| | 1.30 ± 0.04 | 0.066 ± 0.001 | 0.0150 ± 0.0001 |
| | 2.4 ± 0.2 | 0.0630 ± 0.0002 | 0.0150 ± 0.0002 |
| | 5.4 ± 0.4 | 0.059 ± 0.001 | 0.0160 ± 0.0002 |
| | 10.4 ± 0.3 | 0.057 ± 0.002 | 0.0180 ± 0.0003 |
| | 19.8 ± 0.6 | 0.039 ± 0.006 | 0.018 ± 0.003 |
| **7.5** | 0.37 ± 0.04 | 0.071 ± 0.004 | 0.0165 ± 0.0008 |
| | 0.77 ± 0.06 | 0.073 ± 0.002 | 0.0169 ± 0.0002 |
| | 1.62 ± 0.04 | 0.071 ± 0.003 | 0.0167 ± 0.0003 |
| | 2.8 ± 0.2 | 0.072 ± 0.0006 | 0.0166 ± 0.0007 |
| | 5.4 ± 0.1 | 0.069 ± 0.003 | 0.0164 ± 0.0007 |
| | 9.6 ± 0.3 | 0.065 ± 0.003 | 0.0167 ± 0.0003 |
| | 27 ± 1 | 0.068 ± 0.007 | 0.0132 ± 0.0008 |

| | | | |
|---|---|---|---|
| **8.0** | 0.61 ± 0.04 | 0.0730 ± 0.0004 | 0.0289 ± 0.0004 |
| | 1.17 ± 0.03 | 0.078 ± 0.003 | 0.0282 ± 0.0010 |
| | 2.3 ± 0.1 | 0.076 ± 0.001 | 0.0283 ± 0.0006 |
| | 5.0 ± 0.1 | 0.081 ± 0.002 | 0.0284 ± 0.0004 |
| | 9.9 ± 0.3 | 0.079 ± 0.001 | 0.0275 ± 0.0010 |
| | 20.9 ± 0.6 | 0.086 ± 0.005 | 0.0277 ± 0.0004 |
| **8.5** | 0.57 ± 0.03 | 0.074 ± 0.001 | 0.0286 ± 0.0003 |
| | 0.92 ± 0.11 | 0.074 ± 0.002 | 0.0275 ± 0.0008 |
| | 1.6 ± 0.1 | 0.077 ± 0.004 | 0.0276 ± 0.0007 |
| | 4.0 ± 0.1 | 0077 ± 0.002 | 0.0267 ± 0.0006 |
| | 8.4 ± 0.3 | 0.078 ± 0.002 | 0.0261 ± 0.0006 |
| | 18.2 ± 0.5 | 0.088 ± 0.002 | 0.0238 ± 0.0007 |
| **9.0** | 0.53 ± 0.03 | 0.0760 ± 0.0003 | 0.038 ± 0.001 |
| | 1.07 ± 0.03 | 0.077 ± 0.001 | 0.037 ± 0.001 |
| | 2.4 ± 0.1 | 0.086 ± 0.001 | 0.0380 ± 0.0001 |
| | 5.1 ± 0.1 | 0.093 ± 0.003 | 0.036 ± 0.001 |
| | 10.0 ± 0.3 | 0.092 ± 0.006 | 0.035 ± 0.002 |
| | 20.5 ± 0.5 | 0.10 ± 0.01 | 0.033 ± 0.002 |

**Table B11**. Forward and backward conformational rate constants for AcH73 iso-1-cytochrome *c*.

| pH | $k_{HM3}$, ($s^{-1}$) | $k_{MH3}$, ($s^{-1}$) |
|---|---|---|
| 5.0 | 29 ± 1 | 11.8 ± 3.4 |
| 5.5 | 25.5 ± 1.3 | 13.7 ± 5.5 |
| 6.0 | 22.9 ± 0.5 | 17.4 ± 2.5 |
| 6.5 | 19.0 ± 0.2 | 20.5 ± 1.1 |
| 7.0 | 15.2 ± 0.2 | 21.6 ± 1.8 |
| 7.5 | 14.1 ± 0.2 | 27.7 ± 1.5 |
| 8.0 | 13.0 ± 0.1 | 22.5 ± 1.3 |
| 8.5 | 12.5 ± 0.1 | 23.1 ± 1.3 |
| 9.0 | 12.0 ± 0.2 | 26.9 ± 1.8 |

**Figure B1** Plots of absorbance at 550 nm as a function of time at 5 mM $a_6Ru^{2+}$ are shown along with the residuals of fits to the data from pH 5 to 9. Time is shown logarithmically. The red line in each graph and the residuals represent the triple exponential fit while the green line and residuals represent the quadruple exponential fit.

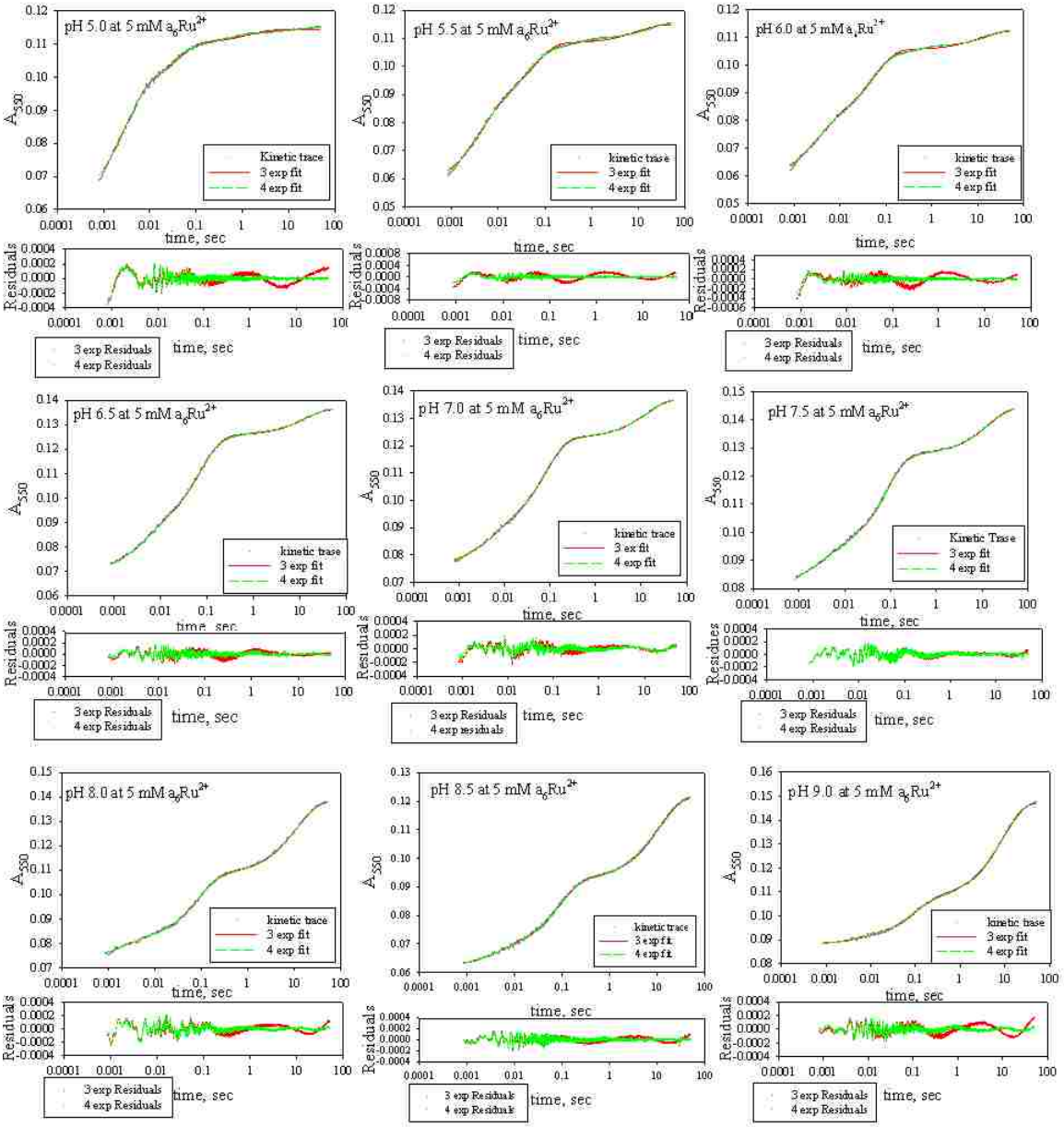

**Figure B2** NMR spectra of the AcH73 variant at 500 MHz in 0.1 M NaCl, $D_2O$ solution at 25 ºC as a function of pH.

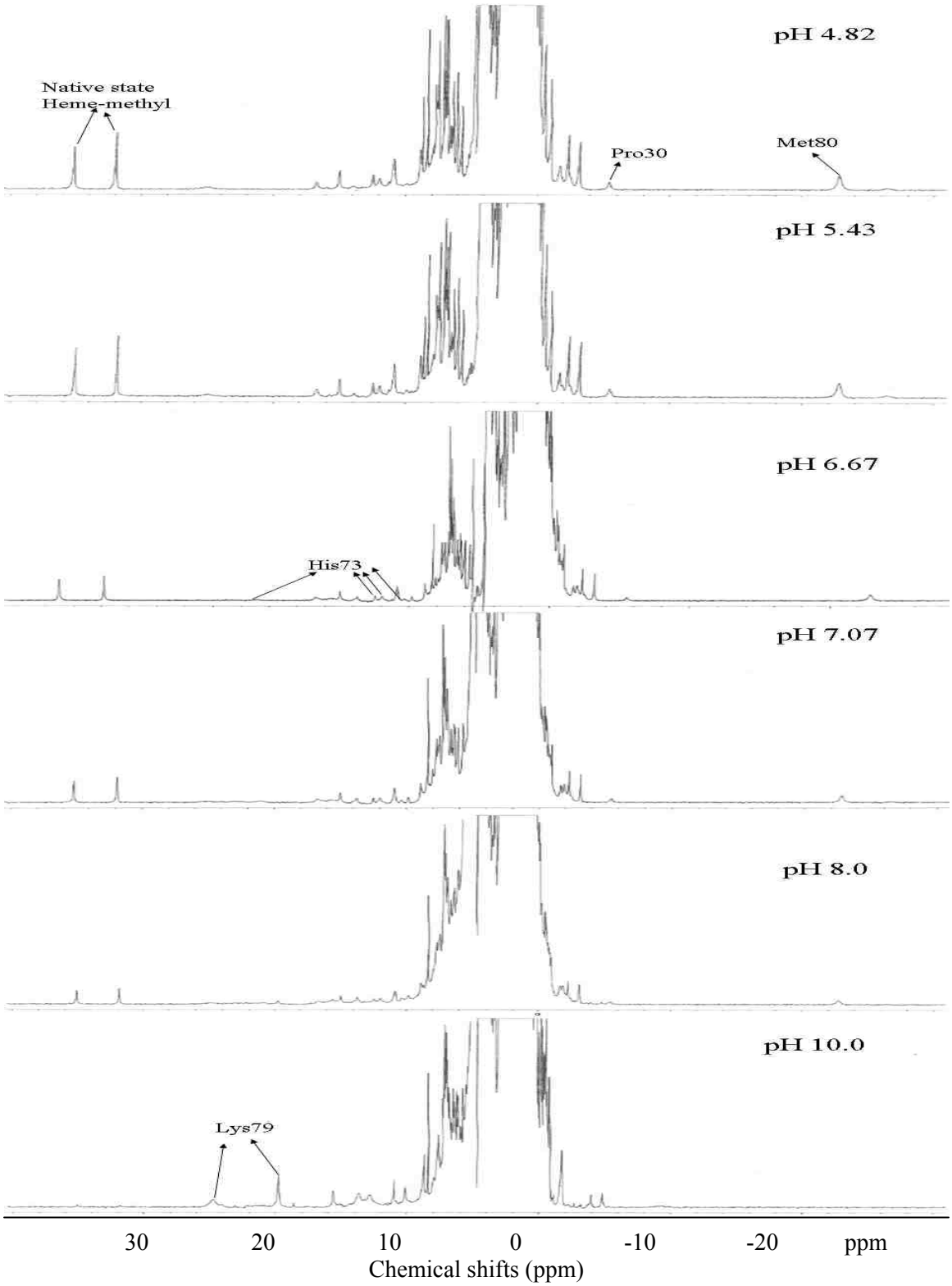

**Figure B3** NMR spectra of the AcH73 variant at 600 MHz in 0.1 M NaCl, $D_2O$ solution at 25 ºC as a function of pH.

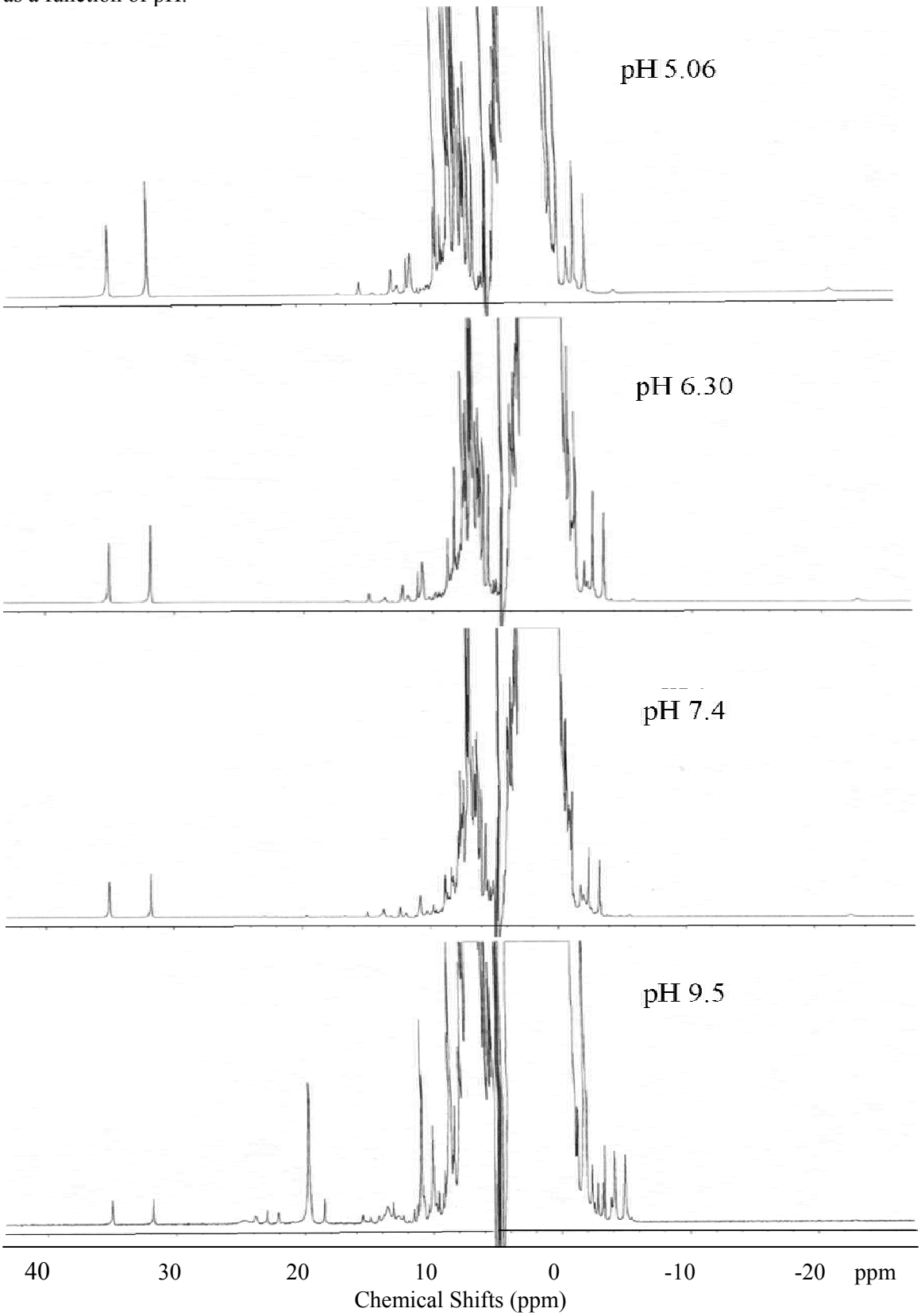

**Figure B4** NMR spectra of the AcH73 variant at 600 MHz showing the upfield region from -1.2 to -24 ppm. Spectra were obtained at 25 ºC in 0.1 M NaCl, $D_2O$ solution.

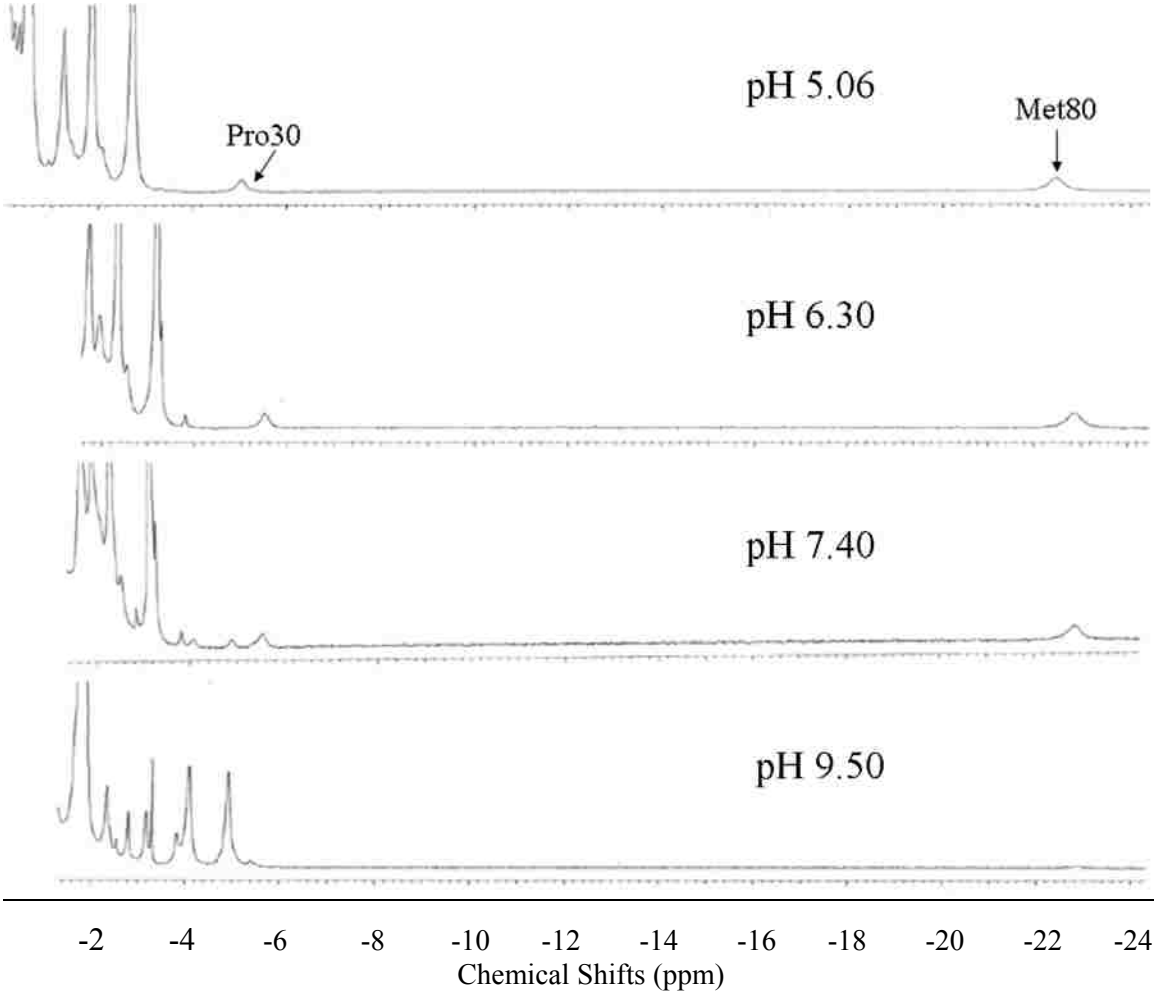

## C. Tables of Rate Constants and Amplitudes for the A79H73 Variant in 0.1 M NaCl and at 25 °C.

**Table C1**. Fast rate constant, $k_1$, and its amplitude for the reduction of A79H73 iso-1-cytochrome *c* by $a_6Ru^{2+}$ as a function of pH and [$a_6Ru^{2+}$] from four exponential fits to the data in figure 4.4.

| pH | [$a_6Ru^{2+}$] mM | $k_{obs}$, $s^{-1}$ | Amplitude |
|---|---|---|---|
| 5.5 | 1.5 ± 0.1 | 438 ± 15 | 0.0298 ± 0.0010 |
| | 2.2 ± 0.2 | 767 ± 73 | 0.0244 ± 0.0020 |
| | 4.7 ± 0.2 | 1263 ± 287 | 0.0108 ± 0.0050 |
| 6.0 | 1.1 ± 0.1 | 358 ± 16 | 0.0254 ± 0.0010 |
| | 2.2 ± 0.1 | 755 ± 65 | 0.0191 ± 0.0020 |
| | 4.7 ± 0.2 | 1254 ± 184 | 0.0082 ± 0.002 0 |
| 6.5 | 1.1 ± 0.1 | 359 ± 16 | 0.0202 ± 0.0002 |
| | 2.4 ± 0.1 | 775 ± 99 | 0.0159 ± 0.0020 |
| | 4.5 ± 0.3 | 1103 ± 97 | 0.0060 ± 0.0006 |
| 7.0 | 1.0 ± 0.1 | 281 ± 14 | 0.0088 ± 0.0020 |
| | 2.2 ± 0.1 | 595 ± 86 | 0.0053 ± 0.0010 |
| | 3.5 ± 0.1 | 1487 ± 325 | 0.0018 ± 0.0010 |
| 7.5 | 1.0 ± 0.1 | 301 ± 10 | 0.0089 ± 0.0010 |
| | 2.0 ± 0.1 | 523 ± 88 | 0.0046 ± 0.0010 |
| | 4.1 ± 0.1 | 1142 ± 237 | 0.0024 ± 0.0005 |
| 8.0 | 1.0 ± 0.1 | 278 ± 16 | 0.0097 ± 0.0020 |
| | 2.1 ± 0.1 | 525 ± 24 | 0.0059 ± 0.0005 |
| | 4.5 ± 0.2 | 1093 ± 101 [a] | 0.0029 ± 0.0004 |
| 8.5 | 1.2 ± 0.1 | 251 ± 91 | 0.0069 ± 0.0003 |
| | 1.9 ± 0.1 | 398 ± 77 | 0.0041 ± 0.0006 |
| | 4.8 ± 0.2 | 913 ± 40[b] | 0.0025 ± 0.0001 |
| 9.0 | 1.2 ± 0.1 | 285 ± 11 | 0.0073 ± 0.0003 |
| | 2.2 ± 0.1 | 428 ± 54 | 0.0045 ± 0.0003 |
| | 4.8 ± 0.1 | 787 ± 52 | 0.0017 ± 0.0001 |
| 9.5 | 0.8 ± 0.2 | 176 ± 15 | 0.0049 ± 0.0004 |
| | 2.2 ± 0.1 | 315 ± 43 | 0.002 ± 0.0002 |
| | 4.5 ± 0.2 | 706 ± 1257.8 | 0.0042 ± 0.0030 |

[a] This rate constant value is taken from one trial of experiment with a three exponential rise fit as values from the other trials and fits to a 4 exponential equation showed variation due to very low amplitude at the highest concentration of $a_6Ru^{2+}$.
[b] This rate constant value is taken from one trial as values from the other trials showed wide variation due to very low amplitude at the highest concentration of $a_6Ru^{2+}$.

**Table C2**. First intermediate rate constant, $k_2$, and its amplitude for the reduction of A79H73 iso-1-cytochrome *c* by $a_6Ru^{2+}$ as a function of pH and [$a_6Ru^{2+}$] from four exponential fits to the data in figure 4.4.

| pH | [$a_6Ru^{2+}$] mM | $k_{obs}$, $s^{-1}$ | Amplitude |
|---|---|---|---|
| 5.5 | 1.5 ± 0.1 | 13.0 ± 0.2 | 0.0122 ± 0.0004 |
| | 2.2 ± 0.2 | 12.4 ± 0.4 | 0.0117 ± 0.0003 |
| | 4.7 ± 0.2 | 12.0 ± 0.4 | 0.0116 ± 0.0003 |
| 6.0 | 1.1 ± 0.1 (1.25) [a] | 9.0 ± 0.1 (9.6 ± 0.3 ) [a] | 0.0154 ± 0.0002 (0.0188 ± 0.0006)[a] |
| | 2.2 ± 0.1 (2.5) [a] | 9.5 ± 0.2 (8.9 ± 0.4) [a] | 0.0150 ± 0.0004 (0.0171 ± 0.0006)[a] |
| | 4.7 ± 0.2 (5) [a] | 9.7 ± 0.4 (9.3 ± 0.1) [a] | 0.0149 ± 0.0003 (0.0171 ± 0.0020)[a] |
| 6.5 | 1.1 ± 0.1 (1.25) [a] | 6.9 ± 0.2 (6.9 ± 0.002)[a] | 0.0216 ± 0.0002 (0.0286 ± 0.0020)[a] |
| | 2.3 ± 0.1 (2.5) [a] | 7.2 ± 0.1 (7.3 ± 1)[a] | 0.0212 ± 0.0002 (0.0237 ± 0.0020)[a] |
| | 4.5 ± 0.3 (5) [a] | 7.4 ± 0.2 (7.0 ± 0.3)[a] | 0.0207 ± 0.0003 (0.0264 ± 0.0007)[a] |
| 7.0 | 1.0 ± 0.1 | 6.3 ± 0.2 | 0.0194 ± 0.0010 |
| | 2.2 ± 0.1 | 6.8 ± 0.3 | 0.0190 ± 0.0007 |
| | 3.5 ± 0.1 | 6.1 ± 0.4 | 0.0196 ± 0.0003 |
| 7.5 | 1.0 ±0.1 (1.25) [a] | 6.0 ± 0.2 (5.2 ± 0.6)[a] | 0.0222 ± 0.0005 (0.0327 ± 0.0060)[a] |
| | 2.0 ± 0.1 (2.5) [a] | 6.1 ± 0.4 (6.3 ± 0.5)[a] | 0.0219 ± 0.0007 (0.0250 ± 0.0008)[a] |
| | 4.1 ± 0.1 (5) [a] | 6.0 ± 0.2 (6.4 ± 0.6)[a] | 0.0223 ± 0.0003 (0.0278 ± 0.0060)[a] |
| 8.0 | 1.0 ± 0.1 | 6.0 ± 0.1 | 0.0272 ± 0.0002 |
| | 2.1 ± 0.1 | 6.0 ± 0.1 | 0.0268 ± 0.0003 |
| | 4.5 ± 0.2 | 6.1 ± 0.2 | 0.0265 ± 0.0005 |
| 8.5 | 1.2 ± 0.1 | 6.0 ± 0.2 | 0.0230 ± 0.0006 |
| | 1.9 ± 0.1 | 6.0 ± 0.1 | 0.0227 ± 0.0004 |
| | 4.8 ± 0.2 | 6.2 ± 0.3 | 0.0223 ± 0.0005 |
| 9.0 | 1.2 ± 0.1 | 6.1 ± 0.1 | 0.0262 ± 0.0090 |
| | 2.2 ± 0.1 | 6.4 ± 0.1 | 0.0283 ± 0.0005 |
| | 4.8 ± 0.1 | 6.7 ± 0.3 | 0.0278 ± 0.0007 |
| 9.5 | 0.8 ± 0.2 | 4.5 ± 0.1 | 0.0317 ± 0.0020 |
| | 2.2 ± 0.1 | 5.3 ± 0.3 | 0.0268 ± 0.0060 |
| | 4.5 ± 0.2 | 5.0 ± 0.9 | 0.0252 ± 0.0030 |

[a] These values are the average and standard deviation from previous ET data [62], which have been refitted to triple exponential rise equations. The values in brackets are from triple exponential fits. For the concentration of $a_6Ru^{2+}$, the assumption is made that the concentrations based on weight were 1.25, 2.5 and 5 mM, as no direct measurement of concentration was done for this data.

**Table C3.** Second intermediate rate constant, $k_3$, and its amplitude for the reduction of A79H73 iso-1-cytochrome *c* by $a_6Ru^{2+}$ as a function of pH and [$a_6Ru^{2+}$] from four exponential fits to the data in figure 4.4.

| pH | [$a_6Ru^{2+}$] mM | $k_{obs}$, $s^{-1}$ | Amplitude |
|---|---|---|---|
| 5.5 | 1.5 ± 0.1 | 0.86 ± 0.04 | 0.0034 ± 0.0002 |
| | 2.2 ± 0.2 | 1.10 ± 0.07 | 0.0025 ± 0.0002 |
| | 4.7 ± 0.2 | 1.20 ± 0.08 | 0.0030 ± 0.0002 |
| 6.0 | 1.1 ± 0.1 (1.25) [a] | 0.75 ± 0.09 (0.70 ± 0.09)[a] | 0.0016 ± 0.0001 (0.0015 ± 0.0001)[a] |
| | 2.2 ± 0.1 (2.5) [a] | 1.2 ± 0.1 (0.71 ± 0.07)[a] | 0.0021 ± 0.0002 (0.0015 ± 0.0002)[a] |
| | 4.7 ± 0.2 (5) [a] | 1.3 ± 0.2 (0.81 ± 0.02)[a] | 0.0026 ± 0.0004 (0.0025 ± 0.0001)[a] |
| 6.5 | 1.1 ± 0.1 (1.25) [a] | 0.9 ± 0.4 (0.16 ± 0.05)[a] | 0.0016 ± 0.0001 (0.0045 ± 0.0020)[a] |
| | 2.3 ± 0.1 (2.5) [a] | 1.2 ± 0.2 (0.24 ± 0.07)[a] | 0.0020 ± 0.0002 (0.0038 ± 0.0010)[a] |
| | 4.5 ± 0.3 (5) [a] | 1.4 ± 0.2 (0.54 ± 0.17)[a] | 0.0024 ± 0.0003 (0.0029 ± 0.0002)[a] |
| 7.0 | 1.0 ± 0.1 | 1.23 ± 0.50 | 0.0019 ± 0.0006 |
| | 2.2 ± 0.1 | 1.32 ± 0.40 | 0.0026 ± 0.0007 |
| | 3.5 ± 0.1 | 1.53 ± 0.30 | 0.0018 ± 0.0007 |
| 7.5 | 1.0 ±0.1 (1.25) [a] | 1.02 ± 0.3 (0.33 ± 0.003)[a] | 0.0023 ± 0.0004 (0.0028±0.0001)[a] |
| | 2.0 ± 0.1 (2.5) [a] | 1.15 ± 0.6 (3.78 ± 0.4)[a] | 0.0022 ± 0.0009 (0.014 ± 0.007)[a] |
| | 4.1 ± 0.1 (5) [a] | 1.37 ± 0.3 (2.41 ± 1.7)[a] | 0.0016 ± 0.0003 (0.0063 ± 0.0050)[a] |
| 8.0 | 1.0 ± 0.1 | 0.64 ± 0.30 | 0.0025 ± 0.0004 |
| | 2.1 ± 0.1 | 0.91 ± 0.20 | 0.0023 ± 0.0003 |
| | 4.5 ± 0.2 | 1.08 ± 0.20 | 0.0023 ± 0.0004 |
| 8.5 | 1.2 ± 0.1 | 0.58 ± 0.20 | 0.0022 ± 0.0002 |
| | 1.9 ± 0.1 | 0.65 ± 0.10 | 0.0022 ± 0.0002 |
| | 4.8 ± 0.2 | 0.73 ± 0.30 | 0.0023 ± 0.0004 |
| 9.0 | 1.2 ± 0.1 | 0.78 ± 0.20 | 0.0027 ± 0.0003 |
| | 2.2 ± 0.1 | 0.92 ± 0.20 | 0.0032 ± 0.0003 |
| | 4.8 ± 0.1 | 0.93 ± 0.10 | 0.0037 ± 0.0004 |
| 9.5 | 0.8 ± 0.2 | 0.68 ± 0.40 | 0.0022 ± 0.0004 |
| | 2.2 ± 0.1 | 1.53 ± 0.30 | 0.0058 ± 0.0070 |
| | 4.5 ± 0.2 | 2.7 ± 0.4 | 0.0048 ± 0.0040 |

[a] These values are the average and standard deviation from previous ET data [62], which have been refitted to triple exponential rise equations. The values in brackets are from triple exponential fits. For the concentration of $a_6Ru^{2+}$, the assumption is made that the concentrations based on weight were 1.25, 2.5 and 5 mM, as no direct measurement of concentration was done for this data.

**Table C4**. Slow rate constant, $k_4$ and its amplitude for the reduction of A79H73 iso-1-cytochrome *c* by $a_6Ru^{2+}$ as a function of pH and [$a_6Ru^{2+}$] from four exponential fits to the data in figure 4.3.

| pH | [$a_6Ru^{2+}$] mM | $k_{obs}$, $s^{-1}$ | Amplitude |
|---|---|---|---|
| 5.5 | 1.5 ± 0.1 | 0.042 ± 0.002 | 0.0071 ± 0.0003 |
| | 2.2 ± 0.2 | 0.052 ± 0.001 | 0.0063 ± 0.0001 |
| | 4.7 ± 0.2 | 0.057 ± 0.001 | 0.0056 ± 0.0002 |
| 6.0 | 1.1 ±0.1 (1.25) [a] | 0.055 ± 0.001 (0.054 ± 0.001)[a] | 0.0092 ± 0.0002 (0.013 ± 0.001)[a] |
| | 2.2 ± 0.1 (2.5) [a] | 0.060 ± 0.001 (0.052 ± 0.001) [a] | 0.0088 ± 0.0003 (0.013 ± 0.001) [a] |
| | 4.7 ± 0.2 (5) [a] | 0.063 ± 0.002 (0.05 ± 0.001) [a] | 0.0081 ± 0.0004 (0.013 ± 0.001)[a] |
| 6.5 | 1.1 ±0.1 (1.25) [a] | 0.059 ± 0.001 (0.049 ± 0.003) [a] | 0.0134 ± 0.0003 (0.015 ± 0.002)[a] |
| | 2.3 ± 0.1 (2.5) [a] | 0.062 ± 0.001 (0.056 ± 0.004)[a] | 0.0132 ± 0.0002 (0.019 ± 0.001)[a] |
| | 4.5 ± 0.3 (5) [a] | 0.068 ± 0.002 (0.058 ± 0.002)[a] | 0.0123 ± 0.0004 (0.018 ± 0.001) |
| 7.0 | 1.0 ± 0.1 | 0.062 ± 0.001 | 0.0120 ± 0.0002 |
| | 2.2 ± 0.1 | 0.063 ± 0.001 | 0.0118 ± 0.0001 |
| | 3.5 ± 0.1 | 0.061 ± 0.004 | 0.0114 ± 0.0010 |
| 7.5 | 1.0 ±0.1 (1.25) [a] | 0.062 ± 0.002 (0.067 ± 0.003)[a] | 0.0133 ± 0.0001 (0.023 ± 0.001)[a] |
| | 2.0 ± 0.1 (2.5) [a] | 0.063 ± 0.001 (0.073 ± 0.001)[a] | 0.0135 ± 0.0002 (0.0242 ± 0.0004)[a] |
| | 4.1 ± 0.1 (5) [a] | 0.065 ± 0.002 (0.072±0.002)[a] | 0.0133 ± 0.0003 (0.0234 ± 0.0002)[a] |
| 8.0 | 1.0 ± 0.1 | 0.061 ± 0.003 | 0.0154 ± 0.0007 |
| | 2.1 ± 0.1 | 0.064 ± 0.001 | 0.0161 ± 0.0002 |
| | 4.5 ± 0.2 | 0.066 ± 0.001 | 0.0162 ± 0.0001 |
| 8.5 | 1.2 ± 0.1 | 0.060 ± 0.001 | 0.0132 ± 0.0006 |
| | 1.9 ± 0.1 | 0.063 ± 0.002 | 0.0131 ± 0.0003 |
| | 4.8 ± 0.2 | 0.064 ± 0.002 | 0.0131 ± 0.0004 |
| 9.0 | 1.2 ± 0.1 | 0.061 ± 0.001 | 0.0157 ± 0.0004 |
| | 2.2 ± 0.1 | 0.062 ± 0.001 | 0.0152 ± 0.0003 |
| | 4.8 ± 0.1 | 0.062 ± 0.001 | 0.0147 ± 0.0003 |
| 9.5 | 0.8 ± 0.2 | 0.056 ± 0.003 | 0.0114 ± 0.0007 |
| | 2.2 ± 0.1 | 0.057 ± 0.002 | 0.0124 ± 0.0007 |
| | 4.5 ± 0.2 | 0.056 ± 0.006 | 0.0118 ± 0.0010 |

[a] These values are the average and standard deviation from previous ET data [62], which have been refitted to triple exponential rise equations. The values in brackets are from triple exponential fits. For concentration of $a_6Ru^{2+}$, the assumption is made that the concentrations based on weight were 1.25, 2.5 and 5 mM, as no direct measurement of concentration was done for this data.

**Table C5**. Forward and backward conformational rate constants for the His73-heme alkaline transition of the A79H73 variant of iso-1-cyt *c* observed with $a_6Ru^{2+}$ ET data.

| pH | $k_{HM3}$ ($s^{-1}$) [a] | $k_{MH3}$ ($s^{-1}$) [b] |
|---|---|---|
| 5.5 | 12.4 ± 0.5 | 0.12 ± 0.5 |
| 6.0 | 9.4 ± 0.4 | 2.7 ± 0.4 |
| 6.5 | 7.1 ± 0.2 | 4.7 ± 0.2 |
| 7.0 | 6.4 ± 0.3 | 5.3 ± 0.3 |
| 7.5 | 6.0 ± 0.1 | 6.2 ± 0.1 |
| 8.0 | 5.9 ± 0.2 | 7.7 ± 0.2 |
| 8.5 | 6.0 ± 0.2 | 9.4 ± 0.2 |
| 9.0 | 6.4 ± 0.3 | 12.1 ± 0.3 |
| 9.5 | 5.0 ± 0.4 | 15.6 ± 0.4 |

[a] This value is the average value taken from 1.25, 2.5 and 5 mM $a_6Ru^{2+}$ concentration data for all pHs.

[b] These values are calculated from the equation, $k_{obs} = k_{HM3} + k_{MH3}$.

Values for $k_{obs}$ are obtained by placing values of the parameters in Table 2 [62] for the fast phase into equation 6 *ref* [62]. Values for $k_{HM3}$ are taken directly from ET experiments for the A79H73 variant of iso-1-cyt *c*.

**Table C6**. Forward and backward proline isomerization rate constant for A79H73 variant of iso-1-cyt *c* by $a_6Ru^{2+}$.

| pH | $k_{ct}$ ($s^{-1}$) [a] | $k_{obs\text{-}cal}$ ($s^{-1}$) [b] | $k_{tc\text{-}cal}$ ($s^{-1}$) [c] | $k_{tc\text{-}pH}$ (eq) ($s^{-1}$) [d] | $k_{pro}$ ($s^{-1}$) [e] | $K_{iso}$ [f] |
|---|---|---|---|---|---|---|
| 5.5 | 0.057 ± 0.001 | 0.067 | 0.01 | 0.007 | 0.064 | 0.54 ± 0.12 |
| 6.0 | 0.063 ± 0.002 | 0.084 | 0.021 | 0.018 | 0.081 | 0.58 ± 0.07 |
| 6.5 | 0.068 ± 0.002 | 0.010 | 0.033 | 0.032 | 0.01 | 0.61 ± 0.05 |
| 7.0 | 0.061 ± 0.004 | 0.110 | 0.049 | 0.034 | 0.095 | 0.61 ± 0.03 |
| 7.5 | 0.065 ± 0.002 | 0.114 | 0.049 | 0.038 | 0.010 | 0.60 ± 0.01 |
| 8.0 | 0.066 ± 0.001 | 0.115 | 0.049 | 0.039 | 0.10 | 0.59 ± 0.03 |
| 8.5 | 0.064 ± 0.002 | 0.116 | 0.052 | 0.037 | 0.10 | 0.58 ± 0.02 |
| 9.0 | 0.062 ± 0.001 | 0.116 | 0.054 | 0.034 | 0.096 | 0.55 ± 0.05 |
| 9.5 | 0.056 ± 0.006 | 0.116 | 0.006 | 0.024 | 0.080 | 0.43 ± 0.13 |

[a] These values are taken from 5 mM $a_6Ru^{2+}$ data from the slowest phase ($k_4$).

[b] These values are calculated from eq 4.3, using parameters from pH jump data in *ref* [62].

[c] These values are calculated from equation $k_{tc} = k_{obs} - k_{ct}$. $k_{obs}$ is calculated from eq 8 from *ref* [62].

[d] These values are calculated from equation 4.5.

[e] These values are the sum of $k_{ct}$ and $k_{tc\text{-}pH}$(eq).

[f] $K_{iso}$ is the proline isomerization equilibrium constant derived from ET amplitude data from figure 4.13.

**Figure C1** Figure of absorbance at 550 nm as a function of time are shown along with their residuals in separate plots from pH 5.5 to 9.5. Time is shown logarithmically. Red lines in the graph and residuals represent the quadruple exponential fit, while the green lines in the graph and the residuals represent the triple exponential fits. (figure continues on next page)

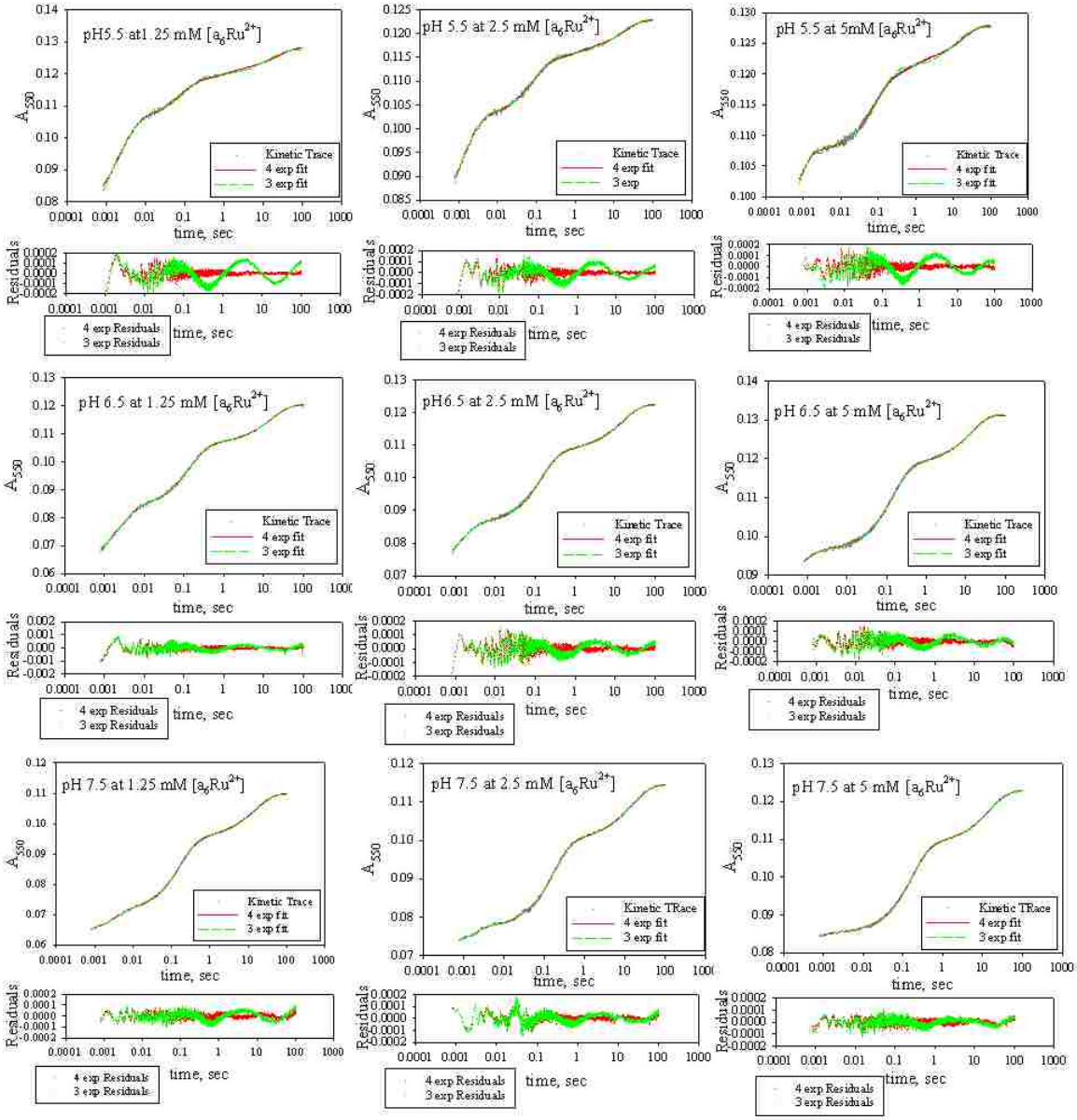

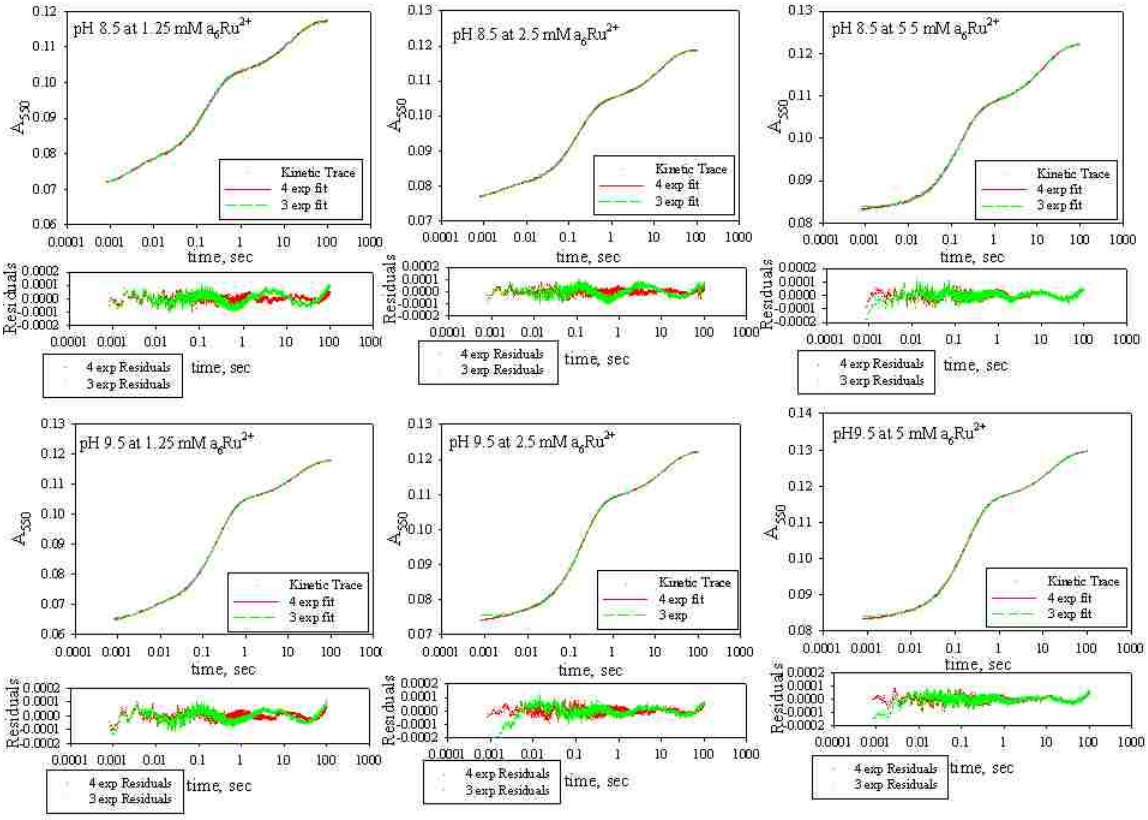
pH 8.5 at 1.25 mM a6Ru2+
pH 8.5 at 2.5 mM a6Ru2+
pH 8.5 at 5.5 mM a6Ru2+
pH 9.5 at 1.25 mM a6Ru2+
pH 9.5 at 2.5 mM a6Ru2+
pH9.5 at 5 mM a6Ru2+
A550
time, sec
Residuals
Kinetic Trace
4 exp fit
3 exp fit
3 exp
4 exp Residuals
3 exp Residuals

## D. Tables of Rate Constants and Amplitudes for the H81 Variant in 0.1 M NaCl and at 25 $^{o}$C from pH jump experiments.

The time scales on which the upward pH jump kinetics data were collected are given in parentheses for each pH: pH 6.0 (50 s), pH 6.2 (20, 50 s), pH 6.4 to 6.8 (100 s), pH 7.0 &7.2 (200 s), pH 7.4 to 7.8 (400 s), pH 8.0 (200 s), pH 8.2 (200, 300 s), pH 8.4 to 8.8 (200 s), pH 9.0 (100 s), pH 9.2 (50 s), pH 9.4 (20, 30, 40 s), pH 9.6 (20, 30 s), pH 9.8 (30, 50 s), pH 10 to 11.2 (50 s).

The time scales for which the downward pH jump kinetics data were collected are given in parentheses for each pH: pH 5.0 (200, 500 s), pH 5.2 (300, 500 s), pH 5.4 (500, 600 s), pH 5.6 (600, 1000 s), pH 5.8 (700, 1000 s), pH 6 to 6.8 (1000 s).

**Table D1.** $k_{obs}$ average data for the fast kinetic phase from upward pH jump experiments.[a]

| pH | $k_{obs}$, $s^{-1}$ | pH | $k_{obs}$, $s^{-1}$ | pH | $k_{obs}$, $s^{-1}$ |
|---|---|---|---|---|---|
| 6.0 | 3.4 ± 0.5[b] | 7.8 | 3.9 ± 0.1 | 9.6 | 2.7 ± 0.6[d] |
| 6.2 | 3.7 ± 0.6[c] | 8.0 | 3.8 ± 0.2 | 9.8 | 2.2 ± 0.1[d] |
| 6.4 | 3.9 ± 0.3[c] | 8.2 | 3.8 ± 0.1 | 10.0 | 2.4 ± 0.1[d] |
| 6.6 | 4.0 ± 0.1[c] | 8.4 | 3.8 ± 0.2 | 10.2 | 2.7 ± 0.06[d] |
| 6.8 | 4.2 ± 0.3 | 8.6 | 3.7 ± 0.1 | 10.4 | 3.3 ± 0.2[d] |
| 7.0 | 4.1 ± 0.2 | 8.8 | 3.5 ± 0.1 | 10.6 | 3.8 ± 0.2[d] |
| 7.2 | 4.1 ± 0.2 | 9.0 | 3.3 ± 0.4[d] | 10.8 | 4.2 ± 0.6[d] |
| 7.4 | 4.0 ± 0.2 | 9.2 | 2.9 ± 0.3[d] | 11.0 | 4.6 ± 0.4 |
| 7.6 | 4.1 ± 0.2 | 9.4 | 2.9 ± 0.3[d] | 11.2 | 7.9 ± 1.6 |

[a] Data fit to a triple exponential rise equation unless otherwise stated.

[b] Data fit to a single exponential rise equation.

[c] Data fit to a double exponential rise equation.

[d] Data fit to a quadruple exponential rise equation.

**Table D2**. $k_{obs}$ average data for the intermediate kinetic phase from upward pH jump experiments.[a]

| pH | $k_{obs}$, $s^{-1}$ | Amplitude (absorbance units) |
|---|---|---|
| 7.0 | 0.019 ± 0.004 | 0.005 ± 0.001 |
| 7.2 | 0.021 ± 0.006 | 0.008 ± 0.001 |
| 7.4 | 0.016 ± 0.002 | 0.009 ± 0.002 |
| 7.6 | 0.019 ± 0.002 | 0.013 ± 0.001 |
| 7.8 | 0.022 ± 0.001 | 0.020 ± 0.003 |
| 8.0 | 0.023 ± 0.002 | 0.023 ± 0.003 |
| 8.2 | 0.026 ± 0.001 | 0.030 ± 0.001 |
| 8.4 | 0.033 ± 0.004 | 0.038 ± 0.007 |
| 8.6 | 0.039 ± 0.005 | 0.036 ± 0.007 |
| 8.8 | 0.051 ± 0.007 | 0.04 ± 0.01 |
| 9.0 | 0.02 ± 0.04 | 0.08 ± 0.03 |
| 9.2 | 0.4 ± 0.1 | 0.034 ± 0.020 |
| 9.4 | 0.7 ± 0.4 | 0.03 ± 0.01 |
| 9.6 | 1.3 ± 0.3 | 0.024 ± 0.010 |

[a] Data fit to a triple exponential rise equation.

**Table D3.** $k_{obs}$ average data for the slow kinetic phase from upward pH jump experiments.[a]

| pH | $k_{obs}$, $s^{-1}$ | pH | $k_{obs}$, $s^{-1}$ | pH | $k_{obs}$, $s^{-1}$ |
|---|---|---|---|---|---|
| 6.2 | 0.05 ± 0.02 [b] | 8.0 | 0.066 ± 0.005 | 9.8 | 0.27 ± 0.01 [c] |
| 6.4 | 0.053 ± 0.008 [b] | 8.2 | 0.070 ± 0.002 | 10.0 | 0.240 ± 0.002[c] |
| 6.6 | 0.052 ± 0.008 [b] | 8.4 | 0.083 ± 0.006 | 10.2 | 0.160 ± 0.003[c] |
| 6.8 | 0.034 ± 0.003 [b] | 8.6 | 0.096 ± 0.004 | 10.4 | 0.110 ± 0.004 [c] |
| 7.0 | 0.07 ± 0.02 [b] | 8.8 | 0.12 ± 0.01 | 10.6 | 0.10 ± 0.05 [c] |
| 7.2 | 0.064 ± 0.01 | 9.0 | 0.098 ± 0.010 [c] | 10.8 | 0.14 ± 0.02 [c] |
| 7.4 | 0.06 ± 0.01 | 9.2 | 0.016 ± 0.008 [c] | 11.0 | 4.6 ± 0.4 |
| 7.6 | 0.060 ± 0.006 | 9.4 | 0.22 ± 0.01 [c] | 11.2 | 7.9 ± 1.6 |
| 7.8 | 0.065 ± 0.004 | 9.6 | 0.27 ± 0.01 [c] | | |

[a] Data fit to a triple exponential rise equation unless otherwise stated.

[b] Data fit to a double exponential rise equation fits.

[c] Data fit to a quadruple exponential rise equation fits.

**Table D4.** $k_{obs}$ average data for the fastest kinetic phase from upward pH jump experiments.[a]

| pH | $k_{obs}$, $s^{-1}$ | Amplitude (absorbance units) |
|---|---|---|
| 9.0 | 138 ± 41 | 0.014 ± 0.002 |
| 9.2 | 147 ± 47 | 0.018 ± 0.003 |
| 9.4 | 86 ± 21 | 0.022 ± 0.001 |
| 9.6 | 89 ± 31 | 0.028 ± 0.002 |
| 9.8 | 86 ± 22 | 0.029 ± 0.009 |
| 10.0 | 96 ± 3 [b] | 0.036 ± 0.030 |
| 10.2 | 51 ± 14 | 0.036 ± 0.008 |
| 10.4 | 85 ± 8 | 0.042 ± 0.010 |
| 10.6 | 91 ± 6 | 0.05 ± 0.20 |
| 10.8 | 112 ± 4 | 0.061 ± 0.004 |
| 11.0 | 136 ± 34 | 0.06 ± 0.02 |
| 11.2 | 219 ± 13 | 0.071 ± 0.004 |

[a] Data fit to a quadruple exponential rise equation unless otherwise stated.

[b] This value is the average of 3 trials as other two trials appeared to be outliers (1876 and 430 $s^{-1}$).

**Table D5. A**verage amplitude data for the fast kinetic phase from upward pH jump experiments.[a]

| pH | Amplitude (absorbance units) | pH | Amplitude (absorbance units) | pH | Amplitude (absorbance units) |
|---|---|---|---|---|---|
| 6.0 | 0.0020 ± 0.0001[b] | 7.8 | 0.0180 ± 0.0003 | 9.6 | 0.048 ± 0.008[d] |
| 6.2 | 0.0040 ± 0.0004[c] | 8.0 | 0.019 ± 0.001 | 9.8 | 0.072 ± 0.001[d] |
| 6.4 | 0.0060 ± 0.0003[c] | 8.2 | 0.0200 ± 0.0002 | 10.0 | 0.085 ± 0.010[d] |
| 6.6 | 0.0080 ± 0.0002[c] | 8.4 | 0.022 ± 0.001 | 10.2 | 0.097 ± 0.004[d] |
| 6.8 | 0.0090 ± 0.0004 | 8.6 | 0.024 ± 0.001 | 10.4 | 0.095 ± 0.008[d] |
| 7.0 | 0.011 ± 0.001 | 8.8 | 0.0260 ± 0.0003 | 10.6 | 0.085 ± 0.010[d] |
| 7.2 | 0.0130 ± 0.0004 | 9.0 | 0.0300 ± 0.001[d] | 10.8 | 0.056 ± 0.020[d] |
| 7.4 | 0.013 ± 0.002 | 9.2 | 0.0350 ± 0.0003[d] | 11.0 | 0.028 ± 0.020 |
| 7.6 | 0.015 ± 0.001 | 9.4 | 0.040 ± 0.005[d] | 11.2 | 0.009 ± 0.007 |

[a] Data fit to a triple exponential rise equation unless otherwise stated.

[b] Data fit to a single exponential rise equation.

[c] Data fit to a double exponential rise equation.

[d] Data fit to a quadruple exponential rise equation.

**Table D6. A**verage amplitude data for the slow kinetic phase from upward pH jump experiments.[a]

| pH | Amplitude (absorbance units) | pH | Amplitude (absorbance units) | pH | Amplitude (absorbance units) |
|---|---|---|---|---|---|
| 6.2 | 0.012 ± 0.020 [b] | 8.0 | 0.020 ± 0.002 | 9.8 | 0.110 ± 0.002 [c] |
| 6.4 | 0.011 ± 0.020 [b] | 8.2 | 0.032 ± 0.002 | 10.0 | 0.088 ± 0.001 [c] |
| 6.6 | 0.0020 ± 0.0003 [b] | 8.4 | 0.051 ± 0.008 | 10.2 | 0.056 ± 0.001 [c] |
| 6.8 | 0.004 ± 0.001 | 8.6 | 0.074 ± 0.007 | 10.4 | 0.034 ± 0.001 [c] |
| 7.0 | 0.003 ± 0.001 | 8.8 | 0.091 ± 0.010 | 10.6 | 0.016 ± 0.001 [c] |
| 7.2 | 0.004 ± 0.001 | 9.0 | 0.066 ± 0.030 [c] | 10.8 | 0.006 ± 0.001 [c] |
| 7.4 | 0.008 ± 0.001 | 9.2 | 0.11 ± 0.02 [c] | 11.0 | 0.03 ± 0.02 |
| 7.6 | 0.011 ± 0.002 | 9.4 | 0.12 ± 0.01 [c] | 11.2 | 0.009 ± 0.007 |
| 7.8 | 0.015 ± 0.002 | 9.6 | 0.120 ± 0.004 [c] | | |

[a] Data fit to a triple exponential rise equation unless otherwise stated.

[b] Data fit to a double exponential rise equation.

[c] Data fit to a quadruple exponential rise equation.

**Table D7.** $k_{obs}$ and amplitude average data for the fast kinetic phase from downward pH jump experiments.[a]

| pH | $k_{obs}$, $s^{-1}$ | Amplitude (absorbance units) |
|---|---|---|
| 5.0 | 3.1 ± 0.1 | 0.014 ± 0.004 |
| 5.2 | 3.4 ± 0.1 | 0.0150 ± 0.0004 |
| 5.4 | 3.8 ± 0.1 | 0.0150 ± 0.0003 |
| 5.6 | 4.0 ± 0.2 | 0.015 ± 0.001 |
| 5.8 | 4.2 ± 0.1 | 0.014 ± 0.001 |
| 6.0 | 4.2 ± 0.2 | 0.0120 ± 0.0002 |
| 6.2 | 4.4 ± 0.1 | 0.0120 ± 0.0002 |
| 6.4 | 4.26 ± 0.15 | 0.0100 ± 0.0004 |
| 6.6 | 4.2 ± 0.3 | 0.0080 ± 0.0003 |
| 6.8 | 4.7 ± 0.6 | 0.007 ± 0.001 |

[a] Data are the average of five data sets. Parameters are fits to a three exponential equation.

**Table D8.** $k_{obs}$ and amplitude average data for the intermediate kinetic phase from downward pH jump experiments.[a]

| pH | $k_{obs}$, $s^{-1}$ | Amplitude (absorbance units) |
|---|---|---|
| 5.0 | 0.015 ± 0.002 | 0.016 ± 0.002 |
| 5.2 | 0.012 ± 0.002 | 0.014 ± 0.002 |
| 5.4 | 0.013 ± 0.002 | 0.016 ± 0.002 |
| 5.6 | 0.001 ± 0.002 | 0.014 ± 0.002 |
| 5.8 | 0.002 ± 0.002 | 0.0160 ± 0.0003 |
| 6.0 | 0.013 ± 0.003 | 0.011 ± 0.006 |
| 6.2 | 0.014 ± 0.002 | 0.014 ± 0.002 |
| 6.4 | 0.015 ± 0.001 | 0.014 ± 0.001 |
| 6.6 | 0.016 ± 0.003 | 0.014 ± 0.001 |
| 6.8 | 0.017 ± 0.001 | 0.0110 ± 0.0002 |

[a] Data are the average of five data sets. Parameters are from fits to a quadruple exponential equation.

**Table D9.** $k_{obs}$ and amplitude average data for the slow kinetic phase from downward pH jump experiments.[a]

| pH | $k_{obs}$, $s^{-1}$ | Amplitude (absorbance units) |
|---|---|---|
| 5.0 | 0.057 ± 0.007 | 0.012 ± 0.001 |
| 5.2 | 0.047 ± 0.006 | 0.015 ± 0.001 |
| 5.4 | 0.050 ± 0.005 | 0.014 ± 0.002 |
| 5.6 | 0.046 ± 0.007 | 0.015 ± 0.003 |
| 5.8 | 0.053 ± 0.004 | 0.012 ± 0.002 |
| 6.0 | 0.048 ± 0.007 | 0.014 ± 0.002 |
| 6.2 | 0.053 ± 0.004 | 0.011 ± 0.001 |
| 6.4 | 0.054 ± 0.002 | 0.010 ± 0.001 |
| 6.6 | 0.055 ± 0.006 | 0.009 ± 0.002 |
| 6.8 | 0.055 ± 0.001 | 0.009 ± 0.001 |

[a] Data are the average of five data sets. Parameters are from fits to a quadruple exponential rise equation.

## E. Tables of Rate Constants and Amplitudes for the A72H76 Variant in 0.1 M NaCl and at 25 $^{o}$C from pH jump experiments.

The time scales on which the upward pH jump kinetics data were collected are given in parentheses for each pH's: pH 5.4 (100 s), pH 5.6 (250, 300 s), pH 5.6 & 5.8 (250, 300 s), pH 6.0 (100, 200, 300 s), pH 6.2 (200 s), pH 6.4 & 6.6 (150 s), pH 6.8 & 7.0 (100 s), pH 7.2 (100, 110 s), pH 7.4 to 8.0 (100 s), pH 8.2 (50, 100 s), pH 8.4 (50 s), pH 8.6 (50, 100 s), pH 8.8 to 9.2 (50 s), pH 9.4 & 9.6 (50, 100 s), pH 9.8 (50 s), pH 10.0 (50, 100 s), pH 10.2 to 10.8 (50 s), pH 11.0 (10, 50, 100 s), pH 11.2 (10, 50 s).

The time scale on which the downward pH jump kinetics data were collected are given in parentheses for each pH's: pH 5 (100, 200, 300 s), pH 5.2 (200, 300 s), pH 5.4 to 5.8 (300 s), pH 6.0 (250, 300 s), pH 6.2 (200, 250 s), pH 6.4 (250, 300 s), pH 6.6 & 6.8 (200, 250, 300 s).

**Table E1.** $k_{obs}$ average data for the fast kinetic phase from upward pH jump experiments.[a]

| pH | $k_{obs}$, $s^{-1}$ | pH | $k_{obs}$, $s^{-1}$ | pH | $k_{obs}$, $s^{-1}$ |
|---|---|---|---|---|---|
| 5.4 | 5.0 ± 0.1 | 7.4 | 10.4 ± 0.7 | 9.4 | 8.6 ± 0.4 |
| 5.6 | 5.6 ± 0.3 | 7.6 | 10.70 ± 0.03 | 9.6 | 8.7 ± 0.7 |
| 5.8 | 5.9 ± 0.2 | 7.8 | 12.0 ± 0.5 | 9.8 | 8.7 ± 0.7 |
| 6.0 | 6.4 ± 0.1 | 8.0 | 10.9 ± 0.2 | 10.0 | 9.9 ± 0.7 |
| 6.2 | 6.9 ± 0.1 | 8.2 | 10.8 ± 0.2 | 10.2 | 11.1 ± 0.6 |
| 6.4 | 7.6 ± 0.2 | 8.4 | 10.8 ± 0.7 | 10.4 | 16.7 ± 0.2 |
| 6.6 | 8.2 ± 0.4 | 8.6 | 10.7 ± 0.7 | 10.6 | 27.0 ± 1.5 |
| 6.8 | 9.0 ± 0.2 | 8.8 | 10.6 ± 0.6 | 10.8 | 42.5 ± 3.6 |
| 7.0 | 9.3 ± 0.3 | 9.0 | 10.0 ± 0.4 | 11.0 | 71 ± 10 |
| 7.2 | 9.7 ± 0.3 | 9.2 | 9.3 ± 0.5 | 11.2 | 102 ± 10 |

[a] Data fit to a triple exponential rise equation. All these values are the average and standard deviation from 7-8 trials.

**Table E2**. $k_{obs}$ average data for the intermediate kinetic phase from upward pH jump experiments.[a]

| pH | $k_{obs}$, $s^{-1}$ | Amplitude (absorbance units) |
|---|---|---|
| 5.4 | 0.001 ± 0.010 | 0.0001 ± 0.0001 |
| 5.6 | 0.016 ± 0.020 | 0.0003 ± 0.0002 |
| 5.8 | 0.034 ± 0.001 | 0.002 ± 0.00 |
| 6.0 | 0.028 ± 0.030 | 0.003 ± 0.003 |
| 6.2 | 0.054 ± 0.010 | 0.002 ± 0.002 |
| 6.4 | 0.046 ± 0.020 | 0.004 ± 0.001 |
| 6.6 | 0.067 ± 0.001 | 0.004 ± 0.001 |
| 6.8 | 0.071 ± 0.009 | 0.005 ± 0.002 |
| 7.0 | 0.074 ± 0.020 | 0.006 ± 0.002 |
| 7.2 | 0.22 ± 0.20 | 0.006 ± 0.006 |
| 7.4 | 0.39 ± 0.20 | 0.008 ± 0.007 |
| 7.6 | 1.01 ± 0.70 | 0.003 ± 0.002 |
| 7.8 | 1.03 ± 0.80 | 0.003 ± 0.001 |
| 8.0 | 1.01 ± 0.70 | 0.003 ± 0.001 |
| 8.2 | 1.03 ± 0.80 | 0.011 ± 0.020 |
| 8.4 | 2.0 ± 1.4 | 0.008 ± 0.004 |
| 8.6 | 1.0 ± 0.9 | 0.021 ± 0.010 |
| 8.8 | 1.6 ± 1.8 | 0.024 ± 0.010 |

[a] Data fit to a triple exponential rise equation.

**Table E3.** $k_{obs}$ average data for the slow kinetic phase from upward pH jump experiments.[a]

| pH | $k_{obs}$, $s^{-1}$ | pH | $k_{obs}$, $s^{-1}$ | pH | $k_{obs}$, $s^{-1}$ |
|---|---|---|---|---|---|
| 5.4 | 0.024 ± 0.007 | 7.4 | 0.064 ± 0.001 | 9.4 | 0.98 ± 0.01 |
| 5.6 | 0.032 ± 0.001 | 7.6 | 0.077 ± 0.001 | 9.6 | 1.05 ± 0.01 |
| 5.8 | 0.034 ± 0.002 | 7.8 | 0.110 ± 0.001 | 9.8 | 1.06 ± 0.02 |
| 6.0 | 0.033 ± 0.001 | 8.0 | 0.130 ± 0.001 | 10.0 | 1.05 ± 0.02 |
| 6.2 | 0.036 ± 0.001 | 8.2 | 0.180 ± 0.001 | 10.2 | 1.30 ± 0.02 |
| 6.4 | 0.037 ± 0.001 | 8.4 | 0.270 ± 0.001 | 10.4 | 1.40 ± 0.01 |
| 6.6 | 0.0400 ± 0.0002 | 8.6 | 0.400 ± 0.003 | 10.6 | 1.9 ± 0.1 |
| 6.8 | 0.043 ± 0.001 | 8.8 | 0.52 ± 0.01 | 10.8 | 2.6 ± 0.3 |
| 7.0 | 0.047 ± 0.001 | 9.0 | 0.710 ± 0.003 | 11.0 | 3.1 ± 0.1 |
| 7.2 | 0.0530 ± 0.0004 | 9.2 | 0.82 ± 0.01 | 11.2 | 4.2 ± 0.4 |

[a] Data fit to a triple exponential rise equation. All these values are the average and standard deviation from 7-8 trials.

**Table E4.** $k_{obs}$ average data for the slow kinetic phase from upward pH jump experiments.[a]

| pH | $k_{obs}$, $s^{-1}$ | Amplitude (absorbance units) |
|---|---|---|
| 10.2 | 0.13 ± 0.01 | 0.0040 ± 0.0002 |
| 10.4 | 0.15 ± 0.01 | 0.0050 ± 0.0002 |
| 10.6 | 0.30 ± 0.04 | 0.006 ± 0.001 |
| 10.8[b] | 0.51 ± 0.07 | 0.009 ± 0.002 |
| 11.0[b] | 0.81 ± 0.1 | 0.004 ± 0.001 |
| 11.2[b] | 0.71 ± 0.4 | 0.006 ± 0.007 |

[a] Data fit to a quadruple exponential rise equation unless otherwise stated.

[b] Data fit to a triple exponential rise equation.

**Table E5.** $k_{obs}$ average data for the fastest kinetic phase from upward pH jump experiments.[a]

| pH | $k_{obs}$, $s^{-1}$ | Amplitude (absorbance units) |
|---|---|---|
| 8.0 | 130 ± 17 | 0.004 ± 0.001 |
| 8.2 | 147 ± 30 | 0.0060 ± 0.0004 |
| 8.4 | 184 ± 85 | 0.009 ± 0.002 |
| 8.6 | 189 ± 25 | 0.013 ± 0.002 |
| 8.8 | 143 ± 46 | 0.015 ± 0.004 |
| 9.0 | 137 ± 11 | 0.020 ± 0.001 |
| 9.2 | 138 ± 16 | 0.023 ± 0.002 |
| 9.4 | 140 ± 19 | 0.025 ± 0.002 |
| 9.6 | 191 ± 23 | 0.029 ± 0.002 |
| 9.8 | 216 ± 41 | 0.027 ± 0.006 |
| 10.0 | 449 ± 104 | 0.036 ± 0.006 |
| 10.2[b] | 626 ± 96 | 0.04 ± 0.01 |
| 10.4[b] | 1795 ± 409 | 0.07 ± 0.04 |
| 10.6[b] | 3315 ± 1076 | 0.09 ± 0.10 |

[a] Data fit to a triple exponential rise equation.

[b] Data fit to a quadruple exponential rise equation.

**Table E6.** Average amplitude data for the fast kinetic phase from upward pH jump experiments.[a]

| pH | Amplitude (absorbance units) | pH | Amplitude (absorbance units) | pH | Amplitude (absorbance units) |
|---|---|---|---|---|---|
| 5.4 | 0.0070 ± 0.0003 | 7.4 | 0.054 ± 0.003 | 9.4 | 0.049 ± 0.001 |
| 5.6 | 0.013 ± 0.001 | 7.6 | 0.057 ± 0.002 | 9.6 | 0.050 ± 0.001 |
| 5.8 | 0.020 ± 0.001 | 7.8 | 0.061 ± 0.002 | 9.8 | 0.052 ± 0.002 |
| 6.0 | 0.026 ± 0.001 | 8.0 | 0.058 ± 0.001 | 10.0 | 0.058 ± 0.002 |
| 6.2 | 0.034 ± 0.001 | 8.2 | 0.058 ± 0.002 | 10.2 | 0.059 ± 0.002 |
| 6.4 | 0.041 ± 0.001 | 8.4 | 0.057 ± 0.003 | 10.4 | 0.062 ± 0.001 |
| 6.6 | 0.045 ± 0.003 | 8.6 | 0.057 ± 0.003 | 10.6 | 0.062 ± 0.001 |
| 6.8 | 0.049 ± 0.001 | 8.8 | 0.057 ± 0.002 | 10.8 | 0.072 ± 0.004 |
| 7.0 | 0.051 ± 0.002 | 9.0 | 0.053 ± 0.002 | 11.0 | 0.081 ± 0.002 |
| 7.2 | 0.052 ± 0.002 | 9.2 | 0.051 ± 0.002 | 11.2 | 0.082 ± 0.004 |

[a] Data fits to a triple exponential rise equation. All these values are the average and standard deviation from 7-8 trials.

**Table E7.** Average amplitude data for slow kinetic phase from upward pH jumps experiments.[a]

| pH | Amplitude (absorbance units) | pH | Amplitude (absorbance units) | pH | Amplitude (absorbance units) |
|---|---|---|---|---|---|
| 5.4 | 0.0040 ± 0.0004 | 7.4 | 0.0047 ± 0.0005 | 9.4 | 0.069 ± 0.001 |
| 5.6 | 0.004 ± 0.001 | 7.6 | 0.052 ± 0.001 | 9.6 | 0.065 ± 0.001 |
| 5.8 | 0.0060 ± 0.0001 | 7.8 | 0.0570 ± 0.0003 | 9.8 | 0.060 ± 0.002 |
| 6.0 | 0.0100 ± 0.0003 | 8.0 | 0.0600 ± 0.0002 | 10.0 | 0.054 ± 0.001 |
| 6.2 | 0.0130 ± 0.0003 | 8.2 | 0.0660 ± 0.0004 | 10.2 | 0.0480 ± 0.0004 |
| 6.4 | 0.0170 ± 0.0004 | 8.4 | 0.0690 ± 0.0004 | 10.4 | 0.0400 ± 0.0004 |
| 6.6 | 0.0200 ± 0.0003 | 8.6 | 0.073 ± 0.001 | 10.6 | 0.0330 ± 0.0004 |
| 6.8 | 0.0260± 0.0003 | 8.8 | 0.074 ± 0.001 | 10.8 | 0.030 ± 0.001 |
| 7.0 | 0.0320 ± 0.0004 | 9.0 | 0.074 ± 0.001 | 11.0 | 0.026 ± 0.001 |
| 7.2 | 0.0390 ± 0.0004 | 9.2 | 0.073 ± 0.001 | 11.2 | 0.020 ± 0.001 |

[a] Data fits to a triple exponential rise equation. All these values are the average and standard deviation from 7-8 trials.

**Table E8.** $k_{obs}$ and amplitude average data for the fast kinetic phase from downward pH jump experiments.[a]

| pH | $k_{obs}$, $s^{-1}$ | Amplitude (absorbance units) |
|---|---|---|
| 5.0 | 4.6 ± 0.1 | 0.022 ± 0.001 |
| 5.2 | 4.8 ± 0.2 | 0.021 ± 0.001 |
| 5.4 | 5.2 ± 0.1 | 0.020 ± 0.001 |
| 5.6 | 5.6 ± 0.1 | 0.0180 ± 0.0004 |
| 5.8 | 6.2 ± 0.1 | 0.0150 ± 0.0003 |
| 6.0 | 7.0 ± 0.2 | 0.013 ± 0.001 |
| 6.2 | 7.7 ± 0.4 | 0.010 ± 0.001 |
| 6.4 | 8.06 ± 0.04 | 0.007 ± 0.001 |
| 6.6 | 8.6 ± 0.9 | 0.0050 ± 0.0004 |
| 6.8 | 10 ± 1 | 0.004 ± 0.001 |

[a] Data are the average of five data sets. Parameters are taken from fits to a three exponential rise equation.

**Table E9.** $k_{obs}$ and amplitude average data for the intermediate kinetic phase from downward pH jump experiments.[a]

| pH | $k_{obs}$, $s^{-1}$ | Amplitude (absorbance units) |
|---|---|---|
| 5.0 | 0.028 ± 0.001 | 0.052 ± 0.006 |
| 5.2 | 0.026 ± 0.003 | 0.045 ± 0.01 |
| 5.4 | 0.027 ± 0.001 | 0.044 ± 0.003 |
| 5.6 | 0.026 ± 0.002 | 0.036 ± 0.009 |
| 5.8 | 0.028 ± 0.002 | 0.038 ± 0.007 |
| 6.0 | 0.030 ± 0.001 | 0.037 ± 0.005 |
| 6.2 | 0.030 ± 0.002 | 0.033 ± 0.007 |
| 6.4 | 0.033 ± 0.003 | 0.032 ± 0.008 |
| 6.6 | 0.036 ± 0.003 | 0.03 ± 0.007 |
| 6.8 | 0.039 ± 0.009 | 0.012 ± 0.007 |

[a] Data are the average of five data sets. Parameters are taken from fits to a quadruple exponential equation.

**Table E10.** $k_{obs}$ and amplitude average data for the slow kinetic phase from downward pH jump experiments.[a]

| pH | $k_{obs}$, $s^{-1}$ | Amplitude (absorbance units) |
|---|---|---|
| 5.0 | 0.057 ± 0.003 | 0.034 ± 0.006 |
| 5.2 | 0.051 ± 0.003 | 0.039 ± 0.01 |
| 5.4 | 0.050 ± 0.001 | 0.033 ± 0.003 |
| 5.6 | 0.047 ± 0.003 | 0.037 ± 0.0009 |
| 5.8 | 0.05 ± 0.0004 | 0.028 ± 0.0008 |
| 6.0 | 0.05 ± 0.004 | 0.021 ± 0.005 |
| 6.2 | 0.053 ± 0.008 | 0.019 ± 0.007 |
| 6.4 | 0.049 ± 0.001 | 0.02 ± 0.003 |
| 6.6 | 0.054 ± 0.005 | 0.014 ± 0.004 |
| 6.8 | 0.039 ± 0.009 | 0.013 ± 0.007 |

[a] Data are the average of five data sets. Parameters are taken from fits to a quadruple exponential equation.

**Figure F1** Plot of $A_{695corr}$ versus gdnHCl concentration for the A72H76 variant of iso-1-cyt *c*. Data were acquired at room temperature (22 ± 1 ºC) in the presence of 20 mM Tris, pH 7.5, 40 mM NaCl.

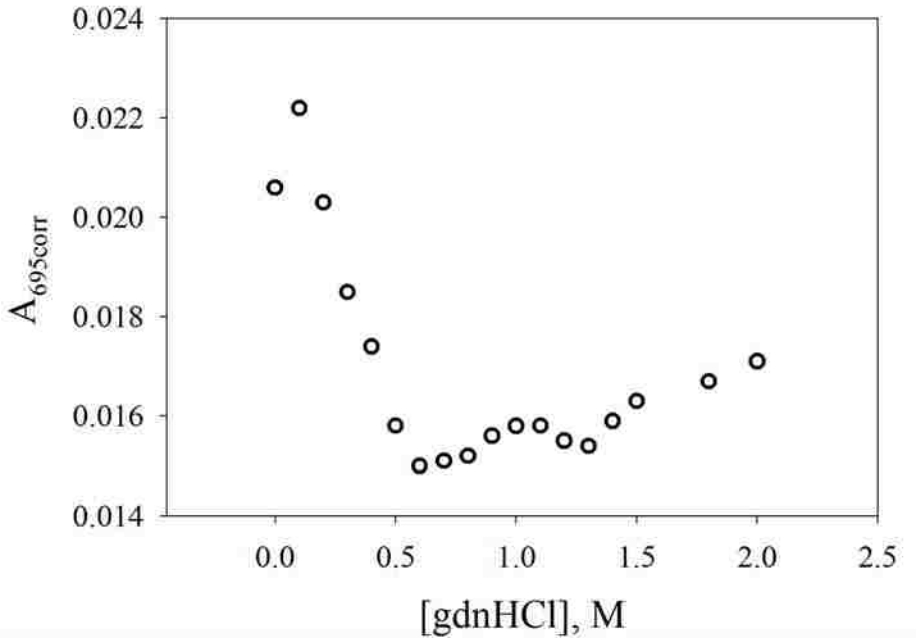


**Figure F2** Plot of $\varepsilon_{695corr}$ versus pH for H81 iso-1-cytochrome *c* in the absence of gdnHCl. Data were collected at room temperature (22 ± 1 ºC) in 0.5 M NaCl. The solid curves are fits to eq 5.1 as described in the Materials and Methods of Chapter 5.

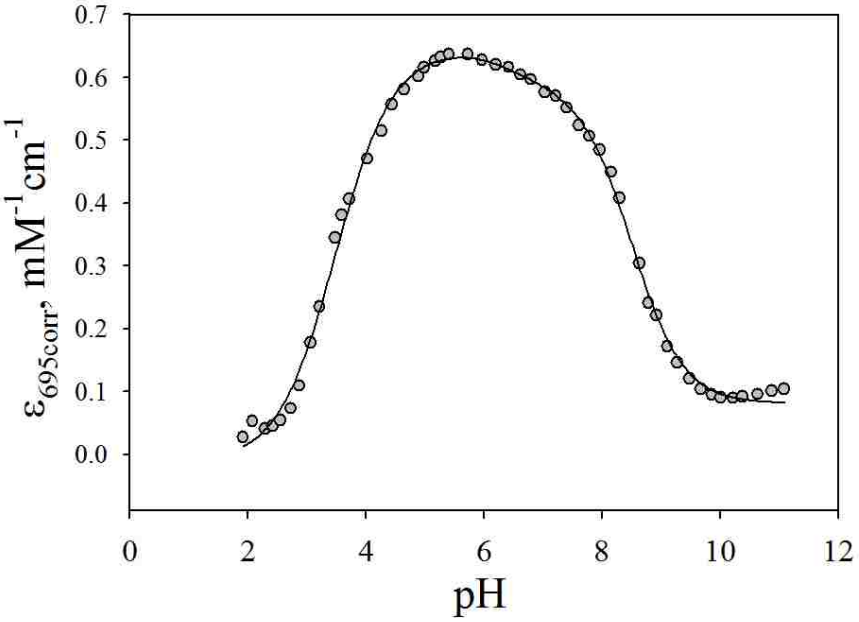

**Figure F3** Plot of absorbance spectra as a function of pH for the H81 variant of iso-1-cyt *c* at 22 ± 1 ºC in the presence of 0.5 M NaCl. (a) pH 1.97 – 2.63 (504, 590, 676 nm) (b) pH 2.91 – 3.46 (505, 596, 665 nm) (c) pH 3.59 – 3.89 (593, 641 nm) (d) pH 4.03 – 6.62 (618 nm) and (e) pH 6.81 – 11.05 (610 nm). Isosbestic points are indicated in brackets.

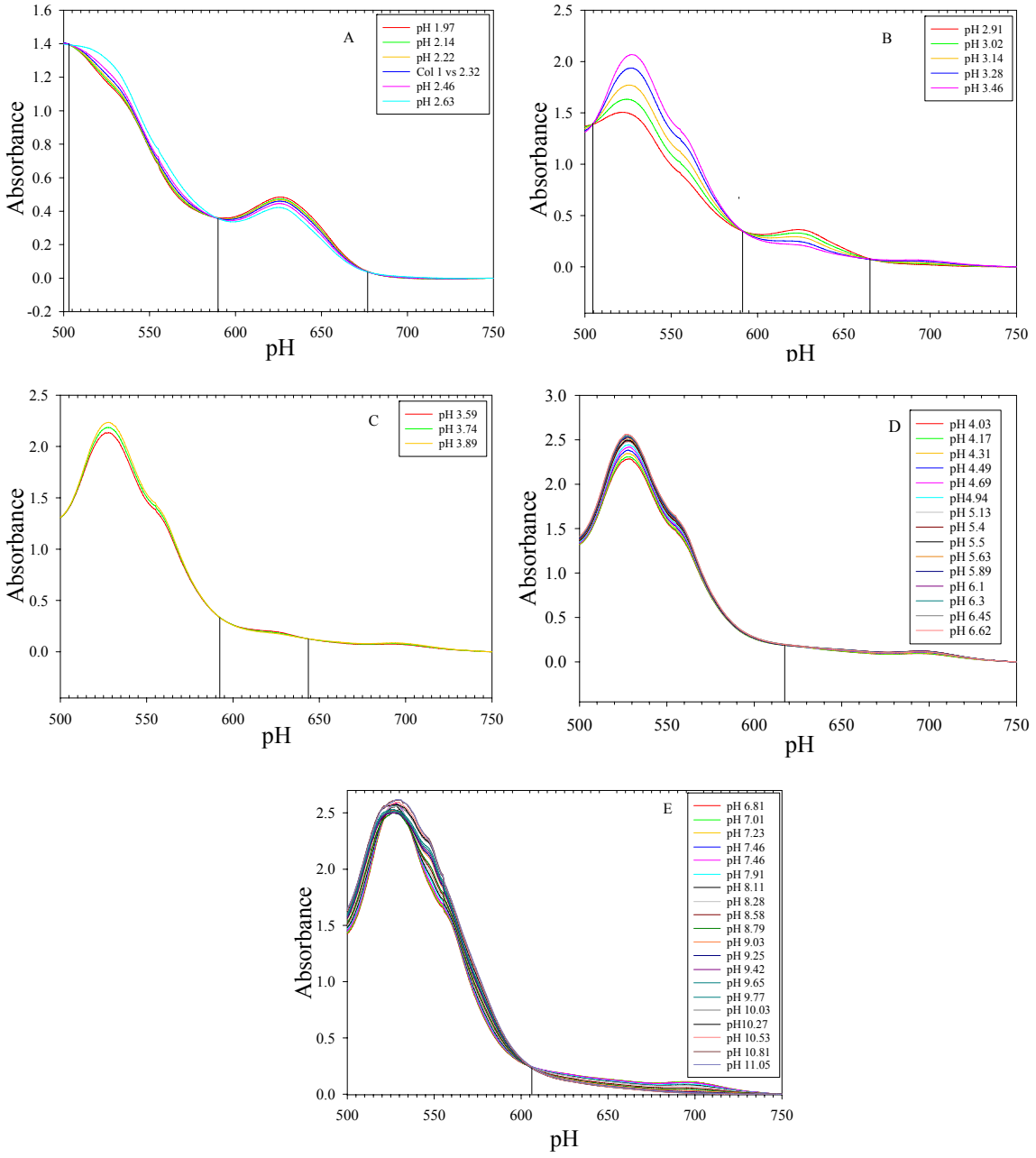

**Figure F4** Plot of $\varepsilon_{695corr}$ versus pH for A72H73G76 iso-1-cytochrome *c* in the absence of gdnHCl. Data were collected at room temperature (22 ± 1 ºC) in 0.1 M NaCl.

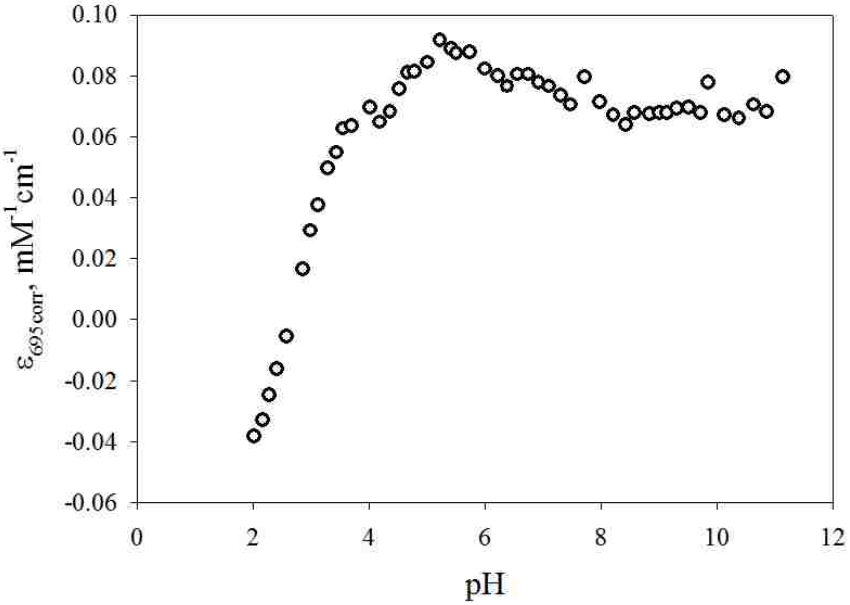


**Figure F5** Plot of $\varepsilon_{695corr}$ versus pH for A72H73G76A79 iso-1-cytochrome *c* in the absence of gdnHCl. Data were collected at room temperature (22 ± 1 ºC) in 0.1 M NaCl.

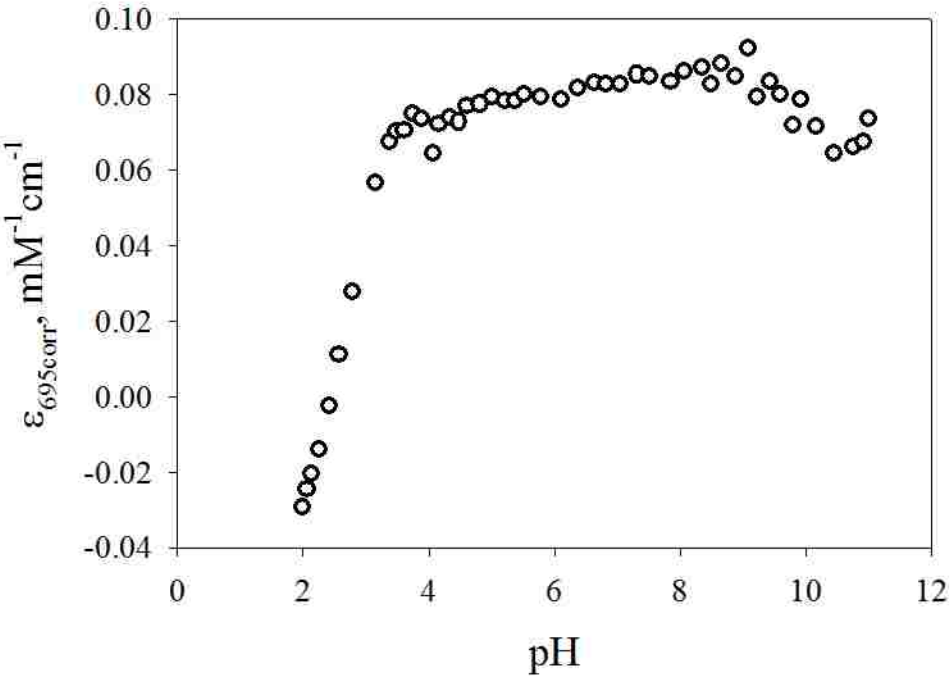

**Figure F6** Plots of absorbance at 405 nm as a function of time at 25 ºC for the H81 variant of iso-1-cyt *c*. (A) pH 5.4, 600 s and (B) pH 6.4, 1000 s time scale data for downward pH jump experiments. (C) pH 7.4, 400 s, (D) pH 8.4, 200 s (E) pH 9.4, 40 s and (F) pH 10.4, 50 s time scale data for upward pH jump experiments. Buffers all contain 0.1 M NaCl as described in the Materials and Methods. The time scale is logarithmic.

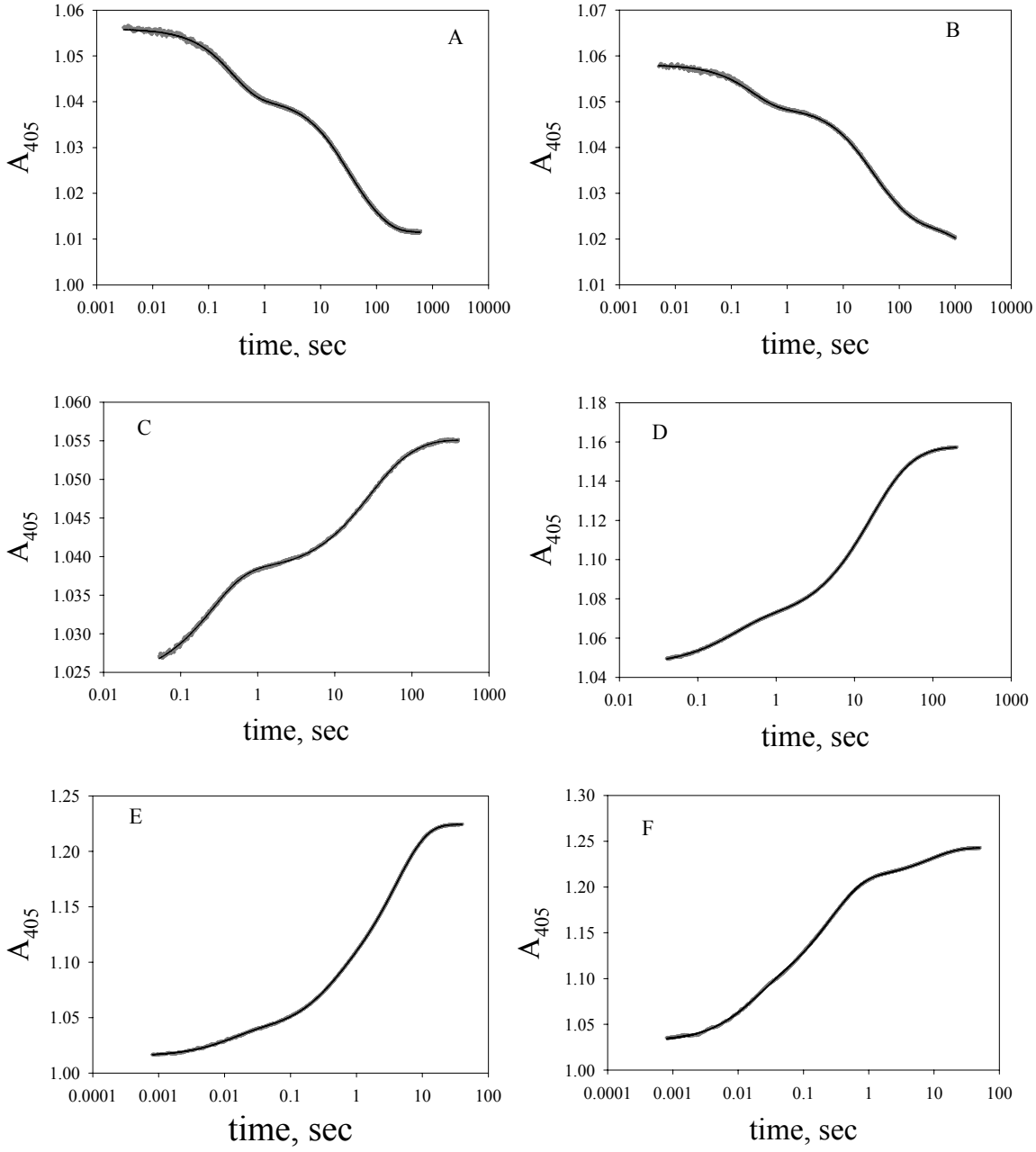

**Figure F7** Plots of absorbance at 405 nm as a function of time at 25 ºC for the A72H76 variant of iso-1-cyt *c*. (A) pH 5.4, 300 s and (B) pH 6.4, 2000 s time scale data for downward pH jump experiments. (C) pH 7.4, 100 s, (D) pH 8.4, (E) pH 9.4, and (F) pH 10.4, at 50 s time scale data for upward pH jump experiments. Buffers all contain 0.1 M NaCl as described in the Materials and Methods. The time scale is logarithmic.

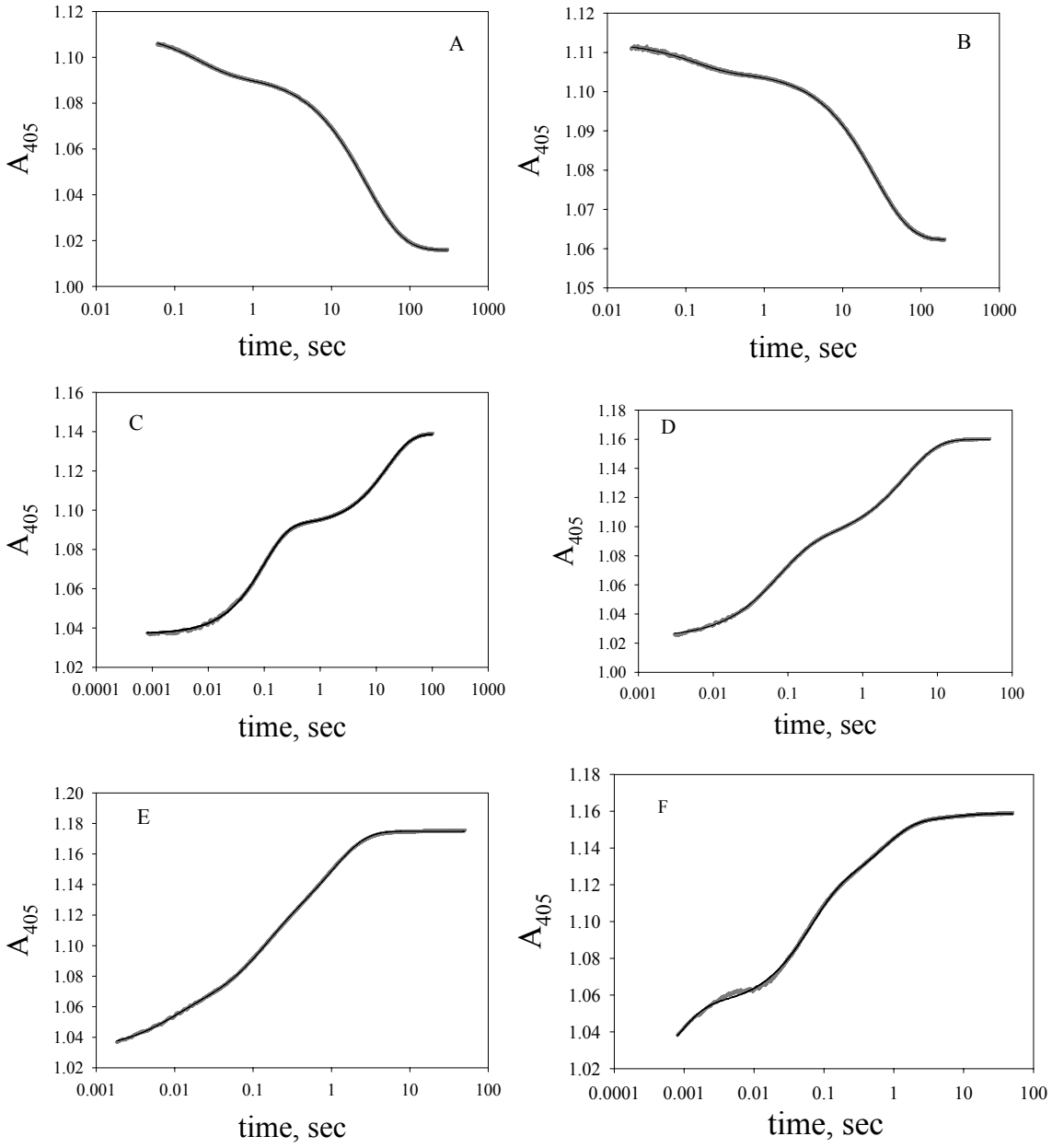

**Figure F8** Plots of absorbance at 550 nm versus time (on logarithmic scale) for reduction of the H81 variant of iso-1-cyt *c* at pH 7.5 and six different concentrations of $a_6Ru^{2+}$. The solid lines are fits to a triple exponential rise equation.

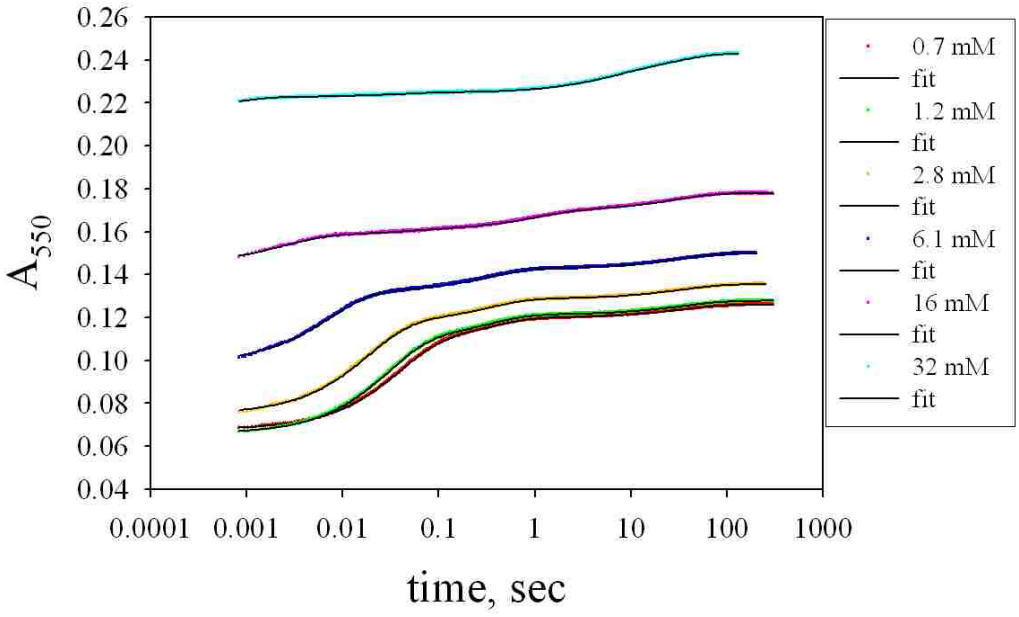


**Figure F9** Plots of absorbance at 550 nm versus time (on logarithmic scale) for reduction of the H81 variant of iso-1-cyt *c* at pH 7.5 and six different concentrations of $[Co(terpy)_2]^{2+}$. The solid lines are fits to a triple exponential rise equation.

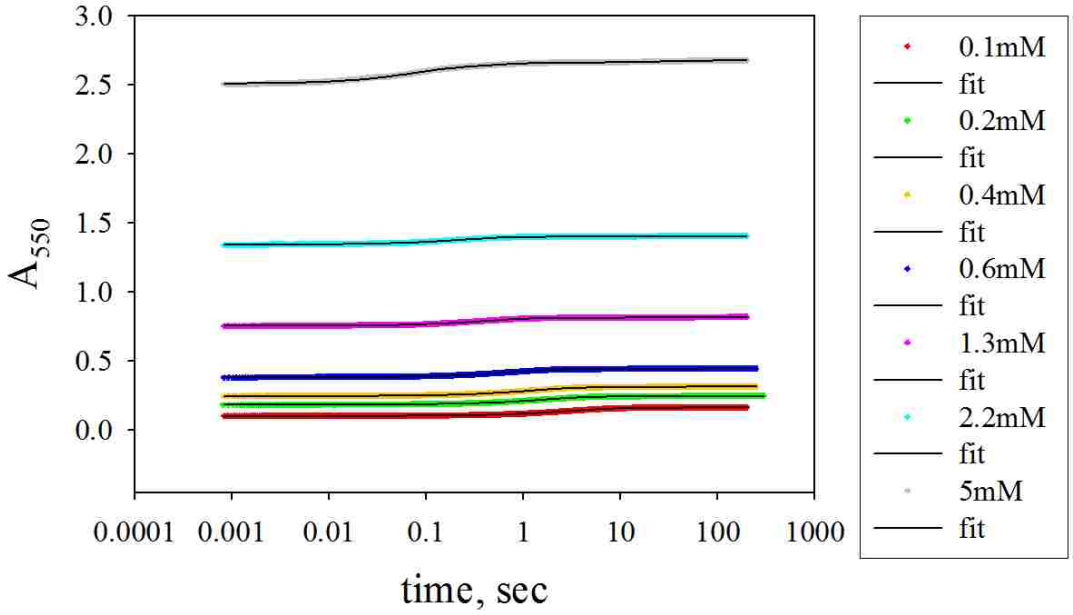

**Figure F10** Plots of absorbance at 550 nm versus time (on logarithmic scale) for reduction of the A72H76 variant of iso-1-cyt *c* at pH 7.5 and six different concentrations of $a_6Ru^{2+}$. The solid lines are fits to a triple exponential rise equation.

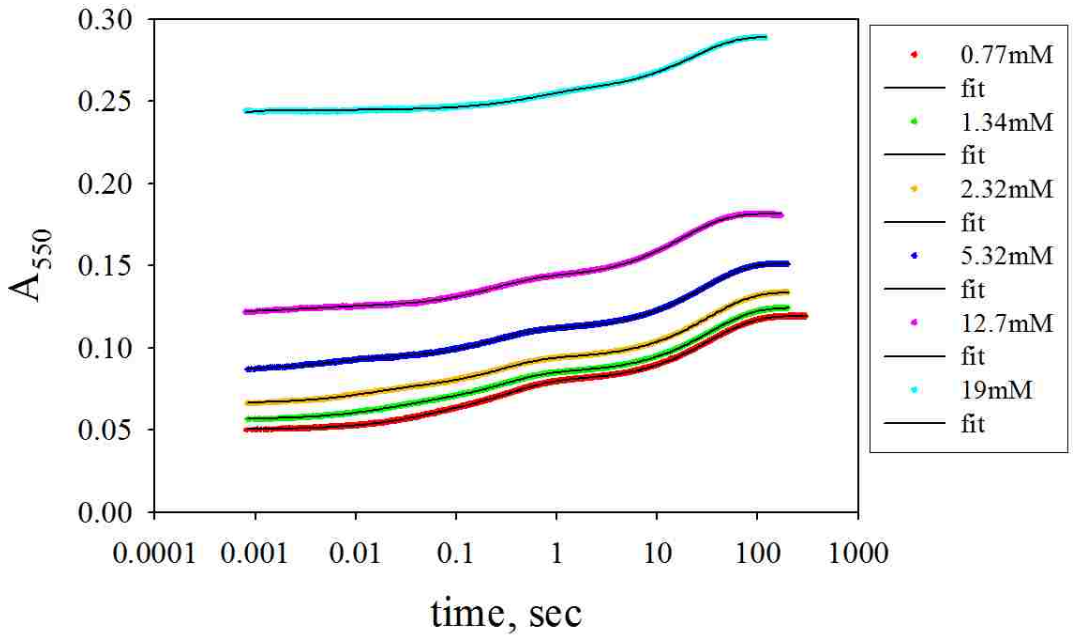


**Figure F11** Plots of absorbance at 550 nm versus time (on logarithmic scale) for reduction of the A72H76 variant of iso-1-cyt *c* at pH 7.5 and six different concentrations of $[Co(terpy)_2]^{2+}$. The solid lines are fits to a double exponential rise equation.

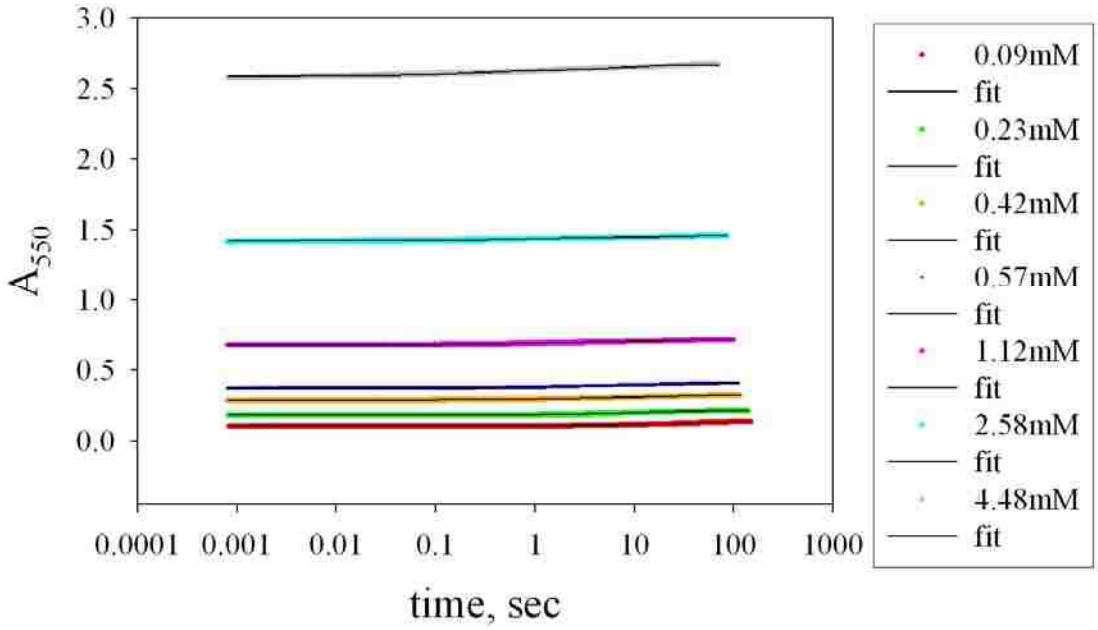

## G. Tables of Rate Constants and Amplitudes for the H81 Variant in 0.1 M NaCl and at 25 °C from ET experiments with $[a_6Ru^{2+}]$.

**Table G1**. Fast phase rate constants and amplitudes for the reduction of H81 iso-1-cyt *c* by $a_6Ru^{2+}$ as a function of $[a_6Ru^{2+}]$ at pH 7.5 derived from three exponential fits to the data in figure F8. [a]

| pH | $[a_6Ru^{2+}]$, mM | $k_{obs}$, $s^{-1}$ | Amplitude |
|---|---|---|---|
| 7.5 | 0.7 ± 0.2 | 28 ± 2 | 0.0430 ± 0.0004 |
| | 1.2 ± 0.1 | 37 ± 2 | 0.0450 ± 0.0002 |
| | 2.8 ± 0.3 | 59 ± 4 | 0.0440 ± 0.0001 |
| | 6.1 ± 0.4 | 144 ± 7 | 0.033 ± 0.001 |
| | 16 ± 3 [b] | 435 ± 46 | 0.014 ± 0.001 |
| | 32 ± 3 [b] | 1157 ± 423 | 0.0050 ± 0.0002 |

**Table G2**. Intermediate phase rate constants and amplitudes for the reduction of H81 iso-1-cyt *c* by $a_6Ru^{2+}$ as a function of $[a_6Ru^{2+}]$ at pH 7.5 derived from three exponential fits to the data in figure F8. [a]

| pH | $[a_6Ru^{2+}]$, mM | $k_{obs}$, $s^{-1}$ | Amplitude |
|---|---|---|---|
| 7.5 | 0.7 ± 0.2 | 3.23 ± 0.01 | 0.013 ± 0.001 |
| | 1.2 ± 0.1 | 3.23 ± 0.08 | 0.013 ± 0.001 |
| | 2.8 ± 0.3 | 3.33 ± 0.04 | 0.012 ± 0.001 |
| | 6.1 ± 0.4 | 3.26 ± 0.10 | 0.012 ± 0.001 |
| | 16 ± 3 [b] | 1.71 ± 0.70 | 0.010 ± 0.001 |
| | 32 ± 3 [b] | 0.26 ± 0.09 | 0.008 ± 0.001 |

**Table G3**. Slow phase rate constants and amplitudes for the reduction of H81 iso-1-cytochrome *c* by $a_6Ru^{2+}$ as a function of $[a_6Ru^{2+}]$ at pH 7.5 derived from three exponential fits to the data in figure F8. [a]

| pH | $[a_6Ru^{2+}]$, mM | $k_{obs}$, $s^{-1}$ | Amplitude |
|---|---|---|---|
| 7.5 | 0.7 ± 0.2 | 0.033 ± 0.004 | 0.014 ± 0.020 |
| | 1.2 ± 0.1 | 0.031 ± 0.001 | 0.007 ± 0.001 |
| | 2.8 ± 0.3 | 0.031 ± 0.001 | 0.0070 ± 0.0001 |
| | 6.1 ± 0.4 | 0.032 ± 0.003 | 0.0070 ± 0.0004 |
| | 16 ± 3 [b] | 0.036 ± 0.001 | 0.0070 ± 0.0004 |
| | 32 ± 3 [b] | 0.040 ± 0.002 | 0.010 ± 0.001 |

[a] Data for different $[a_6Ru^{2+}]$ were collected on the time scales as given in brackets: 0.7 mM (100, 200, 300, 500 s), 1.2 mM (300 s), 2.8 mM (250 s), 6.1 mM (200 s), 16 mM (160, 200, 300 s) and 32 mM (130, 200 s).

[b] Parameter is from quadruple exponential fits to the data.

## H. Tables of Rate Constants and Amplitudes for the H81 Variant in 0.1 M NaCl and at 25 °C from ET experiments with $[Co(terpy)_2]^{2+}$.

**Table H1**. Fast phase rate constants and amplitudes for the reduction of H81 iso-1-cytochrome *c* by $[Co(terpy)_2]^{2+}$ as a function of $[Co(terpy)_2]^{2+}$ at pH 7.5 derived from three exponential fits to the data in figure F9.

| pH | $[Co(terpy)_2]^{2+}$, mM | $k_{obs}$, $s^{-1}$ | Amplitude |
|---|---|---|---|
| 7.5 | 0.09 ± 0.01 | 0.7 ± 0.2 | 0.0077± 0.0007 |
| | 0.24 ± 0.02 | 1.5 ± 0.8 | 0.0062 ± 0.0004 |
| | 0.34 ± 0.03 | 1.4 ± 0.3 | 0.0063 ± 0.0001 |
| | 0.60 ± 0.05 | 2.5 ± 1.7 | 0.014 ± 0.02 |
| | 1.3 ± 0.1 | 3.8 ± 1.1 | 0.038 ± 0.01 |
| | 2.2 ± 0.1 | 6.6 ± 1.6 | 0.042 ± 0.001 |
| | 5.1 ± 0.6 | 15.0 ± 1.3 | 0.022 ± 0.001 |

**Table H2**. Intermediate phase rate constants and amplitudes for the reduction of H81 iso-1-cytochrome *c* by $[Co(terpy)_2]^{2+}$ as a function of $[Co(terpy)_2]^{2+}$ at pH 7.5 derived from three exponential fits to the data in figure F9.

| pH | $[Co(terpy)_2]^{2+}$, mM | $k_{obs}$, $s^{-1}$ | Amplitude |
|---|---|---|---|
| 7.5 | 0.09 ± 0.01 | 0.32 ± 0.03 | 0.052 ± 0.006 |
| | 0.24 ± 0.02 | 0.63 ± 0.04 | 0.0540 ± 0.0004 |
| | 0.34 ± 0.03 | 0.82 ± 0.06 | 0.053 ± 0.001 |
| | 0.60 ± 0.05 | 1.3 ± 0.1 | 0.054 ± 0.001 |
| | 1.3 ± 0.1 | 1.4 ± 0.5 | 0.019 ± 0.020 |
| | 2.2 ± 0.1 | 1.9 ± 0.4 | 0.022 ± 0.010 |
| | 5.1 ± 0.6 | 2.3 ± 0.2 | 0.010 ± 0.001 |

**Table H3**. Slow phase rate constants and amplitudes for the reduction of H81 iso-1-cytochrome *c* by $[Co(terpy)_2]^{2+}$ as a function of $[Co(terpy)_2]^{2+}$ at pH 7.5 derived from three exponential fits to the data in figure F9.

| pH | $[Co(terpy)_2]^{2+}$, mM | $k_{obs}$, $s^{-1}$ | Amplitude |
|---|---|---|---|
| 7.5 | 0.09 ± 0.01 | 0.027 ± 0.001 | 0.0067 ± 0.0003 |
| | 0.24 ± 0.02 | 0.026 ± 0.003 | 0.0065 ± 0.0004 |
| | 0.34 ± 0.03 | 0.031 ± 0.001 | 0.0063 ± 0.0002 |
| | 0.60 ± 0.05 | 0.031 ± 0.003 | 0.0063 ± 0.0004 |
| | 1.3 ± 0.1 | 0.032 ± 0.003 | 0.0064 ± 0.0004 |
| | 2.2 ± 0.1 | 0.033 ± 0.003 | 0.0073 ± 0.0004 |
| | 5.1 ± 0.6 | 0.031 ± 0.004 | 0.005 ± 0.001 |

[a] Data for different $[Co(terpy)_2]^{2+}$ were collected on the time scales as given in brackets: 0.09 to 0.6 mM (200, 250 s), 1.3 and 2.2 mM (200 s) and 5.1 mM (200, 300 s).

## I. Tables of Rate Constants and Amplitudes for the A72H76 Variant in 0.1 M NaCl and at 25 °C from ET experiments with [$a_6Ru^{2+}$].

**Table I1**. Fast phase rate constants and amplitudes for the reduction of A72H76 iso-1-cyt *c* by $a_6Ru^{2+}$ as a function of [$a_6Ru^{2+}$] at pH 7.5 derived from three exponential fits to the data in figure F10. [a]

| pH | [$a_6Ru^{2+}$], mM | $k_{obs}$, $s^{-1}$ | Amplitude |
|---|---|---|---|
| 7.5 | 0.8 ± 0.1 | 31 ± 3 | 0.0082 ± 0.0006 |
| | 1.3 ± 0.1 | 52 ± 3 | 0.0089 ± 0.0002 |
| | 2.3 ± 0.3 | 85 ± 4 | 0.0084 ± 0.0002 |
| | 5.3 ± 0.4 | 177 ± 9 | 0.0073 ± 0.0006 |
| | 12.7 ± 0.6 | 274 ± 60 | 0.0031 ± 0.0003 |
| | 19 ± 8 | 520 ± 552 | 0.003 ± 0.002 |

**Table I2**. Intermediate phase rate constants and amplitudes for the reduction of A72H76 iso-1-cyt *c* by $a_6Ru^{2+}$ as a function of [$a_6Ru^{2+}$] at pH 7.5 derived from three exponential fits to the data in figure F10. [a]

| pH | [$a_6Ru^{2+}$], mM | $k_{obs}$, $s^{-1}$ | Amplitude |
|---|---|---|---|
| 7.5 | 0.8 ± 0.1 | 3.19 ± 0.08 | 0.0220 ± 0.0004 |
| | 1.3 ± 0.1 | 3.60 ± 0.02 | 0.0200 ± 0.0003 |
| | 2.3 ± 0.3 | 3.87 ± 0.06 | 0.0190 ± 0.0002 |
| | 5.3 ± 0.4 | 4.11 ± 0.08 | 0.0180 ± 0.0002 |
| | 12.7 ± 0.6 | 4.25 ± 0.08 | 0.0180 ± 0.0003 |
| | 19 ± 8 | 1.8 ± 0.4 | 0.012 ± 0.001 |

**Table I3**. Slow phase rate constants and amplitudes for the reduction of A72H76 iso-1-cyt *c* by $a_6Ru^{2+}$ as a function of [$a_6Ru^{2+}$] at pH 7.5 derived from three exponential fits to the data in figure F10. [a]

| pH | [$a_6Ru^{2+}$], mM | $k_{obs}$, $s^{-1}$ | Amplitude |
|---|---|---|---|
| 7.5 | 0.8 ± 0.1 | 0.0300 ± 0.0005 | 0.0408 ± 0.0008 |
| | 1.3 ± 0.1 | 0.0300 ± 0.0003 | 0.0405 ± 0.0006 |
| | 2.3 ± 0.3 | 0.0310 ± 0.0004 | 0.0408 ± 0.0004 |
| | 5.3 ± 0.4 | 0.0340 ± 0.0005 | 0.0403 ± 0.0003 |
| | 12.7 ± 0.6 | 0.054 ± 0.001 | 0.0398 ± 0.0004 |
| | 19 ± 8 | 0.044 ± 0.001 | 0.036 ± 0.002 |

[a] Data for different [$a_6Ru^{2+}$] were collected on the time scales as given in brackets: 0.8 mM (200, 300, 500 s), 1.3 mM (200, 250, 300 s), 2.3 mM (200, 500 s), 5.3 mM (170, 200 s), 13 mM (100, 170 s) and 19 mM (100, 120 s).

## J. Tables of Rate Constants and Amplitudes for the H81 Variant in 0.1 M NaCl and at 25 °C from ET experiments with $[Co(terpy)_2]^{2+}$.

**Table J1**. Fast rate constants and amplitudes for the reduction of A72H76 iso-1-cytochrome *c* by $[Co(terpy)_2]^{2+}$ as a function of $[Co(terpy)_2]^{2+}$ at pH 7.5 derived from two exponential fits to the data in figure F11. [a]

| pH | $[Co(terpy)_2]^{2+}$, mM | $k_{obs}$, $s^{-1}$ | Amplitude |
|---|---|---|---|
| 7.5 | 0.09 ± 0.01 | 0.19 ± 0.02 | 0.0060 ± 0.0002 |
| | 0.23 ± 0.02 | 0.29 ± 0.04 | 0.0110 ± 0.0001 |
| | 0.42 ± 0.04 | 0.39 ± 0.02 | 0.0140 ± 0.0002 |
| | 0.57 ± 0.06 | 0.50 ± 0.05 | 0.0150 ± 0.0004 |
| | 1.12 ± 0.04 | 0.82 ± 0.08 | 0.0170 ± 0.0004 |
| | 2.6 ± 0.2 | 1.1 ± 0.2 | 0.0150 ± 0.0004 |
| | 4.5 ± 0.7 | 1.2 ± 0.6 | 0.017 ± 0.001 |

**Table J2**. Slow rate constants and its amplitudes for the reduction of A72H76 iso-1-cytochrome *c* by $[Co(terpy)_2]^{2+}$ as a function of $[Co(terpy)_2]^{2+}$ at pH 7.5 derived from two exponential fits to the data in figure F11. [a]

| pH | $[Co(terpy)_2]^{2+}$, mM | $k_{obs}$, $s^{-1}$ | Amplitude |
|---|---|---|---|
| 7.5 | 0.09 ± 0.01 | 0.0280 ± 0.0004 | 0.027 ± 0.001 |
| | 0.23 ± 0.02 | 0.033 ± 0.001 | 0.025 ± 0.001 |
| | 0.42 ± 0.04 | 0.036 ± 0.001 | 0.022 ± 0.001 |
| | 0.57 ± 0.06 | 0.037 ± 0.001 | 0.021 ± 0.001 |
| | 1.12 ± 0.04 | 0.039 ± 0.001 | 0.0210 ± 0.0002 |
| | 2.6 ± 0.2 | 0.046 ± 0.004 | 0.018 ± 0.001 |
| | 4.5 ± 0.7 | 0.052 ± 0.014 | 0.020 ± 0.001 |

[a] Data for different $[Co(terpy)_2]^{2+}$ were collected on the time scales as given in brackets: 0.09 mM (150, 170, 200 s), 0.2 mM (140, 200 s), 0.4 mM (115 s), 0.6 mM (112, 200 s), 1.1 mM (100, 200 s), 2.6 mM (85, 200 s) and 4.5 mM (70, 75, 100 s).